
GEAP-3766

# CRITICAL HEAT FLUX AND FLOW PATTERN CHARACTERISTICS OF HIGH PRESSURE BOILING WATER IN FORCED CONVECTION

By
Frank E. Tippets

April 1962

Atomic Power Equipment Department
General Electric Company
San Jose, California

UNITED STATES ATOMIC ENERGY COMMISSION · DIVISION OF TECHNICAL INFORMATION

## DISCLAIMER

# LEGAL NOTICE



USAEC Division of Technical Information Extension, Oak Ridge, Tennessee

GEAP-3766

REACTOR TECHNOLOGY

# CRITICAL HEAT FLUX AND FLOW PATTERN CHARACTERISTICS OF HIGH PRESSURE BOILING WATER IN FORCED CONVECTION

By

Frank E. Tippets

General Electric Company
Atomic Power Equipment Department
San Jose, California

April 1962

Prepared for the
U. S. ATOMIC ENERGY COMMISSION

under
Fuel Cycle Development Program
(Contract No. AT(04-3)-189, P.A. 11)

Approved By: D. H. Imhoff
D. H. Imhoff, Manager
Engineering Development

Approved By: C. L. Howard
C. L. Howard,
Project Engineer
Fuel Cycle Development
Program

Atomic Power Equipment Department
General Electric Company
San Jose, California

Prints of the motion picture films referenced in this report are available, on loan, from either of the following organizations: (1) U. S. Atomic Energy Commission, Washington 25, D. C., Attention: Chief, Engineering Development Branch, Division of Reactor Development, or (2) U. S. Atomic Energy Commission, San Francisco Operations Office, 211 Bancroft Way, Berkeley 4, California, Attention: Director, Reactor Division. Inquiries concerning purchase of prints of the films should be directed to: General Electric Co., Atomic Power Division, P. O. Box 254, 2151 S. First Street, San Jose, California, Attention: Roger Baird, Specialist, Government Research and Development Sales.

## ACKNOWLEDGMENT

The work reported here was done under the U. S. Atomic Energy Commission Fuel Cycle Development Program at General Electric Company, Atomic Power Equipment Department (Contract Number AT(04-3)-189, P.A.11). This report is submitted to the Atomic Energy Commission and, with the Commission's permission, to Stanford University, Department of Mechanical Engineering as a dissertation under the Stanford University Honors Cooperative Program.

Professor A. L. London was the author's Faculty Research Supervisor at Stanford University during the course of this work. The work was done in connection with the author's assignment under Dr. S. Levy at General Electric Company. The author gratefully thanks these two gentlemen for the substantial encouragement, opportunity and help they gave him.

The assistance of the several people at General Electric Company who applied their special skills and efforts to various aspects of the project is acknowledged with the author's gratitude. Finally, the author is grateful to Mrs. Annalee Wright for her careful typing of the report.

## ABSTRACT

High speed motion pictures of boiling water flow patterns in conditions of forced flow at 1000 psia pressure in a vertical heated rectangular channel were taken over the range of mass velocities from 50 to 400 lbs/sec-ft$^2$, fluid states from 170 Btu/lb bulk enthalpy of subcooling to 0.66 bulk steam quality, and heat fluxes up to and including the critical heat flux level. Thirty-three sequences from the motion pictures, covering this range of variables, have been made up in suitable form for further study.

The motion pictures show substantial, but not indisputable, evidence that the general arrangement of the flow, in conditions of bulk boiling, at heat fluxes near and including the critical heat flux level, is characteristically a wavy turbulent liquid film, in which there is vapor formation, flowing along the channel walls with the balance of the liquid being carried as either dispersed droplets or as an emulsion with the vapor in an adjacent more rapidly and steadily moving core.

Eighty valid critical heat flux determinations were made in the course of the experiment at conditions of bulk boiling with forced flow in the rectangular channel over the range of variables:

| | |
|---|---|
| Mass Velocity | 50 to 400 lbs/sec-ft$^2$ |
| Bulk Steam Quality | 0.033 to 0.75 |
| Pressure | 1000 psia |
| Heated Length | 37 inches |
| Hydraulic Diameter | 0.46 in. and 0.81 in. |

Theoretical analysis based on a representation of the flow pattern

which is generally consistent with the evidence observed in the motion pictures resulted with a useful working equation which relates the critical heat flux to the significant local fluid properties and flow parameters in conditions of bulk boiling with forced flow. This working equation was used to correlate and study the critical heat flux data obtained in the present work together with a selection, intended to be representative, of 742 additional data points from the major available sources. The equation includes three empirical constants which were determined by application to a limited portion of the data. Critical heat fluxes calculated by this expression are in good general agreement with measured values over the following range of variables considered:

| | |
|---|---|
| Duct Geometry | Rectangular, Circular, Annular |
| Mass Velocity | 27 to 1096 lbs/sec-ft$^2$ |
| Steam Quality | 0.00 to 0.75 |
| Pressure | 585 to 2500 psia |
| Hydraulic Diameter | 0.095 to 0.875 in. |
| Heated Length | 6.0 to 108 inches |

An objective of the work was that the results might be found useful in continued experimental and theoretical investigation of the critical heat flux phenomenon in forced flow bulk boiling systems. The results are intended to be applicable to design and development of nuclear power reactors employing high pressure boiling water as a working fluid.

TABLE OF CONTENTS


| | | Page |
|---|---|---|
| ACKNOWLEDGMENT | | iii |
| ABSTRACT | | iv |
| LIST OF FIGURES | | ix |
| NOMENCLATURE | | xi |
| I. | INTRODUCTION | 1 |
| II. | BACKGROUND INFORMATION | 2 |
| III. | RELEVANT LITERATURE | 8 |
| | Two-Phase Flow Patterns | 8 |
| | Liquid Film Flows and Interface Instability | 12 |
| | Critical Heat Flux Condition | 14 |
| IV. | EXPERIMENTAL EQUIPMENT | 25 |
| | Test Loop | 25 |
| | Observational Test Section | 27 |
| | Instrumentation and Measurements | 29 |
| | Photography | 32 |
| V. | EXPERIMENTAL METHOD | 41 |
| | Start-Up Procedure | 41 |
| | Classification of Runs | 42 |
| | Critical Heat Flux Determinations | 43 |
| | Photography | 44 |
| VI. | EXPERIMENTAL RESULTS | 47 |
| | Critical Heat Flux Determinations | 47 |
| | Motion Pictures of Flow Patterns | 52 |

Page

VII. THEORETICAL ANALYSIS . . . . . 100

Summary (Hypotheses) . . . . . 100

Part A: Analysis of the Liquid Film Stability . . . 104

Part B: Analysis of the Liquid Film Thickness . . . 115

Parc C: Analysis of the Critical Heat Flux . . . . 126
Condition

VIII. COMPARISON OF THEORETICAL RESULTS WITH CRITICAL HEAT . . 138
FLUX DATA

Description of Data . . . . . 138

Application of Equation (52) . . . . . 141

IX. DISCUSSION OF RESULTS. . . . . 158

Summary . . . . . 158

Flow Pattern Observations. . . . . 159

Critical Heat Flux Determinations. . . . . 164

Theoretical Analysis and Application . . . . . 166

Uses of the Results. . . . . 171

X. CONCLUSIONS. . . . . 173

XI. RECOMMENDATIONS . . . . . 175

APPENDICES:

A. DESCRIPTION OF THE OBSERVATIONAL TEST SECTION . . . 177

B. DESCRIPTION OF THE CRITICAL HEAT FLUX DETECTOR . . . 188

C. EXPERIMENTAL CRITICAL HEAT FLUX DATA . . . . . 201

D. MOTION PICTURES OF BOILING WATER FLOW PATTERNS . . . 206

E. EXPERIMENTAL CRITICAL HEAT FLUX DATA USED FOR . . . 217
COMPARISON WITH THEORETICAL ANALYSIS

F. ANALYSIS OF THE LIQUID FILM INTERFACE . . . . . 221
VELOCITY

Page

REFERENCES. . . . . 224

SUPPLEMENTARY MOTION PICTURES:

"SUMMARY OF SELECTED HIGH SPEED MOTION PICTURES OF BOILING WATER FLOW PATTERNS" (Summary Reel)

"SELECTED HIGH SPEED MOTION PICTURES OF BOILING WATER FLOW PATTERNS" (Five Data Reels)

## LIST OF FIGURES


| Figure | | Page |
|---|---|---|
| II-1 | ILLUSTRATION OF SURFACE TEMPERATURE CHANGES IN TRANSITION BOILING . . . . . | 7 |
| IV-1 to IV-7 | PHOTOGRAPHS AND DIAGRAMS OF THE EQUIPMENT . . . | 34 - 40 |
| V-1 | GRAPH OF THE TEST CONDITIONS . . . . . | 46 |
| VI-1 | GRAPH OF THE CRITICAL HEAT FLUX DATA . . . . . | 55 |
| VI-2 to VI-14 | RECORDER TRACES AT AND NEAR THE CRITICAL HEAT FLUX CONDITION . . . . . | 56 - 85 |
| VI-15 to VI-18 | PHOTOGRAPHS OF USED HEATER ELEMENTS . . . . . | 87 - 89 |
| VI-19 to VI-23 | ENLARGEMENTS OF SELECTED FRAMES FROM MOTION PICTURES . . . . . | 91 - 99 |
| VII-1 | REPRESENTATION OF THE TWO-PHASE FLOW PATTERN . | 102 |
| VII-2 to VII-5 | SKETCHES FOR ANALYSIS (included in text of Section VII) | 111 - 127 |
| VII-6 | GRAPH OF THE TWO-PHASE FRICTION MULTIPLIER $\Phi_{TPF}$ FOR WATER . . . . . | 135 |
| VII-7 | GRAPH OF LAUFER'S MEASUREMENTS OF THE FLUCTUATING TURBULENT VELOCITY COMPONENT . . . . . | 136 |
| VII-8 | GRAPH OF MEASURED AND CALCULATED STEAM VOLUME FRACTIONS . . . . . | 137 |
| VIII-1 | NON-DIMENSIONAL GRAPH OF DATA OF APPENDIX C AND EQUATION (52) . . . . . | 145 |
| VIII-2 | ERROR PLOT COMPARING DATA FROM APPENDIX C WITH CORRESPONDING HEAT FLUXES CALCULATED BY EQUATION (52) . . . . . | 146 |
| VIII-3 | ERROR PLOT COMPARING DATA OF REF. (15) WITH CORRESPONDING HEAT FLUXES CALCULATED BY EQUATION (52) . . . . . | 147 |
| VIII-4 | ERROR PLOT SHOWING CHANNEL SIZE EFFECT ON CRITICAL HEAT FLUX CALCULATIONS BY EQUATION (52) . . . . . | 148 |

| Figure | | Page |
|---|---|---|
| VIII-5 to VIII-13 | GRAPHS OF MEASURED AND CALCULATED CRITICAL HEAT FLUXES AS FUNCTIONS OF VARIOUS SYSTEM PARAMETERS . . . . . | 149 - 157 |
| A-1 | OBSERVATIONAL TEST SECTION ASSEMBLY DRAWING . . . . . | 186 |
| A-2 | HEATER ELEMENT ASSEMBLY DRAWING . . . . . | 187 |
| B-1 | DIAGRAM OF CRITICAL HEAT FLUX DETECTOR CIRCUIT . . . . . | 198 |
| B-2 | REPRESENTATION OF THE CRITICAL HEAT FLUX DETECTOR BRIDGE CIRCUIT FOR ANALYSIS . . . . . | 199 |
| B-3 | GRAPH OF CALCULATED TEMPERATURE RISES FOR RECTANGULAR PATCHES IN THE CRITICAL HEAT FLUX CONDITION . . . . . | 200 |

## NOMENCLATURE*

| | |
|---|---|
| $A_f$ | flow area, ft.$^2$ |
| b | hydraulic radius $\mathcal{R}_H$ for rectangular channels and annuli; radius $D_e/2$ for circular tubes, ft. |
| C',C" | constants (equations (49),(52), Sec. VII), dimensionless |
| $D_e$ | hydraulic diameter, $4A_f/P_f$, ft. |
| $f_F$ | Fanning friction factor, dimensionless |
| g | gravitational acceleration, ft./sec$^2$ |
| G | total flow rate per flow area (mass velocity), lb/sec-ft$^2$ |
| $G_d$ | net diffusion flux of liquid, lb/sec-ft$^2$ |
| h | mean mixed specific enthalpy, Btu/lb. |
| $h_f$ | specific enthalpy of the liquid at saturation, Btu/lb. |
| $h_{fg}$ | specific enthalpy of vaporization, Btu/lb. |
| $\Delta h_s$ | mean mixed specific enthalpy of sub-cooling, $h_f$-h, Btu/lb. |
| k | wave number, $2\pi/\lambda$ , ft.$^{-1}$ |
| K | Prandtl mixing length constant (equation (30), Sec. VII), dimensionless |
| $K_1$, $K_2$, $K_3$, $K_4$, K' | constants (equations (31),(32),(36),(40),(45),Sec. VII), dimensionless |
| $\ell$ | Prandtl mixing length, ft. |
| $\ell'$ | mixing length for turbulent diffusion, ft. |
| $\ell''$ | half-width of the zone of influence adjacent to the interface, ft. |
| L | heated duct length, ft. |
| m | constant (equations (45),(52), Sec. VII), dimensionless |

* The analysis in Section VII is constructed to employ without change any consistent unit system using the three fundamental units of length, mass and time. For convenience the corresponding English units foot (ft.), pound-mass (lb.) and second (sec.) are listed in the Nomenclature. The British Thermal Unit (Btu) is used for the unit of thermal energy.

| | |
|---|---|
| $p$ | pressure, lb/ft- $sec^2$ |
| $P_f$ | wetted wall area per unit duct length, ft. |
| $q$ | heat flux, Btu/sec-$ft^2$ |
| $q_c$ | critical heat flux, Btu/sec-$ft^2$ |
| $\mathcal{R}_H$ | hydraulic radius, $A_f/P_f$, ft. |
| $R_e$ | Reynolds number, $GD_e/\mu_L$ , dimensionless |
| $t$ | time, sec. |
| $\Delta T$ | temperature difference, $^oF$ |
| $\Delta T_{SH}$ | liquid superheat, $^oF$ |
| $u$ | local velocity in the Z-direction, ft/sec. |
| $u'$ | root-mean-square turbulent fluctuating velocity component in the Z-direction, ft/sec. |
| $u_t$ | turbulent fluctuating velocity component in the Z-direction, ft/sec. |
| $U$ | mean velocity in the Z-direction near the interface, ft/sec. |
| $U_{gL}$ | relative velocity between the gaseous core and the liquid film, ft./sec. |
| $v$ | local velocity in the y-direction, ft/sec. |
| $v'$ | root-mean-square turbulent fluctuating velocity component in the y-direction, ft/sec |
| $v_t$ | turbulent fluctuating velocity component in the z-direction, ft/sec. |
| $v_*$ | friction velocity, $\sqrt{\tau_0/\rho}$ , ft/sec. |
| $X$ | steam quality, $(h-h_f)/h_{fg}$, dimensionless |
| $y$ | coordinate normal to the mean flow, ft. |
| $Z$ | coordinate parallel to the mean flow, ft. |
| $\left(\frac{dp}{dZ}\right)_{TPF}$ | friction pressure gradient in two-phase flow, lbs/$ft^2$-$sec^2$ |
| $\left(\frac{dp}{dZ}\right)_o$ | friction pressure gradient for total flow of saturated liquid, lb/$ft^2$-$sec^2$ |

Greek

| | |
|---|---|
| $\alpha$ | local vapor or gas volume fraction, dimensionless |
| $\bar{\alpha}$ | channel cross-sectional average vapor or gas volume fraction, dimensionless |
| $\alpha_c$ | local vapor or gas volume fraction in the gaseous core, dimensionless |
| $\bar{\alpha}_c$ | cross-sectional average vapor or gas volume fraction in the gaseous core, dimensionless |
| $\beta$ | disturbance growth factor, $sec.^{-1}$ |
| $\delta$ | liquid film mean thickness, ft. |
| $\Delta$ | finite difference or increment, dimensionless |
| $\zeta$ | transport property (Sec. VII-B) |
| $\eta$ | deflection of the interface from the mean position, ft. |
| $\eta_o$ | amplitude of the interfacial waves, ft. |
| $\lambda$ | wave length of interfacial waves, ft. |
| $\lambda_c$ | critical wave length (equations (25b),(33), Sec. VII), ft. |
| $\lambda_m$ | wave-length of disturbances which grow fastest (equation (35),Sec. VII), ft. |
| $\lambda_o$ | dominant wave-length of disturbance motion impressed on the interface (equation (36), Sec. VII), ft. |
| $\mu$ | absolute viscosity, lbs/ft-sec. |
| $\nu$ | kinematic viscosity, $\mu/\rho$ , $ft^2/sec$ |
| $\xi$ | dimensional group (equation (52), Sec. VII), $ft^2$-sec/Btu |
| $\pi$ | 3.14... |
| $\rho$ | density, $lbs/ft^3$ |
| $\sigma$ | surface tension at the interface, $lbs/sec^2$ |
| $\tau$ | fluid shear stress, $lbs/ft\text{-}sec^2$ |
| $\tau_o$ | fluid shear stress at the wall, $lbs/ft\text{-}sec^2$ |
| $\phi$ | velocity potential, $ft^2/sec$ |

| | |
|---|---|
| $\Phi_{TPF}$ | two-phase friction multiplier, $(dp/dZ)_{TPF} / (dp/dZ)_o$, dimensionless |
| $\psi$ | dimensionless group (equation (52), Sec. VII), |
| $\omega$ | radian frequency of the interfacial waves, $sec.^{-1}$ |

Subscripts

| | |
|---|---|
| c | critical condition |
| g | gas or vapor |
| L | liquid |
| TPF | two-phase flow |

# I. INTRODUCTION

Recent developments in nuclear power reactor technology have resulted in need for more precise determination and understanding of the nature of the critical heat flux condition and the factors governing its onset in high thermal performance systems using pressurized boiling water in forced flow.

The work reported here was undertaken for the particular purpose of obtaining photographic evidence of the general flow patterns in vertical upward flow of high pressure boiling water in a duct at heat fluxes near and including the "critical heat flux" level[1] and to derive at least a preliminary theory of the phenomenon based on this experimental evidence.

The work was largely exploratory in nature, and to that extent it is preliminary, as there have been no previous experimental investigations along these same lines for high pressure flows of water in bulk boiling with large heat fluxes. It is intended that the results of the work might be found useful to better define the nature of the critical heat flux phenomenon and thereby to help clarify the directions succeeding researches would most fruitfully follow. The results are intended to be particularly applicable to design and development of nuclear power reactors employing high pressure boiling water as a working fluid.

The main results obtained are summarized in Section IX, and the conclusions and recommendations are listed in Sections X and XI.

---

[1] Sometimes called "burnout" or "departure from nucleate boiling."

## II. BACKGROUND INFORMATION

For some time design and operation of modern nuclear power reactors using high pressure water, either in bulk boiling or with sub-cooled surface boiling, have been governed by the limiting criterion of avoiding the condition of the critical heat flux. Economic and technically feasible nuclear fuels capable of withstanding without destruction onset of the critical heat flux condition at the high heat fluxes used are not yet available. Due to the cost of nuclear reactor components there is a large economic incentive to know more precisely the conditions of operation which would cause onset of the critical heat flux condition in reactors so that design margins can be reduced to a minimum consistent with good design practice (ref. (106)).

As a result of the large economic factors involved, there has been an immense effort over about the last fifteen years in the United States and, more recently, in Russia, England and Europe to investigate the critical heat flux condition, both by laboratory research and engineering test at simulated nuclear reactor conditions. Due to the urgency of the need to develop bases for design, the effort has been expended principally on engineering test work.

Critical heat flux data points that have been taken number in the thousands. The earlier data is characterized by large scatter, due to lack of precise control of the governing variables in the process and substantial uncertainties of definition and measurement of the critical heat flux condition. It is evident in the literature that only recently (since about 1957 to 1959) have even the main trends of variation of the critical heat flux with system parameters in forced convection been

generally recognized. At the time of this writing there have not been published any general correlations that can be used with confidence to extrapolate from test conditions or that, in fact, predict with reasonable certainty the results of tests at much different conditions than the ones to which the correlations are fitted. Progress in development of a sound theory to explain and reliably predict onset of the critical heat flux condition in forced flow with bulk boiling has been small, with the results largely speculative and semi-empirical at the present time.

Most success in theoretical development and laboratory investigation and measurement of the critical heat flux phenomenon has been confined to small systems in pool boiling (non-flow). High speed photography of the flow process has been a significant factor in success of development of a good theory describing the critical heat flux in pool boiling systems (refs. (77) and (10)).

Absence of knowledge of the general arrangement of the two-phase flow pattern at the critical heat flux condition in bulk boiling with forced flow, particularly the nature of the flow process at the heated surface, has been one of the largest impediments to development of theoretical understanding of the process, especially at the higher pressures of significance to nuclear reactor design (refs. (7), (2), (3)). Investigations dealing with observations of two-phase and boiling water flow patterns date back to at least as early as that of Barbet in 1914 (ref. (88)). With the exception of Leppert's observations of two-phase water flow at pressures up to 300 psia in a boiler sight glass at the end of a horizontal heated test section (ref. (108)), the work has been confined to low temperatures and pressures in the range of less than

60 psia. Many of the studies have been with low pressure air-water systems. Only a very few have been done with local heating (refs. (88), (75), (76)).

Various definitions of the critical heat flux condition,[1] both operational and theoretical, have been used on occasion, depending on the application (ref. (12)). These include definitions based on: measurement of abrupt rise or start of fluctuation of the heated surface temperature; visual observations of the walls of the channel becoming reddened as a result of high temperature; physical damage by melting or rupture[2] of the heater elements; or, simply, the heat flux at which heater element temperature rises cause an electronic circuit ("burnout detector") to shut off the power supply to electrical resistance heated elements.[3]

Before closing this Section it is desirable to review briefly, in combination, the facts that are in hand concerning the character of behavior of the heated surface temperature as the heat flux is raised slowly from a condition analogous to "nucleate boiling" to the critical heat flux condition and beyond it through "transition boiling" to establishment of stable "film boiling" (or "liquid deficit" regime, ref. (7)), for high pressure water in bulk boiling with forced flow.

---

[1] Alternate terms that have been used are: "burnout" (ref. (101)); "departure from nucleate boiling" or "DNB" (refs. (1),(93)); and the boiling "crisis" (refs. (10),(11)).

---

[2] Usually due to the yield stress of the metal decreasing with the increased temperature until it becomes less than the load stress.

---

[3] The definition used in the present work for purposes of data taking is a combination of the first and last definitions, discussed in detail in Section V and Appendix B.

These terms are borrowed from the terminology common in pool boiling investigations to describe apparently analogous general situations. The main source of data for the description which follows is ref. (14), together with published results of other critical heat flux investigations and the results of the present work.

At heat fluxes slightly less than the critical heat flux in the "nucleate boiling" regime (Fig. II-1), the temperature difference between the heated surface and the bulk fluid is quite uniform with time and is relatively small, due to the large order of magnitude of the convection heat transfer coefficient in nucleate boiling ($\geq 10^4$ Btu/hr-ft$^2$-F$^o$). As the heat flux is raised, with the other system variables maintained approximately constant, the surface temperature difference increases in considerably lesser proportion and remains uniform with time until the critical heat flux condition is reached. Further increases of heat flux beyond the critical level result in either:

(1) irregular oscillations of the surface temperature difference, if the steam quality is in the higher ranges with correspondingly lower critical heat flux levels; or

(2) abrupt rise of the temperature to a level frequently high enough to cause damage to the surface (preceded sometimes by slight temperature oscillations), if the steam quality is in the lower ranges with correspondingly higher critical heat flux levels (Fig. II-1).

At heat fluxes slightly above the critical level, depending on the steam quality, heat flux level and local flow turbulence, the surface temperature characteristically oscillates in an irregular manner between a lower level, only a little above that for sub-critical heat fluxes, and

a slightly higher level. The frequency of these oscillations is characteristically in the range of 2 to 10 cycles per second. As the heat flux is raised further into the "transition boiling" regime, the mean level of the surface temperature rises steeply and the amplitude of the temperature oscillations increases to a maximum, at the higher ranges of steam quality, as depicted in Figure II-1. Finally, as the heat flux is raised still further, the surface temperature oscillation amplitude becomes less and the mean surface temperature difference begins to stabilize to a level which, in the cases investigated at the higher steam qualities is about an order of magnitude higher than that corresponding to the inception of the critical heat flux condition (ref. (14)). The point where the heat transfer again becomes steady is sometimes called the beginning of the "film boiling" regime (or "liquid deficit" regime) and is apparently characterized by there being almost pure superheated steam, rather than liquid, in contact with the surface.

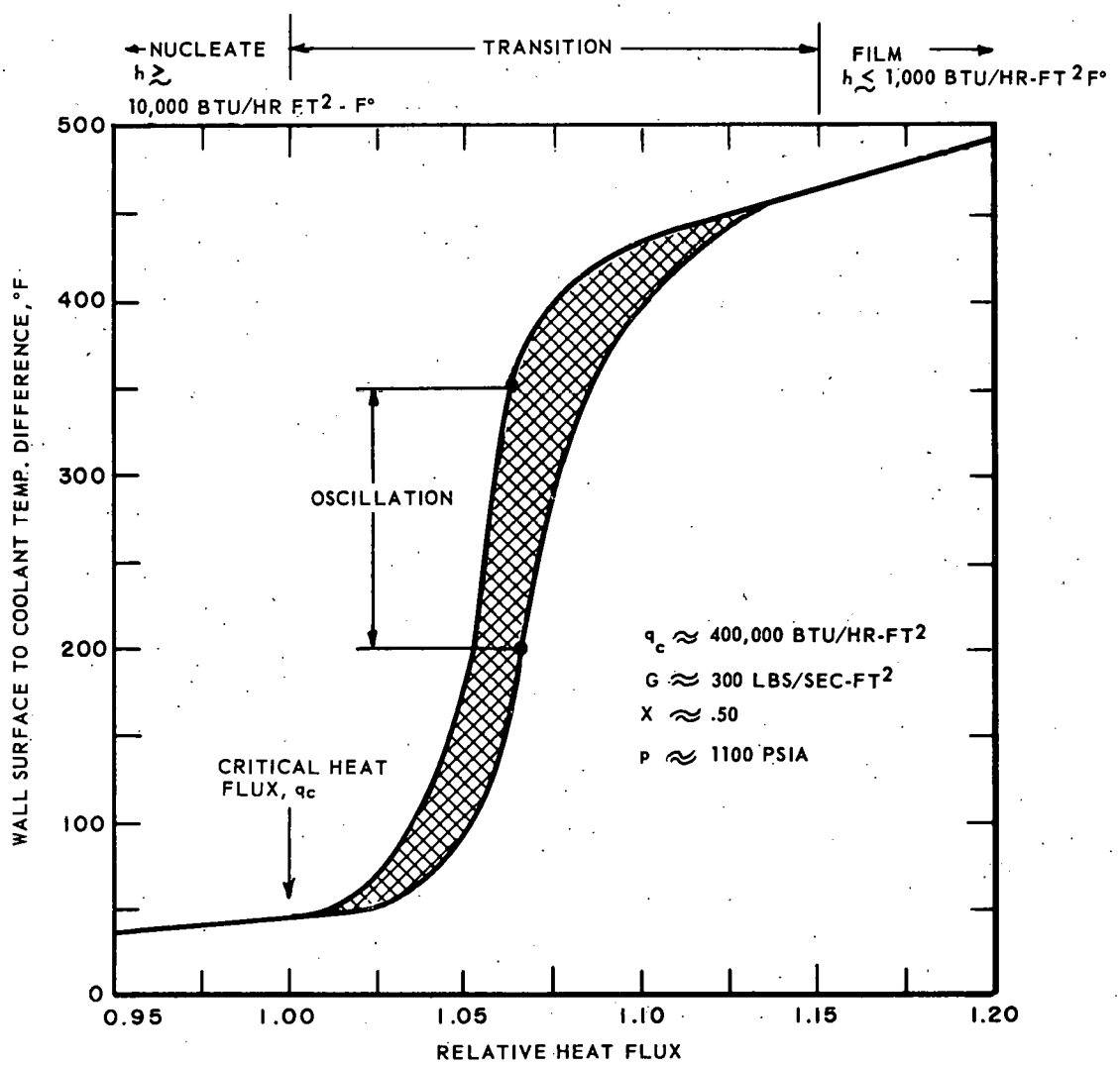


FIGURE II-1

ILLUSTRATION OF SURFACE TEMPERATURE CHANGES
IN "TRANSITION BOILING"

Based on Experimental Data in Ref. (14)

## III. RELEVANT LITERATURE

The published literature dealing with boiling water flow and heat transfer is very voluminous. Since there already exist several published reviews of the main aspects of the field,[1] this Section is confined to brief mention of some of the principal works which are particularly relevant to this investigation. References which pertain especially to parts of the Theoretical Analysis and are not mentioned here are discussed briefly in footnotes in Section VII.

### Two-Phase Flow Patterns

The earliest work dealing with observations of boiling water flow patterns to which reference has been found is that of Barbet (1914) described by Brooks and Badger (ref. (88)). Barbet's experiments were repeated by Brooks and Badger using a small vertical tube heated by a glass-walled steam jacket, with sub-cooled liquid water entering the tube at the bottom at slightly above atmospheric pressure. In substantial agreement with Barbet's results, the following general patterns were observed at progressively higher elevations up the tube:

(1) Over a short length near the bottom of the channel the vapor and liquid were almost uniformly distributed, both transversely and longitudinally.

(2) Further up the channel the flow was composed of alternate slugs of liquid and vapor.

(3) Towards the top of the channel the flow became arranged as a core of vapor with most of the liquid climbing as an irregular film on the walls of the tube.

---

[1] See, for example, refs. (64), (65), (66), (67), (68), (69), (71), (72), (73), (74), (6), (1), and (109).

Later studies involving direct observation and photography of the boiling heat transfer process were conducted at conditions of sub-cooled surface boiling in pools (ref. (77)) and with forced flow of sub-cooled liquid (refs. (78), (79)).

More recently, observations and photography of bulk boiling water at low pressure ($p \lesssim 30$ psia) with heat fluxes up to the critical level were done with a 1 in. x 1 in. x 8 in. long glass channel fitted with a four-rod heater element by Janssen (ref. (75)). Janssen's motion pictures indicate the low pressure boiling flow to be swirling and eddying, with mixing across the channel and a tendency to surge at the higher heat fluxes and lower flows.

Research work has been in progress at Columbia University by Vohr to observe and photograph the flow pattern regimes for boiling water at low pressure ($p \lesssim 50$ psia) with sub-critical heat fluxes in a 3-3/4 in. x 3/8 in. x 48 in. long channel heated on one side (ref. (76)).

The observations by Dengler (ref. (80)) of flow patterns with vertical upward flowing boiling water at low pressures (up to 30 psia) were made with an unheated glass tube attached to the top of a steam jacketed heater section. The flow pattern observations of Kozlov were made with a vertical glass tube with unheated air-water mixtures at about 23 psia (ref. (81), Russia). Kosterin's observations of vertical, inclined and horizontal flow of unheated air and water were at 45 to 60 psia (ref. (84), Russia). The work of Govier, et.al., on flow pattern observations in vertical upward flow was also with air-water mixtures at about 70 F. and 36 psia (refs. (82), (83), Canada).

Observations of flow patterns in horizontal flow and attempts to correlate the boundaries of the various regimes in terms of fluid and

system properties have been reported by Kosterin (ref. (84)), Baker (ref. (85)), Richardson (ref. (86)), Mologin (ref. (87), Russian), and others (ref. (64)). All of these works appear to have been confined to unheated mixtures of air and water or other liquids at atmospheric temperature and pressure, or slightly above. Leppert, et.al. (ref. (108)), have reported visual observations of two-phase water flow at pressures up to 300 psia in an unheated sight-glass attached to the end of a horizontal heated test section. The flow appeared to be a fog-like mixture of steam and water droplets, with frequent bursts of apparently higher velocity vapor passing through the mixture (ref. (108)).

While their terminology differs slightly in detail, the several observers seem to be in general agreement that the following flow pattern effects occur in smooth circular vertical tubes with upward adiabatic flow of liquid and gas (or vapor) at low pressure, as the flow rate of gas or vapor is increased relative to that of the liquid. This verbal description is based primarily on Dengler's thesis (ref. (80)) and Kozlov's paper (ref. (81)).

(1) Bubble Flow:

The bubbles are first small and well distributed throughout the liquid phase. As vaporization or gas flow rate increases the bubbles grow in size, decrease in number, and tend to occupy the center of the tube. The bubbles grow to about one-quarter of the tube diameter and then they start to combine and lose their identity.

(2) Slug Flow:

As more liquid is vaporized or, equivalently, the gas flow rate is increased, the bubbles coalesce further and form slugs of vapor

or gas which fill the cross-section of the tube and alternate with liquid slugs along the length of the tube. The vapor or gas slugs grow in length with increased vaporization or gas flow rate until they tend to unite and displace the liquid from the center of the tube.

(3) Froth Flow:

This regime appears to be a transition between the preceding "slug flow" and the following "annular" or climbing film flow. The structure of the flow changes to a mixed flow of both phases in the form of a very coarse emulsion with elements which are continually collapsing and reforming. According to Dengler, annuli of liquid seem repeatedly to separate and are temporarily held up on the wall by the central vapor (or gas) stream and then tumble back into the center of the tube, thereby momentarily blocking the vapor or gas flow. Pressure pulsations are experienced.

(4) Annular or "Climbing Film" Flow:

With further vaporization or increased gas flow rate, the previous agitation and pressure pulsations subside and the vapor or gas, now moving at high velocity, forces the liquid up the tube wall as an irregular annulus in contact with the tube walls. The gas or vapor moves as a central core. According to Kozlov, an amount of entrained liquid is carried along in the gas or vapor stream. At the interface between the climbing liquid film and the gas or vapor core, there is apparently a capillary wave structure superimposed on waves of larger length. In this flow regime there is, according to Kozlov, always a continuous process of liquid droplets being torn from the film surface and absorbed further up the tube.

(5) Homogeneous (Fog) Flow:

At very high gas or vapor flow rates, the amount of liquid entrainment appears to increase to a maximum and the liquid is apparently carried as a mist or fog. The presence of a liquid film along the tube walls was, according to Kozlov, difficult to observe but might exist. Dengler's observations did not extend to this regime due to limitations of his equipment.

Liquid Film Flows and Interface Instability

A substantial amount of work has been done to investigate the mechanics and stability characteristics of liquid film flows in tubes in application to liquid film cooling of rocket engines (refs. (29), (34), (30)),chemical engineering heat transfer and flow processes (refs. (90), (89)), and to improve bases for calculation of pressure losses and phase distributions in nuclear reactor systems (refs. (31), (32), (91)). The analyses in these references are based on application of single-phase turbulent velocity profiles to describe the liquid film flow.

Knuth observed by means of high speed motion pictures that small disturbances, apparently associated with the stream turbulence, were always present on the liquid film interface. For liquid flow rates larger than some critical value, long wave-length disturbances appeared on the film and liquid droplets started to be entrained by the gas stream from the crests of the long wave-length disturbances (ref. (34)).

Several recent investigations have explored the mechanism of energy transfer at interfaces in shear flows (refs. (20), (21), (22)), the structure and stability characteristics of interfacial waves in relation to the liquid film thickness and flow velocities (refs. (30), (19)), and entrainment rates from the liquid film into the co-current gaseous core

(ref. (31)), for air-water flows at atmospheric pressure. Charvonia found that both the thickness of the liquid film and the maximum interfacial wave amplitude tended to decrease as either the gas core velocity was increased or the liquid flow rate was decreased (ref. (30)). According to the results of Collier and Hewitt (ref. (31)), the proportion of liquid entrained in the gaseous core increases as the liquid flow rate is increased until finally the film flow rate becomes constant, independent of total liquid flow and governed only by the gas flow rate. At the highest gas and liquid mass flow rates, approximately 90 per cent of the liquid flowing at the top of the vertical test section is carried as entrained droplets in the gas core and the remainder is carried as a thin film on the wall. A proven quantitative relationship between the interface motion and the stream turbulence, as needed for direct application of these results to analysis of other systems (Section VII), apparently has not yet been found.

The studies of wave formation and mechanism of disintegration of free-flowing liquid sheets done originally by York, Stubbs and Tek (ref. (17)) and extended by Hagerty and Shea (ref. (18)) formed a major part of the basis for the analysis of liquid film stability given in Part A of Section VII. These two works established that instability and wave formation at the interface are the major factors in the break up of a free-flowing sheet of liquid into drops. The sheets were considered to be in potential flow for analysis and the "method of small disturbances" was employed to linearize the equations of motions. The resulting predictions of the growth of instabilities on the interface and the conditions for maximum instability are supported by short-exposure photographs of the sheets in various stages of disinte-

gration.[2]

Critical Heat Flux Condition

Largely as a result of the need to define precise design limits of heat flux and fluid enthalpy for nuclear reactor systems employing water as a coolant there has been an extensive test and research effort all over the world for the past 15 years or so to determine the critical heat flux characteristics of boiling water in forced flow.[3]

Much of this work, especially the earlier portions of it, was done more from the standpoint of engineering tests at simulated nuclear reactor conditions rather than to discover and explore systematically the principal variables governing the critical heat flux condition. Also, in several cases, neither the definition nor the measurement of the critical heat flux condition were uniform or precise and in the reports of the work the actual character of the determinations are not described in sufficient detail for a reliable assessment of the validity

---

[2] It appears from the photographs in the paper of Hagerty and Shea that the dominant wave lengths on the film at breakup are of the same order of magnitude as the sheet thickness (Figs. 8, 9, 10 in ref. (18)), in support of the assumption made in Section VII, Part B for derivation of equation (33).

---

[3] The effort in the United States alone is immense, as represented by the data included in refs. (1), (15), (93), (101) and various large test and research programs in existence under sponsorship of the U. S. Atomic Energy Commission (refs. (76), (99)). Apparently a comparable effort has been underway in Russia (refs. (11), (74), (92), (94), (95), (96), (97)). A substantial program of investigation is in progress in Italy, with principal emphasis on the higher steam quality regions (refs. (6), (12), (13), (98)). A program of research similar to the one in Italy, at the higher range of steam qualities is being done at Harwell in England (ref. (8)), and another is in preparation at Winfrith, England, to perform experiments at simulated nuclear reactor conditions (ref. (99)).

of the data to be made.[4] Because of these features of the available data, only a fraction of the thousands of critical heat flux data points reported appear to be sufficiently well described and accurate enough to justify their use in attempts to develop general correlations and theoretical analysis. Often even the major trends of the data have escaped notice or have been incorrectly ascribed.[5]

In contrast, investigation of the critical heat flux condition in pool boiling has progressed more rapidly and along lines of more precise determination of the phenomena. It now appears the main facts of the process are known and the theoretical representation is in good agreement with measurements and photographic observations (refs. (9), (10)).

Earliest correlations of the critical heat flux data for forced flow of water in channels were principally for purposes of nuclear reactor design. Typically, only the fluid enthalpy (or, equivalently, the local enthalpy of sub-cooling or steam quality, whichever was appropriate) was employed as the independent variable (ref. (101)). The effect of mass velocity as an independent variable was either ignored in

---

[4] See, for example, discussions in refs. (6),(7) and (12), which note in particular the distinction between the so-called "burnout heat flux" at which a self-heated element melts or is otherwise damaged by overheating and the true "critical heat flux condition" as characterized by abrupt rise or fluctuation of the heater element surface temperature with further small increases of the heat flux. Cicchetti, et.al. note that deviations of the data from empirical "best fit" correlations are not infrequently as much as 100 per cent, with 15 to 20 per cent being minimum (ref. (6)).

[5] It has been only lately recognized, for example, that the early data of Westinghouse (Bettis), ANL and MIT (tabulated in ref. (1) and treated further in ref. (93)) exhibit a trend of decreasing critical heat flux with increased mass velocity in conditions of bulk boiling, $X > 0$, (refs. (4),(6),(100)). Reynolds' correlation (ref. (100)) was apparently the first to correctly find the trend in these data of decreasing critical heat flux with increased pressure over the range from 500 to 2000 psia.

these design correlations or it was incorporated to predict an increase of the critical heat flux with increasing mass velocity for both sub-cooled enthalpies and bulk boiling (refs. (1), (92), (93)), in contrast with the true trends in the data discovered later. The resulting scatter of the data around these correlations was allowed for in application to designs by constructing "limit lines" representing loci of heat fluxes below which the critical heat flux condition (the so-called "burnout") had not been experienced in the several tests (refs. (1), (93), (101)).

Reynolds was apparently the first in this country to correlate the trends in some of the data of reduction of critical heat flux with increased mass velocity and increased pressure (500 to 2000 psia) for $X > 0$. The correlation was constructed from dimensional reasoning based on all the liquid flowing as an annulus attached to the heater tube wall, using the early data from MIT and ANL (ref. (100)). A short time later Bell (ref. (4)) discovered by statistical correlation the same trend of decreasing critical heat flux with increased mass velocity in the Westinghouse 2000 psia data (ref. (1)) and found that the previously ascribed trend of variation with length to diameter ratio was fictitious, due apparently to confusion with the mass velocity effect in the previous design correlations (ref. (1), also ref. (93)). Immediately following, Bell's results were corroborated independently by Cicchetti, et.al. in a further semi-empirical treatment of the same data (ref. (6), Italy).

During about the same interval of time, the Russian investigators were beginning to note similar trends in some of their data of decreasing critical heat flux with increased pressure for sub-cooled average

enthalpies over the pressure range from 585 to 3000 psia (ref. (97)), increasing critical heat flux with increased mass velocity for subcooled average enthalpies (refs. (94), (97)), and decreasing critical heat flux with increased mass velocity in the range of bulk boiling (ref. (96)). An apparent trend of decreasing critical heat flux with increased channel length to diameter ratio (over the range of ratios 11 to 50) was noted by Styrikovich and Faktorovich for their data at bulk boiling conditions, but they were unable to conclude that this apparent trend was definitely not connected with the mass velocity effect over the limited range of their experiment (ref. (96)).

The results from several of the Russian experiments are presented together in ref. (11). In this summary presentation the trends of decreasing critical heat flux with increased mass velocity and independence of the length to diameter ratio are noted together with the trends of decreasing critical heat flux with increased channel diameter and apparent independence of channel heated wall thickness and surface roughness (ref. (11)). A trend of decreasing critical heat flux with increasing pressure can be found in the Russian data given in ref. (11) (see Section VIII).

Aladyev, et. al. (ref. (11)) distinguish between conditions of operation when the flow and pressure are steady, for which the critical heat flux decreases monotonically with increasing fluid enthalpy or steam quality, and conditions when the flow and pressure are pulsating (sometimes by intention in the experiments), for which the critical heat flux appears to increase with increasing enthalpy or steam quality to a maximum (magnitude less than for corresponding steady conditions) and

then decrease monotonically with further increases in steam quality.[6] It is noted in some of the earlier Russian works (e.g., ref. (96)) that the trend of a *maximum* in the variation of the critical heat flux with enthalpy is observed mainly at the lesser pressure levels (380 psia) and disappears at higher pressures (2650 psia).

Ivashkevich has presented a general correlation of much of the Russian data taken through 1958 (ref. (92)), which, according to Ivashkevich, correlates the majority of the data to within about $\pm$ 30 per cent.[7] This correlation appears to have been constructed using the data at sub-cooled enthalpies as the principal basis, although it was offered for general use in the bulk boiling range as well. Hence, although it seems to predict correctly the general trend of decreasing critical heat flux with increasing pressure, it represents the critical heat flux as increasing with increased mass velocity, as is apparently true for sub-cooled enthalpies and perhaps the lower steam quality range but is incorrect for intermediate and higher steam qualities. The correlation predicts correctly a monotonic decrease of the critical heat flux with increasing steam quality. It represents the critical heat flux as decreasing with increased length to diameter ratio for $L/D_e < 125$ and independent of length to diameter ratio for $L/D_e > 125$.

---

[6] This same trend in some of the CISE data is discussed by Silvestri (ref. (12)).

---

[7] Using symbols from the Nomenclature, the correlation is, for $X > 0$:

$$q_c = \frac{1.9 \times 10^{-5} \; Re\left[g\sigma(\rho_l - \rho_g)\right]^{1/4} h_{fg}(1 - X_c)\sqrt{\rho_g}}{1 + 1.8 \times 10^{-6} \; Re \; \left[K_3 + K_4\right]} \; ; \quad K_3 = \begin{cases} K_3', & K_3' < 50 \\ 50, & K_3' > 50 \end{cases}$$

$$K_3' = L\left[g(\rho_l - \rho_g)/\sigma\right]^{1/2} \; ; \quad K_4 = \begin{cases} L/D_e, & L/D_e < 125 \\ 125, & L/D_e > 125 \end{cases}$$

Silvestri has presented a modification and extension of the earlier correlation scheme of Cicchetti, et.al., (ref. (6)) in his presentation of some of the recent CISE data (ref. (12), Italy). The correlation correctly predicts, for bulk boiling, the trends of decrease of the critical heat flux with increasing mass velocity and decrease of critical heat flux with increasing steam quality (for conditions of stable operation (see footnote 6 ). Silvestri's correlation of the CISE data does not include treatment of the trends of variation with pressure, duct size or other system variables.

Aside from the unpublished work of Reynolds (ref. (100)), the only other published attempts to improve correlation of the existing critical heat flux data by means of analysis using definite physical representations or models of the process apparently are the recent works of Isbin and associates (ref. (2)) and Goldmann and associates (ref. (3)). The two analyses are similar to each other to the extent that both consider that the onset of the critical heat flux condition is governed by the nature of the turbulent diffusion of liquid droplets from a liquid-bearing vapor core to the wall. The critical heat flux condition is considered to occur when the diffusion rate of liquid from the core to the wall becomes less than equal to the liquid evaporation rate at the wall.

The analysis of Isbin and co-workers (ref. (2)) proceeds on the basis of a definite liquid film being attached to the wall for conditions of heat fluxes less than the critical level and considers a material flow balance comprised of: liquid removal from the film by vaporization together with re-entrainment into the core; and liquid supply to the film by means of droplets diffusing (because of the turbulence) to

the liquid film interface, to which they attach. The critical heat flux condition is then defined as the condition for which liquid supply to the film becomes less than liquid removal. Droplet diffusion is treated in the customary manner for turbulent flow, in analogy to the usual treatment of turbulent convective heat transfer, by expressing the droplet diffusion rate in terms of a "diffusion coefficient" and the local liquid concentration at the film interface.[8] The resulting constants in the expression obtained are then determined empirically by comparison with measured critical heat flux data. Liquid concentration at the wall is taken as zero at the critical heat flux condition. The results of the analysis are applied in ref. (2) to a selection of the Westinghouse 2000 psia data (ref. (1)) and a best fit of the constants is obtained. The resulting semi-empirical correlation agrees well with the data treated and correctly predicts the trend of reducing critical heat flux with increased mass velocity and increased enthalpy or steam quality. Since all of the data treated was at 2000 psia with duct hydraulic diameters of approximately 0.19 to 0.20 inch only, an assessment of the correlation prediction of the variations with duct size and pressure is not available. Although the analytical model includes the channel diameter as a variable it does not include the liquid-vapor surface tension, which appears to be a significant fluid property in determination of the dependence on saturation pressure.[9]

---

[8] Specifically, $G_d = k_g C$, $k_g = bG^j$, where $G_d$ is the mass flux of liquid to the film, C is the concentration of liquid in the vapor core, $k_g$ is the diffusion coefficient, G is the flow mass velocity, and b and j are parameters to be determined empirically.

---

[9] See Sections VII and VIII. Also refer to Zuber's treatment for pool boiling in either ref. (9) or (10).

In contrast to a basic assumption in the analysis of Isbin, et.al., the analysis of Goldmann and co-workers (ref. (3)) proceeds on the basis of there being no liquid attached to the wall. The analysis is considered to be representative for the so-called "fog-flow" regime, for which all of the liquid is assumed to be carried as dispersed droplets in the vapor. The mechanism of heat transfer is considered to be by evaporation of liquid droplets in a layer of superheated steam adjacent to the wall. Similarly to the analytical model of Isbin, et.al. (ref. (2)), liquid supply to the superheated steam layer at the wall is considered to occur by means of turbulent diffusion from the liquid-bearing stream and the critical heat flux condition is considered to occur when the liquid supply rate by this means becomes less than the vaporization rate at the wall. Also similarly to the analysis in ref. (2), the droplet diffusion rate is expressed as being equal to a "diffusion coefficient" times the local liquid concentration gradient (equivalent to the expression in footnote 8 from ref. (2)). The result of the analysis, a non-dimensional grouping involving the critical heat flux, mass velocity, steam quality and enthalpy of vaporization, is plotted against the gas phase Reynolds number[10] in Figure 2 of ref. (3) using critical heat flux data from several sources over a pressure range from about 500 to 1550 psia. The data does not appear to have been correlated, as the spread with respect to the parameter[10] $K_G$ is as large as a factor of ten, although the general trend of reduced critical heat

---

[10] Specifically,

$$K_G = \frac{q_c}{(1-x)\, h_{fg}\, G} \quad \text{vs.} \quad \frac{G\, De}{\mu g}$$

flux with increasing mass velocity can be discerned.

In both the analyses of Isbin, et.al. (ref. (2)) and Goldmann, et.al. (ref. (3)), a main assumption is that the liquid droplet diffusion rate is represented at the critical heat flux condition by an expression equivalent to

$$G_d = k_g C = bG^j C,$$

in which the symbols are those given in footnote 8. In both attempts to correlate the data it was found that in order to achieve a "fit" the exponent j had to be negative, in contrast with the value $j = 0.8$, expected from experience with turbulent diffusion in single-phase fluids.[11]

In a series of two papers, Collier (ref. (7)) and, most recently, Lacey, Hewitt and Collier (ref. (102)) have suggested several possible mechanisms for the onset of the critical heat flux condition and the inverse dependence on the mass velocity in the range of higher steam qualities. In agreement with suggestions advanced earlier in refs. (100), (6), (2), these authors base their ideas on the concept of a liquid film wetting the wall at conditions of heat flux up to the critical level. The critical heat flux condition is considered to occur when the film no longer wets the wall. Reference (102) summarizes several of the possible mechanisms which have been suggested in the literature to explain, in terms of a liquid film attached to the heated surface, why the critical heat flux condition occurs, as characterized by abrupt rise or start of fluctuation of the heated wall temperature. No analyses or numerical

---

[11] The authors of ref. (2) suggest a mechanistic explanation for this as being at least in part due to the possibility of changes in droplet size and, hence, effective droplet diffusion rates, depending on the stream mass velocity.

correlation of critical heat flux data are presented in refs. (7) and (102).

Lastly, attention is called to some of the work that has been done to investigate the heat transfer characteristics of forced flow boiling water systems at heat fluxes above the critical heat flux level in transition and stable film boiling, described in refs. (14) and (103).

In summary, the works reported appear to be in approximate agreement that the main trends of variation of the critical flux $q_c$ for high pressure water in forced flow appear to be:

(1) $q_c$ decreases as mass velocity is increased, in conditions of bulk boiling (refs. (2), (4), (6), (11), (12), (96), (100)); and increases as mass velocity is increased, in conditions of sub-cooled bulk enthalpies (refs. (1), (92), (94), (97)).

(2) $q_c$ decreases monotonically with increased steam quality or specific enthalpy, if the flow is stable and steady (all refs.); and may have maxima with respect to steam quality, in conditions of bulk boiling if the flow is unsteady or oscillating (refs. (11), (12)).

(3) $q_c$ decreases monotonically as pressure is increased, for the range above about 600 psia (refs. (92), (97), (100)).

(4) $q_c$ decreases as hydraulic diameter is increased, for some of the data (ref. (11)).

(5) $q_c$ is virtually independent of duct length to diameter ratio, for ratios larger than about 100 (refs. (4), (6), (11), (92)); and increases with decreased length to diameter ratios, for ratios less than about 100 (refs. (92), (96)).

Selections, intended to be representative, from the data of

Westinghouse (ref. (1)), Harwell (ref. (8), England), CISE (refs. (12), (13), Italy), and the Russian data (ref. (11)), together with the data of Janssen and Kervinen (ref. (15)) and the new data obtained in this work (Appendix C) are treated in detail in Section VIII using the results of the theoretical analysis in Section VII.

## IV. EXPERIMENTAL EQUIPMENT

The observational test section and other equipment associated with the experiment were installed in the north loop of the large twin-loop heat transfer test facility at General Electric Company, Atomic Power Equipment Department. Figure IV-1 gives a partial view of the test facility showing the observational test section in the left background, installed in its safety enclosure with the high speed motion picture camera and photographic lights mounted. In the foreground is the main power, flow and thermal control and recording equipment. The Sanborn recorder used to record relative coolant flow rate, relative power level, Critical Heat Flux Detector output signal, and camera operation is shown in the right background together with the cabinet containing the Critical Heat Flux Detector. Operation of the camera and lights was controlled remotely by switches located on the control panel and at the recorder.

### Test Loop

The test loop used for the experiment and the principal instrumentation components are diagrammed in Figure IV-5. All piping and fittings in the loop are made of stainless steel.

Slightly sub-cooled liquid water circulates from a nine-foot vertical steam drum down a four-inch downcomer in which mixing with sub-cooled liquid from the bypass sub-cooler system is done and in which a standard flow orifice is installed to measure coolant flow rate to the test section. The flow is circulated by a packless canned rotor centrifugal pump installed at the bottom together with the flow throttle, pump bypass and recirculation lines and the connections for draining and filling. The pipe size is reduced from four inches to two inches in the

horizontal bottom cross-over at inlet to the test section. The flow discharges from the test section into a two-inch vertical riser at an elevation of 6 feet 3 inches above the inlet and then flows upward an additional 17 feet 1 inch to a horizontal top cross-over which returns the fluid to the vertical steam drum. Steam is separated by gravity in the steam drum, after which it is condensed and slightly sub-cooled in the condenser located at the top of the facility and then returned to the downcomer at the outlet connection from the bottom of the steam drum.

A by-pass demineralizer system installed in the sub-cooler loop was used to maintain water quality in the range of 0.2 to 1.0 megohm-cm. resistivity. No other means were employed to control water purity, other than to thoroughly flush the loop at the start of each 24-hour period of test operation.

Control of the system pressure and degree of sub-cooling at inlet to the test section is done either automatically or manually at the main control panel. Precise adjustment of coolant flow is done manually by means of the throttle valve and pump by-pass loop used together with a manometer installed at the main flow orifice.

Single-phase alternating current is used to generate heat in the test section heater element. The main power supply and control system includes an induction type voltage regulator which is fed by a 12,000 volt three-phase source. The regulator is adjusted to prescribed output voltage by a remote unit in the main control panel. The regulator automatically compensates for variations in supply voltage. The load terminals of the induction regulator are connected to the high voltage side of a three-phase transformer. As used in conjunction with the induction regulator, the windings of this transformer are such that

regulated constant voltage output from 30 to 360 volts can be obtained in three overlapping steps for each of the three phases, by changing connections on a link-board between transformer winding taps. Multiple cable conductors carry the electrical current from the link-board terminals to the test section heater element electrodes. A main power circuit breaker, installed in the 12,000 volt supply system, is actuated by the Critical Heat Flux Detector to shut off power at the onset of the critical heat flux condition in the test section.

Observational Test Section

The test section is shown in Figure IV-2, installed in its partially assembled safety enclosure together with the photographic lights and mounted high speed motion picture camera. Figure IV-3 shows the complete test section in disassembly, with one of the .50-inch spacing heater elements. Figure IV-4 shows a closer view of the photographic window section. A more detailed description of the main construction features of the test section is given in Appendix A.

The observational test section is basically a heated rectangular flow channel 58.8 inches long, mounted vertically with sub-cooled liquid water entering as coolant at the bottom. Width of the channel is nominally uniform and at the photographic window section at the exit end of the heater element it is measured to be 2.10 $\pm$ .02 inches wide. Thickness of the channel is nominally uniform and is measured at the photographic window section to be either .50 in. or .25 in. ($\pm$ .01 in.), depending on the type of heater element used. Corresponding channel hydraulic diameters are .81 in. and .46 in. The channel is heated uniformly on either one or both of the two wide sides, depending on the type of heater element installed. The heated section extends 37.0 inches

from the channel inlet to an abrupt termination located at about the middle of the photographic window assembly. The channel is continued upward with nominally no change in geometry or cross-section for 21.8 inches of unheated length to the channel outlet.

Five types of heater elements were used, depending on heater ribbon thickness (.006 in. and .010 in.), spacing between ribbons (.50 in. and .25 in.) and number of heated sides. As shown in Figures IV-3 and IV-4, the heater element ribbons cover the two wide sides of the flow channel to provide a uniform, virtually unobstructed rectangular flow geometry. The heater element is held in tension by a double-spring assembly in the inlet terminal head and the heater ribbons are pressed tightly against their insulated backing strips (not shown in Figures IV-3 and IV-4) by small leaf and wire springs located at their edges along the heated length.

The photographic window assembly is comprised of a mono-crystalline sapphire filler block and holder which form the front edge of the flow channel, a pressure-bearing pyrex window and gaskets, a steel retaining cover or frame, and a coated front surface mirror mounted on the retaining cover. The window assembly at the adjacent back side was similar except that a pyrex filler block was used rather than the sapphire filler block, and no mirror was attached. The photographic window assembly was used only at the second window section from the top adjacent to the end of the heated section. The other three window sections were fitted with stainless steel "blanks" to form the edges of the flow channel at those locations.

The test section and connecting piping were thoroughly insulated to reduce heat losses from the section to a negligible level.

Instrumentation and Measurements

The main instrumentation used in the experiment is diagrammed in Figure IV-5.

Measurement of pressure for determination of fluid properties was done by two standard Heise gauges connected in parallel to a tap in the test section slightly below the outlet end of the heated section. Calibration of these gauges and comparison of their respective readings indicate a maximum error less than 5 psi at 1000 psia.

Heat fluxes and flow channel powers were calculated, based on known heater element dimensions and fabrication tolerances, using system electrical power measurements together with an estimated allowance of 2 per cent for power losses in the electrical connections and system in series with the heater ribbons. System electrical power was recorded as data by a General Electric Company recording watt-meter, which was compared by direct check at the start of each set of critical heat flux or camera runs with the steady power calculated from measurement of the rotator speed of a standard General Electric Company watt-hour meter on the same circuit. Comparison of these two measurements together with previous calibrations of both instruments indicates a maximum error in power measurement of less than 1-1/2 per cent. Assuming all heater elements were fabricated to specified tolerances and assuming an allowance for maximum heater ribbon resistance variation of 3 per cent in the critical heat flux zone at the end of the heater ribbon due to observed dimensional changes occasionally caused by making of the silver-soldered step-joint there, the corresponding maximum error in determination of the critical heat fluxes is estimated to be less than

5 per cent.[1] Relative power was recorded simultaneously on the Sanborn recorder in order to have a definite history of the character of the approach to each critical heat flux data point.

The specific enthalpy of the fluid at test section inlet was calculated from mean fluid temperatures measured by thermocouples located in the test section inlet terminal head (TC-2) and in the inlet pipe about one foot upstream from the inlet (TC-1) and about four feet upstream (TC-10). The thermocouples were Chromel-Alumel type made by Conax Corporation. Thermocouple outputs were recorded on a Brown recorder. The arithmetic averages of the TC-1 and TC-2 readings were used as the inlet temperature and the TC-10 readings were used as a check. The TC-1 and TC-2 thermocouples were calibrated over the temperature range of interest against a certified mercury in glass thermometer and a calibrated platinum-rhodium standard thermocouple. By comparison of the TC-1, TC-2 and TC-10 readings, and allowing for a maximum of 1-1/2°F variation in the Brown recorder potentiometer and reference cold junction system, it is estimated that the measured coolant inlet temperatures are correct to within less than 3-1/2°F maximum error. The corresponding maximum error in determination of the specific enthalpy of sub-cooling at the inlet is less than 5 Btu/lb.

Test section coolant flow was measured using a 60-inch oil-in-glass manometer connected to flange taps of a calibrated standard orifice in the downcomer. Flow rate was also recorded on a Bristol flow recorder

---

[1] As is discussed in Section IX, there is indication by the critical heat flux data that some of the thinner ribbon heater elements (.006 in.) may have been subject to a greater variation of heat flux than allowed for here.

connected through a diaphragm transmitter to the orifice. Relative flow rate was recorded continuously on the Sanborn recorder using the voltage output from a Pace reluctance type transducer connected to the orifice taps. All data calculations are based on the average manometer reading over the time of operation at the critical heat flux condition or time of operation of the camera. The orifice flow calculations account for local fluid temperature, variation of discharge coefficient with Reynolds number and thermal expansion of the orifice. Calculated flow rates are estimated to be correct to within less than 2 per cent maximum error.

Detection of the onset of the critical heat flux condition and automatic shut off of power to prevent destruction of the heater element was accomplished with the Critical Heat Flux Detector, described in Appendix B. The Detector system includes a channel in the Sanborn recorder to record changes in the degree of heater element voltage unbalance between two tapped sections at the exit end of the heated section. The character of these traces at the critical heat flux condition formed the main basis for judgment of the validity of each critical heat flux determination and provided information required to judge when to start the high speed motion picture camera in order to synchronize with the critical heat flux condition.

A master switch, located at the Sanborn recorder, was actuated manually to simultaneously start the high speed motion picture camera and switch the photographic lights from dim to full bright at onset of the critical heat flux condition, based on judgment of the character of Sanborn recorder trace of the Critical Heat Flux Detector output signal. The camera would then run for about 1.2 seconds to expose 100 feet of film, after which it automatically shut off. The period of camera

operation was recorded by a marker on the Sanborn recorder, thereby giving immediate indication of the time sequencing of the motion picture with the critical heat flux condition.

Several representative Sanborn recorder traces showing the instrumentation readouts at or near critical heat flux conditions are displayed in Figures VI-2 through VI-14. Frequency response of the Sanborn recorder appears to be adequate for the present purposes. According to the manufacturer's specifications the pen response at 71 per cent of critical damping is: (1) Step input, 90 per cent of full deflection in 10 milliseconds; (2) Sinusoidal input, 71 per cent of full deflection at 42 cps.

Photography

The photographic setup used in conjunction with the observational test section is diagrammed in Figure IV-6 together with a tabulation of the main photographic data.

The camera was located outside the test section enclosure on an adjustable mount together with two photo-spot lamps spread at an angle of about 25° above and below the camera axis, as shown in Figure IV-2. The optical path from the plane of focus through the mirror to the film plane was about 29 inches. Back lighting was provided by two photo-spot lamps spread at an angle of about 10° above and below horizontal in their location 6 inches from the back side of the test section in the safety enclosure.

The four lamps were positioned to converge axes at the plane of focus of the camera in the flow channel. Due to some flexibilities inherent in the lamp mountings and the inaccessibility of the back lights during operation, alignment of the lamps with the camera axis

and the transverse plane of the flow channel was approximate rather than precise. Some variations in the motion picture images due to this can be noticed.

The camera was focused sharply on the wire focusing target shown in Figure IV-6 and was in reasonably good focus over a depth of field from the inside face of the sapphire filler block back to a distance of about .20 inch beyond the focusing target. The heater elements used for the camera runs were positioned during assembly in the test section so that the 1/8-inch long perpendicular focusing target, attached .25 in. from the end of the heated section, was located about .15 in. inside the channel from the filler block face. The camera position was adjusted, as part of the focusing procedure for each run, so that it was in reasonably accurate alignment with the plane of the flow channel and so that the horizontal focusing target was at approximately the middle of the image field. The camera lens and extension tube set used resulted in an image field, measured to be about .56 in. high, which covered approximately the last 1/2 inch of the heated section of the flow channel. There is evidence from the heater element damages sometimes experienced during valid critical heat flux determinations that this size and location of the image field included the critical heat flux zone (see, for example, Figures VI-15, VI-16 and VI-18).

Examination and measurements of the motion picture data films were done with the Projector-Analyzer, shown in Figure IV-7, which was made for this job. The Analyzer was used together with a Bell and Howell Time and Motion Study Projector, Model 173. The apparatus was adjusted to give a definite enlargement ratio for the projected image on the glass back-projector screen (ten times actual size), thereby permitting reasonably accurate measurements of flow pattern dimensions to be made.

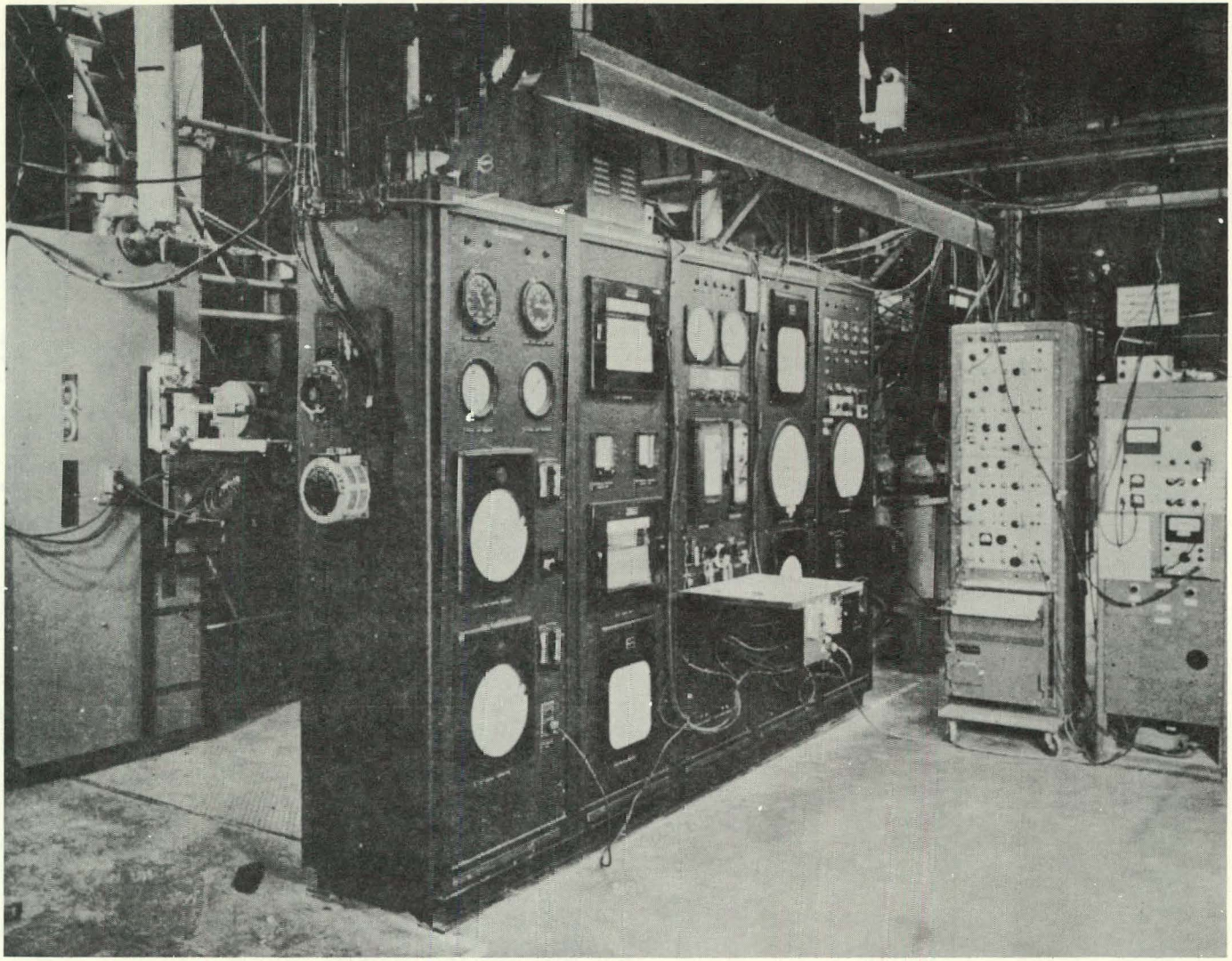

FIGURE IV-1

GENERAL VIEW OF EXPERIMENTAL EQUIPMENT SHOWING
ENCLOSED TEST SECTION IN LEFT BACKGROUND

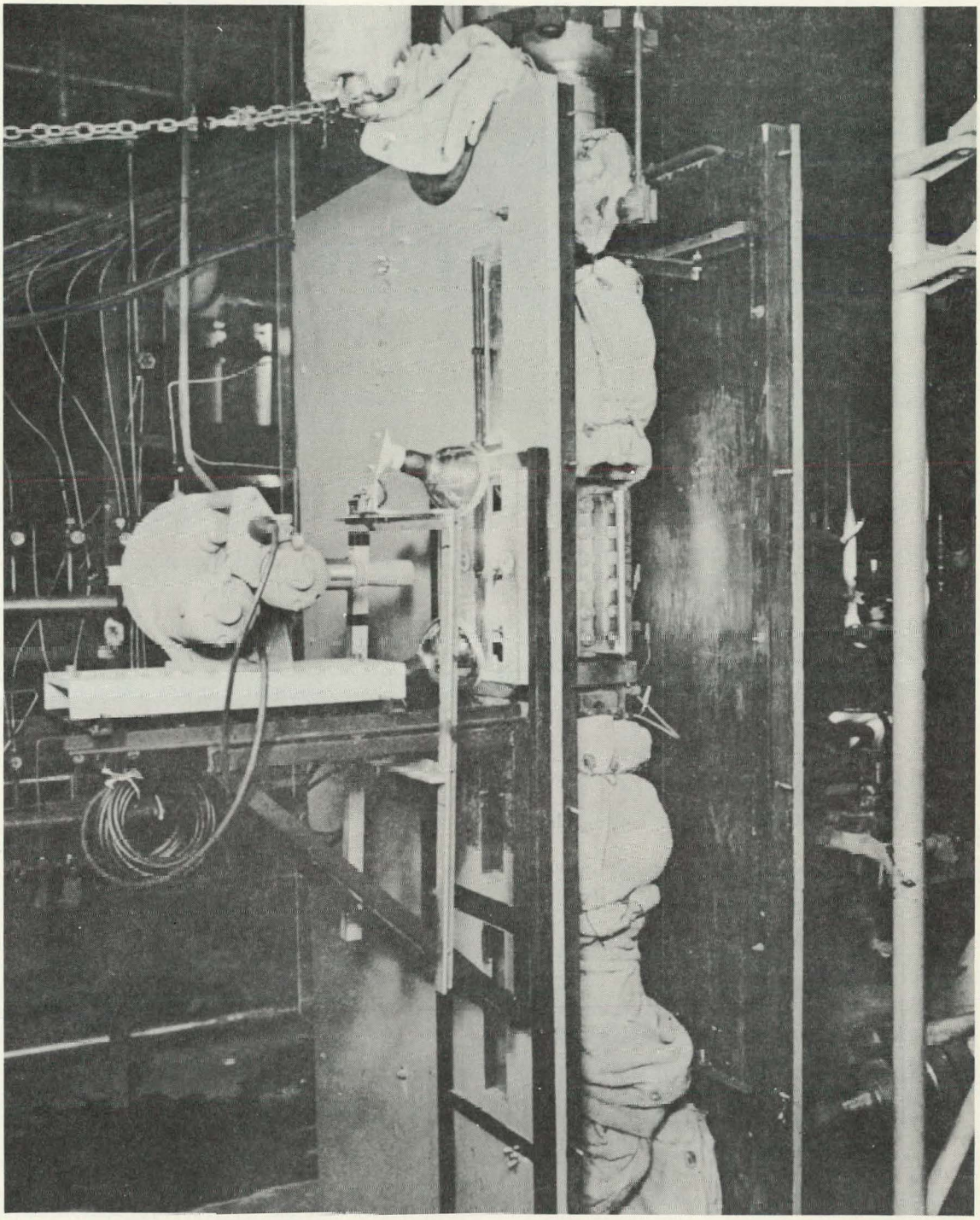

FIGURE IV-2

TEST SECTION INSTALLATION

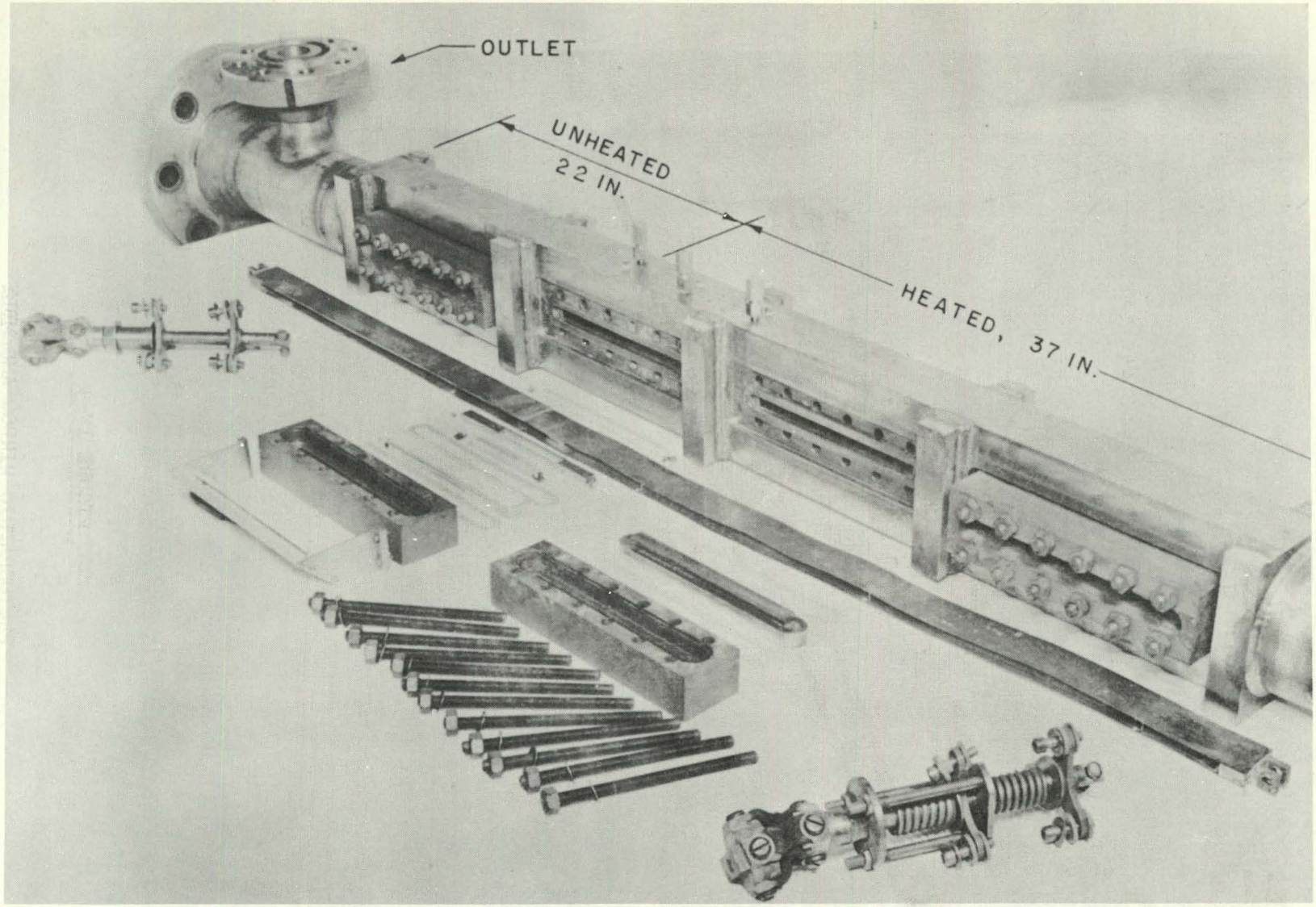


FIGURE IV-3

TEST SECTION ASSEMBLY

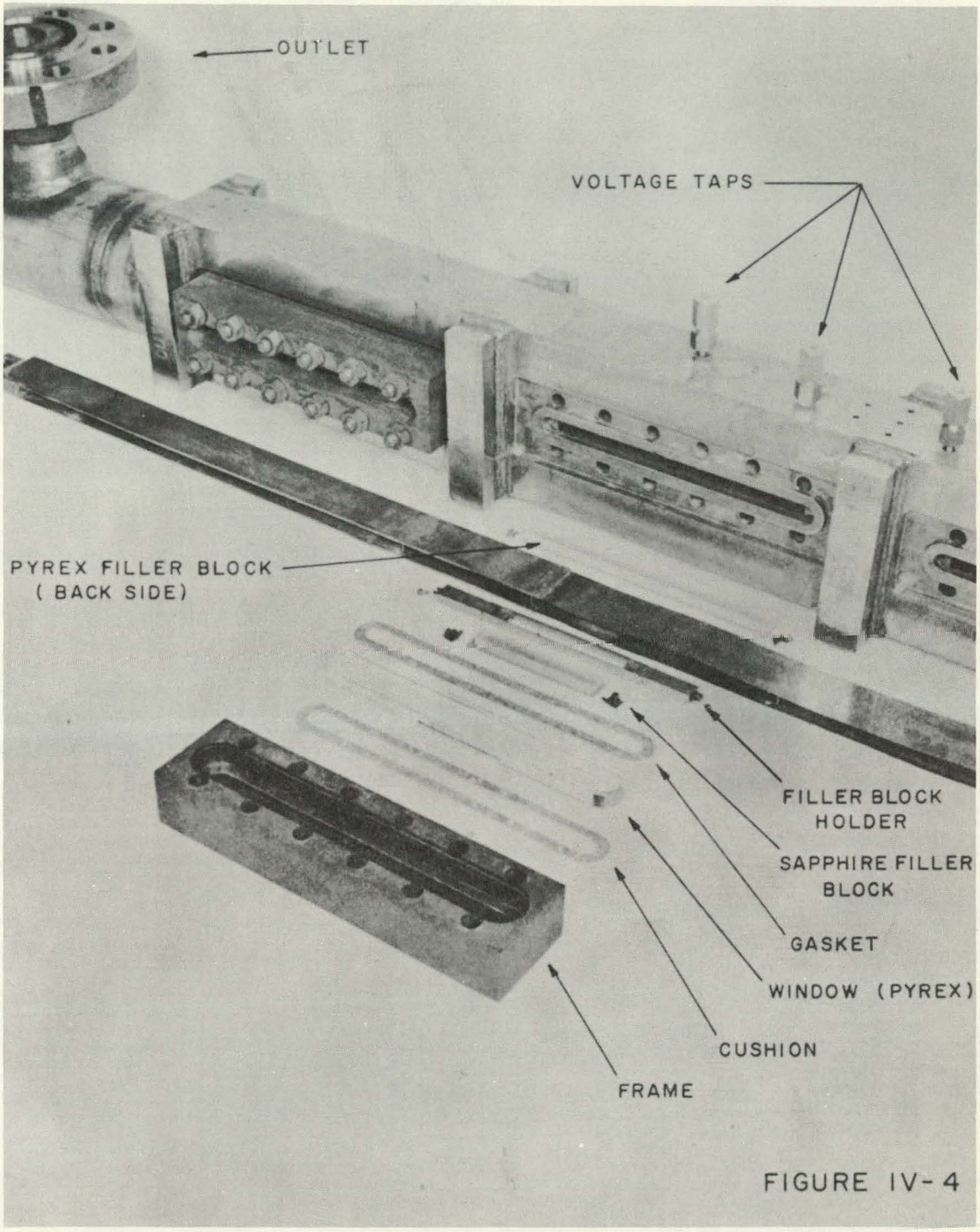


FIGURE IV-4

PHOTOGRAPHIC WINDOW ASSEMBLY

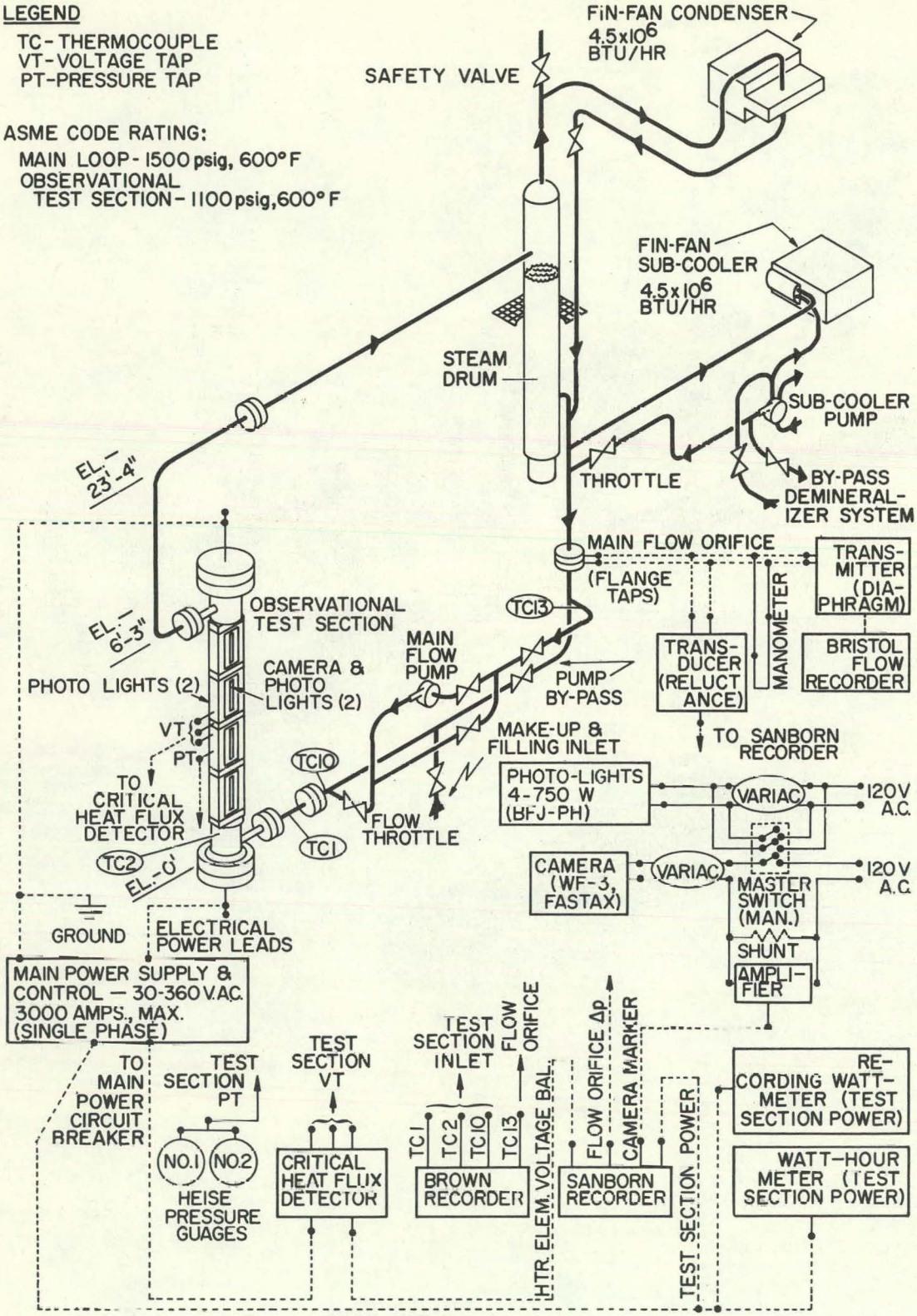


FIGURE IV-5

DIAGRAM OF FLOW LOOP AND INSTRUMENTATION

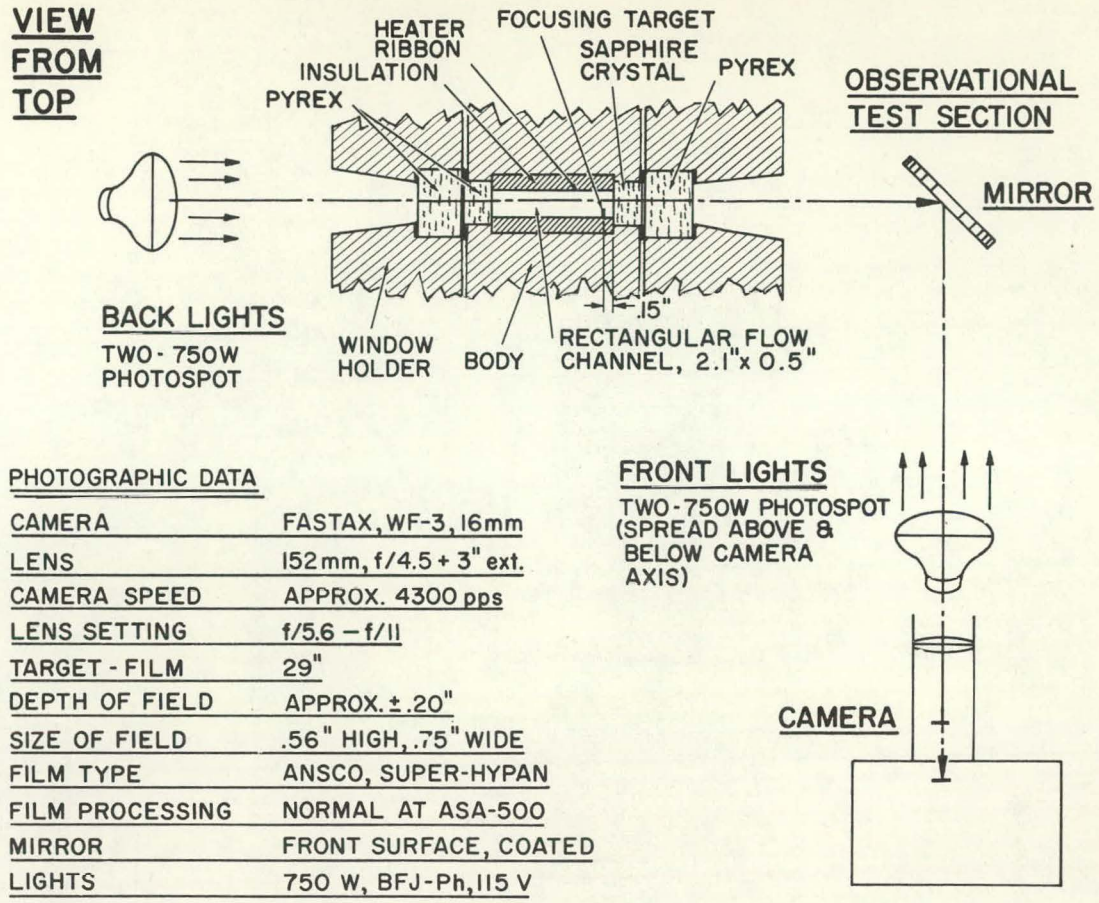


| PHOTOGRAPHIC DATA | |
|---|---|
| CAMERA | FASTAX, WF-3, 16mm |
| LENS | 152mm, f/4.5 + 3" ext. |
| CAMERA SPEED | APPROX. 4300 pps |
| LENS SETTING | f/5.6 – f/11 |
| TARGET - FILM | 29" |
| DEPTH OF FIELD | APPROX. ± .20" |
| SIZE OF FIELD | .56" HIGH, .75" WIDE |
| FILM TYPE | ANSCO, SUPER-HYPAN |
| FILM PROCESSING | NORMAL AT ASA-500 |
| MIRROR | FRONT SURFACE, COATED |
| LIGHTS | 750 W, BFJ-Ph, 115 V |

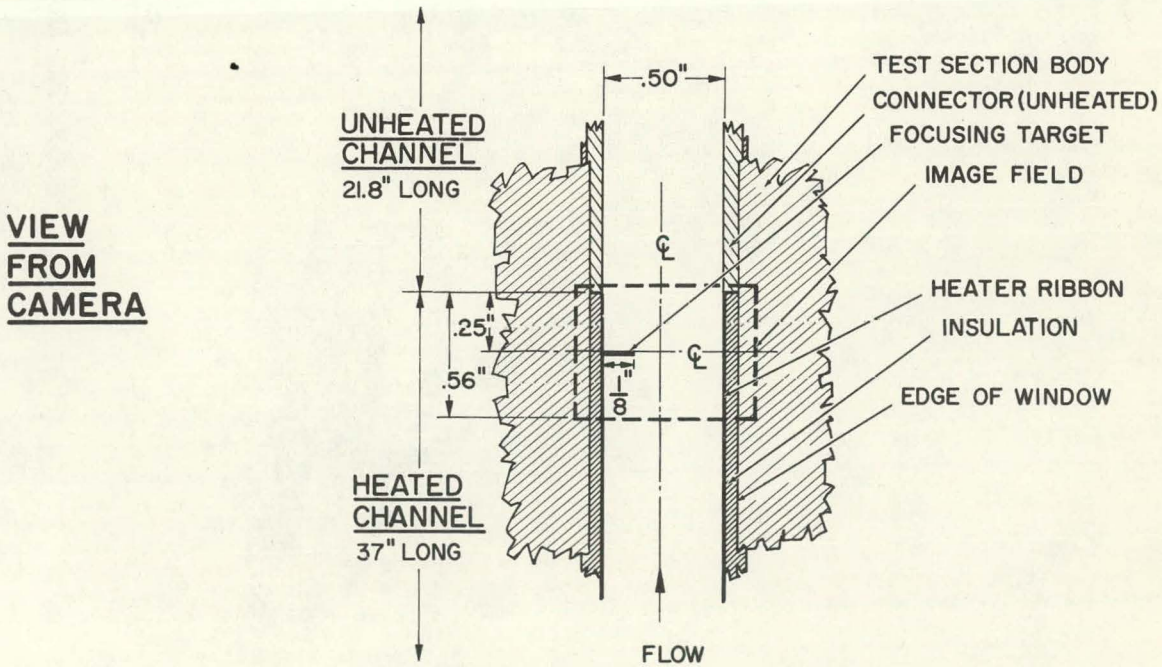


FIGURE IV-6

DIAGRAM OF PHOTOGRAPHIC SYSTEM

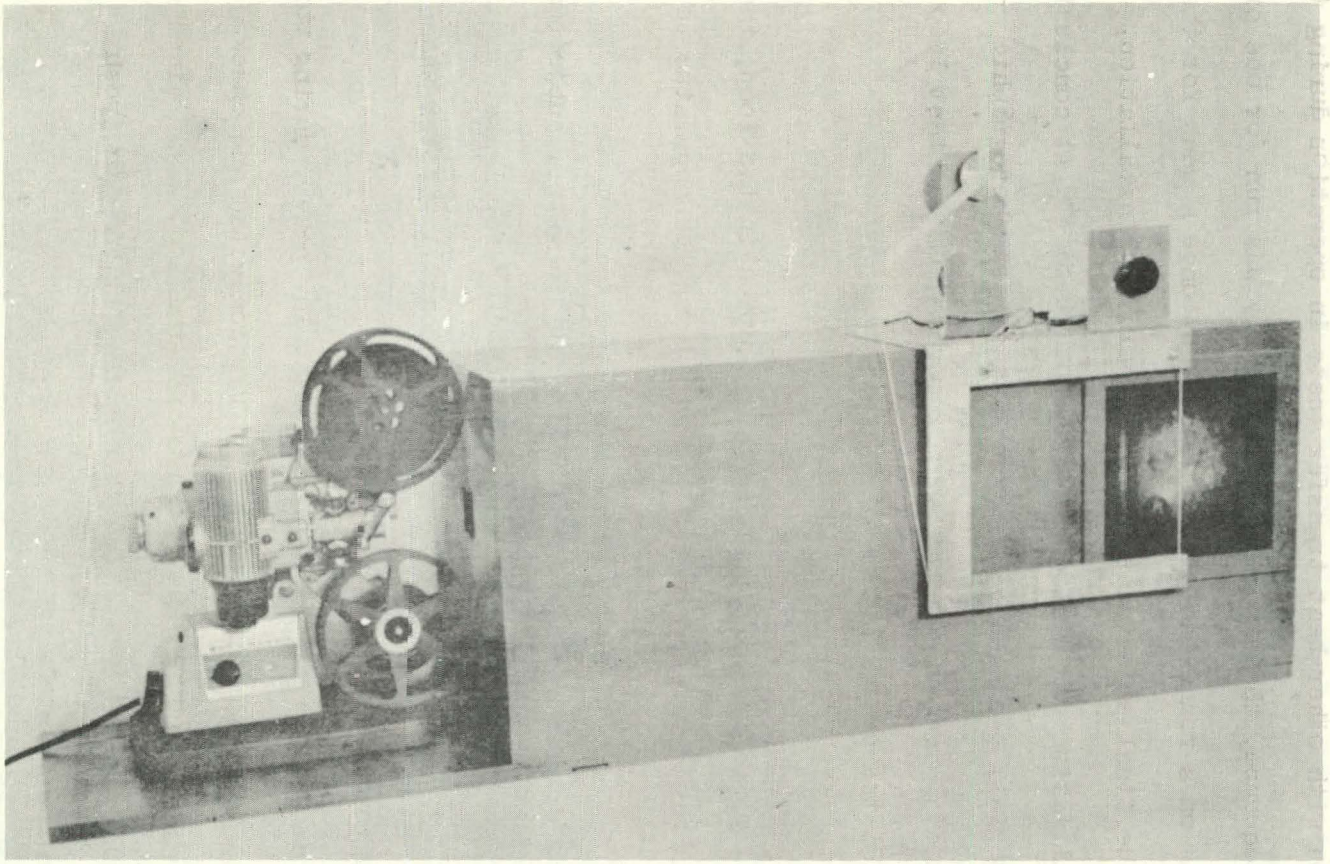

FIGURE IV-7

PROJECTOR-ANALYZER APPARATUS

## V. EXPERIMENTAL METHOD

Use of the heat transfer test facility for the experiment was in joint cooperation with other heat transfer tests in operation during the period. In consequence, the experiment typically was run for one or two day intervals on a round-the-clock basis about once a week for the four months of the final experimental phase, including installation, warmup and stabilization of the loop at test conditions.[1] At conclusion of each test interval, the test section and associated photographic equipment and special instrumentation were removed from the test loop to be prepared for the next interval of operation.

### Start-Up Procedure

After installation of the assembled test section in the loop, the following general procedure was carried out to bring the apparatus to approximate test conditions.

1. The loop was filled with fresh demineralized water, subjected to hydrostatic test at 1050 psig and checked for leaks.
2. The coolant circulation pump was started and low power was applied (65 KW).
3. After one hour (minimum) circulation at low power, during which the balance of the instrumentation was connected and checked out, the flow and power were shut off, the loop was drained completely at the bottom and then again filled with fresh demineralized water.

---

[1] Installation of the test equipment and operation of the test loop was done by the technician staff of the heat transfer test facility under Mr. C. D. Endsley, Manager of Test Operations, with the author in attendance to direct each critical heat flux determination and to do the photography.

4. The loop was again pressurized, the coolant circulation pump was started, low power was applied, and the loop was vented at the top to maintain pressure between 900 and 1000 psig and to release dissolved gases coming out of solution.
5. Power was slowly raised as the loop warmed. Towards the end of the warm-up period, the flow, pressure and inlet sub-cooling were trimmed to approximately the values to be used for the first experimental run and the power was held to a value which caused the test section heat flux to be about one-half or less of the expected critical heat flux level.
6. After the warm-up period (about 4 hours), flow, pressure and inlet sub-cooling were adjusted to the values to be used for the experimental run. Loop temperatures were allowed to stabilize before the run was started.

Classification of Runs

Three general types of experimental runs were made: camera operation only to photograph flow patterns; critical heat flux determinations only; combined critical heat flux determination and camera operation to photograph flow patterns associated with the critical heat flux condition. Individual runs were further categorized according to the type of heater element used (channel wall spacing and number of heated sides)[2] and channel mass velocity.

The numbered curves in Figure V-1 are approximate plots of the operating characteristics of the system in terms of the test section power and heat flux as functions of steam quality X at exit from the

---

[2] Variation of heater ribbon thickness between runs (.006 in. and .010 in. thickness) formed a sub-category.

heated section for various test section inlet sub-coolings $\Delta h_s$, as calculated from an energy balance for one-dimensional flow in thermodynamic equilibrium. The sub-coolings span approximately the ranges used for each group of runs. The arrows represent approximately the loci of the critical heat flux conditions found for each group and, hence, are approximate plots of the terminal conditions of the runs.

Critical Heat Flux Determinations

As elaborated upon further in Appendix B, determination of the critical heat flux condition was defined, for the purpose of taking data, in terms of the Detector setting to trip the power upon deflection of the Detector signal recorder pen 6 mm to the right from the null balance position, signifying an abrupt temperature rise or fluctuation over the last 4-1/4 inches of the heated section.[3] As discussed in Section II, the critical heat flux phenomenon is more correctly defined as the condition of incipient local temperature variation, either as a fluctuation or an abrupt rise with time. The operating definition used here for the taking of data was necessary with the equipment used, in order to be sure that the determination was not spurious, due to unrelated flow or electrical transients. Examination of the recorder traces shows that for all the valid critical heat flux determinations the heat flux which caused 6 mm deflection of the recorder pen and power trip did not exceed the heat flux at which the first indication of change of the heater element temperature could be discerned by more than 5 to 6 per cent. In most cases, especially at the lower steam qualities, the differences in these heat flux levels were about 1 or 2

[3] Estimates of the local heater element temperature rises corresponding to deflections of the recorder pen are plotted in Fig. B-3.

per cent. (See, for example, Figures VI-3 and VI-7 through VI-14)

Each new critical heat flux determination was approached by first stabilizing the system at the pressure (1000 psia), inlet sub-cooling and flow rate prescribed for the run, with the power adjusted to make the test section heat flux about one-half of the expected critical value. The power was then slowly raised to the critical heat flux point, with occasional pauses as required to allow the system temperatures to stabilize, while the pressure, inlet sub-cooling and flow rate were maintained almost exactly constant.[4] At the instant of power trip or, as was sometimes done, manual reduction of power from the critical heat flux level (see, for example, Figure VI-8), a signal was given and all relevant data was recorded on standard data sheets immediately.

Photography

For runs during which only photography of the flow patterns was to be done, at heat fluxes substantially less than the critical heat flux, it was necessary only to stabilize the system at the prescribed conditions preparatory to operating the camera.

For runs during which the camera was operated at heat flux levels near or at the critical heat flux level the same general procedure was followed as for the critical heat flux determinations. This type of run was usually made as a nearly exact duplication of a previous critical heat flux run. The character of the recorder trace of the Critical Heat Flux Detector output signal in comparison with the trace obtained during a previous critical heat flux run at very nearly the

[4] The power control regulator permits increments of steady-state power increase of about 1/2 to 2 per cent, minimum, depending on the power level. During the final portion of each run, an operator was stationed at the flow throttle to manually adjust it as required in order to maintain constant flow, based on the orifice manometer readings.

same operating conditions was used as the main basis for judgment of when to start the camera. Typically, a motion picture of the channel flow pattern would be taken at the heat flux level at which the first indication of change of the heater element temperature was observed (see, for example, Figure VI-3). Next, the heat flux level would be raised slightly until the fluctuations of the Detector output signal indicated the heat flux was very nearly at the power trip level, a motion picture of the channel flow pattern would again be made, and the heat flux level would then be reduced slightly (see, for example, Figures VI-2, VI-4, VI-6 and VI-8). Depending on the character of the Detector output signal trace for the particular run, an attempt would sometimes next be made to synchronize the camera with the power trip at the critical heat flux condition (see, for example, Figures VI-10 and VI-11).

The camera alignment and focus on the heater element focusing target were checked through the camera eyepiece using special Fastax focusing film, as part of the camera loading procedure for each run. In order that a clear view of the focusing target could be seen, the test section power was momentarily shut off and the photographic lights were placed on dim for the focusing check.

A mark identifying the camera run was scribed in the emulsion at the beginning and end of each negative exposed. The edited sequences which have been selected as data for the experiment include these field marks at their ends.

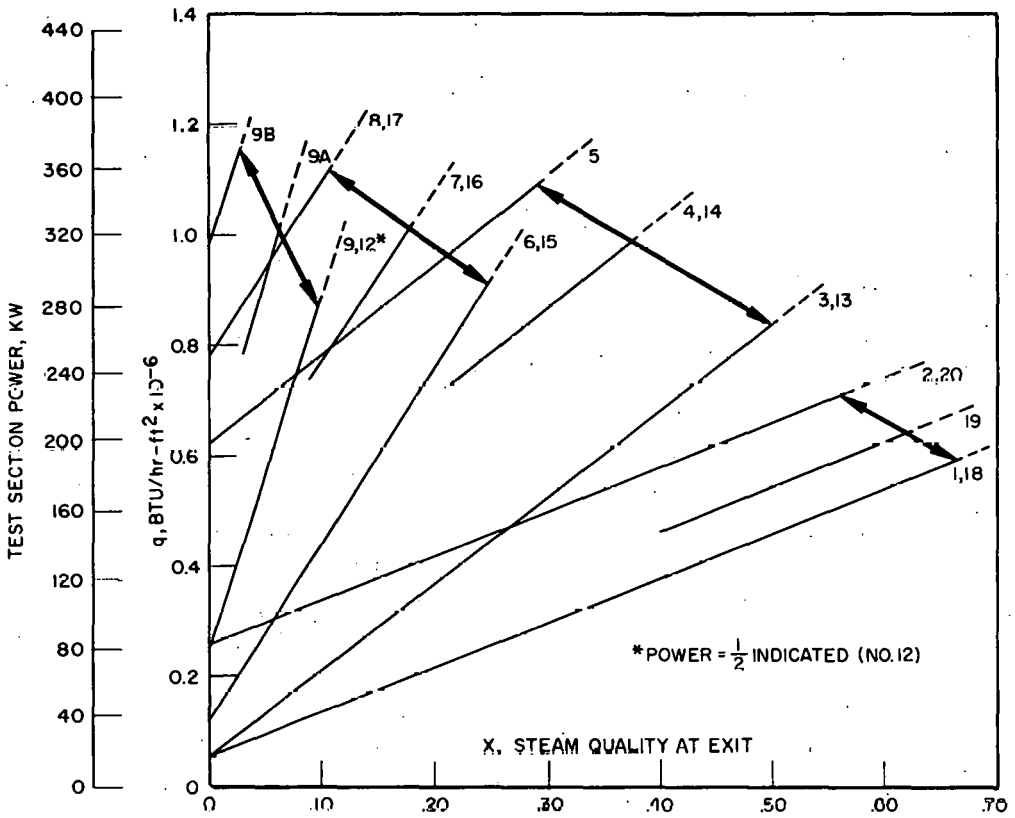


| SET NO. | HEATER ELEMENT | G, lb/sec-ft² | $\Delta h_s$, BTU/lb |
|---|---|---|---|
| 1 | .50 IN.-2 | 50 | 75 |
| 2 | .50 IN.-2 | 50 | 215 |
| 3 | .50 IN.-2 | 100 | 30 |
| 4 | .50 IN.-2 | 100 | 160 |
| 5 | .50 IN.-2 | 100 | 230 |
| 6 | .50 IN.-2 | 200 | 30 |
| 7 | .50 IN.-2 | 200 | 90 |
| 8 | .50 IN.-2 | 200 | 160 |
| 9 | .50 IN.-2 | 400 | 25 |
| 9A | .50 IN.-2 | 400 | 60 |
| 9B | .50 IN.-2 | 400 | 100 |
| 12* | .50 IN.-1 | 200 | 25 |
| 13 | .25 IN.-2 | 200 | 30 |
| 14 | .25 IN.-2 | 200 | 160 |
| 15 | .25 IN.-2 | 400 | 30 |
| 16 | .25 IN.-2 | 400 | 90 |
| 17 | .25 IN.-2 | 400 | 160 |
| 18 | .25 IN.-2 | 100 | 75 |
| 19 | .25 IN.-2 | 100 | 130 |
| 20 | .25 IN.-2 | 100 | 215 |

APPROXIMATE LOCUS OF $q_c(X)$

FIGURE V-1

GRAPH OF THE TEST SECTION OPERATING CHARACTERISTICS SHOWING THE APPROXIMATE RANGE OF CONDITIONS EXPLORED

Run settings are grouped according to:

| | |
|---|---|
| Heater Element Spacing | .50, .25 in. |
| Number of Heated Sides | 2, 1 |
| Mass Velocity | 50, 100, 200, 400 lbs/sec-ft$^2$ |

The first one or two digits of each run number designation in Appendix C matches the number of the corresponding run setting in Figure V-1.

The locus of critical heat fluxes for each group of run settings was found by varying inlet sub-cooling $\Delta h_s$ over the ranges indicated while holding mass velocity constant.

## VI. EXPERIMENTAL RESULTS

The experimental results are 89 critical heat flux determinations, of which 80 are selected as valid, and 33 selected high speed motion picture data films of boiling water flow patterns. The critical heat flux data are tabulated in Appendix C and are plotted in Figure VI-1. Operating conditions for the selected data films are tabulated in Appendix D together with notes describing observed characteristics of the flow patterns.

### Critical Heat Flux Determinations

Judgment of validity of the critical heat flux determinations was in each case based on there being evidence from the Critical Heat Flux Detector output signal that the heater element had experienced an abrupt rise or substantial fluctuation of its surface temperature in the 4-1/4 inch long section between Detector voltage taps at the outlet end of the heated section (see Appendix C). Several representative recorder traces are reproduced in Figures VI-2 through VI-14, which show the nature of the variations in the Critical Heat Flux Detector output signal, the test section coolant flow, sequencing of the motion pictures, and the history of the heat flux changes during operation to the critical heat flux condition. Appendix B includes an idealized analysis of the corresponding heater element temperature changes associated with the Detector output signal (Figure B-3). The codings designating the types of runs are defined in Appendix C.

Determinations for which there was evidence of overheating in the upstream parts of the heater element, as indicated either by heater element damage there or by the nature of the Detector output signal, were rejected as invalid. Examples of rejected runs are given in

Figures VI-4 and VI-5, which show Detector pen deflections to the left, indicating temperature rises upstream from the heated section exit.

Typical zones of high temperature rise can be seen on the heater ribbons in Figures VI-15 through VI-18. Stains and blemishes on the back sides of the ribbons are from the insulated backing strips adhering to the ribbons during operation. The heater elements in Figures VI-15 and VI-18 experienced almost identical severances of both heater ribbons within 1/4 inch of the end of the heated section, at steam qualities of 51 per cent and 75 per cent, respectively. Two small local patches of overheating can be seen on the single-ribbon element in Figure VI-16, which occurred during critical heat flux conditions at an exit steam quality of about 14 per cent. Figure VI-17 shows a photograph of the upstream section of a heater element which experienced the critical heat flux condition and consequent heater ribbon damage about 22 inches upstream from the exit of the heated section (rejected run 3A-2). The two long sections of overheated metal extending downstream from the point of severance on one of the ribbons in Figure VI-17 were caused by local flow obstructions resulting from the severed section of the other ribbon moving across the channel and blocking flow at the surface. Damages to other heater elements during valid critical heat flux determinations were very similar to those in Figures VI-15 and VI-18 (runs 3T-6, 3TRR-5 and 7R-1, in Appendix C).

The character of the traces of the Detector output signal at onset of the critical heat flux condition show a definite general similarity throughout the entire range of steam qualities, mass velocities and heater element geometries (Figures VI-3 and VI-7 through VI-14). Typically, as the heat flux was slowly raised to the critical condition,

the first indication of abrupt change of the heater element temperature occurred at heat fluxes about 94 to 99 per cent of the heat flux at which the Detector would trip the power or physical damage to the heater ribbons would occur. At this point the recorded Detector output signal would commence pulsing slightly. As the heat flux was raised further, a definite fluctuation or oscillation would usually develop with a characteristic frequency of about 2 to 5 cycles per second and a minimum deflection about equal to or slightly above the previous steady-state level. Further increases in heat flux would increase the amplitude of fluctuation to the power trip point (6 mm deflection of the recorder pen to the right) or would cause an abrupt transient rise of the output signal through the power trip point, depending on the levels of steam quality and heat flux. Occasionally the Detector response was too slow to trip the power in time to prevent damage to the heater element (see, for example, Figure VI-9 for run 7R-1). At the lower steam qualities and higher critical heat flux levels the span of heat fluxes between initial indication of onset of critical conditions and the power trip point tended to be least and the Detector output signal tended to rise more abruptly than at the higher steam qualities and lesser critical heat flux levels (compare, for example, Figure VI-10 with Figures VI-3 or VI-14).

At the lower steam qualities (less than about 50 per cent) and correspondingly higher critical heat flux levels there appears to be little or no detectable difference between the heat flux level to cause a power trip and the corresponding level which would cause damage to the element at a particular critical heat flux condition (compare repeat data points in Figure VI-1). For run 18RR-1, the power trip

component of the Detector was shut off and the heat flux was raised slowly above the level for which the Detector output signal would normally trip the power. Figures VI-14 a, b, c show the record of the run up to near the heat flux level at which the heater ribbons failed. The damaged heater element used is shown in Figure VI-18. The heat flux level at which the element failed was about 11 per cent above the normal power "trip" level at a corresponding steam quality of .751. This run is the highest steam quality run made during the experiment. The change in the character of the Detector output signal during the run beyond the "trip" point appears to be principally an increase in mean level as the heat flux was raised, with only little change in frequency and amplitude of oscillation around the mean level. Speed-up of the chart during the last part of the run reveals irregular harmonics in the signal output at roughly 8 cps.

The recorder traces indicate no detectable variation of coolant flow, as measured at the main flow orifice, associated with onset of the critical heat flux condition.

The pattern of the Detector output signal for a particular set of conditions appears to be approximately reproducible and it appears to have little hysteresis during reductions of heat flux from critical conditions (see, for example, Figures VI-2, VI-4 and VI-8).

Examination of the plotted data in Figure VI-1 and the tabulation in Appendix C indicates very close repeatibility of the critical heat fluxes at repeat conditions with the same heater element. Several of the points were repeated with a deviation of less than 1 per cent of the critical heat flux. The average deviation from the means for repeat points over the range of the experiment is less than 2 per cent.

Steam qualities at exit from the heated section were calculated for each critical heat flux condition using the following test section energy balance together with measured electrical powers, corrected for external losses, flow rates, and inlet fluid temperature.

$$X_c = \frac{1}{h_{fg}} \left[ \frac{Q_c}{W} - \Delta h_{s_{inlet}} \right] \qquad (1)$$

where $X_c$ = exit steam quality at the critical heat flux condition.

$Q_c$ = test section power at the critical heat flux condition

$W$ = test section flow rate

$\Delta h_{s_{inlet}}$ = specific enthalpy of sub-cooling at the test section inlet.

$h_{fg}$ = specific enthalpy of vaporization

As mentioned in Section IV, the measurements are subject to the following estimated maximum errors: $Q_c$, less than 1-1/2 per cent; $W$, less than 2 per cent; $\Delta h_{s_{inlet}}$, less than 5 Btu/lb. Using the method of Kline and McClintock (ref. (107)), the corresponding maximum errors in the critical steam quality ($\Delta X_c$) are estimated to be as listed in Table VI-1, to the same confidence level as the foregoing errors.

TABLE VI-1

| Run No. | $q_c$, $\frac{10^6 \text{ Btu}}{\text{hr-ft}^2}$ | $G$, $\frac{\text{lbs.}}{\text{sec-ft}^2}$ | $\Delta h_{s,\text{inlet}}$, Btu/lb. | $X_c$ | Max. error in $X_c$, $(\Delta X_c)$ |
|---|---|---|---|---|---|
| 1-3 | .591 | 50.1 | 67.0 | .650 | .020 |
| 2-5 | .698 | 50.1 | 216.0 | .556 | .023 |
| 3-5 | .898 | 98.6 | 45.5 | .511 | .016 |
| 4R-1 | .979 | 99.4 | 161.0 | .381 | .017 |
| 6RR-1 | .916 | 199 | 16.0 | .269 | .011 |
| 8-2 | 1.089 | 199 | 166.4 | .095 | .012 |
| 9-1 | .832 | 397 | 19.0 | .104 | .008 |
| 9B-1 | 1.136 | 397 | 97.3 | .033 | .009 |

Maximum error in determination of the critical heat fluxes is estimated to be less than 5 per cent, based on the estimated maximum error in the power measurements, heater element fabrication tolerances and an assumed maximum variation in heater ribbon thickness due to making of the silver-solder step-joint at the end of the heated section.[1]

Motion Pictures of Flow Patterns

Operating conditions for each of the thirty-three edited high speed motion picture sequences, together with notes describing the salient features of the flow patterns observed in each case, are tabulated in Appendix D. The films are made up as a set in five data reels plus a summary reel. In all cases the camera was focused sharply on the 1/8-inch long, .020-inch diameter wire focusing target attached normal to one heater ribbon .25 inch down the end of the heated section and located about .15 inch inside the channel from the window. The view seen is approximately the last 1/2 inch of the heated section, covering the critical heat flux zone. Nominal operating pressure was 1000 psia and the flow was vertically upward. Enlargements of selected frames from the data reels are presented in Figures VI-19 through VI-23. For each of these the channel width is .50 inch and the apparent magnification is approximately four times real size.

Since the liquid water, water vapor and window material are all almost equally transparent and colorless as far as the eye can discern,

---

[1] There is evidence that some of the thinner ribbon heater elements (.006 in.) may have been subject to a greater variation of heat flux than this allowance. (See, for example, the data for curves 5, 9, and 10 in Figure VI-1. Also refer to footnote 6 in Section IX.)

observed images in the motion picture films are mainly optical effects resulting from different degrees of light reflection and transmission at the interfaces. Because of this, observations tend to be subjective, and, hence, subject to error. An effort was made to minimize errors by having other observers make independent examinations of the films[2] and by considering all aspects of the observed image to arrive at a coherent and uncontradictory description of the pattern seen.

Discrete small bubbles in liquid were virtually certain of correct interpretation because of their regular spherical shape and their general similarity to known bubbles observed in the sub-cooled nucleate boiling runs. With this fact in mind, the fluid immediately adjacent to such a bubble is concluded to be liquid. Hence, any nearby interfaces, as marked by either luminescences due to local reflections from the front lamps or dark shadows due to local interruption of the light coming through the channel from the rear lamps, could reasonably be interpreted as indicating a boundary of continuous vapor adjacent to the liquid containing the observed bubble. This general line of reasoning was followed, for example, in deducing that the arrangement of the phases for several of the sequences involved a wavy liquid film covering the inside face of the window and extending around the corners of the channel to include the edges of the heater ribbons and at least a portion of their surfaces (shadow of the heater ribbon surface film evident in profile), with irregular streamers of vapor issuing from the heater ribbon edges into the film, and probably continuous vapor

---

[2] The author is grateful to Dr. S. Levy of General Electric Company and Professor A. L. London of Stanford University for their careful reviews of all the selected data films.

containing small droplets or conglomerates of liquid, or an emulsion of liquid and vapor, flowing in the core of the channel.[3]

Distinction between bubbles flowing inside the channel and those which occasionally appeared in the .03 inch thick liquid filled space between the filler block and the outer pressure-bearing window could always readily be made by noting their apparent position relative to the heater ribbon edges and focusing target and by noting their direction and velocity of motion relative to the channel flow. Observed irregularities in the motion of the external bubbles were useful indications of corresponding local pressure variations in the flow channel.

Evidence of "slugging" is apparent in some of the sequences, as indicated by almost periodic variations of the general flow pattern and intensity of light transmitted from the rear.[4]

---

[3] See, for example, the film sequences in Reel I; sequences 3S-4 through 3R-3 in Reel II; sequences 6R-1 through 8-3 in Reel III; sequences 9R-1 through 9B-2 in Reel IV; and sequence 12-2 in Reel V.

[4] See, for example, sequences 2-1, 1-1 and 2-2 in Reel I; sequences 3S-3, 3S-4, 3R-1 and 4-5-a in Reel II; sequence 6R-1 in Reel III; and sequence 18S-1 in Reel V.

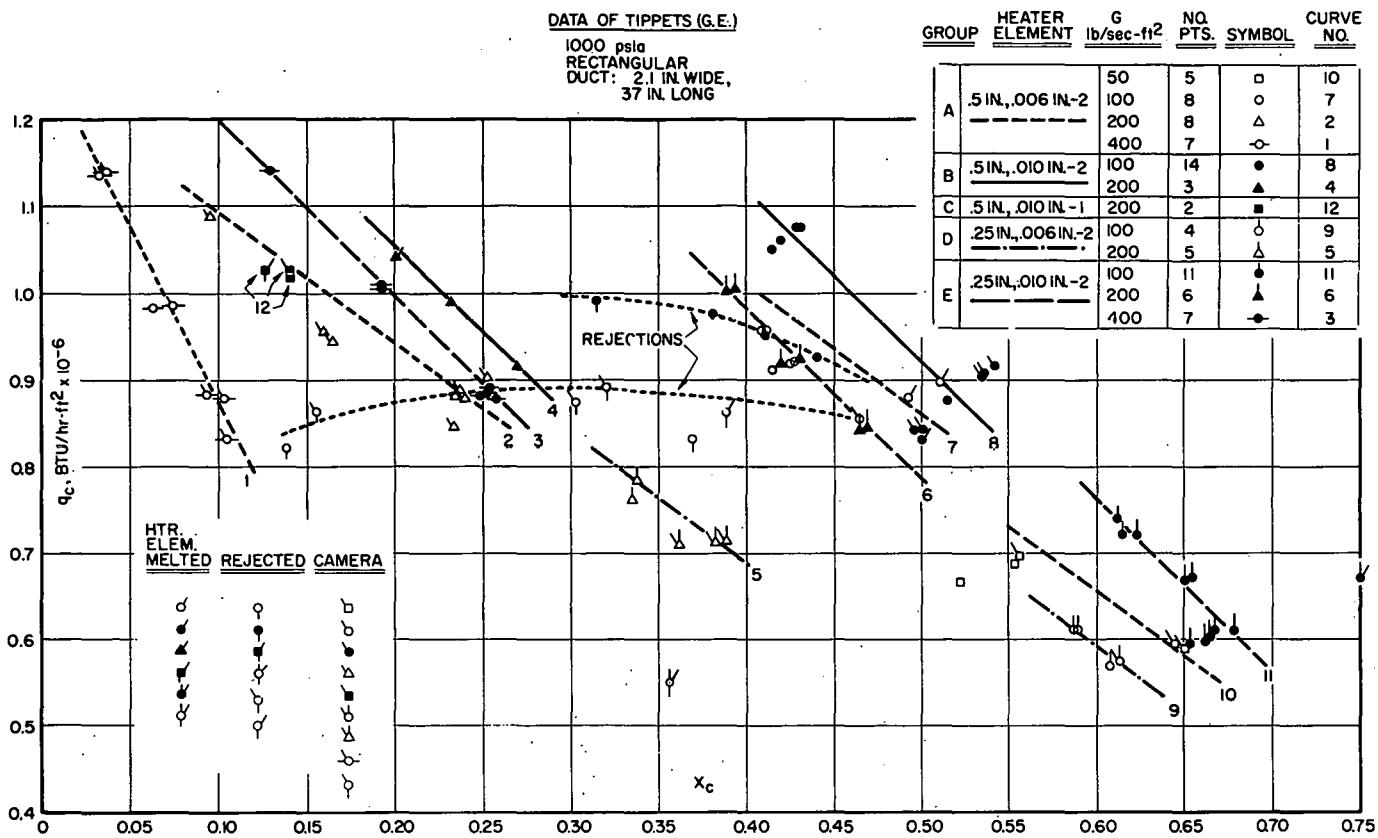


FIGURE VI-1

GRAPH OF CRITICAL HEAT FLUX DATA

1. Points for which the camera was operated simultaneously, points for which the heater element melted, and rejected points are separately coded.

2. Variation of $q_c$ with mass velocity can be seen by comparing curves 1, 2, 7, and 10; curves 4 and 8; curves 5 and 9; and curves 3, 6, and 11.

3. Variation of $q_c$ with hydraulic diameter (.46 in. to .81 in., corresponding to .25 in. and .50 in. spacing) can be seen by comparing curves 2 and 5; curves 7 and 9; curves 4 and 6; and curves 8 and 11.

4. Variation of $q_c$ with heater ribbon thickness (.006 in. and .010 in.) can be seen by comparing curves 2 with 4 and 7 with 8, for .50 in. spacing; and curves 5 with 6 and 9 with 11, for .25 in. spacing.

5. The effect of having one side only heated compared with the two sides heated can be seen by comparing points number 12 (Group C) with curve 4.

6. The trends of the rejected points, shown by dotted lines, appear to possess maxima of $q_c$ with respect to $X_c$.

7. Scatter of some of the data along particular operating characteristics can be discerned, corresponding to the plots in Figure V-1 (e.g., some of the data for curves 7, 8, 10, 11).

FIGURE VI-2

RECORDER CHART SHOWING OPERATING CONDITIONS FOR FILM NO. 1-2
NEAR CRITICAL HEAT FLUX "TRIP" LEVEL

Type Run* : SSC-O

Type 1A Heater Element: .50 in., .006 in. -2

The trace of the Detector signal indicates little hysteresis of the heater element temperature fluctuations with small manual reduction of heat flux from near the critical heat flux "trip" point.

---

* Codings designating the types of runs are defined in Appendix C.

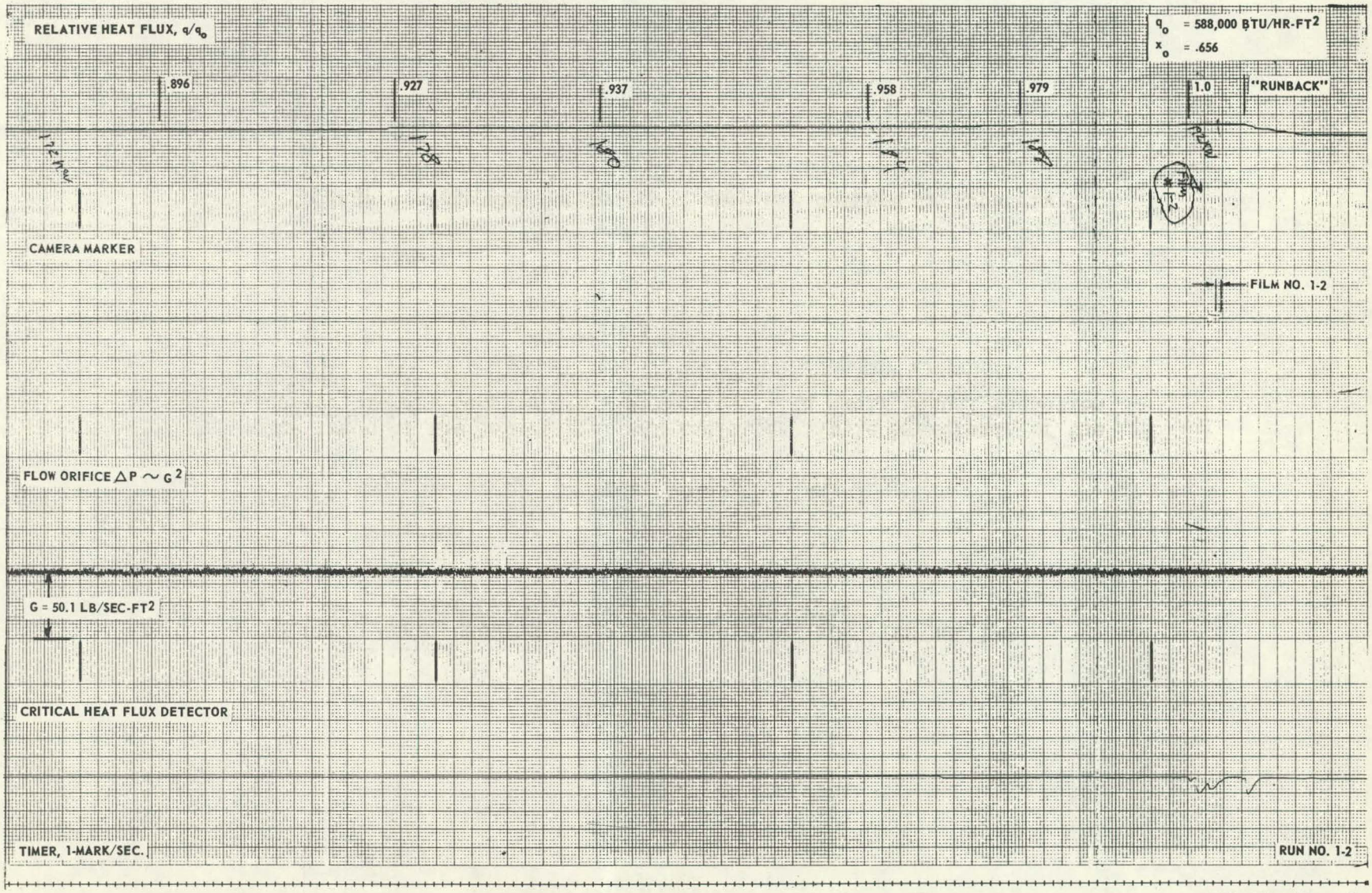
RELATIVE HEAT FLUX, q/q0
q0 = 588,000 BTU/HR-FT2
x0 = .656
.896
.927
.937
.958
.979
1.0
"RUNBACK"
CAMERA MARKER
FILM NO. 1-2
FLOW ORIFICE ΔP ~ G2
G = 50.1 LB/SEC-FT2
CRITICAL HEAT FLUX DETECTOR
TIMER, 1-MARK/SEC.
RUN NO. 1-2

FIGURE VI - 2

FIGURE VI-3

RECORDER CHART SHOWING OPERATING CONDITIONS FOR CRITICAL HEAT FLUX DETERMINATION NO. 1-4 AND FILM NO. 1-4*

Type Run : BOC-T

Type 1A Heater Element: .50 in., .006 in. -2

There were slight fluctuations of the Detector signal as the "trip" point was approached and an abrupt rise of the signal to the right causing the "trip," indicating heater element temperature rise at the outlet end.

---

* Film No. 1-4 discarded due to inadequate photographic quality (not included in tabulation in Appendix D).

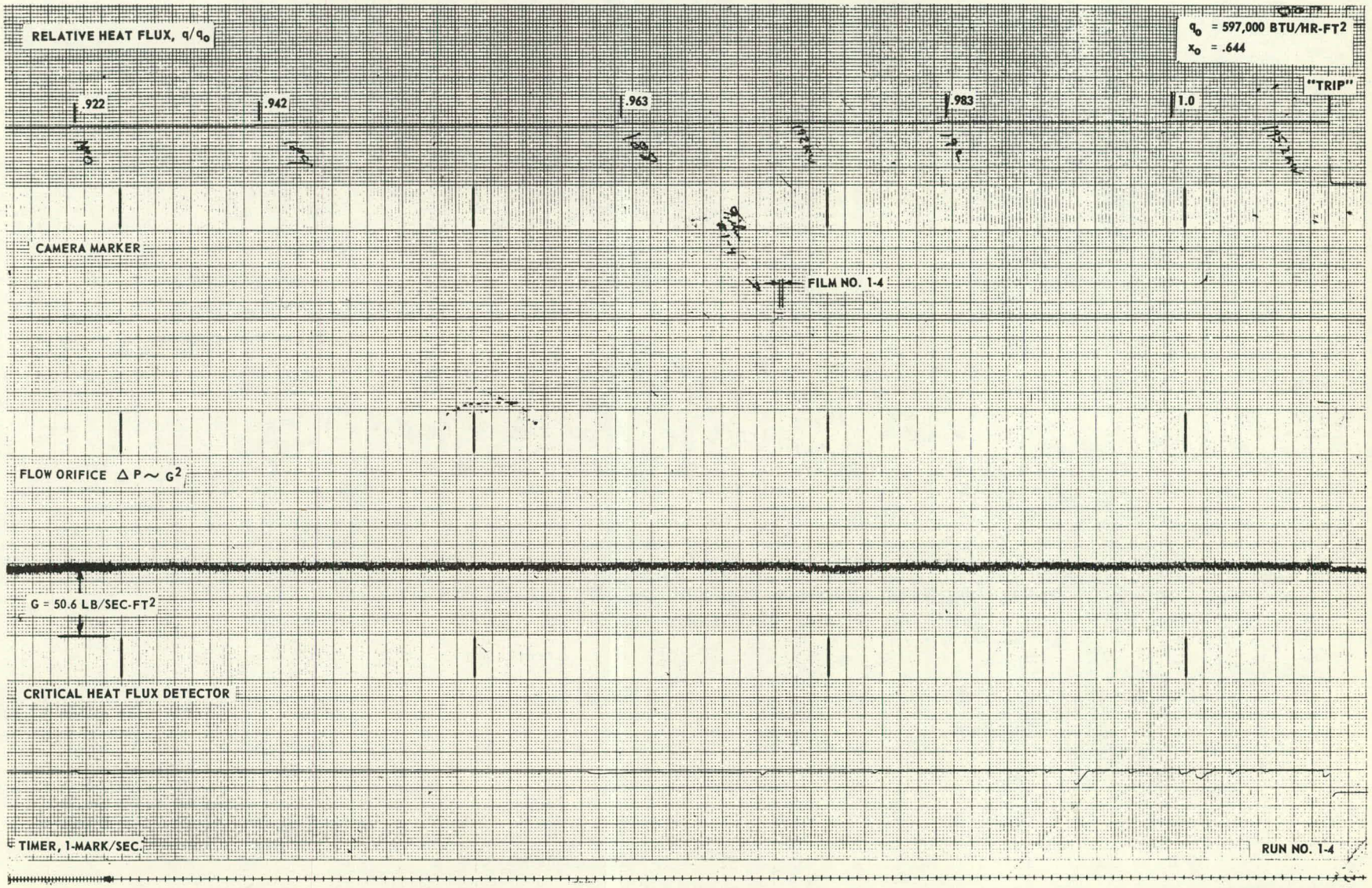
RELATIVE HEAT FLUX, q/q₀
q₀ = 597,000 BTU/HR-FT²
x₀ = .644
.922
.942
.963
.983
1.0
"TRIP"
CAMERA MARKER
FILM NO. 1-4
FLOW ORIFICE ΔP ~ G²
G = 50.6 LB/SEC-FT²
CRITICAL HEAT FLUX DETECTOR
TIMER, 1-MARK/SEC.
RUN NO. 1-4

FIGURE VI-3

## FIGURE VI-4

RECORDER CHART SHOWING OPERATING CONDITIONS DURING CRITICAL HEAT FLUX CONDITION UPSTREAM (REJECTED RUN NO. 4-4) AND FILM NO. 4-5-a

Type Run : BOC-S-R

Type 1A Heater Element: .50 in., .006 in. -2

Deflection of the Detector signal trace to the left to near the "trip" level indicates heater element temperature rise upstream from the outlet end.

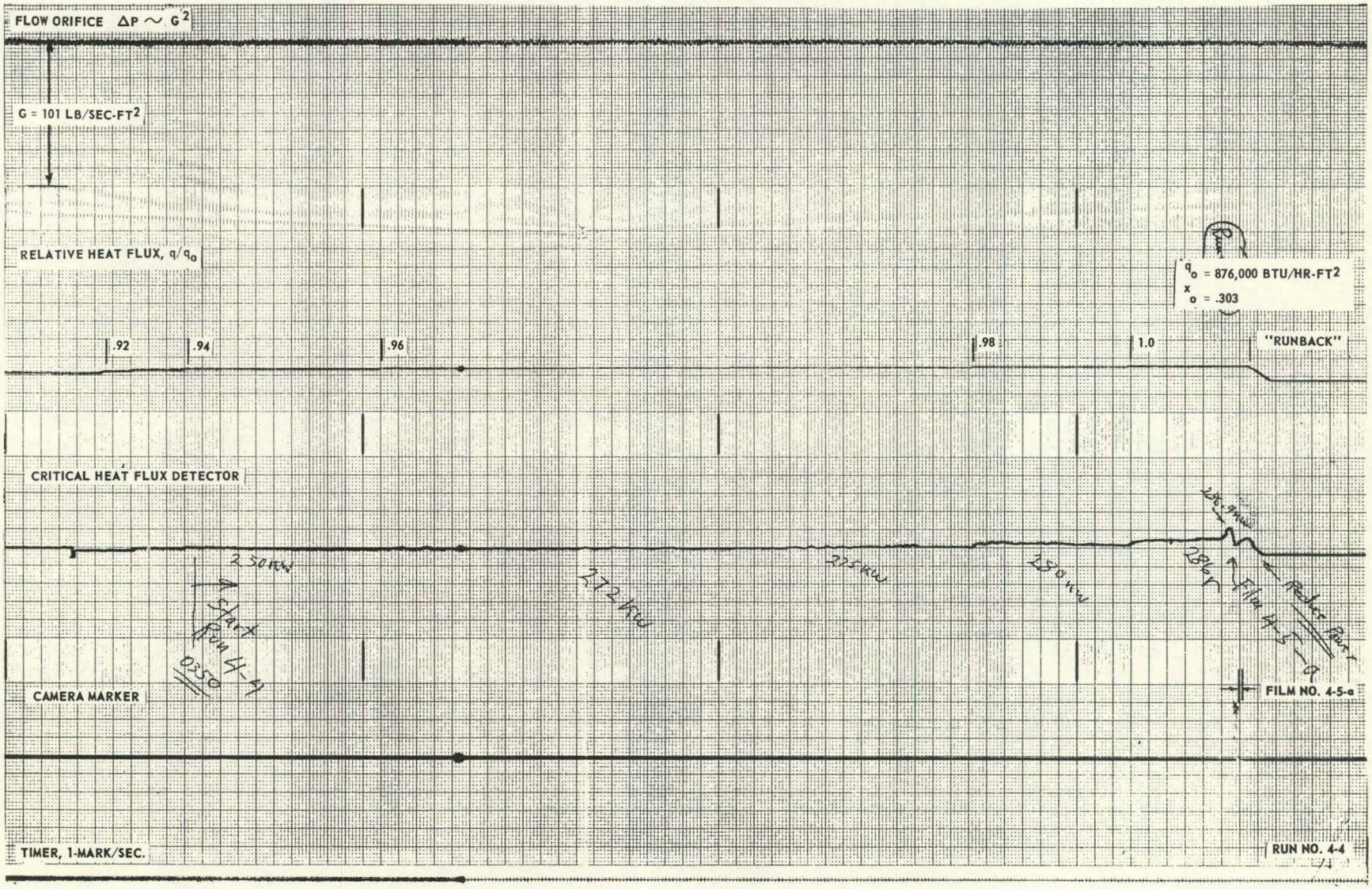
FLOW ORIFICE ΔP ~ G²
G = 101 LB/SEC-FT²
RELATIVE HEAT FLUX, q/q₀
q₀ = 876,000 BTU/HR-FT²
x₀ = .303
.92
.94
.96
.98
1.0
"RUNBACK"
CRITICAL HEAT FLUX DETECTOR
2.50 KW
2.72 KW
2.25 KW
2.50 KW
1.84 KW
Reactor Power
FILM NO. 4-5-a
CAMERA MARKER
TIMER, 1-MARK/SEC.
RUN NO. 4-4

FIGURE VI - 4

## FIGURE VI-5

RECORDER CHART SHOWING OPERATING CONDITIONS DURING CRITICAL HEAT FLUX CONDITION UPSTREAM (REJECTED RUN NO. 5A-1)

Type Run : BO-T-R

Type 1B Heater Element: .50 in., .010 in. -2

Deflection of the Detector signal trace to the left to the "trip" level indicates heater element temperature rise upstream from the outlet end.

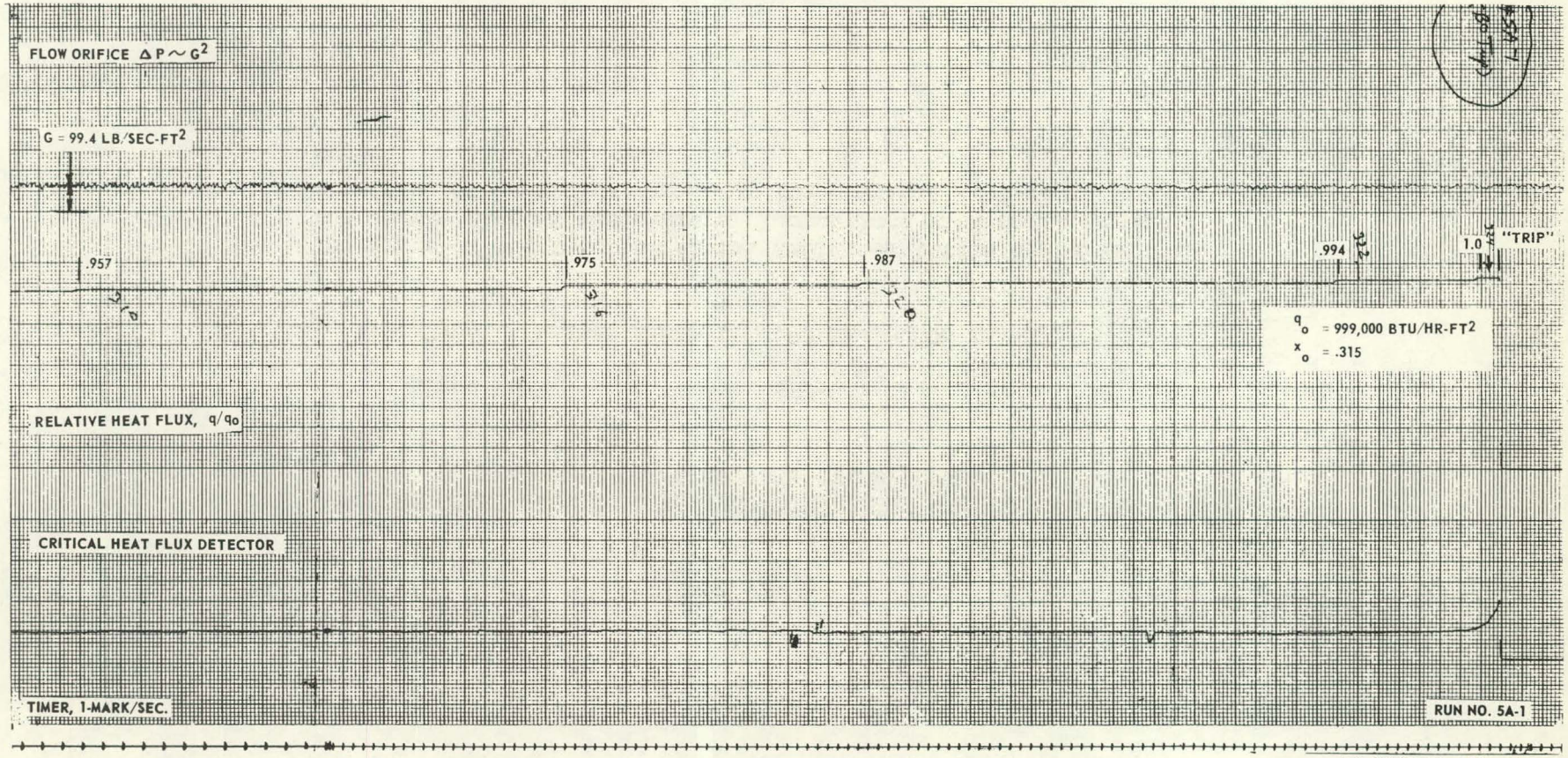
FLOW ORIFICE ΔP ~ G²
G = 99.4 LB/SEC-FT²
.957
.975
.987
.994
1.0
"TRIP"
$q_o$ = 999,000 BTU/HR-FT²
$x_o$ = .315
RELATIVE HEAT FLUX, q/$q_o$
CRITICAL HEAT FLUX DETECTOR
TIMER, 1-MARK/SEC.
RUN NO. 5A-1

FIGURE VI-5

## FIGURE VI-6

RECORDER CHART SHOWING OPERATING CONDITIONS FOR FILM NO. 3R-3
NEAR CRITICAL HEAT FLUX "TRIP" LEVEL

Type Run : SSC-0

Type 1A Heater Element: .50 in., .006 in.-2

The trace of the Detector signal indicates little hysteresis of the heater element temperature fluctuations with small manual reduction of heat flux from near the critical heat flux "trip" point.

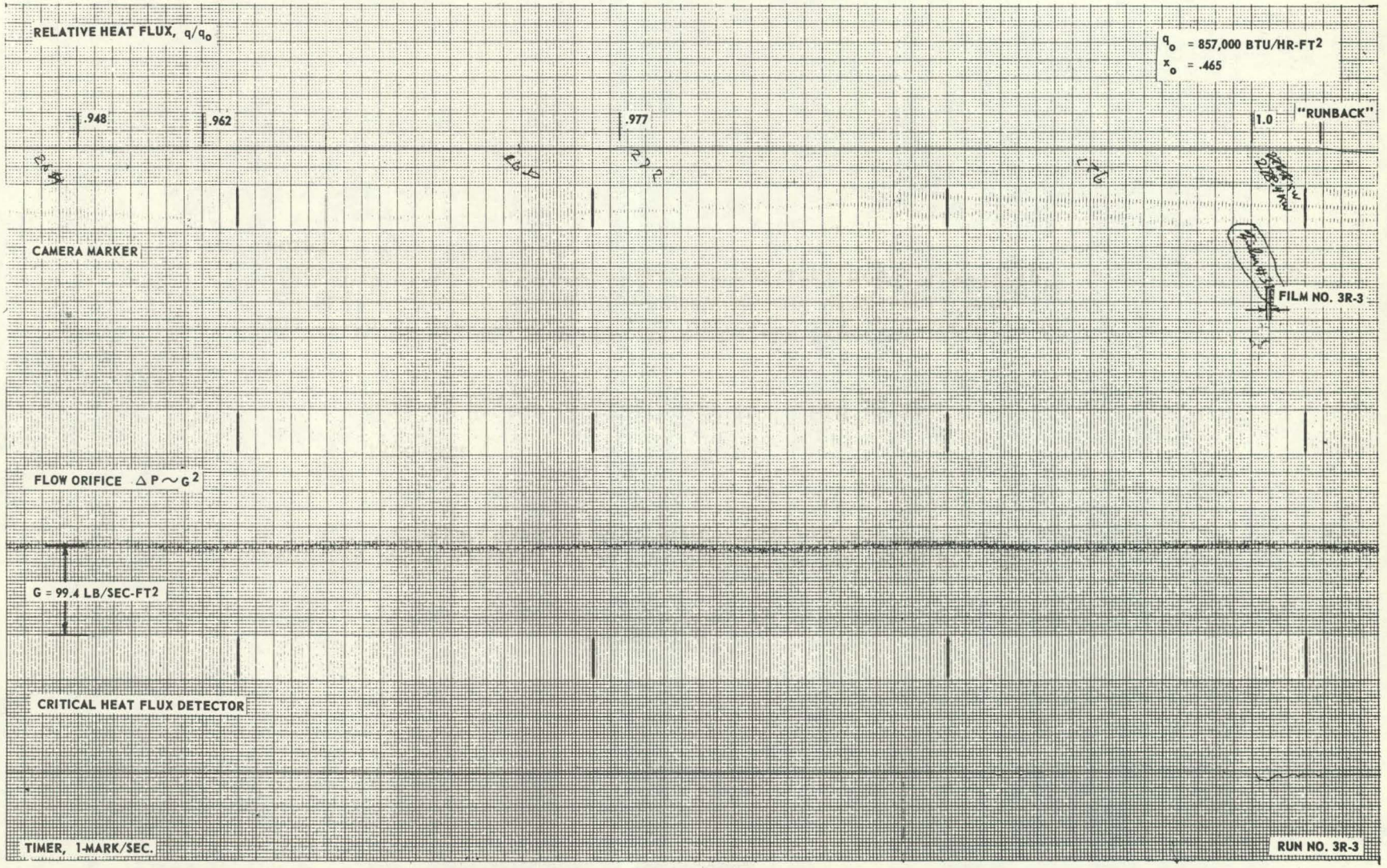
RELATIVE HEAT FLUX, q/q₀
q₀ = 857,000 BTU/HR-FT²
x₀ = .465
.948
.962
.977
1.0
"RUNBACK"
CAMERA MARKER
FILM NO. 3R-3
FLOW ORIFICE ΔP ~ G²
G = 99.4 LB/SEC-FT2
CRITICAL HEAT FLUX DETECTOR
TIMER, 1-MARK/SEC.
RUN NO. 3R-3

FIGURE VI - 6

## FIGURE VI-7

RECORDER CHART SHOWING OPERATING CONDITIONS FOR
CRITICAL HEAT FLUX DETERMINATION NO. 3RR-1

Type Run : BO-T

Type 1B Heater Element: .50 in., .010 in.-2

There were increasing oscillations of the Detector signal, indicating corresponding variations of the heater element temperature at the outlet end, as the critical heat flux "trip" point was approached.

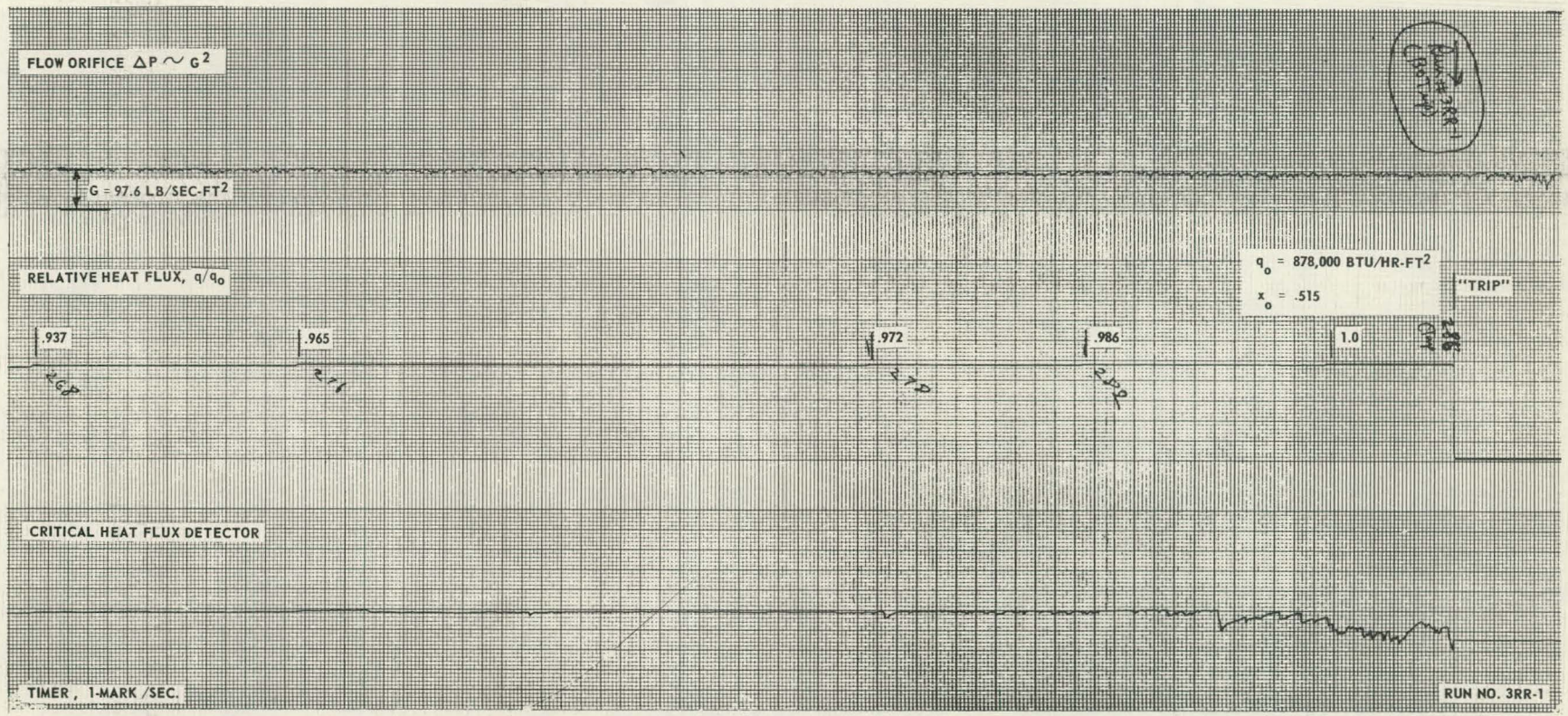
FLOW ORIFICE ΔP ~ G²
G = 97.6 LB/SEC-FT²
RELATIVE HEAT FLUX, q/q₀
q₀ = 878,000 BTU/HR-FT²
x₀ = .515
"TRIP"
.937
.965
.972
.986
1.0
CRITICAL HEAT FLUX DETECTOR
TIMER , 1-MARK /SEC.
RUN NO. 3RR-1

FIGURE VI - 7

FIGURE VI-8

RECORDER CHART SHOWING OPERATING CONDITIONS FOR CRITICAL HEAT FLUX DETERMINATION NO. 7-5 AND FILM NO. 7-5

Type Run : BOC-S

Type 1A Heater Element: .50 in., .006 in.-2

The trace of the Detector signal indicates little hysteresis of the heater element temperature fluctuations with small manual reduction of heat flux from near the critical heat flux "trip" point.

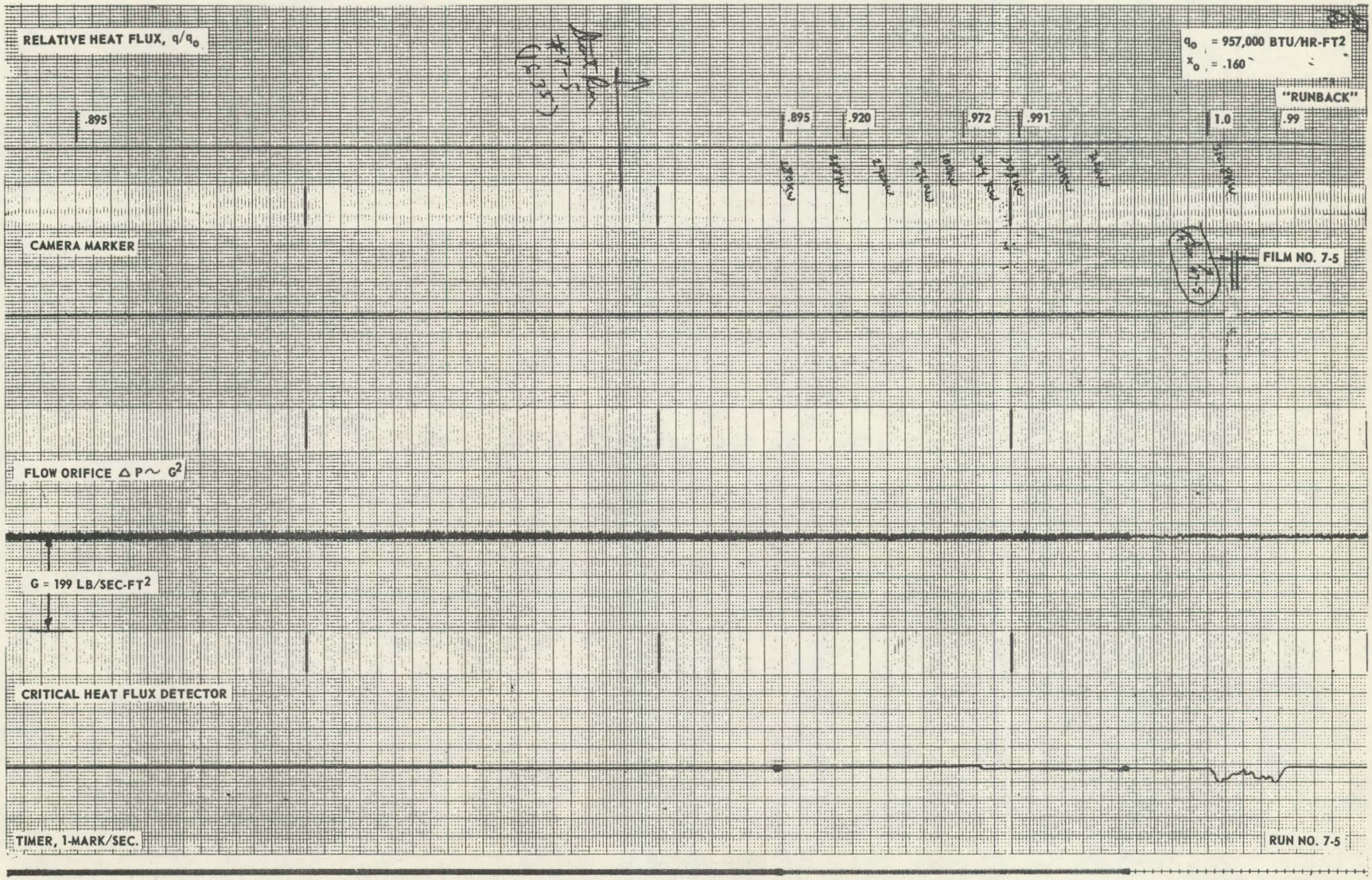
RELATIVE HEAT FLUX, q/q0
.895
.895
.920
.972
.991
1.0
.99
"RUNBACK"
q0 = 957,000 BTU/HR-FT2
x0 = .160
CAMERA MARKER
FILM NO. 7-5
FLOW ORIFICE ΔP ~ G2
G = 199 LB/SEC-FT2
CRITICAL HEAT FLUX DETECTOR
TIMER, 1-MARK/SEC.
RUN NO. 7-5

FIGURE VI-8

FIGURE VI-9

RECORDER CHART SHOWING OPERATING CONDITIONS FOR CRITICAL HEAT FLUX DETERMINATION NO. 7R-1 (HEATER ELEMENT MELTED)

Type Run : BO-A

Type 1B Heater Element: .50 in., .010 in.-2

There were increasing oscillations of the Detector signal, indicating corresponding variations of the heater element temperature at the outlet end, as the point of melting of the heater element was approached. Melting was apparently caused by extremely rapid and abrupt rise of the temperature at the outlet end.

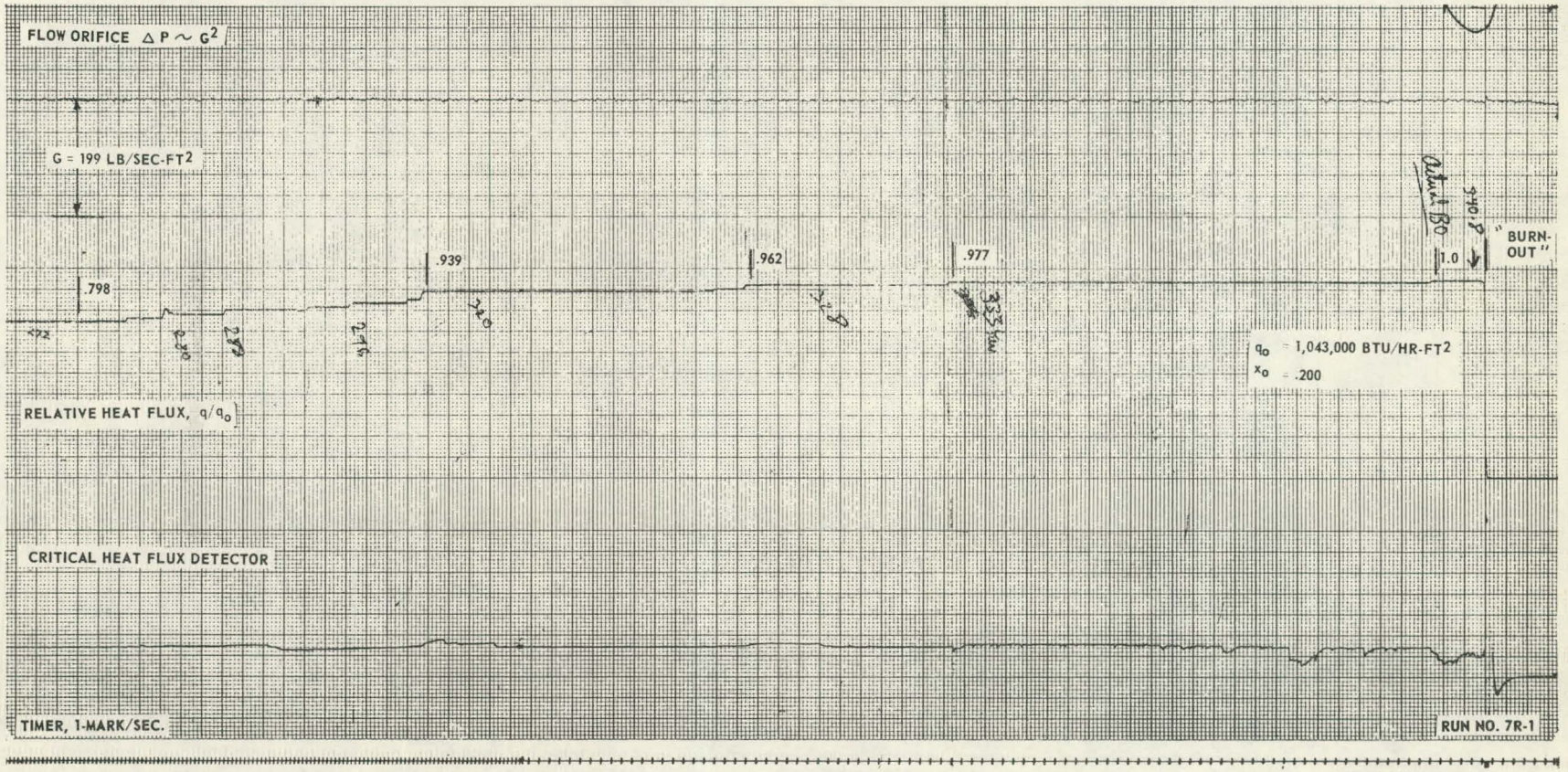
FLOW ORIFICE ΔP ~ G²
G = 199 LB/SEC-FT²
.798
.939
.962
.977
1.0
"BURN-OUT"
q₀ = 1,043,000 BTU/HR-FT²
x₀ = .200
RELATIVE HEAT FLUX, q/q₀
CRITICAL HEAT FLUX DETECTOR
TIMER, 1-MARK/SEC.
RUN NO. 7R-1

FIGURE VI - 9

FIGURE VI-10

RECORDER CHART SHOWING OPERATING CONDITIONS FOR CRITICAL HEAT FLUX DETERMINATION NO. 9A-2 AND SYNCHRONIZED FILM NO. 9A-1

Type Run : BOC-T

Type 1A Heater Element: .50 in., .006 in.-2

There were slightly increasing oscillations of the Detector signal, indicating corresponding variations of the heater element temperature at the outlet end, as the critical heat flux "trip" point was approached, followed by an abrupt rise to the "trip" point synchronized with the camera.

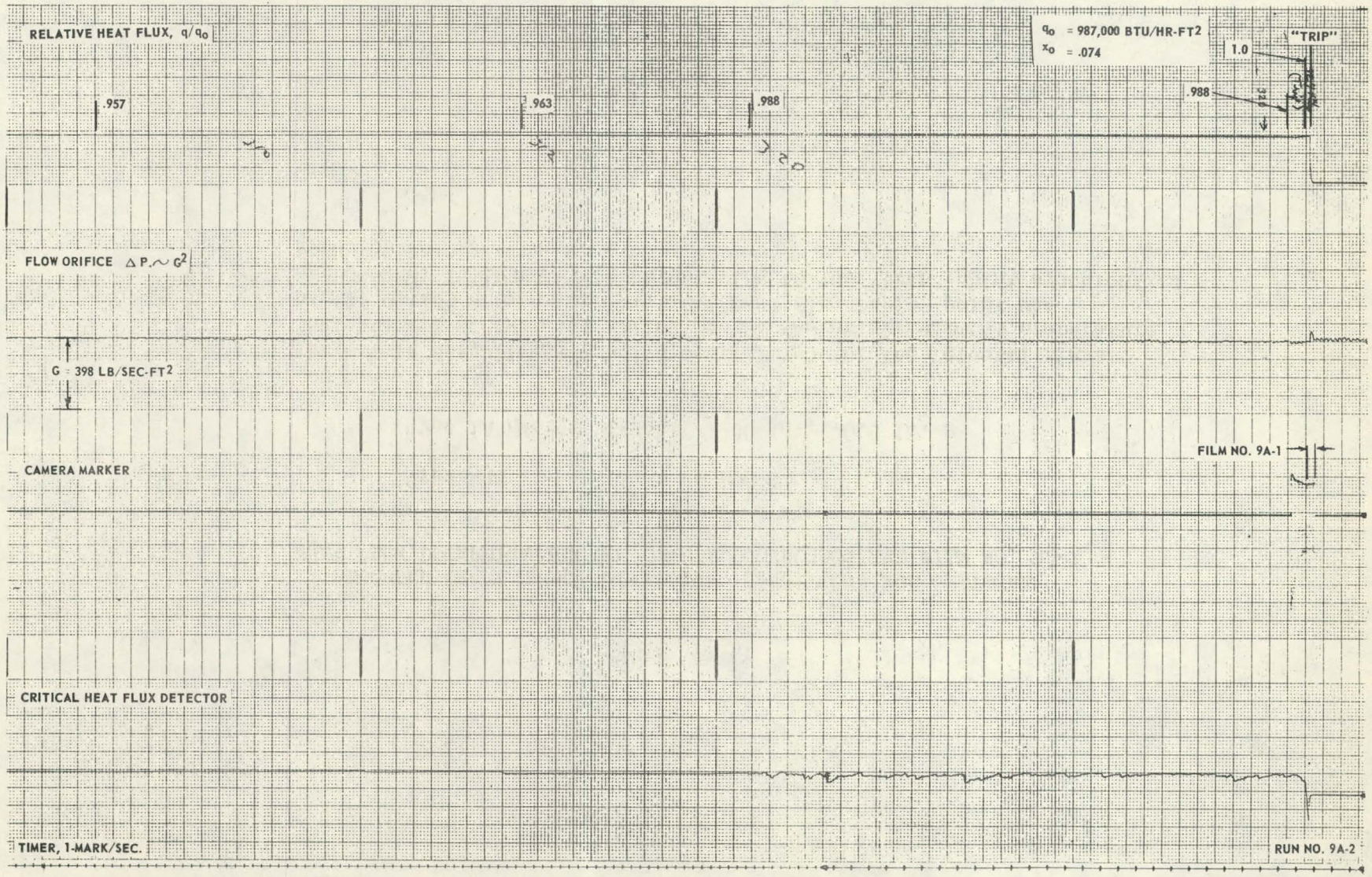
RELATIVE HEAT FLUX, q/q0
q0 = 987,000 BTU/HR-FT2
x0 = .074
1.0
"TRIP"
.988
.957
.963
.988
FLOW ORIFICE ΔP ~ G2
G = 398 LB/SEC-FT2
FILM NO. 9A-1
CAMERA MARKER
CRITICAL HEAT FLUX DETECTOR
TIMER, 1-MARK/SEC.
RUN NO. 9A-2

FIGURE VI-10

## FIGURE VI-11

RECORDER CHART SHOWING OPERATING CONDITIONS FOR CRITICAL HEAT FLUX DETERMINATION NO. 9B-2 AND SYNCHRONIZED FILM NO. 9B-2

Type Run BOC-T

Type 1A Heater Element: .50 in., .006 in.-2

There were very slight oscillations of the Detector signal, indicating corresponding variations of the heater element temperature at the outlet end, as the critical heat flux "trip" point was approached, followed by an abrupt rise to the "trip" point synchronized with the camera.

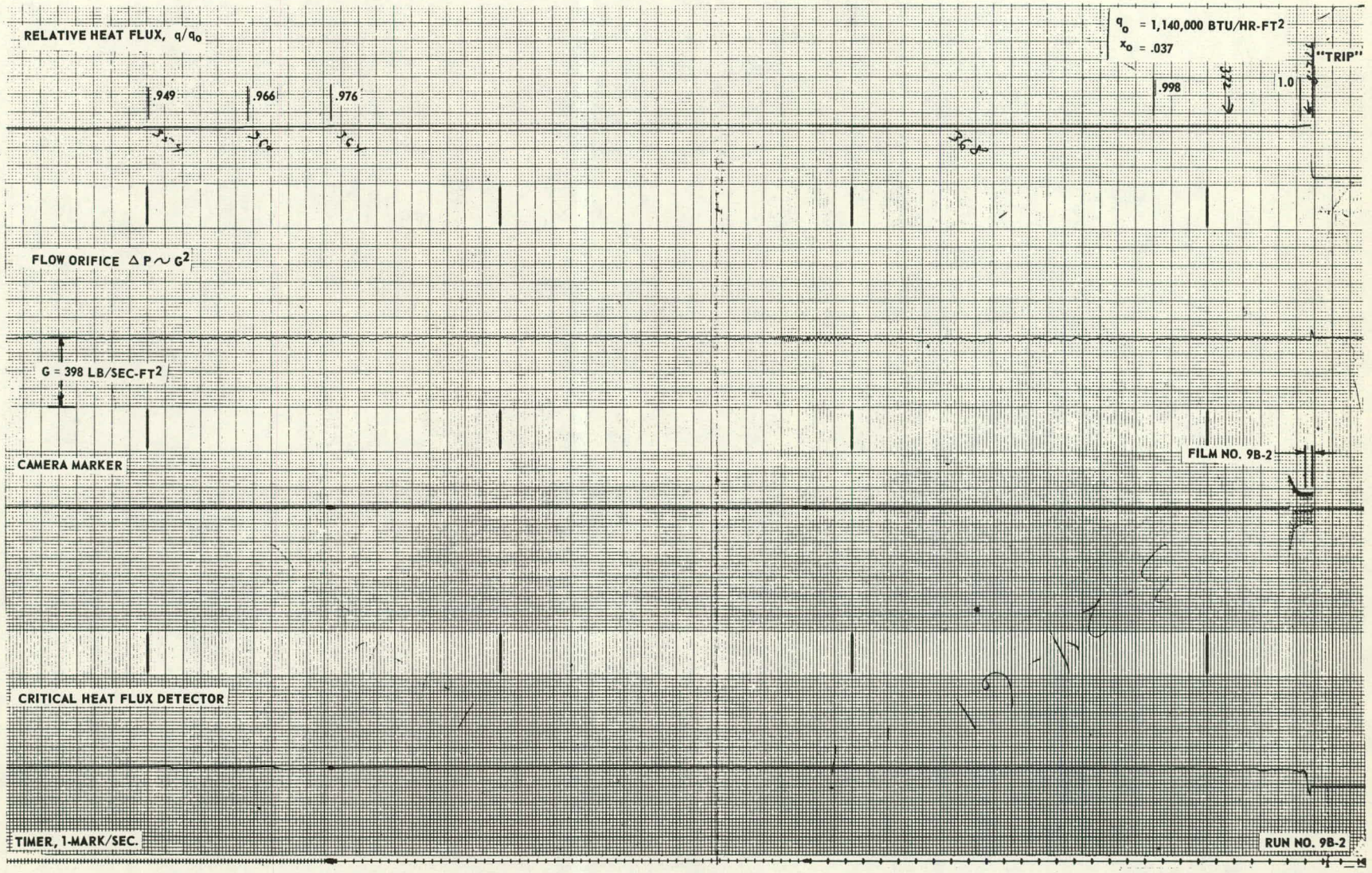
RELATIVE HEAT FLUX, q/q₀
q₀ = 1,140,000 BTU/HR-FT²
x₀ = .037
"TRIP"
.949
.966
.976
.998
1.0
FLOW ORIFICE ΔP ~ G²
G = 398 LB/SEC-FT²
CAMERA MARKER
FILM NO. 9B-2
CRITICAL HEAT FLUX DETECTOR
TIMER, 1-MARK/SEC.
RUN NO. 9B-2

FIGURE VI - 11

FIGURE VI-12

RECORDER CHART SHOWING OPERATING CONDITIONS FOR CRITICAL HEAT FLUX DETERMINATION NO. 20R-3

Type Run : BO-T

Type 2B Heater Element: .25 in., .010 in.-2

There were increasing oscillations of the Detector signal, indicating corresponding variations of the heater element temperature at the outlet end, as the critical heat flux "trip" point was approached.

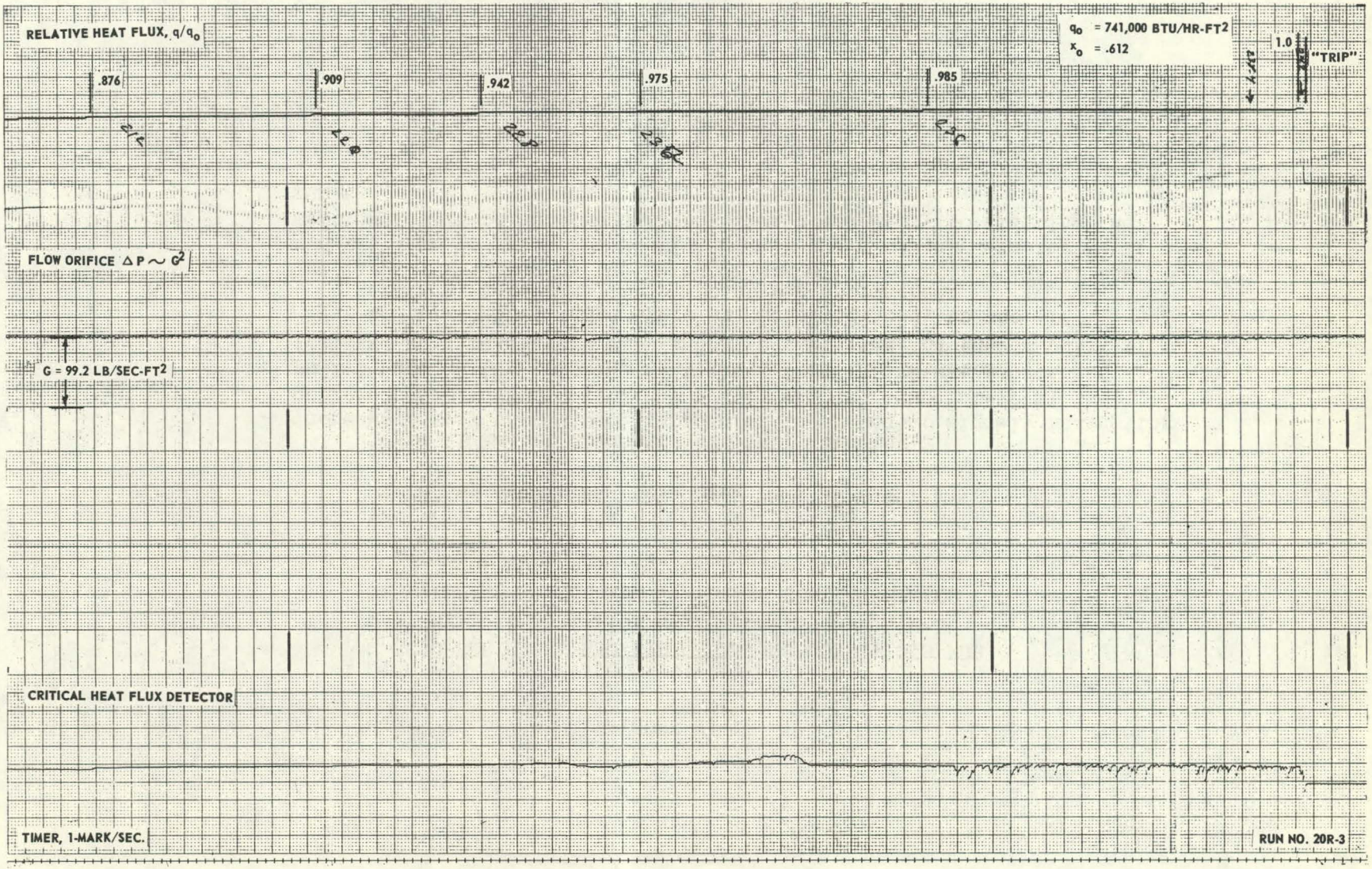
RELATIVE HEAT FLUX, q/q0
q0 = 741,000 BTU/HR-FT2
x0 = .612
.876
.909
.942
.975
.985
1.0
"TRIP"
FLOW ORIFICE ΔP ~ G2
G = 99.2 LB/SEC-FT2
CRITICAL HEAT FLUX DETECTOR
TIMER, 1-MARK/SEC.
RUN NO. 20R-3

FIGURE VI-12

FIGURE VI-13

RECORDER CHART SHOWING OPERATING CONDITIONS FOR
CRITICAL HEAT FLUX DETERMINATION NO. 15R-1

Type Run : BO-T

Type 2B Heater Element: .25 in., .010 in.-2

There were very slight oscillations of the Detector signal, indicating corresponding variations of the heater element temperature at the outlet end, as the critical heat flux "trip" point was approached, followed by a relatively slow and irregular rise and then a pulse of the signal to the critical heat flux "trip" point.

The large deflection of the Detector signal trace near start of the run was done as part of a routine manual check of the Detector "trip" setting and re-balance to null position preparatory to starting the run.

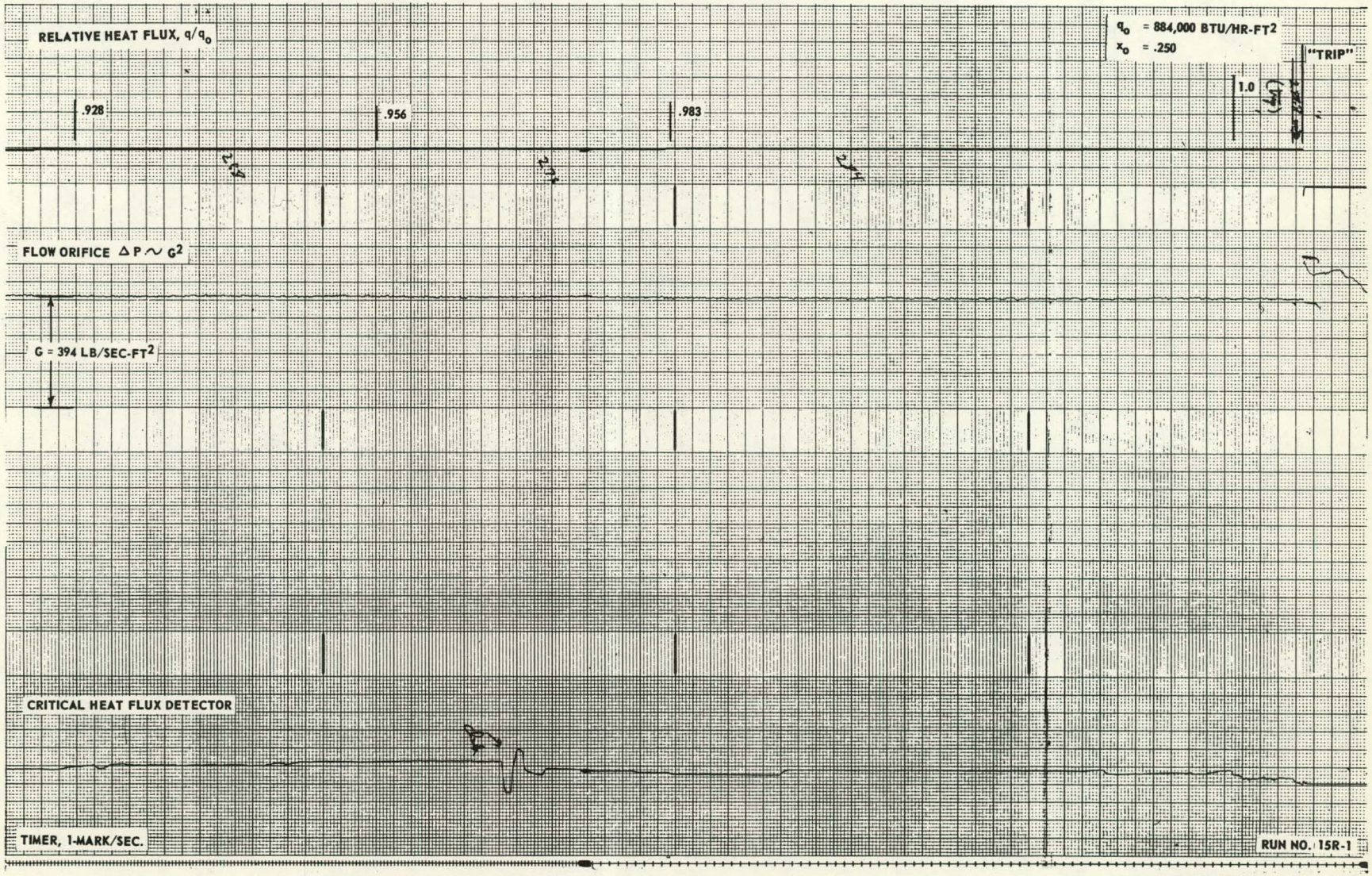
RELATIVE HEAT FLUX, $q/q_o$
$q_o$ = 884,000 BTU/HR-FT2
$x_o$ = .250
"TRIP"
1.0
.928
.956
.983
FLOW ORIFICE $\Delta P \sim G^2$
G = 394 LB/SEC-FT2
CRITICAL HEAT FLUX DETECTOR
TIMER, 1-MARK/SEC.
RUN NO. 15R-1

FIGURE VI-13

FIGURE VI-14a

RECORDER CHART SHOWING ONSET OF CRITICAL HEAT FLUX CONDITIONS DURING RUN NO. 18RR-1 TO DELIBERATE HEATER ELEMENT DESTRUCTION

Type Run : BC-A

Type 2B Heater Element: .25 in., .010 in.-2

There were increasing oscillations of the Detector signal, indicating corresponding variations of the heater element temperature at the outlet end, as the critical heat flux "trip" point ($q/q_o = 1.0$) was approached. The power trip component of the Detector was shut off during the run.

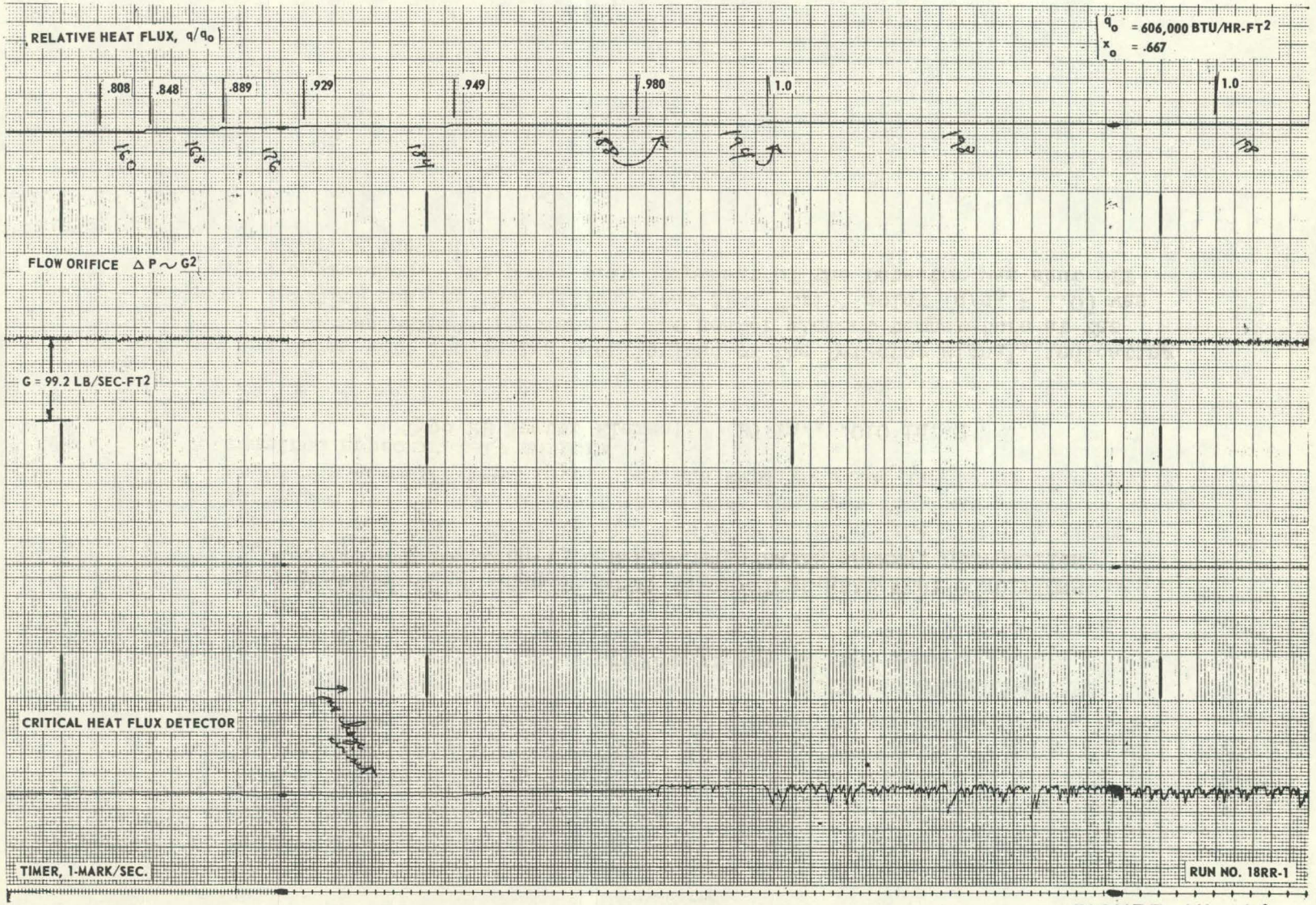


FIGURE VI - 14 a

Figure VI-14b

CONTINUED RECORDER CHART SHOWING OPERATING CONDITIONS AT HEAT FLUXES ABOVE THE POWER "TRIP" LEVEL FOR RUN NO. 18RR-1

The amplitude and frequency of oscillation of the Detector signal remained approximately uniform while the heat flux was held constant at the normal critical heat flux "trip" level. The mean level of the Detector signal increased by a factor of about three when the heat flux was raised slightly above the normal "trip" level, but the amplitude and frequency of oscillation remained approximately uniform.

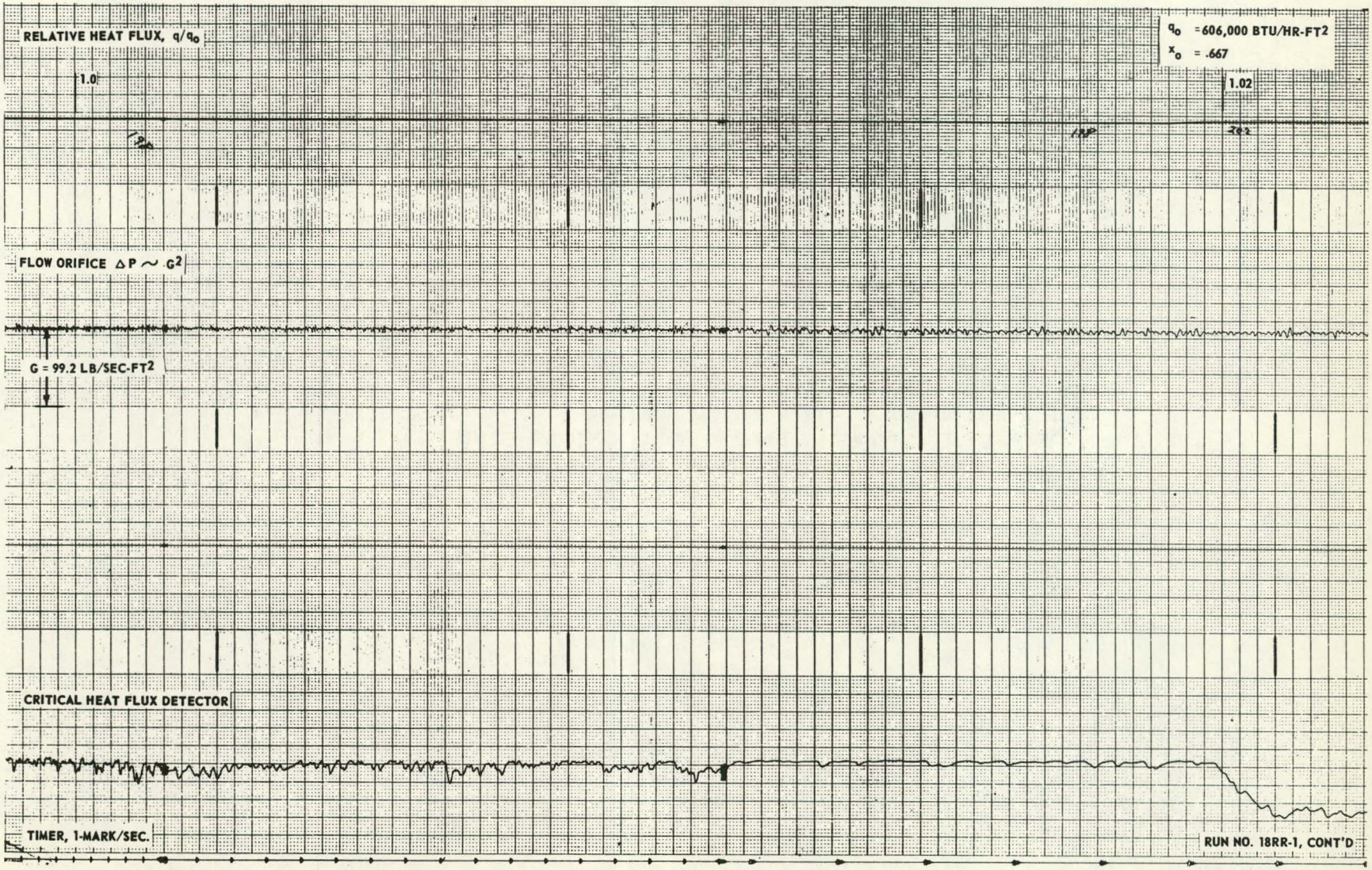


FIGURE VI - 14 b

FIGURE VI-14c

CONTINUED RECORDER CHART SHOWING OPERATING CONDITIONS AT HEAT FLUXES ABOVE THE POWER "TRIP" LEVEL NEAR THE POINT OF HEATER ELEMENT DESTRUCTION

The amplitude and frequency of oscillation of the Detector signal remained approximately uniform while the heat flux was held constant at slightly above the normal "trip" level. Speed-up of the recorder chart reveals harmonics in the oscillations at about 8 cps. Further slight rise of the heat flux resulted in deflection of the recorder pen off the chart. The heater element melted at a heat flux 11 per cent above the normal critical heat flux "trip" point (see Fig. VI-18). The flow remained constant throughout the run, except for the uniform "noise" in the flow orifice recorder trace (similar to the other runs).

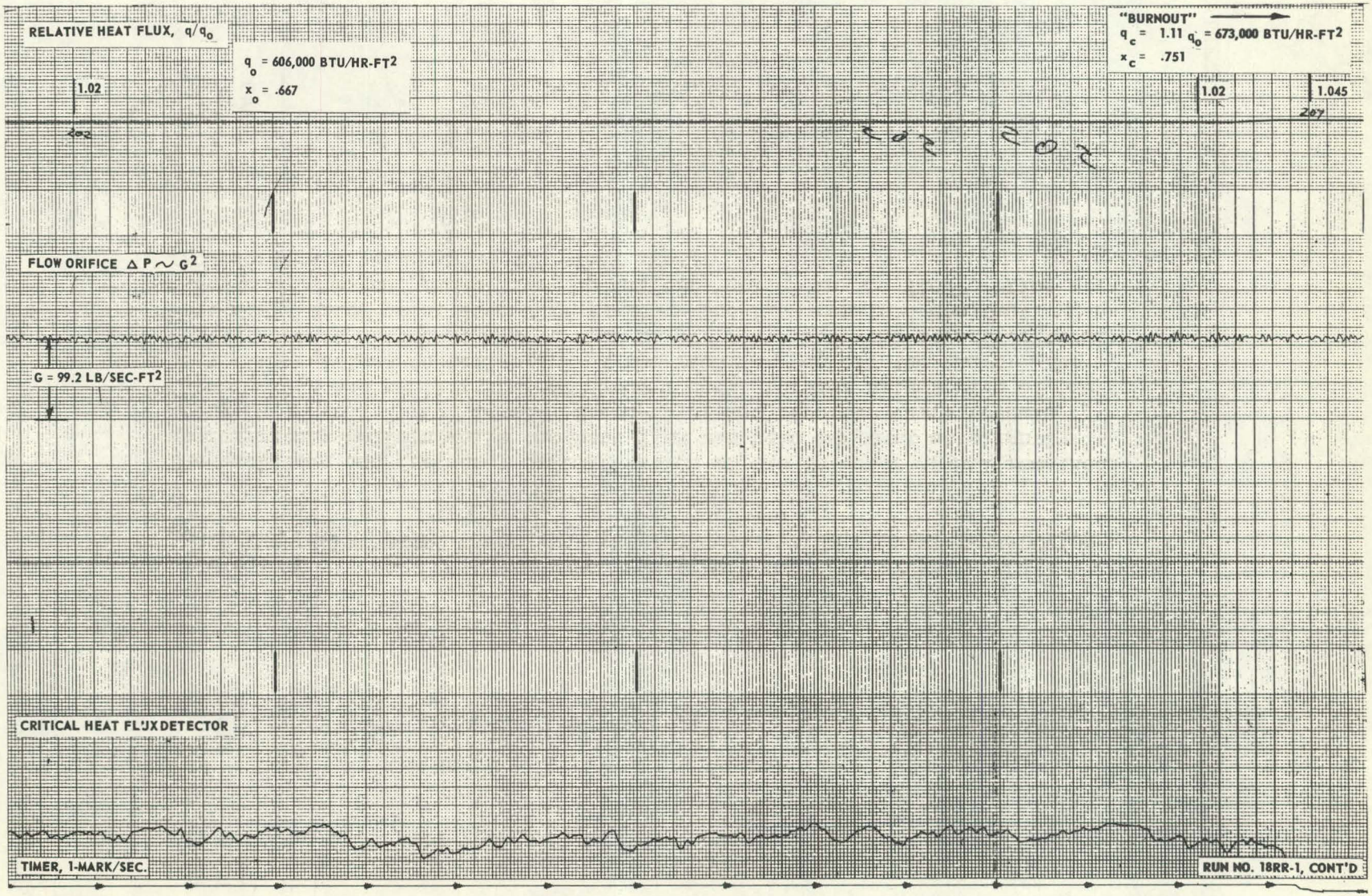


FIGURE VI-14c

## FIGURE VI-15

PHOTOGRAPH OF AN UNUSED .50 IN. SPACING DOUBLE-RIBBON HEATER ELEMENT COMPARED WITH A USED ELEMENT DESTROYED AT THE CRITICAL HEAT FLUX CONDITION

| Run No. | Type Run | G, $\frac{\text{lbs.}}{\text{sec-ft}^2}$ | $q_c$ $\frac{10^6 \text{ Btu}}{\text{hr-ft}^2}$ | $X_c$ |
|---|---|---|---|---|
| 3-5 | BO-A | 98.6 | .898 | .511 |

## FIGURE VI-16

PHOTOGRAPH OF A USED .50 IN. SPACING SINGLE-RIBBON HEATER ELEMENT SHOWING PATCHES OF LOCAL HIGH TEMPERATURE RISE

| Run No. | Type Run | G, $\frac{\text{lbs.}}{\text{sec-ft}^2}$ | $q_c$ $\frac{10^6 \text{ Btu}}{\text{hr-ft}^2}$ | $X_c$ |
|---|---|---|---|---|
| 12-3 | BO-T | 199 | 1.018 | .140 |
| 12-4 | BOC-T | 199 | 1.027 | .140 |
| 12-5* | BO-A-R | 201 | 1.027 | .126 |

* Heater ribbon melted upstream near inlet end.

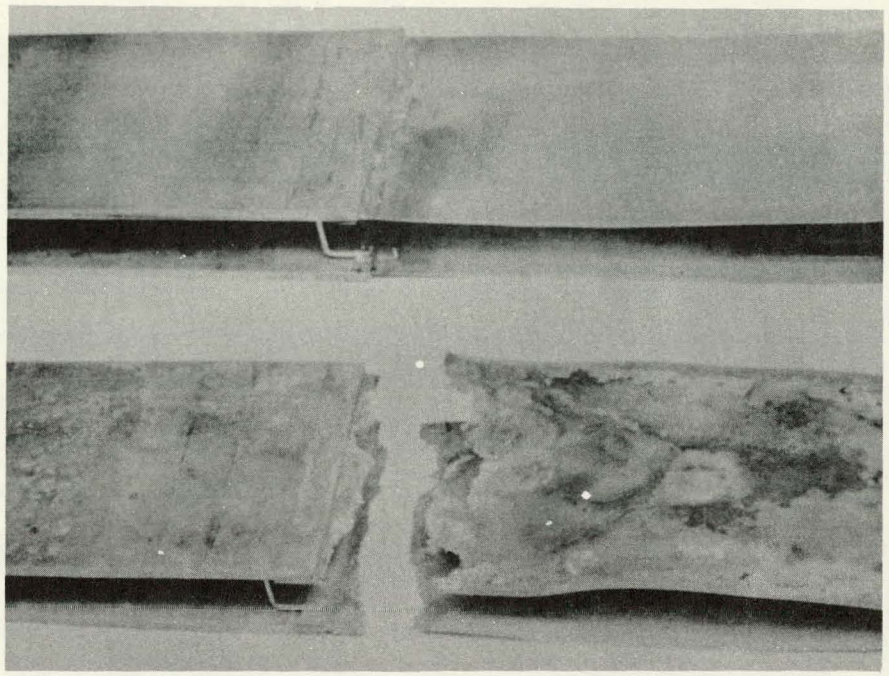


FIGURE VI-15

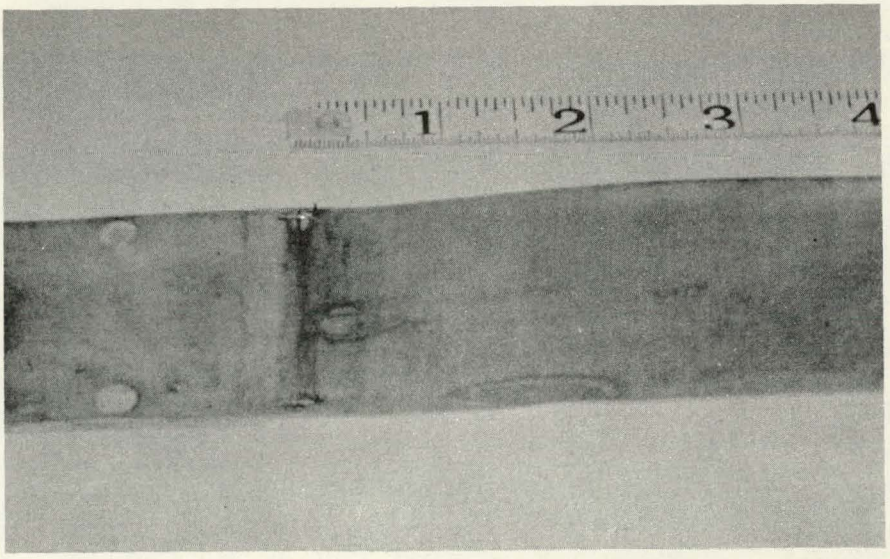


FIGURE VI-16

FIGURE VI-17

PHOTOGRAPH OF A USED .50 IN. SPACING DOUBLE-RIBBON HEATER ELEMENT SHOWING DAMAGES AFTER ONSET OF THE CRITICAL HEAT FLUX CONDITION UPSTREAM TOWARDS THE INLET (DATA REJECTED)

| Run No. | Type Run | G, $\frac{\text{lbs.}}{\text{sec-ft}^2}$ | $q_c$ $\frac{10^6 \text{ Btu}}{\text{hr-ft}^2}$ | $X_c$ |
|---|---|---|---|---|
| 3A-2 | BO-A-R | 99.4 | .864 | .389 |

FIGURE VI-18

PHOTOGRAPH OF A USED .25 IN. SPACING DOUBLE-RIBBON HEATER ELEMENT DESTROYED AFTER DELIBERATE OPERATION TO A HEAT FLUX 11 PER CENT ABOVE THE NORMAL TRIP LEVEL*

| Run No. | Type Run | G, $\frac{\text{lbs.}}{\text{sec-ft}^2}$ | $q_c$ $\frac{10^6 \text{ Btu}}{\text{hr-ft}^2}$ | $X_c$ |
|---|---|---|---|---|
| 18RR-1 | BO-A | 99.2 | .673 | .751 |

* See recorder trace of Detector signal in Figs. VI-14a,b,c.

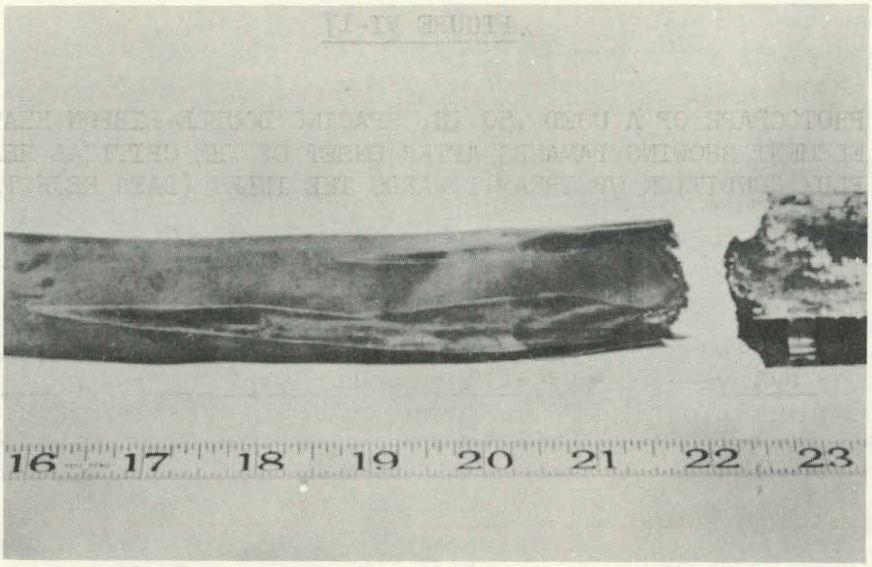


FIGURE VI-17

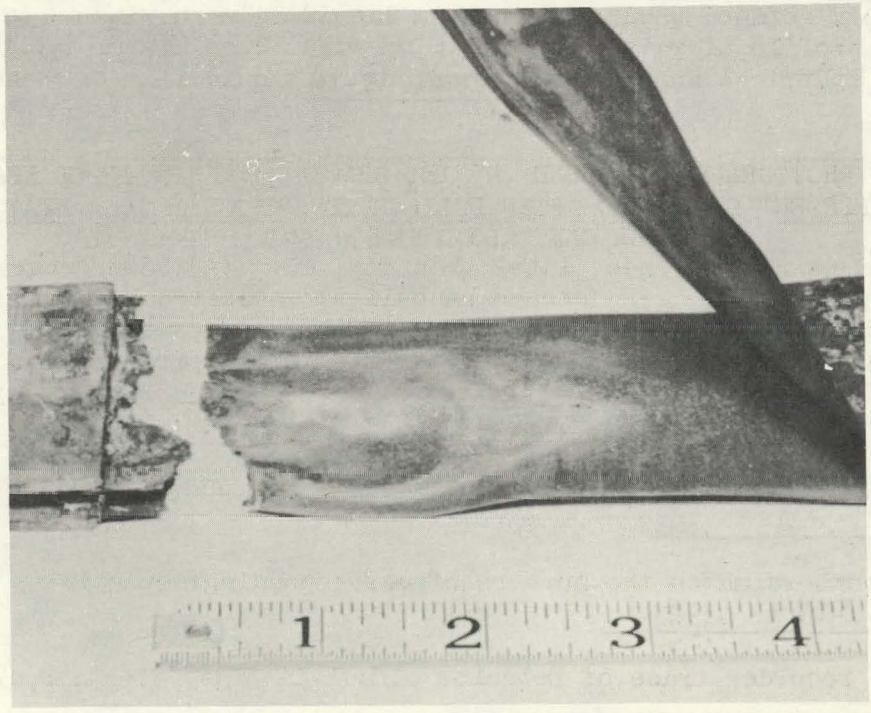


FIGURE VI-18

## FIGURE VI-19*

ENLARGED FRAMES FROM REEL I

G = 50 lbs/sec-ft$^2$, both sides heated

| Fig. | Seq. No. | Type Run | X | q, $10^6$ Btu / hr-ft$^2$ | $\frac{q}{q_c}$ |
|---|---|---|---|---|---|
| a | 2-1 | SSC | .258 | .465 | $<<1.0$ |

(1) Liquid film wave structure on window surface. (2) Shadow of wavy liquid film profile on right-hand heater ribbon. (3) Focusing target on right-hand side.

| | | | | | |
|---|---|---|---|---|---|
| b | 2-2 | SSC-0 | .450 | .616 | $<<1.0$ |

(1) Shadows of focusing target and profile of wavy liquid film on heater ribbon at right-hand side. (2) Increased back-light intensity indicates higher vapor content in core than in No. 2-1.

| | | | | | |
|---|---|---|---|---|---|
| c | 1-2 | SSC-0 | .656 | .588 | $\approx 1.0$ |

(1) Sharply defined wave structure on liquid film on window. (2) Distinct profile of wavy liquid film on right-hand heater ribbon. (3) Tiny spherical bubbles carried along in liquid film on window.

| | | | | | |
|---|---|---|---|---|---|
| d | 1-2 | SSC-0 | .656 | .588 | $\approx 1.0$ |

(1) Frame exposed .07 sec. later than Fig. c. (2) Same general pattern as Fig. c. (3) Intense back-light indicates high vapor content in core. (4) Streamers of vapor from edges of heater ribbons into liquid film. (5) Heater element temperature oscillating.

* Arrow numbers match the numbers of corresponding notes in Figs. VI-19 to VI-23.

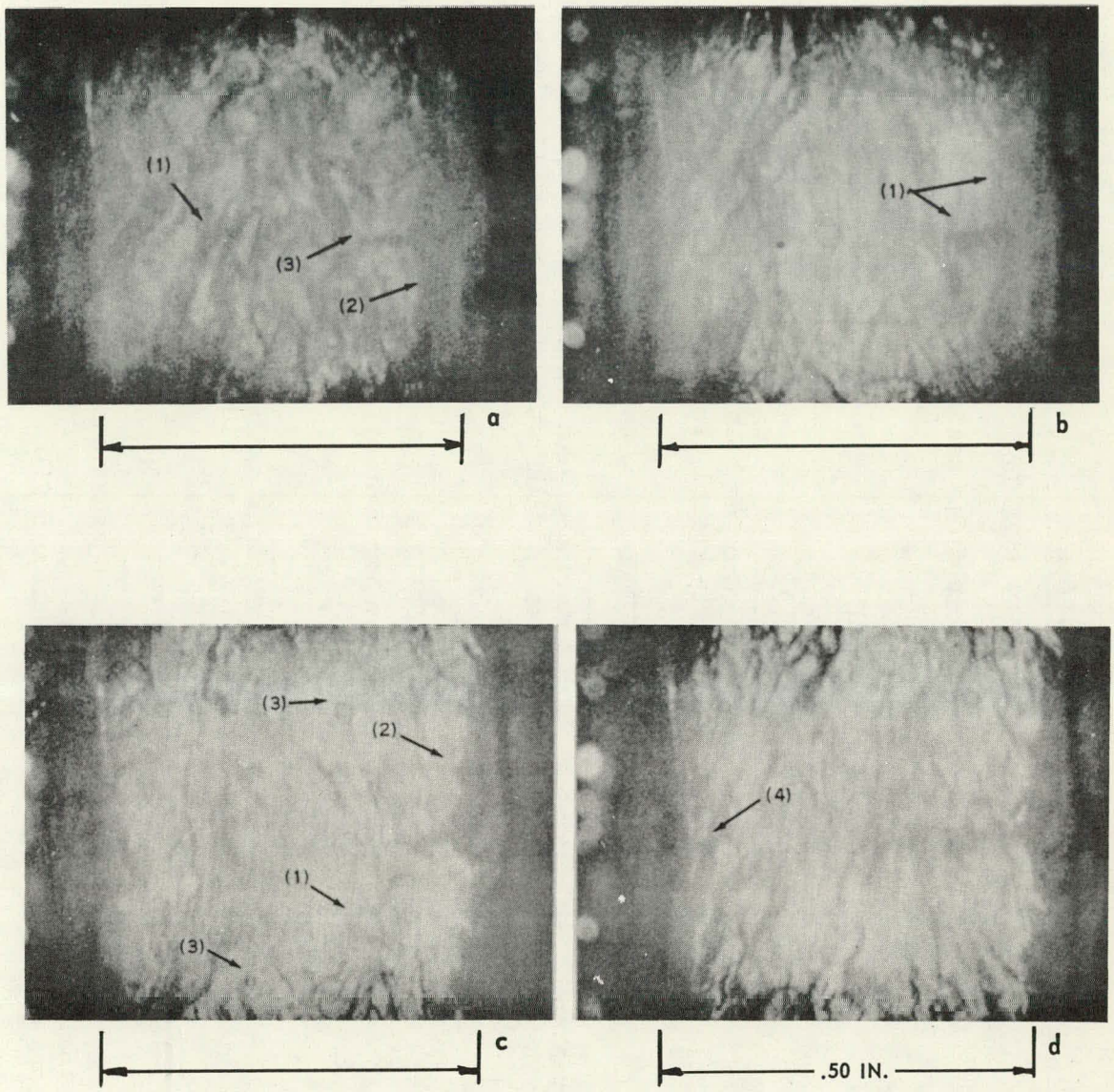


FIGURE VI - 19

## FIGURE VI-20

### ENLARGED FRAMES FROM REEL II

G = 100 lbs/sec-ft$^2$, both sides heated

| Fig. | Seq. No. | Type Run | X or ($\Delta h_s$, Btu/lb.) | q, $10^6$ Btu / hr-ft$^2$ | $\frac{q}{q_c}$ |
|---|---|---|---|---|---|
| a | 3S-1 | SC | (91.4) | .245 | $<<1.0$ |

(1) Sub-cooled nucleate boiling at heater surfaces. (2) Growing bubbles slide along the surface, moving with the stream. (3) Bubbles tend to grow in periodically spaced, irregular clumps.

| | | | | | |
|---|---|---|---|---|---|
| b | 3S-2 | SSC | .056 | .492 | $<<1.0$ |

(1) General froth-like appearance, with large bubbles interlaced with continuous liquid containing a range of smaller bubbles. (2) Larger bubbles centrally located. (3) Frothy structure of fine bubbles in liquid at heater surfaces.

| | | | | | |
|---|---|---|---|---|---|
| c | 3S-4 | SSC | .166 | .491 | $<<1.0$ |

(1) Flow is "slugging." (2) Frame exposed during a "light" slug, indicative of thick placid liquid layer on window, containing small bubbles, with probably high vapor content in core. (3) Frothy structure of fine bubbles in liquid against heater surfaces.

| | | | | | |
|---|---|---|---|---|---|
| d | 3S-4 | SSC | .166 | .491 | $<<1.0$ |

(1) Frame exposed .02 sec. later than Fig. c, during "dark" slug. (2) Small spherical bubbles in foreground in both frames are outside channel. (3) "Dark" slugs indicative of finely divided "froth" of vapor and liquid in core. (4) Heater temperature steady.

| | | | | | |
|---|---|---|---|---|---|
| e | 3R-3 | SSC-O | .465 | .857 | .96 |

(1) Shadow of profile of highly turbulent wavy liquid film against heater ribbon surfaces. (2) Finely divided structure of waves on liquid film against window. (3) Heater element temperature oscillating. (4) Streamers of vapor from edges of heater ribbons into liquid film.

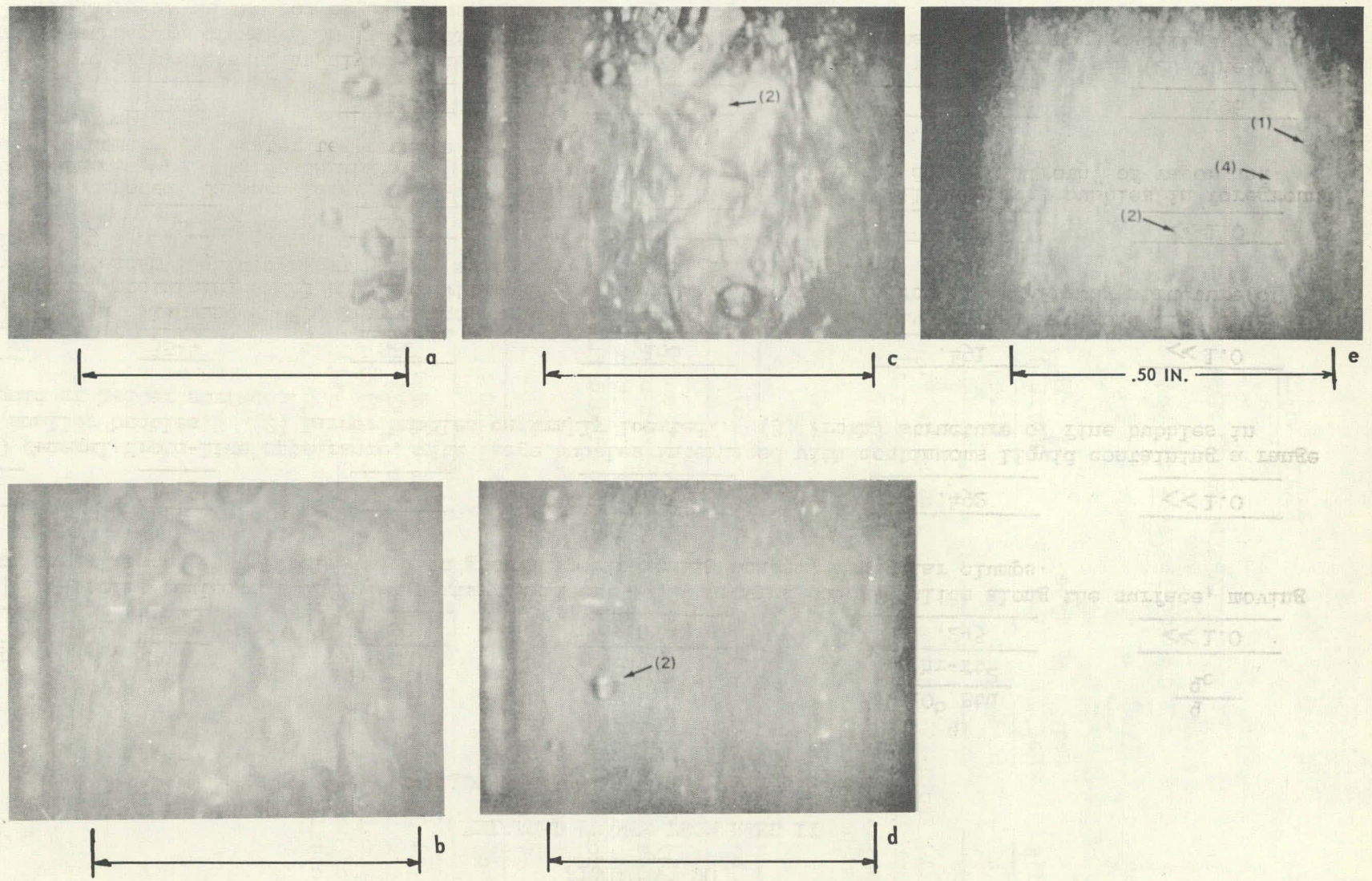


FIGURE VI - 20

## FIGURE VI-21

ENLARGED FRAMES FROM REEL III

G = 200 lbs/sec-ft$^2$, both sides heated

| Fig. | Seq. No. | Type Run | X or ($\Delta h_s$, Btu/lb.) | q, $10^6$ Btu / hr-ft$^2$ | $\frac{q}{q_c}$ |
|---|---|---|---|---|---|
| a | 6S-1 | SC | (2.8) | .298 | $\ll 1.0$ |

(1) Froth-like appearance, similar to Figure VI-20 b, with large bubbles interlaced with continuous liquid containing a range of smaller bubbles. (2) Frothy structure of fine bubbles in liquid at heater surfaces.

| | | | | | |
|---|---|---|---|---|---|
| b | 6R-1 | SSC | .167 | .612 | $\ll 1.0$ |

(1) Flow structure is finely divided and indistinct (rapidly moving) near middle, indicative of very short wave lengths on liquid film against windows. (2) Irregular streamers of vapor vaguely apparent from edge of heater ribbons into liquid film.

| | | | | | |
|---|---|---|---|---|---|
| c | 7-5 | BOC-S | .160 | .957 | 1.0 |

(1) Shadow of profile of wavy liquid film vaguely apparent against right-hand heater ribbon surface. (2) Flow structure on window more finely divided than in Figure b. (3) Streamers of vapor from edge of heater ribbons into liquid film. (4) Heater temperature oscillating.

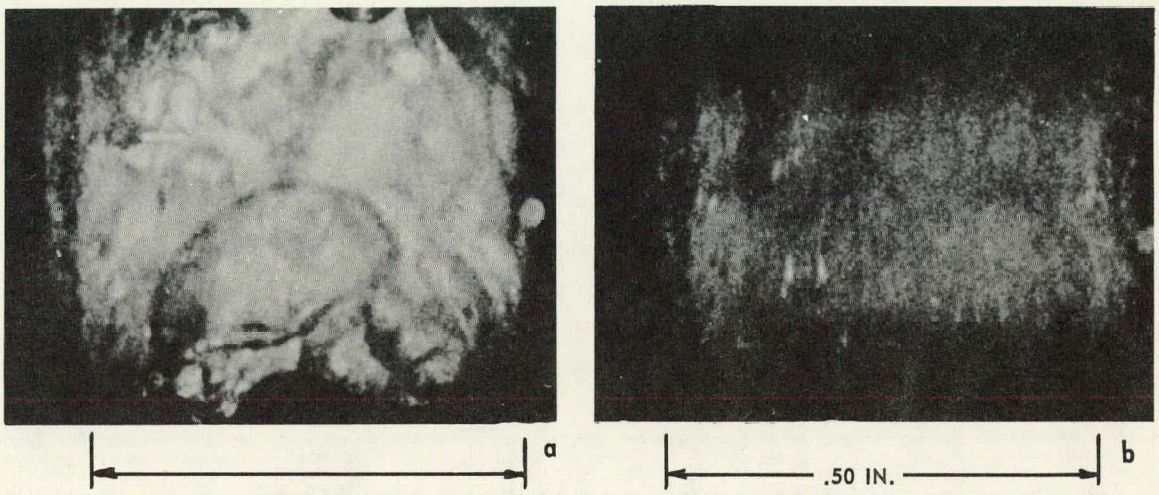


FIGURE VI - 21

## FIGURE VI-22

ENLARGED FRAMES FROM REEL IV

G = 400 lbs/sec-ft$^2$, both sides heated

| Fig. | Seq. No. | Type Run | X or ($\Delta h_s$, Btu/lb.) | $q_c$, $10^6$ Btu / hr-ft$^2$ | $\frac{q}{q_c}$ |
|---|---|---|---|---|---|
| a | 9S-1 | SC | (61.3) | .245 | $\ll 1.0$ |

(1) Start of sub-cooled nucleate boiling. (2) Bubbles against left-hand heater ribbon appear to grow from patches as flat domes, changing to long irregular vapor streamers before disengaging or fracturing. (3) Large, irregular conglomerates at right-hand side slide along with the stream.

| | | | | | |
|---|---|---|---|---|---|
| b | 9S-2 | SC | (17.6) | .493 | $\ll 1.0$ |

(1) Many discrete bubbles in the stream interlaced by almost pure liquid at channel middle. (2) Froth structure of tiny bubbles and liquid in thick layer against both heater surfaces.

| | | | | | |
|---|---|---|---|---|---|
| c | 9A-1 | BOC-T | .074 | .987 | 1.0 |

(1) Shadow of profile of wavy liquid film vaguely apparent against heater ribbon surfaces. (2) Finely divided indistinct liquid film structure on window. (3) Irregular streamers of vapor flowing in liquid at edges of both heater ribbons. (4) Heater element temperature oscillating. (5) Frame is .01 sec. before power "trip."

| | | | | | |
|---|---|---|---|---|---|
| d | 9A-1 | BOC-T | .074 | Shut-off | 0.0 |

(1) Frame was exposed .06 sec. after power "trip." (2) Flow pattern is in the process of re-arranging into a "frothy" structure of large bubbles interlaced with liquid, as steam is "swept" from channel. (3) Focusing target evident at left-hand side. (4) Spherical bubbles in foregrounds of both frames are outside channel.

| | | | | | |
|---|---|---|---|---|---|
| e | 9B-2 | BOC-T | .037 | 1.141 | 1.0 |

(1) Appearance similar to Fig. c. (2) Especially distinct vapor streamer from edge of left-hand heater ribbon into liquid film. Less distinct vapor streamers at right-hand heater ribbon. (3) Heater temperature oscillating and pulsing. (4) Spherical bubbles in foreground are outside channel. (5) Frame is .01 sec. before power "trip."

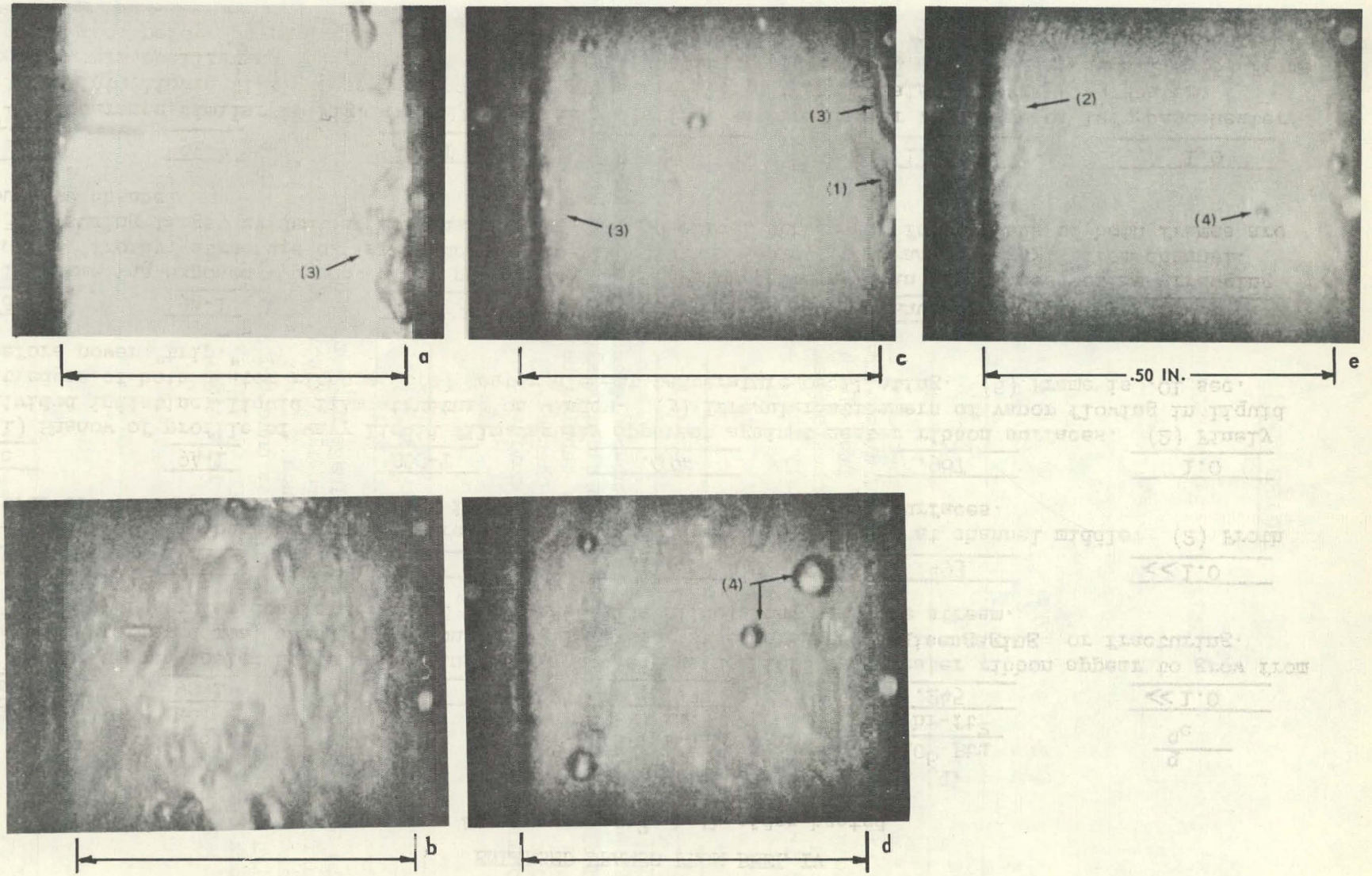


FIGURE VI - 22

## FIGURE VI-23

ENLARGED FRAMES FROM REEL V

G = 100 and 200 lb/sec-ft$^2$, left side heated

| Fig. | Seq. No. | Type Run | X or ($\Delta h_s$, Btu/lb.) | q, $10^6$ Btu / hr-ft$^2$ | $\frac{q}{q_c}$ |
|---|---|---|---|---|---|
| a | 11S-2 | SC | (72.4) | .612 | $\ll 1.0$ |

(1) G = 100 lbs/sec-ft$^2$. (2) Sub-cooled nucleate boiling. (3) Bubbles grow in large irregular frothy clumps of tiny bubbles sliding along the heater ribbon surface, from which occasional large bubbles form. (4) Little mixing with unheated half of channel. (5) Shadow of irregular, wavy thermal boundary layer against unheated side.

| | | | | | |
|---|---|---|---|---|---|
| b | 12S-2 | SC | (151.2) | .612 | $\ll 1.0$ |

(1) G = 200 lbs/sec-ft$^2$. (2) Sub-cooled nucleate boiling. (3) Bubbles grow in irregular clumps sliding along the heater ribbon surface with a frothy layer of tiny bubbles between clumps. (4) Almost no mixing with unheated half of channel. (5) Shadow of wavy thermal boundary layer against unheated surface.

| | | | | | |
|---|---|---|---|---|---|
| c | 12-2 | SSC-0 | .113 | .844 | $\simeq .80$ |

(1) G = 200 lbs/sec-ft$^2$. (2) Image hazy due to fouled window surface. (3) Hazy shadow of profile of wavy liquid film against heated surface at left. (4) Much thicker (more placid) layer of high liquid concentration against unheated surface at right. (5) Dark curved line at right is edge of window gasket, out of position. (6) Target partially visible at left side.

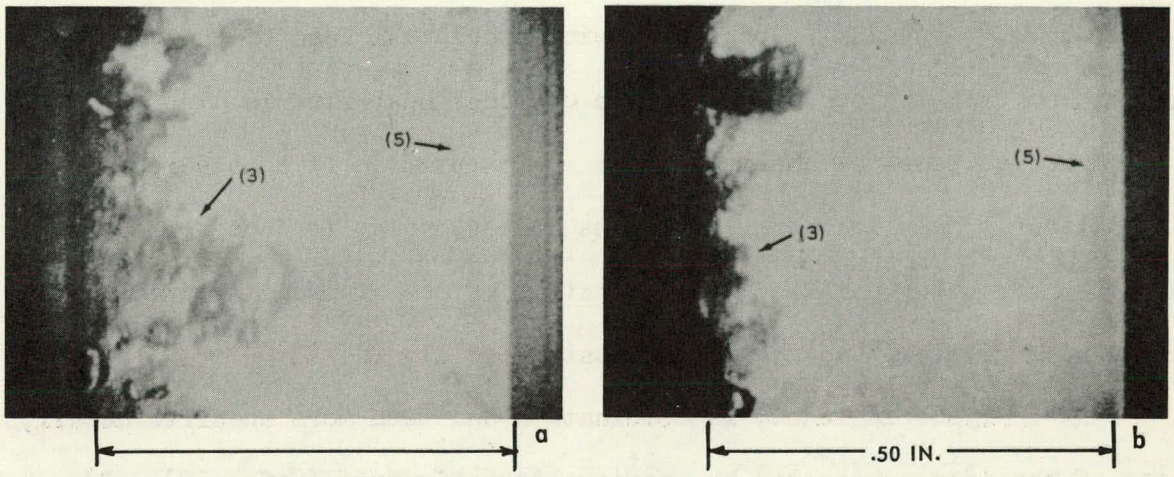


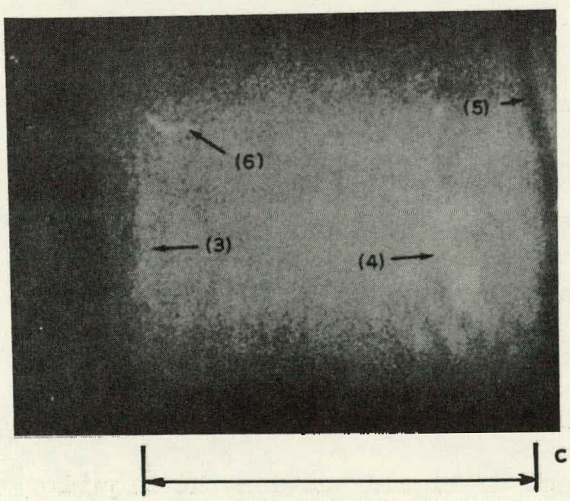


FIGURE VI - 23

# VII. THEORETICAL ANALYSIS


## Summary

The purpose of this Section is to derive a theoretical expression describing the critical heat flux condition in terms of the common properties of the flow.

Based on the visual evidence observed in the motion pictures (Section VI , Appendix D), the following conceptual idea of the mechanism associated with the conditions of the critical heat flux is hypothesized for purposes of analysis. The representation is considered to be applicable only to those conditions corresponding to ducted flow of two-phase water parallel to the heated surface at mean mixture enthalpies greater than that of the saturated liquid ($X>0$).

The analysis includes, in combination and with more specific detail, some of the ideas suggested by previous investigators (refs. (2), (3), (5), (6), (7), (12)). There is no evidence in the literature of previous detailed attempts along the particular line of attack taken here.

The five main hypotheses on which the analysis is based are (Fig. VII-1):

1. A liquid film exists on all heated and unheated surfaces of the channel, traveling in the direction of the general stream flow, under the forces of the pressure gradient and turbulent shear stress exerted on the interface by the core.
2. Not all of the liquid is carried in the liquid film, some being carried as droplets or conglomerates in the gaseous inner core. There is a continual interchange of liquid between the liquid film and the gaseous core at the interface. Thus, the interface of the liquid film is hypothesized to be always at a condition of instability, to the extent that adherence of any

more liquid is matched, on the average, by removal of an equal amount by re-entrainment and boiling in the film. This condition establishes the mean thickness of the film.

3. Heat transfer from the heated surface is principally by convection and conduction in the adjacent liquid (ref. (73)). A portion of the heat goes to form steam in the liquid film and at the core-film interface. The remainder is transferred to the core by turbulent convection in the vapor adjacent to the interface and by removal of superheated liquid particles from the film. The interface and closely adjacent liquid can be only a small amount superheated above the saturation temperature of the core. It is hypothesized therefore that, due to the small film to core temperature differences involved, the heat transfer to the core by convection and conduction is negligibly small compared to the heat transferred to form vapor directly in the film and at the interface.
4. Supply of liquid from the core to the liquid film takes place by a process akin to turbulent diffusion. The net flow of liquid to the film by this process is superimposed on the mean flow of steam away from the liquid film.
5. The critical heat flux condition occurs when the liquid consumption rate in the film, due to steam formation, exceeds the net liquid supply rate from the core.

Figure VII-1A is an idealized representation of the general flow pattern assumed according to hypothesis 1. A wavy irregular liquid film

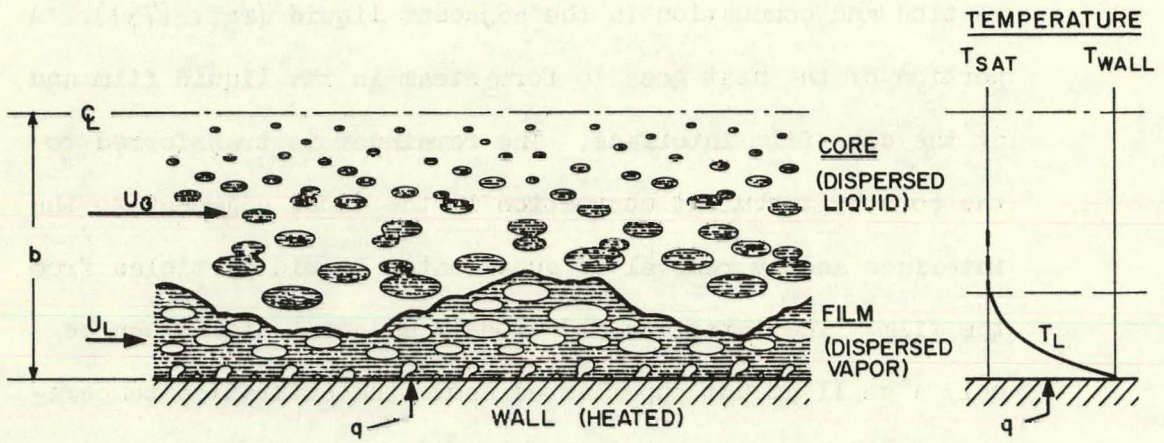


A. REPRESENTATION OF ACTUAL SYSTEM

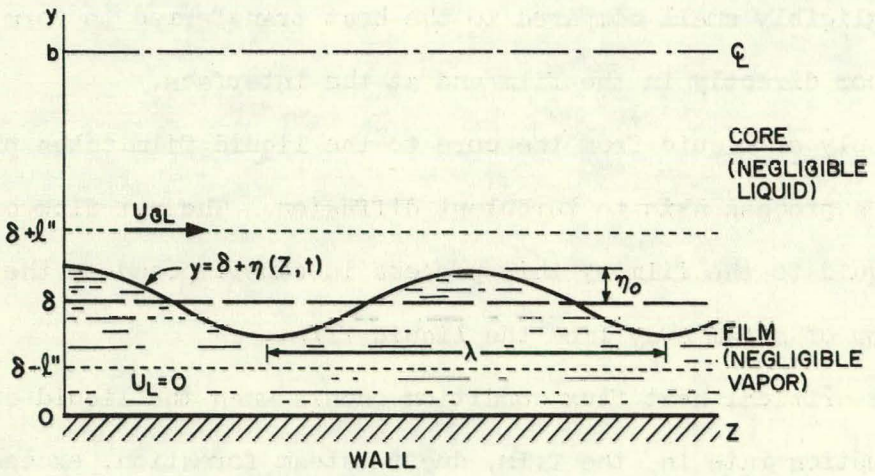


B. REPRESENTATION OF IDEALIZED SYSTEM
FOR FILM STABILITY ANALYSIS

FIGURE VII-1

flows along the heated wall, with bubbles forming at the wall surface and steam being carried along as irregular bubbles in the film. The faster flowing core is represented as continuous vapor carrying discrete particles or conglomerates of liquid.

Hypothesis 2 is applied in Part A to develop an approximate analysis describing the condition of instability of the film-core interface. In order to make the problem tractable but still preserve the essential character of interface motion at incipient instability, it is assumed for Part A that the liquid borne in the core and the vapor formation in the film have a negligible effect and, hence, that the core and film have the densities $\rho_g$ and $\rho_L$. The fluids are assumed to be in potential flow, with the resulting restriction that viscous shear effects are negligible in the region of the interface.

Results of Part A are used in Part B to relate the thickness of the liquid film at the condition of instability to the common properties of the flow. The wave motion on the interface is assumed to be dominated by the turbulence. Since the essence of this part of the problem is the local turbulent motion and momentum transfer at the interface, the fluid is considered to be in fully developed turbulent flow for Part B, in contrast to the assumption of potential flow to develop the underlying stability analysis in Part A. The essential features of the motion, for the purposes of Part B, are developed from the approximate Prandtl mixing length theory of turbulence.

In Part C a mixing length representation of the process of turbulent diffusion is developed, using hypothesis 4, to relate the liquid supply rate from the core to the mean liquid film thickness. This result, together with the expression for the liquid film thickness

obtained in Part B, is then used in conjunction with hypotheses 3 and 5 to form a simple material and energy balance which expresses the critical heat flux in terms of the fluid properties and common properties of the flow.

The densities of the core and film are assumed to be those of the pure vapor and the pure liquid, respectively, for the analyses in Parts A and B. This idealization is justified on the basis of the considerable simplification it provides and the fact that the relevant features of the motion are preserved in both cases. In contrast, for Part C the essential feature of the problem is turbulent diffusion of liquid to the interface from the core, which depends on the local liquid concentration. Consequently, for Part C the core is considered to be carrying liquid dispersed in continuous vapor, as depicted in Figure VII-1A.

The result of the analysis, expressed by equation (52), is applied in Section VIII to a selection of all available critical heat flux data, for the purpose of investigating the characteristics of the data and to test the validity of equation (52).

## A. Analysis of the Liquid Film Stability

The two-phase flow system is represented by Figure VII-1B. The liquid film of thickness $\zeta$ is adhered to the wall and has at its interface a wave structure taken to be of sinusoidal form $\eta(z,t) = \eta_0(t)\cos(kz-\omega t)$. This representation of the interfacial waves may be assumed to be a single term from a possible series of such terms which could be constructed from a Fourier analysis to describe the complete surface. The coordinate system is considered to be moving with the general flow so that the liquid film velocity is zero and the velocity

of the gaseous core at $y = \delta + \ell''$ is the effective relative velocity $U_{gL}$. Strictly, the analysis is based on a discontinuity of stream velocity from zero to $U_{gL}$ across the interface. Since this is impossible for real fluids, correction is made in Part B by taking the velocity change to occur across a zone of influence extending from $y = \delta - \ell''$, $U(y) = U_L$ to $y = \delta + \ell''$, $U(y) = U_g$.

In order to make this part of the analysis tractable, the following idealizations are made: the density of the core is the density of the saturated vapor $\rho_g$ ; the density in the film is the density of the saturated liquid $\rho_L$ ; forces impressed on the film due to vapor formation within it or at its interface are ignored; the flow is two-dimensional; body forces are ignored; a definite interface exists between the liquid film and gaseous core, to the extent that there is the effect of a tangent force on the interface, corresponding to the physical property surface tension $\sigma$ , which acts to stabilize small disturbances of the liquid film surface; there is no motion at the wall.

The analysis is formulated using the method of small disturbances for a perfect fluid in potential flow (ref. (16)). The analysis in this Part is similar in general form to the analyses of free liquid sheets presented in refs. (17) and (18).

With the assumption of potential flow the continuity equations describing the gaseous core and the liquid film are, in terms of the velocity potentials $\phi_L$ and $\phi_g$ ,

$$\frac{\partial^2 \phi_L}{\partial z^2} + \frac{\partial^2 \phi_L}{\partial y^2} = 0 , \qquad 0 < y < \delta \qquad \text{(1a)}$$

$$\frac{\partial^2 \phi_g}{\partial z^2} + \frac{\partial^2 \phi_g}{\partial y^2} = 0 , \qquad \delta < y < \delta + \ell'' \qquad \text{(1b)}$$

wherein the velocity potentials are defined as usual by

$$u_L = -\frac{\partial \phi_L}{\partial z}\ ,\ u_g = -\frac{\partial \phi_g}{\partial z}\ ;\ v_L = -\frac{\partial \phi_L}{\partial y}\ ,\ v_g = -\frac{\partial \phi_g}{\partial y}$$

The process is specified by the boundary conditions on (1):

$$\operatorname{LIM}\left(\frac{-\partial \phi_L}{\partial y}\right)_{y \to \delta^-} = \dot{\eta}_0 \cos(kz - \omega t) + \omega \eta_0 \sin(kz - \omega t) \tag{2}$$

$$\left(-\frac{\partial \phi_L}{\partial y}\right)_{y=0} = 0 \tag{3}$$

$$\operatorname{LIM}\left(\frac{-\partial \phi_g}{\partial y}\right)_{y \to \delta^+} = \operatorname{LIM}\left[\frac{\partial \eta}{\partial t} + \frac{\partial \eta}{\partial z}\left(\frac{dz}{dt}\right)\right]_{y \to \delta^+}$$

$$= \dot{\eta}_0 \cos(kz - \omega t) + (\omega - k U_{gL})\, \eta_0 \sin(kz - \omega t) \tag{4}$$

$$\left(\frac{-\partial \phi_g}{\partial z}\right)_{y = \delta + \ell''} = U_{gL} \tag{5}$$

The length $\ell''$ is the half-width of the zone of influence around the interface. The motion of fluid beyond this zone at $y > \delta + \ell''$ is considered to not affect the interface.

A general form for $\phi_L$ which will satisfy (1a), (2) and (3) is, assuming a product solution for (1),

$$\phi_L = P_L'(y)\left[A \sin(kz - \omega t) + B \cos(kz - \omega t)\right]$$

Substituting this into (1a) gives the ordinary differential equation

$$\frac{d^2 P_L'}{dy^2} - k^2 P_L' = 0$$

which has the general solution

$$P_L'(y) = C e^{ky} + D e^{-ky}$$

Thus, the velocity potential for the liquid film has the form

$$\phi_L = \left(C e^{ky} + D e^{-ky}\right)\left(A \sin(kz - \omega t) + B \cos(kz - \omega t)\right) \tag{6}$$

with the derivative

$$-\frac{\partial \phi_L}{\partial y} = -k\left(C e^{ky} - D e^{-ky}\right)\left(A \sin(kz - \omega t) + B \cos(kz - \omega t)\right) \tag{7}$$

Boundary condition (3) together with (7) gives D = C. Using this result in (7), recalling that $(e^{ky}-e^{-ky})=2\sinh(ky)$, substituting the resulting form of (7) into boundary condition (2) and collecting like terms in the equation obtained gives

$$A = \frac{-\omega\eta_0}{2kC\sinh(k\delta)}$$

$$B = \frac{-\dot{\eta}_0}{2kC\sinh(k\delta)}$$

Finally, substitution of these quantities into (6), together with C = D and $(e^{ky}+e^{-ky}) = 2\cosh(ky)$, results for the velocity potential of the liquid film with

$$\phi_L = \frac{-\cosh(ky)}{k\sinh(ky)}\left[\omega\eta_0\sin(kz-\omega t) + \dot{\eta}_0\cos(kz-\omega t)\right] \qquad (8)$$

Derivatives of $\phi_L$ which will be used later are, all evaluated at the interface $y=\delta$:

$$(\partial\phi_L/\partial y)_{y=\delta} = -\omega\eta_0\sin(kz-\omega t) - \dot{\eta}_0\cos(kz-\omega t) \qquad (9a)$$

$$(\partial\phi_L/\partial z)_{y=\delta} = -\coth(k\delta)\left[\omega\eta_0\cos(kz-\omega t) - \dot{\eta}_0\sin(kz-\omega t)\right] \qquad (9b)$$

$$(\partial\phi_L/\partial t)_{y=\delta} = \frac{\coth(k\delta)}{-k}\left[2\omega\dot{\eta}_0\sin(kz-\omega t) - (\omega^2\eta_0 - \ddot{\eta}_0)\cos(kz-\omega t)\right] \qquad (9c)$$

For two-dimensional flow in the absence of body forces, density changes and viscous effects the Euler momentum equations are applicable (ref. (16), ch. 1):

$$\frac{\partial p}{\partial z} = -\rho\left[\frac{\partial u}{\partial t} + u\frac{\partial u}{\partial z} + v\frac{\partial u}{\partial y}\right] \quad ; \quad \frac{\partial p}{\partial y} = -\rho\left[\frac{\partial v}{\partial t} + u\frac{\partial v}{\partial z} + v\frac{\partial v}{\partial y}\right]$$

For potential flow with

$$u = -\partial\phi/\partial z \ , \ v = -\partial\phi/\partial y$$

so that

$$\frac{\partial v}{\partial z} = \frac{\partial u}{\partial y}$$

the momentum equations can be expressed as

$$\frac{\partial p}{\partial z} = \rho\left[\frac{\partial^2\phi}{\partial t\partial z} - u\frac{\partial u}{\partial z} - v\frac{\partial v}{\partial z}\right]\ ;\quad \frac{\partial p}{\partial y} = \rho\left[\frac{\partial^2\phi}{\partial t\partial y} - u\frac{\partial u}{\partial y} - v\frac{\partial v}{\partial y}\right]$$

Integrating these with respect to their space coordinates gives for each

$$p = K'' + \rho\left[\frac{\partial\phi}{\partial t} - \frac{1}{2}(u^2+v^2)\right]\ ,\ K'' = \text{constant}$$

In terms of the velocity potential $\phi$ this becomes

$$p = K'' + \rho\left[\frac{\partial\phi}{\partial t} - \frac{1}{2}\left\{\left(\frac{\partial\phi}{\partial z}\right)^2 + \left(\frac{\partial\phi}{\partial y}\right)^2\right\}\right] \qquad (10)$$

In order to permit derivation of a linear differential equation of motion of the interface the idealization will be assumed that the disturbance amplitude $\eta_0$ and its derivative $\dot{\eta}_0$ are small so that terms containing their products as factors may be taken as negligible. This idealization restricts the analysis to determination of conditions for which an infinitesimal disturbance will grow. Consideration of (9a,b) together with (10) shows that the physical implication of this assumption is that the kinetic energy of motion $\frac{\rho}{2}(u^2+v^2)$ is small compared with the quantity $\rho\frac{\partial\phi}{\partial t}$, which is proportional to the acceleration.

With this idealization, substitution of equations (9) into (10) gives for the total pressure of the liquid film at the interface $y = \delta$

$$p_i = K_L'' - \frac{\rho_L}{k}\coth(k\delta)\left[2\omega\dot{\eta}_0\sin(kz-\omega t) - (\omega^2\eta_0 - \ddot{\eta}_0)\cos(kz-\omega t)\right] \qquad (11)$$

The pressure of the gaseous core at the interface can be derived in a similar fashion as follows.

A general form for $\phi_g$ which will satisfy (1b), (4) and (5) is

$$\phi_g(y) = P_g'(y)\left[E\sin(kz-\omega t) + F\cos(kz-\omega t)\right] - U_{gL}\,z$$

Substituting this into (1b) gives the ordinary differential equation

$$\frac{d^2P_g'}{dy^2} - k^2P_g = 0\ ,$$

which has the general solution

$$P_g'(y) = He^{ky} + Je^{-ky}$$

Thus, the velocity potential for the gaseous core has the form

$$\phi_g = \left(He^{ky} + Je^{-ky}\right)\left(E\sin(kz-\omega t) + F\cos(kz-\omega t)\right) - U_{gL}z \tag{12}$$

with the derivatives

$$-\partial\phi_g/\partial y = -k\left(He^{ky} - Je^{-ky}\right)\left(E\sin(kz-\omega t) + F\cos(kz-\omega t)\right) \tag{13a}$$

$$-\partial\phi_g/\partial z = -k\left(He^{ky} + Je^{-ky}\right)\left(E\cos(kz-\omega t) - F\sin(kz-\omega t)\right) + U_{gL} \tag{13b}$$

Boundary condition (5) together with equation (13b) gives

$$\frac{H}{J} = -e^{-2k(\delta'+\ell'')} \tag{14a}$$

Combining equation (13a) with boundary condition (4) and collecting like terms in the equation obtained gives

$$k\left(He^{k\delta'} - Je^{-k\delta'}\right)E = -(\omega - kU_{gL})\eta_0 \tag{14b}$$

and

$$\frac{F}{E} = \frac{\dot{\eta}_0}{\eta_0(\omega - kU_{gL})} \tag{14c}$$

Combining equations (14a) and (14b),

$$EJ = \eta_0(\omega - kU_{gL})e^{k\delta'}/k\left(1 + e^{-2k\ell''}\right) \tag{14d}$$

Substitution of equations (14a), (14c) and (14d) into (12) gives finally for the velocity potential of the gaseous core

$$\phi_g = \frac{e^{-k(y-\delta')}}{k\left(1+e^{-2k\ell''}\right)}\left[1 - e^{2k(y-\delta'-\ell'')}\right]\left[\eta_0(\omega - kU_{gL})\sin(kz-\omega t) + \dot{\eta}_0\cos(kz-\omega t)\right] - U_{gL} \tag{15}$$

Derivatives of $\phi_g$ evaluated at the interface $y=\delta'$, which will be

used later are:

$$\left(\partial\phi_g/\partial y\right)_{y=\delta} = -\left[\eta_0(\omega - k U_{gL})\sin(kz-\omega t) + \dot{\eta}_0\cos(kz-\omega t)\right] \tag{16a}$$

$$\left(\partial\phi_g/\partial z\right)_{y=\delta} = \tanh(kl'')\left[\eta_0(\omega - kU_{gL})\cos(kz-\omega t) - \dot{\eta}_0\sin(kz-\omega t)\right] - U_{gL} \tag{16b}$$

$$\left(\frac{\partial\phi_g}{\partial t}\right)_{y=\delta} = \frac{\tanh(kl'')}{k}\left[(2\omega - kU_{gL})\dot{\eta}_0\sin(kz-\omega t) - \left(\omega\eta_0(\omega - kU_{gL}) - \ddot{\eta}_0\right)\cos(kz-\omega t)\right] \tag{16c}$$

Substituting the derivatives (16a), (16b) and (16c) into the integrated momentum equation (10) and again discarding terms having as factors the products of $\eta_0$ and $\dot{\eta}_0$ gives finally for the total pressure of the gas at the interface $y = \delta$

$$p_g = K_y'' - \frac{\rho_g U_{gL}^2}{2} + \frac{\rho_g \tanh(kl'')}{k}\left[2\dot{\eta}_0(\omega - kU_{gL})\sin(kz-\omega t) + \left\{\ddot{\eta}_0 - \eta_0(\omega - kU_{gL})^2\right\}\cos(kz-\omega t)\right] \tag{17}$$

The interface between the liquid film and the gaseous core is considered to be unbroken and subject to a unit tension $\sigma$. As a simplification it is assumed that all deflections of the interface are two-dimensional only in the $y$-$z$ plane. A force balance will be made across the interface using equations (11) and (17) in conjunction with the normal forces caused by the surface tension property $\sigma$ when the surface is curved.

Consider a short curved segment of the interface of arc length $\Delta S$ subtending a correspondingly small angle $\Delta\theta$ at the center of curvature (Fig. VII-2). $\Delta S$ and $\Delta\theta$ are considered to be sufficiently small that the arc may be approximated as a segment of a cylindrical surface of radius R. The gaseous core pressure $p_g$ acts normal to the surface on one side of the segment and immediately opposite on the other side the liquid film pressure $p_l$ acts.

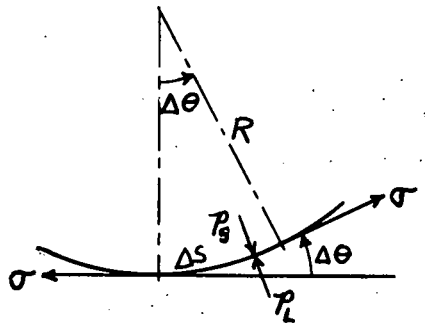


Fig. VII-2: REPRESENTATION OF INTERFACE FORCES

For the interface segment in equilibrium a resolution of forces gives, for $\Delta\theta$ and $\Delta S$ small, $(p_g - p_L)\Delta S = \sigma \tan(\Delta\theta)$

$$\cong \sigma(\Delta\theta)$$

Also $$\frac{\Delta\theta}{\Delta S} = \frac{1}{R}$$

Hence, $$p_g - p_L = \frac{\sigma}{R}$$

Now, $$R = \left[1 + (\partial y/\partial z)^2\right]^{3/2} \Big/ \frac{\partial^2 y}{\partial z^2}$$

so that for small curvature,

$$\frac{1}{R} \cong \frac{\partial^2 y}{\partial z^2} = \frac{\partial^2 \eta}{\partial z^2} \quad , \quad y = s$$

Recalling from the initial statement of the problem that $\eta = \eta_0 \cos(kz - \omega t)$ and combining the foregoing relations gives for the pressure difference across the interface

$$p_g - p_L = -\sigma k^2 \eta_0 \cos(kz - \omega t) \qquad (18)$$

Consistent with the basic assumption of the analysis that single-valued velocity potentials $\phi_L$ and $\phi_g$ exist, it may be assumed that the small disturbance motion $\dot{\eta}_0$ and its amplitude $\eta_0$ have arisen from rest and are superimposed on the general motion described at the beginning

by $U_{gL}$ (ref. (16), ch. 2). With this consideration the initial condition is taken as $\eta_0 , \dot{\eta}_0 , \ddot{\eta}_0 = 0$ so that by combination of (11), (17) and (18) the arbitrary constants $K_L''$ and $K_g''$ can be found to be related according to

$$K_L'' = K_g'' - \frac{1}{2} \rho_g U_{gL}^2 \tag{19}$$

Combining equations (11), (17), (18), and (19),

$$2\dot{\eta}_0 \left[ (\omega - k U_{gL}) \tanh(k\ell'') + \frac{\rho_L}{\rho_g} \omega \coth(k\delta') \right] \sin(kz - \omega t) +$$

$$+ \left\{ \left[ \frac{\rho_L}{\rho_g} \coth(k\delta') + \tanh(k\ell'') \right] \ddot{\eta}_0 - \left[ (\omega - k U_{gL})^2 \tanh(k\ell'') + \frac{\rho_L}{\rho_g} \omega^2 \coth(k\delta') - \frac{\sigma k^3}{\rho_g} \right] \eta_0 \right\} \cos(kz - \omega t) = 0 \tag{20}$$

The coefficients of the sine and cosine terms in (20) must be identically zero. Therefore,

$$\left[ (\omega - k U_{gL}) \tanh(k\ell'') + \frac{\rho_L}{\rho_g} \omega \coth(k\delta') \right] \dot{\eta}_0 = 0 \tag{21a}$$

and

$$\ddot{\eta}_0 - \frac{(\omega - k U_{gL})^2 \tanh(k\ell'') + \frac{\rho_L}{\rho_g} \omega^2 \coth(k\delta') - \sigma k^3 / \rho_g}{\frac{\rho_L}{\rho_g} \coth(k\delta') + \tanh(k\ell'')} \eta_0 = 0 \tag{21b}$$

Since $\dot{\eta}_0$ is not in general zero, equation (21a) establishes a relationship between the wave frequency $\omega$ and the wave number $k = \frac{2\pi}{\lambda}$ as

$$\omega = \frac{k U_{gL}}{1 + \frac{\rho_L}{\rho_g} \frac{\coth(k\delta')}{\tanh(k\delta')}} \tag{22}$$

The remainder of the analysis proceeds using equations (21b) and (22) as the principal working equations.

In particular, the second-order differential equation (21b) is seen to be linear and homogeneous with the form

$$\ddot{\eta}_0 + \beta'^2 \eta_0 = 0 \tag{23}$$

where

$$\beta'^2 = -\frac{(\omega - k U_{s1})^2 \tanh(k\ell'') + \frac{\rho_l}{\rho_g}\omega^2 \coth(k\delta') - \frac{\sigma k^3}{\rho_g}}{\frac{\rho_l}{\rho_g}\coth(k\delta') + \tanh(k\ell'')} \tag{23a}$$

If $\beta'$ is real and $\beta'^2 > 0$, then the solution of (23) can be expressed as

$$\eta_0(t) = C_1 \cos\beta' t + C_2 \sin\beta' t \,, \quad \beta'^2 > 0 \tag{24a}$$

Therefore, for $\beta'^2 > 0$, $\eta_0$ is periodic but has a finite amplitude, and the interface is stable.

If $\beta'$ is real and $\beta'^2 = 0$, equation (23) reduces to

$$\ddot{\eta}_0 = 0$$

with the solution

$$\eta_0(t) = C_1' t + C_2' \,, \quad \beta'^2 = 0 \tag{24b}$$

Therefore, for $\beta'^2 = 0$, $\eta_0$ either grows or subsides linearly with time, or it is constant, according to whether $C_1' = \dot{\eta}_0$ is positive, negative or zero. Since $\eta_0$ is considered to be the amplitude of displacement of the interface due to disturbance from a previously flat condition, it follows that $\dot{\eta}_0 = \dot{\eta}_0(0) > 0$. Thus, if $\beta'^2 = 0$ the amplitude $\eta_0$ of a small disturbance will grow linearly with time according to (24b) until eventually, due to the effect of heretofore neglected aspects, the interface disintegrates.

Finally, if $\beta'$ is imaginary, corresponding to $\beta'^2 < 0$ so that $\beta' = i\beta$ where $\beta$ is real, then the solution of (23) is

$$\eta_0(t) = C_1'' e^{-\beta t} + C_2'' e^{\beta t} \,, \quad \beta'^2 < 0 \tag{24c}$$

Therefore, according to the form of (24c), for $\beta'^2 < 0$ the amplitude $\eta_0$ will grow exponentially with time until the interface disintegrates.

From the results expressed by (24a,b,c) it is evident that a necessary condition for stability of the interface is $\beta'^2 > 0$. Therefore, using equation (23a) together with (22) obtains the corresponding relation for the condition of stability in terms of the wave number $k = 2\pi/\lambda$ as

$$k > \frac{\rho U_{gL}^2/\sigma}{\coth(k\ell'') + \frac{\rho_g}{\rho_L}\tanh(k\delta')} \tag{25a}$$

Equation (25a) defines the range of wave numbers for which the interface is stable, to the extent that a small disturbance of the interface will have a peak amplitude $\eta_0$ which does not grow indefinitely with time.

The critical wave-length $\lambda_c = \frac{2\pi}{k_c}$, corresponding to $\beta'^2 = 0$, is then, from (25a),

$$\lambda_c = \frac{2\pi\sigma}{\rho_g U_{gL}^2}\left[\coth(k\ell'') + \frac{\rho_g}{\rho_L}\tanh(k\delta')\right] \tag{25b}$$

The critical wave-length $\lambda_c$, given by (25b), is the least wave length of simple sinusoidal disturbances which will grow with time to cause instability of the interface. Hence, $\lambda_c$ is the disturbance wave-length for incipient instability.

The growth rate $\dot{\eta}_0(t)$ for disturbances of wave length greater than $\lambda_c$ is found by differentiation of (24c) to be

$$\dot{\eta}_0(t) = \beta\left[C_1'' e^{\beta t} - C_1'' e^{-\beta t}\right]$$

Thus, the growth rate $\dot{\eta}_0(t)$ is proportional to $\beta = -i\beta'$. The growth factor $\beta$ is found for later use by combining equations (23a) and (22) to obtain

$$\beta = \frac{k U_{gL}}{\left[\frac{\rho_L}{\rho_g}\coth(k\delta') + \tanh(k\ell'')\right]^{1/2}}\left\{\frac{1}{\coth(k\ell'') + \frac{\rho_g}{\rho_L}\tanh(k\delta')} - \frac{\sigma k}{\rho_g U_{gL}^2}\right\}^{1/2} \tag{26}$$

The analysis in Part B will employ equations (25b) and (26) to derive an estimate of the liquid film thickness corresponding to the interface being in the unstable condition.

B. Analysis of the Liquid Film Thickness

In this Part an attempt is made to relate the gross properties of the turbulence (i.e., the magnitude of the fluctuating turbulent velocity components and the scale or size of the turbulent eddies) to the dynamical condition of the interface. Thereby, using equations (25b) and (26), an estimate is made of the liquid film thickness in terms of the fluid properties and the properties of the mean flow. The analysis is restricted to those cases for which the Reynolds number of the mean flow is sufficiently large that the turbulence at the interface is fully developed (negligible viscous shear).

The Prandtl "mixing length" theory is employed to describe the statistical properties of the turbulent motion in terms of mean quantities. Although it is approximate, the method has the virtue of simplicity and in several applications, such as the generalizing of velocity profiles for turbulent flow across surfaces, prediction of shear stresses on surfaces and prediction of the spreading of jets, it has provided a basis for estimates which are in rather good agreement with experimental measurements (ref. (25)).

In analogy to the theory of molecular diffusion the statistical effect of the turbulence on the mean flow is represented by the transverse movement of discrete masses of fluid from one layer in the stream, where their transport properties are the mean values of those of the neighboring fluid, to adjacent layers a transverse distance $\ell'$ away,

where they mix with the fluid in the new neighborhood, thereby causing their transport properties to become the same as the mean values of those of the fluid in the new neighborhood. Continual repetition of this process along the stream causes net transfer of mass, heat or momentum in the direction of the gradients of intensity of the respective transport properties, density or mass concentration, temperature, or velocity.

Consider the variation of a transport property $\zeta$ in a direction normal to the mean flow along a wall, in the vicinity of a plane located at $y_o$ . The local mean value of $\zeta$ is considered to vary with distance from the wall, according to $\zeta = \zeta(y)$, but is independent of $z$ . $u'$ and $v'$ are the square roots of the mean squares of the fluctuating turbulent velocity components in the $z$ and $y$ directions, respectively (Fig.VII-3).

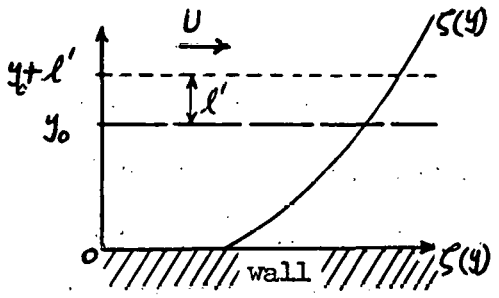


Fig. VII-3: MIXING ZONE AND GRADIENT OF $\zeta$

Imagine a lump of fluid, located initially at $y_o$ where it had the value of $\zeta = \zeta(y_o)$, to move with the time average velocity $v'$ normal to the main flow to a new position at $y = y_o + \ell'$ where it mixes with the fluid there and loses its identity. At the same time imagine another lump of fluid of the same dimensions, located initially at $y_o + \ell'$ where it had the value of $\zeta = \zeta(y_o + \ell')$, to move simultaneously with the same time average velocity $v'$ normal to the main flow to a new position at $y = y_o$ where it mixes with the fluid there and loses its identity. Assume that both lumps of fluid have lineal dimensions approximately equal to $\ell'$ and

that their time of transfer is $t'' = \ell'/v'$. Consider that this sort of exchange of fluid between $y_o$ and $y_o + \ell'$ is repeated continually, thereby causing net transfer of the transferable quantities associated with the transport property $\zeta$ from $y+\ell'$ to $y_o$ (assuming $\zeta(y_o+\ell') > \zeta(y_o)$ ) at the time average rate per unit area normal to $y$

$$Q_\zeta = v' \left[ \zeta(y_o+\ell') - \zeta(y_o) \right] \tag{27a}$$

Expansion of the quantity in brackets by a Taylor series for values of $y$ near $y_o$ and assuming that $\ell'$ is small so that all but the lead derivative term in the expansion can be dropped gives for the net flux

$$Q_\zeta(y) = -\ell' v' \left( \frac{d\zeta}{dy} \right) \tag{27b}$$

In general, $\ell'$ , $v'$ and the gradient $d\zeta/dy$ are functions of $y$ .

Equation (27b) is a slight generalization of the theory of momentum transfer in turbulent flow, as put forth by Prandtl. Take the mean local stream velocity $U$ to be constant with $z$ and variable with distance from the wall according to $U = U(y)$. Following Prandtl's assumption that momentum is a transferable quantity permits then the identification of the mean local momentum per unit volume as $\zeta = \rho U(y)$. With this identification $Q_\zeta$ is the mean flux of momentum per unit volume in the $y$ direction and, hence, is identified with the Reynolds stress $\tau = -\rho \overline{u_i v_i}$ wherein $u_i$ and $v_i$ are the local fluctuating turbulent velocity components (ref. (25)). Thus, taking the density $\rho$ as constant and substituting into (27b)

$$\tau = -\rho \overline{u_i v_i} = \rho \ell' v' \frac{dU}{dy} \tag{28}$$

The basic hypothesis of Prandtl's theory is that there is a length $\ell$, analogous to $\ell'$, so that[1]

$$-\overline{u_t v_t} = \ell^2 \left(\frac{dU}{dy}\right)\left|\frac{dU}{dy}\right|$$

Substitution of this into (28) gives Prandtl's equation for the turbulent shear stress

$$\tau = \rho \ell^2 \left(\frac{dU}{dy}\right)\left|\frac{dU}{dy}\right| \qquad (29)$$

As originally suggested by Prandtl, representing the mixing length $\ell$, for regions close to the wall, by

$$\ell = Ky \qquad (30)$$

where K = 0.4, gives rather good agreement between experimental data and shear stress and velocity profile predictions by equation (29).[2]

The liquid film is assumed to be always in a condition of instability with the maximum wave amplitude $\eta_0(t)$ at any point on the interface

---

[1] As mentioned by Goldstein (ref. (24), pg. 207), the idea underlying this hypothesis is the experimental evidence that the root-mean-square turbulent fluctuating velocity components $u'$ and $v'$ tend to be equal. If they were equal so that $|\overline{u_t}| = |\overline{v_t}|$, then $|\overline{u_t v_t}| = u'^2$. Since the momentum is assumed transferable so that $|\overline{u_t}| = u' = U(y+\ell') - U(y) = \ell'(dU/dy)$ for $\ell'$ small, then

$$-\overline{u_t v_t} = \ell'^2 (dU/dy)\left|dU/dy\right|$$

and, consequently, $\ell' = \ell$.

See ref. (27) for some recent experimental data for the fluctuating velocity components.

---

[2] Schlicting (ref. (25), pg. 408) presents the results of calculations of $\ell$ from Nikuradse's velocity profile measurements, using equation (29). The deviation of $\ell = 0.4y$ from these data varies from zero at the wall to about ±10%, at a distance from the wall of 0.10 times the pipe radius. $\ell/b$ apparently reaches a maximum of about 0.14 at the center of the pipe. According to these data $\ell$ is virtually independent of Reynolds number ($1.1 < 10^{-5}$ Re $< 32$) and has the same values for smooth and rough pipe walls.

tending to increase with time to some size for which the wave becomes distorted by the turbulent motion of the stream, particles of liquid may be torn off and carried away in the gaseous core, the wave subsides due to surface tension effects, other particles of liquid are deposited from the core, and the process repeats indefinitely.

Assuming that the motion near the interface is dominantly turbulent, it is hypothesized that the characteristic or dominant wave length of the interface $\lambda_c$ is related to the size scale of the turbulence. For flow near the wall, the scale of the turbulence appears to be nearly proportional to the "mixing lengths" $\ell$ and $\ell'$, which in turn are proportional to distance from the wall, for regions near the wall. Therefore, in the absence of complete information as to the dependence of the dominant wave length on distance from the wall (film thickness, $\delta$), $\lambda_c$ will be assumed to be proportional to the liquid film thickness,[3] according to

$$\lambda_c = K_1 \delta \tag{31}$$

The half-width of the zone of influence around the interface $\ell''$, used in equation (5) to define $U_{GL}$, is assumed to be identical with the turbulent mixing length $\ell'$, so that

$$\ell'' = \ell' = K_2 \delta \tag{32}$$

where $K_2 \approx K = 0.4$.

---

[3] The actual structure of the interface motion in turbulent two-phase flows has not yet been learned in detail. (See, for example, refs. (35), (19), (21), (22), (23).) While not conclusive, the few visual observations and measurements of the liquid film wave structure that have been reported (refs. (19), (29), (30), (34)) and the appearance of the liquid films shown in the high speed motion pictures taken during this investigation indicate that at least the trend expressed by equation (31) is in gross agreement with the physical evidence. The motion pictures indicate characteristic film wave lengths in the range $1 \lesssim \lambda_c/\delta \lesssim 5$ (Appendix D).

The half-length of the dominant waves on the interface are assumed to be approximately the same as the characteristic dimensions of the turbulent eddies near the interface $\ell'$. That is $\lambda_o \approx 2\ell' \approx 0.8\delta$, from equation (32). Hence, the order of magnitude of the dominant wave-length $\lambda_o$ is assumed to be the same as the film thickness $\delta$.[3]

With these assumptions and noting that by hypothesis 2 (pg.78) $\lambda_c < \lambda_o$, the hyperbolic functions containing $\delta$ and $\ell'$ in equations (25b) and (26) are nearly unity. Hence, using $k = 2\pi/\lambda$, equations (25b) and (26) reduce to

$$\lambda_c = \frac{2\pi\sigma}{\rho_g U_{gL}^2}\left(1 + \frac{\rho_g}{\rho_L}\right) \tag{33}$$

$$\beta = \frac{2\pi U_{gL}}{\lambda(\rho_g+\rho_L)}\left[\rho_L\rho_g - \frac{2\pi\sigma}{\lambda U_{gL}^2}(\rho_g+\rho_L)\right]^{1/2} \tag{34}$$

According to (24c), the amplitude $\eta_o$ of disturbances with wave lengths greater than $\lambda_c$ will grow exponentially with time in proportion to the magnitude of $\beta$. Depending on the variation of $\beta$ with $\lambda$, it is reasonable to expect that interface motion will be dominated by those disturbances which grow fastest. The fastest growing disturbances are those having a wave length $\lambda_m$ which maximizes the growth factor $\beta$. Thus, differentiating (34) with respect to $\lambda$, setting the result equal to zero and solving for $\lambda = \lambda_m$ gives

$$\lambda_m = \frac{3\pi\sigma}{\rho_g U_{gL}^2}\left(1 + \rho_g/\rho_L\right) \tag{35}$$

Due to the character of turbulent flow there exists a spectrum of disturbance wave-lengths extending from the dimensions of the molecular

motion up to within an order of magnitude of the duct dimensions.[4] In accord with hypothesis 2, disturbances of the interface having wave-lengths less than $\lambda_c$ can be ignored since their amplitude will remain small. Disturbances having wave-lengths larger than $\lambda_m$ can also be ignored because their growth rates will be no faster than those of disturbances with wave-lengths slightly less than or equal to $\lambda_m$. Thus, the dominant wave length $\lambda_o$ of the characteristic disturbance motion impressed on the interface by the turbulence may be assumed to be bounded according to $\lambda_c < \lambda_o < \lambda_m$.

Hence, assuming $\lambda_o$ is constant for a given flow condition, equations (33) and (35) can be used to express the dominant wave length as

$$\lambda_o = \frac{K_3 \sigma}{\rho_g U_{gL}^2} \left(1 + \rho_g/\rho_L\right) \tag{36}$$

where

$$2\pi < K_3 < 3\pi \tag{36a}$$

Substituting this into (31) gives for the corresponding liquid film thickness

$$\delta = \left(\frac{K_3}{K_1}\right) \frac{\sigma}{\rho_g U_{gL}^2} \left(1 + \rho_g/\rho_L\right) \tag{37}$$

According to the conceptual ideas of the analysis to this point, the actual liquid film thickness will tend to vary around a mean value given

---

[4] According to Dryden (ref. (36)), the scale of the turbulence in a particular flow may be expected to span the range from the microscopic sizes associated with the molecular motion up to a size scale determined by the size and geometry of the general flow path. See also the paper of Fage & Townend regarding their microscope observations of fluid motion near the wall in turbulent flow (ref. (63)).

by (37) as liquid is exchanged between the film and the gaseous core in consequence of the local turbulent motion. When the film is thicker than $\delta$ unstable disturbances will grow more rapidly causing a net transfer of liquid from the film to the gaseous core with consequent reduction of the film thickness. When the film is thinner than $\delta$ the disturbances will either become stable or will grow less rapidly thereby permitting a net transfer of liquid from the gaseous core to the film with consequent increase of the film thickness.

Finally, an estimate can be made of the effective relative velocity between the gaseous core and the liquid film, $U_{gL}$, using some of the preceding results of Prandtl's mixing length theory. In a manner similar to that used in the derivation of equation (27b) take the general property $\zeta$ to be, for $\rho$ constant, $\zeta(y) = \rho U(y)$.

Consider $y = \delta$, the location of the interface, surrounded by a zone of influence extending from $y = \delta - \ell''$, where $U = U_L$, the effective liquid film velocity, to $y = \delta + \ell''$, where $U = U_g$, the effective gaseous core velocity.[5] Identify the half-width of the zone of influence, $\ell''$, with the effective mixing length $\ell'$ (Fig. VII-4).

---

[5] The analysis in Part A proceeded with the implication of a discontinuity of velocity at the interface corresponding to the velocity difference $U_{gL}$. Actually, for turbulent flow at the interface it is more likely that the velocity will change sharply, but not discontinuously, at the interface over a mixing region or zone of influence extending on both sides of the interface a distance $\ell''$. $\ell''$ is assumed to be proportional to and approximately the same magnitude as the mixing length $\ell'$.

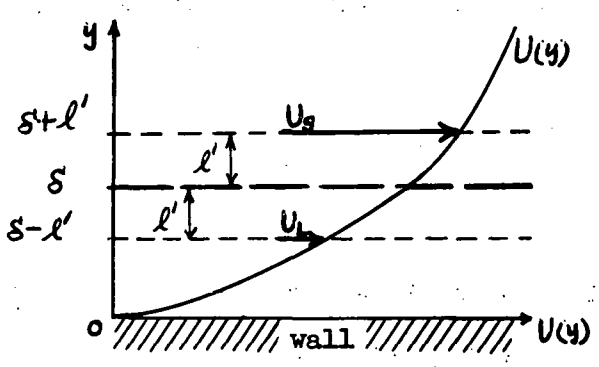


Fig. VII-4: MIXING ZONE AND GRADIENT OF U

The effective velocity of the gaseous core relative to the interface is then

$$U_{g_i} = U_g(\delta+\ell') - U_g(\delta)$$

Expanding this in a Taylor series and taking only the lead term, for $\ell'$ small, gives

$$U_{g_i} = \ell'\left(\frac{dU_g}{dy}\right)_{y=\delta}$$

Similarly, the effective liquid film velocity relative to the interface is

$$U_{L_i} = U_L(\delta-\ell') - U_L(\delta)$$

$$= -\ell'\left(\frac{dU_L}{dy}\right)_{y=\delta}$$

Therefore, the effective velocity difference across the interface is

$$U_{gL} = U_{gi} - U_{Li} = \ell'\left[\left(\frac{dU_g}{dy}\right) + \left(\frac{dU_L}{dy}\right)\right]_{y=\delta}$$

Recall the definition of the friction velocity $v_* = \sqrt{\tau/\rho}$ and, following Prandtl, consistent with the assumption $\ell' \propto \ell = Ky$ for regions near the wall,[6] assume that the shear stress is approximately

---

[6] See Schlicting, page 395 (ref. (25)).

constant across the film at the value for the wall $\tau_o$ , for thin films.

Then,

$$v_{*L} = \sqrt{\tau_o/\rho_L} \tag{38a}$$

and, for continuity of shear stress across the interface, and discontinuity of density from $\rho_L$ to $\rho_g$ ,

$$v_{*g} = \sqrt{\tau_o/\rho_g} = v_{*L}\sqrt{\rho_L/\rho_g} \tag{38b}$$

Substitution of these relations together with Prandtl's shear stress equation (29) into the foregoing relation for $U_{gL}$ and using equations (30) and (32) for the mixing lengths $\ell$ and $\ell'$ gives for the effective relative velocity between the gaseous core and the liquid film

$$U_{gL} = \left(\frac{K_2}{K}\right) v_{*L}\left[1 + \sqrt{\rho_L/\rho_g}\right] \tag{39}$$

Finally, substitution of (39) into equation (37) gives the expression for the liquid film thickness to be used in the remainder of the analysis

$$\delta = \frac{K_3 K_4 \sigma}{\rho_g v_{*L}^2} \cdot \frac{(1+\rho_g/\rho_L)}{(1+\sqrt{\rho_L/\rho_g})^2} \tag{40}$$

where the constants have been combined into

$$K_4 = \frac{1}{K_1}\left(\frac{K}{K_2}\right)^2 \tag{40a}$$

The friction velocity $v_{*L} = \sqrt{\tau_o/\rho_L}$ in equation (40) can be related to the mean properties of the two-phase flow as follows.

Using a method common in the field[7] the pressure gradient due to

[7] See refs. (38), (39), (40) for examples of typical correlations of $\Phi_{TPF}$ and comparisons with data. Fig. VII-6 shows the Martinelli-Nelson correlation of $\Phi_{TPF}$.

wall friction alone can be calculated from

$$(dp/dz)_{TPF} = \Phi_{TPF}\, f_F\, G^2/2\rho_L\, r_H$$

where $r_H = A_f/P_f$ , the hydraulic radius

$f_F = \tau_0 / \frac{G^2}{2\rho_L}$ , the Fanning friction factor[8]

$G$, mass velocity, average stream mass flow rate per unit flow area

$\Phi_{TPF} = (dp/dz)_{TPF} / (dp/dz)_0$ , two-phase friction multiplier[7]

$\left(\frac{dp}{dz}\right)_0$, friction pressure gradient for all of the fluid flowing as saturated liquid at the mass velocity G.

A force balance on a section of the channel of length dZ, cross-sectional area $A_f$ and total wetted area parallel to the flow $P_f dz$ gives, for steady two-phase flow,

$$A_f \left(\frac{dp}{dz}\right)_{TPF} dz = \tau_0 P_f dz$$

Thus,

$$(dp/dz)_{TPF} = \frac{\tau_0}{r_H}$$

Combining the two relations for $(dp/dz)_{TPF}$ and expressing $v_{*L} = \sqrt{\tau_0/\rho_L}$ gives for the friction velocity in two-phase flow

$$v_{*L} = \left(\frac{1}{2}\, \Phi_{TPF}\, f_F\right)^{1/2} \frac{G}{\rho_L} \qquad (41)$$

Substituting this into equation (40) gives as a final working equation for the liquid film thickness

$$\delta = \frac{2 K_3 K_4 \sigma \rho_L (1 + \rho_L/\rho_g)}{\Phi_{TPF}\, f_F\, G^2 \left(1 + \sqrt{\rho_L/\rho_g}\right)^2} \qquad (42)$$

---

[8] See refs. (41) and (42) for correlations of friction factor data. Note that $f_F = f/4$, using the Darcy-Weisbach form of f given by Moody (ref. (42)).

This expression will be used in the analysis of the critical heat flux condition in Part C.

C. Analysis of the Critical Heat Flux Condition

The condition associated with the critical heat flux is assumed to occur when the rate of liquid consumption in the film due to steam formation exceeds the maximum liquid supply rate due to turbulent diffusion of liquid particles from the core (hypothesis 5, page 79). At heat fluxes higher than the critical heat flux the liquid consumption rate in the film becomes increasingly larger than the liquid supply rate and consequently the film becomes increasingly thinner until finally there is insufficient liquid adjacent to the heated wall to provide complete "wetting" by liquid and a patch forms in which the wall is in direct contact with steam. As a consequence, due to the relatively poor heat transfer properties of steam in comparison to boiling liquid water, the temperature of the wall rises sharply to a level dependent on the average heat flux level and the flow conditions.[9] The average wall heat flux level at which this condition is incipient is defined as the "critical heat flux" $q_c$.

It is assumed for this part of the analysis that all but a negligible fraction of the heat transfer from the wall goes to form steam

---

[9] According to the experimental results (see also ref. (14)), the wall temperature typically may start to oscillate rather randomly at the onset of the critical condition, fluctuating between a value only slightly above that for stable nucleate boiling and a higher value approaching that corresponding to steady heat transfer in the liquid deficient or film boiling regime. It is postulated that this is due to alternate growth and collapse of the vapor patches caused by local turbulent flow fluctuations at the critical condition. (See recorder traces in Section VI.)

in the liquid film and at the vapor-film interface (hypothesis 3). Forces on the film due to steam formation are assumed to have a negligible effect on the film stability, and the effect on the local shear stresses and velocities due to liquid particles in the core and vapor in the film are ignored, so that the results from Parts A and B can be used directly. Net transfer of liquid from the core to the film is assumed to occur by a process of turbulent diffusion, described by equations (27a, b) (hypothesis 4).

Consider the general property $\zeta(y)$ in the derivation of equation (27a) in Part B to be the local time average concentration of liquid particles in the gaseous core near the interface so that

$$\zeta(y) = \rho_l \left[1 - \alpha_c(y)\right] , \quad y > \delta$$

where $\alpha_c(y)$ is the local time average vapor volume fraction in the gaseous core (Fig. VII-5).

Correspondingly, identify $Q_\zeta(y)$ in equation (27a) as the liquid transfer rate per unit interface area between the gaseous core and the liquid film due to turbulent diffusion, $G_d'$ .

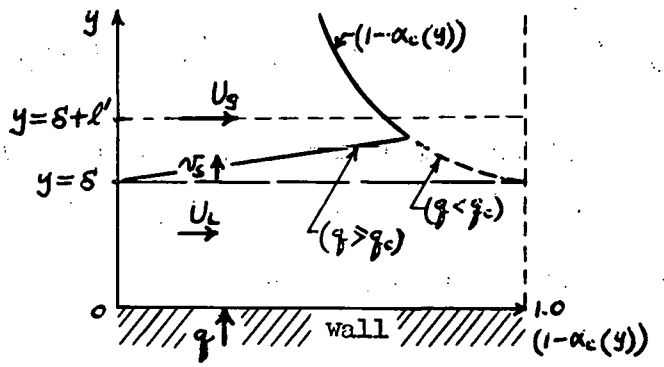


Fig. VII-5: LIQUID VOLUME FRACTION DISTRIBUTION AT THE CRITICAL CONDITION

Thus, using equation (27a), the net liquid mass diffusion flux to the interface due to turbulent diffusion is

$$G_d' = \rho_L v_{TPF}' \left[ (1-\alpha_c(\delta+\ell')) - (1-\alpha_c(\delta)) \right]$$

where $v_{TPF}'$ is the root-mean-square turbulent fluctuating velocity component for two-phase flow. There is in the vicinity of the interface a mean flow of steam in the $y$ direction away from the interface at the mean velocity

$$v_s = \frac{q}{\rho_g h_{fg}} ,$$

assuming all of the wall heat flux $q$ goes to form steam in the liquid film and at its interface (hypothesis 3). As a consequence of this mean flow of vapor there is a component mass flux of liquid away from the interface region at the rate $G_d'' = \rho_L v_s [1-\alpha_c(\delta+\ell')]$, assuming $\ell'$ is small. Due to entrainment of liquid particles torn from the interface there is an additional component mass flux of liquid leaving the interface at the net entrainment rate $G_d'''$. Summation of these component fluxes gives the net mass flux of liquid from the core to the interface, $G_d = G_d' - G_d'' - G_d'''$, as

$$G_d = \rho_L v_{TPF}' \left[ (1-\alpha_c(\delta+\ell')) - (1-\alpha_c(\delta)) \right] - \frac{q}{h_{fg}} \left( \frac{\rho_L}{\rho_g} \right) \left[ 1-\alpha_c(\delta+\ell') \right] - G_d''' \quad (43a)$$

Assuming all heat transferred goes to make steam in the film and at its interface, it follows from an energy and material balance, for steady-state conditions ($q < q_c$), that

$$G = \frac{q}{h_{fg}} \quad (43b)$$

It is postulated that when the critical heat flux condition exists, due to excess of liquid consumption over liquid supply to the film, the film thins slightly causing the interface instabilities to cease growing, thereby momentarily reducing the rate of entrainment of liquid

from the interface. At the limit as the film becomes thinner the local entrainment rate $G_d'''$ reduces to zero and all liquid adjacent to the film which comes in contact with the interface will be absorbed into the film due to surface tension effects.[10] At this condition turbulent diffusion of liquid from the core to the film will behave, in the limit, as though the interface were a sink corresponding to $[1-\alpha_c(\delta)]=0$. This condition is associated with the onset of the critical heat flux condition, corresponding to $q = q_c$ (Fig. VII-5). Thus, combining (43a) and (43b), with $q = q_c$, $G_d'''=0$ and $[1-\alpha_c(\delta)]=0$ gives for the critical heat flux

$$\left(\frac{q_c}{\rho_L h_{fg}}\right)\left[\frac{1}{1-\alpha_c(\delta+\ell')} + \frac{\rho_L}{\rho_g}\right] = v'_{TPF} \qquad (44)$$

There are no analyses which predict $v'_{TPF}$ and the only experimental measurements of turbulent fluctuating velocity components are for single-phase systems. According to the data of Laufer (ref. (27)), the root-mean-square turbulent fluctuating velocity component for single-phase flow is a function of distance from the wall, varying from zero at the wall to a maximum approximately equal to the friction velocity $v_*$ at a distance near the wall, and reducing slightly for the regions near the center of the duct. Variation of $v'$ with Reynolds number is small in the range of fully developed turbulence (Fig. VII-7).

In analogy with the character of $v'(y)$ for single-phase flow, the

---

[10] The term "surface tension" $\sigma$ is taken to mean the physical property of the exposed liquid surface (interface) behaving as though it were in uniform tension. Provided that momentarily there are no forces on the interface which exceed the forces arising from the surface tension (as is assumed here), the surface will flatten and liquid particles which contact the interface immediately become part of the surface system and are pulled into the film (see ref. (43), ch. 6).

effective turbulent fluctuating velocity component for two-phase flow $\nu'_{TPF}(y)$ is assumed for this part of the analysis to be represented adequately near the wall by a simple power law of the form[11]

$$\nu'_{TPF}(y) = K' \nu_* (y/b)^m \qquad (45)$$

where $K'$ and $m$ are constants and $b$ is the radius, for circular pipes, and the hydraulic radius $r_H = A_f/P_f$, for thin rectangular ducts and annuli.[12]

Substituting equation (45) into (44) and evaluating at the interface, $y = \delta$, yields for the critical heat flux in terms of the liquid film thickness

$$\frac{q_{fc}}{\rho_L \sqrt{R/\rho_g}\ \nu_{*L}\ h_{fg}} \left[ \frac{1}{1 - \alpha_c(\delta + \ell')} + \frac{\rho_L}{\rho_g} \right] = K' \left( \frac{\delta'}{b} \right)^m \qquad (46)$$

---

[11] Equation (45) can be considered to be the lead term of a possible power series describing $\nu'_{TPF}$ exactly. This expression of $\nu'_{TPF}$ as a function of distance from the wall is in accord with Laufer's data for single-phase flow, for regions near the wall (Fig. VII-7); it is, however, at variance with the assumption implicit in the mixing length theory, used in preceding parts of the analysis, that $\nu' = \nu_*$. The mixing length theory is justified on the grounds that the single-phase velocity distributions and shear stresses predicted with it are correct in magnitude and trends (ref. (25)). In contrast, for this part of the analysis the essential feature being examined is the variation of turbulent liquid diffusion rate with distance from the wall, and consequently, for the line of attack taken, it is necessary here to consider the corresponding variation of $\nu'_{TPF}$.

---

[12] Laufer's results, given in Fig. VII-7 for a 10-in. diameter pipe, agree well with his earlier data for a rectangular channel (ref. (26)) for $y/b > .05$, if $b$ is taken as the pipe radius in the first case and as the hydraulic radius $r_H$ for the rectangular channel.

For rectangular channels of large aspect ratio $r_H$ approaches the channel half-width. For concentric annuli of radius ratios not far from unity the appropriate value of $b$ would be, by inference, half of the radius difference, which is identical with $r_H$. These definitions of $b$ are in general agreement with usual procedures for prediction of mean velocity profiles from mixing length theory and prediction of turbulent wall shear stresses in ducts (ref. (25), chs. 19 and 20).

wherein the friction velocity, from equation (45), is taken as that for the core, $v_{*g} = \sqrt{\frac{\tau_c}{\rho_g}} = v_{*L}\sqrt{\rho_L/\rho_g}$ , assuming continuity of shear stress and discontinuity of density from $\rho_L$ to $\rho_g$ across the interface. The constants $K'$ and $m$ will be evaluated in combination with other constants by comparison of the final theoretical relation for $q_c$ with the measured critical heat flux data (Section VIII). In this way variations between $\varepsilon_{TPF}(y)$ for two-phase flow and that for single-phase flow will be accounted for.[13]

No data nor reliable means of prediction are yet available giving the transverse steam volume fraction distribution in heated channels with bulk boiling.[14] Consequently, in order to proceed, the steam volume fraction distribution in the core part of the channel flow, $\alpha_c(y)$ will be assumed to be approximately uniform at an effective average value for the core, $\bar{\alpha}_c$ . Thus,

$$\alpha_c(\delta+\ell') \approx \bar{\alpha}_c \qquad (47)$$

It is usual to express the average steam volume fraction for the overall channel cross-section in terms of an effective average phase

---

[13] According to analysis and data given by Longwell and Weiss in ref. (45), the diffusion rates for liquid droplets in a gas stream can be substantially less than for single-phase diffusion, due to inertia effects of the higher density droplets. In effect, for the application here, this would tend to make $\varepsilon_{TPF}(y)$ less than Laufer's data.

[14] Levy has prepared an analytical prediction of the density distribution for two-phase flow in unheated ducts which agrees well with available data for air-water systems (refs. (46) and (47)). It is possible Levy's method could be extended for application at the critical heat flux condition. Petrick's data indicates an almost parabolic variation of $\alpha(y)$ from the maximum at the channel centerline for low pressure air-water flows (ref. (48)).

velocity ratio $S = \bar{U}_g/\bar{U}_L$ and the steam quality as [15]

$$\frac{\bar{\alpha}}{1-\bar{\alpha}} = \frac{1}{S}\left(\frac{\rho_L}{\rho_g}\right)\frac{X}{1-X} \qquad (48)$$

Since neither experimental data nor analytical methods are yet available to relate $\bar{\alpha}_c$ to $\bar{\alpha}$, the relationship is assumed to be

$$\frac{\bar{\alpha}_c}{1-\bar{\alpha}_c} = K_S\frac{\bar{\alpha}}{1-\bar{\alpha}} = C'\left(\frac{\rho_L}{\rho_g}\right)\frac{X}{1-X}, \qquad (49)$$

where $K_S$ is a constant and $C' = K_S/S$.

In effect, $K_S$ serves as a correction factor to account for the reduced liquid concentration in the core due to accumulation in the liquid film on the wall. Hence, it is expected that $K_S > 1$, corresponding to $(1-\bar{\alpha}_c) < (1-\bar{\alpha})$. It is reasonable to expect that $K_S$ is not actually a constant but rather will vary to some extent with the steam quality, pressure, mass velocity and other system variables which affect the thickness of the liquid film relative to the duct wall spacing. The velocity ratio $S$ is also subject to some variance with system conditions (footnote 15). Hence, the degree of variation of $C'$ and whether it

---

[15] Contrary to the prediction of equation (48), $\bar{\alpha}(0)$ may be greater than zero in heated ducts, depending on the excess of the wall surface temperature over the saturation temperature (refs. (50), (51), (52); also ref. (54)). In Figure VII-8 are plots of Larson's data at 1015 psia for flow in an unheated tube; data of Foglia, et.al., at 1030 psia with a wall heat flux of 557,000 Btu/hr-ft$^2$; and values calculated with equation (48) using S = 1.0 and 2.0. For the heated wall data, $\bar{\alpha}(0) = 0.1$. The heated and unheated data appear to be in agreement for $X > .05$. Calculated values for S = 1.0 are higher than the data, except at near $X \cong 0$, indicating $\bar{U}_g > \bar{U}_L$. Calculated values for S = 2.0 are in reasonably good agreement with the data for $X > .03$. The trend of deviation of the calculations from the data for S = 2.0 is to predict slightly low at the lower range of steam qualities and to cross through the data to predict slightly high at the higher range of steam qualities. This trend indicates that S tends to increase at the higher qualities. It is possible that the increase of S at higher steam qualities is due to increased fraction of the liquid being held in the slower moving film at the wall.

approaches being a constant over a range of system variables cannot be concluded at this point.

Introduction of $\alpha_c(\delta+\ell')=\bar{\alpha}_c$ into (49) from equation (47) gives after rearrangement

$$\frac{1}{1-\alpha_c(\delta+\ell')} = 1 + C'\left(\frac{\rho_L}{\rho_g}\right)\frac{X}{1-X} \tag{50}$$

Substitution of equation (50) into equation (46) gives for the critical heat flux in terms of $X_c$, $v_{*L}$, $\delta/b$ and the fluid properties

$$\frac{q_c}{\rho_L\sqrt{\rho_L/\rho_g}\, v_{*L}\, h_{fg}}\left[1+\left(1+C'\frac{X_c}{1-X_c}\right)\frac{\rho_L}{\rho_g}\right] = K'\left(\frac{\delta}{b}\right)^m \tag{51}$$

Finally, substitution into (51) from equation (41) for the friction velocity $v_{*L}$ and from equation (42) for the liquid film thickness $\delta$ gives after rearrangement

$$q_c = C''\frac{\psi^m}{\xi} \tag{52}$$

where

$$\psi = \frac{\sigma\rho_L(1+\rho_L/\rho_g)}{\Phi_{TPF} f_F G^2 b\left(1+\sqrt{\rho_L/\rho_g}\right)^2} \tag{52a}$$

$$\xi = \frac{1+\left(1+C'\frac{X_c}{1-X_c}\right)\frac{\rho_L}{\rho_g}}{\left(\frac{\rho_L}{\rho_g}\Phi_{TPF} f_F\right)^{1/2} G\, h_{fg}} \tag{52b}$$

$$C'' = \frac{2^m}{\sqrt{2}} K'(K_3K_4)^m \tag{52c}$$

The length $b$ is the radius for circular ducts and the hydraulic radius $r_H = A_f/P_f$ for rectangular and concentric annular ducts (see footnote 12). Other quantities are defined in the Nomenclature.

Equation (52) is the final form of the derived critical heat flux

relation for application to the experimental critical heat flux data (Section VIII). The method of application will be to determine values of the constants $C'$, $C''$ and $m$ which cause predictions with (52) to agree best with the critical heat flux data. Since the available data cover a wide range of duct geometries and flow conditions for water, the degree to which (52) can correlate the data will provide basis for an assessment of the general validity of the analysis of this Section and the usefulness of equation (52).[16]

A value of m = 0.75 is found in Section VIII to result with reasonably good agreement between calculations and experimental data, for $f_F \sim G^{-0.2}$. Using this value some of the trends of variation of $q_c$ calculated by equation (52) over the range of steam qualities $0 \leq X_c < 1$ are:

(1) $q_c$ decreases monotonically with increasing steam quality $X_c$.

(2) $q_c$ decreases monotonically with increasing pressure (over the range examined, 585 to 2500 psia).

(3) $q_c$ decreases with increased mass velocity G.

(4) $q_c$ decreases with increased duct size b ($b \sim D_e$).

Further discussion of these trends is given in Sections VIII and IX.

---

[16] Analysis is continued in Appendix F to derive an expression for the velocity of the liquid at the film interface, for possible future use in connection with measurements of the film interface velocity.

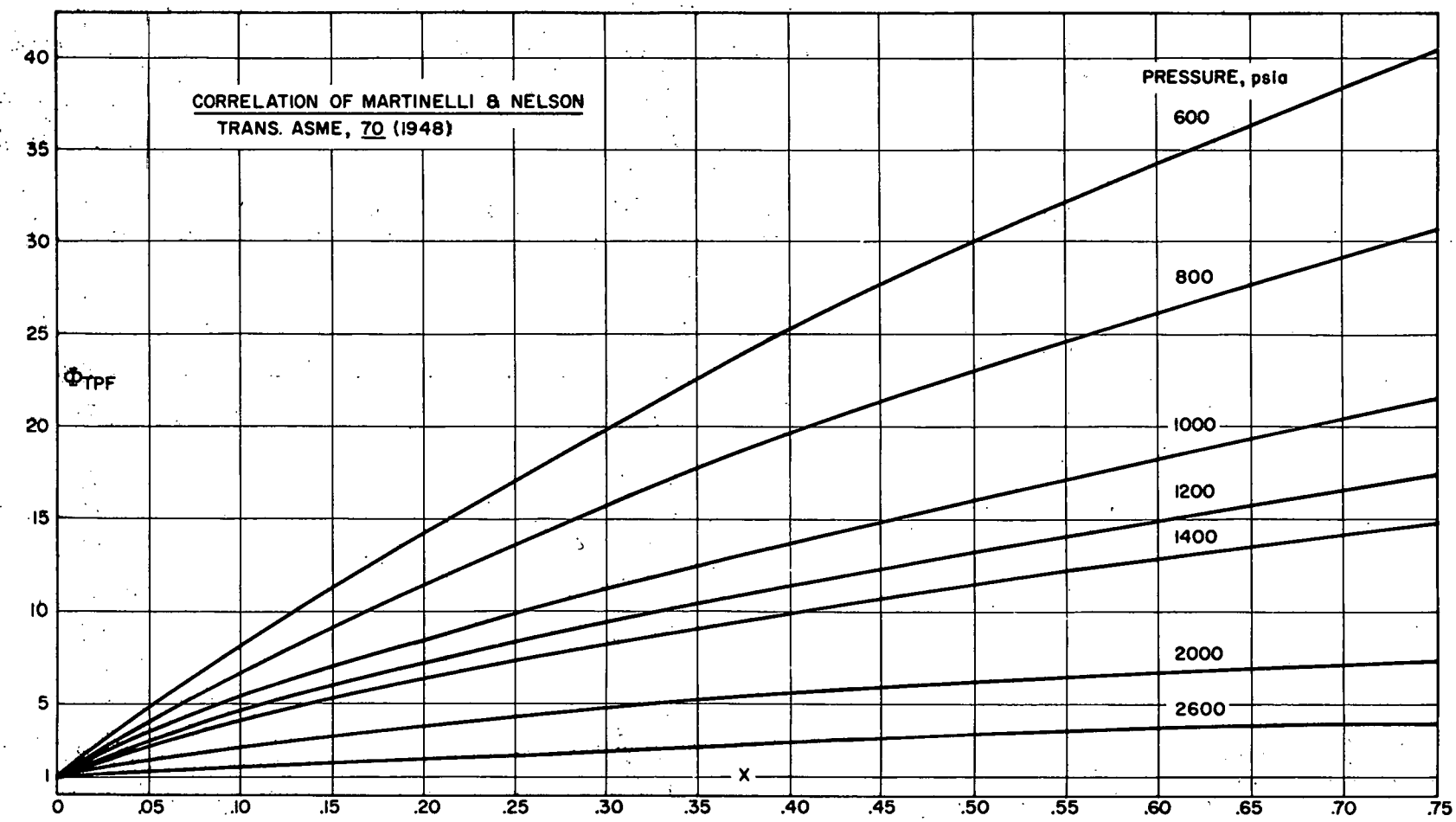


FIGURE VII-6

GRAPH OF THE TWO-PHASE FRICTION MULTIPLIER $\Phi_{TPF}$ FOR WATER

Correlation of Martinelli and Nelson (ref. (38))

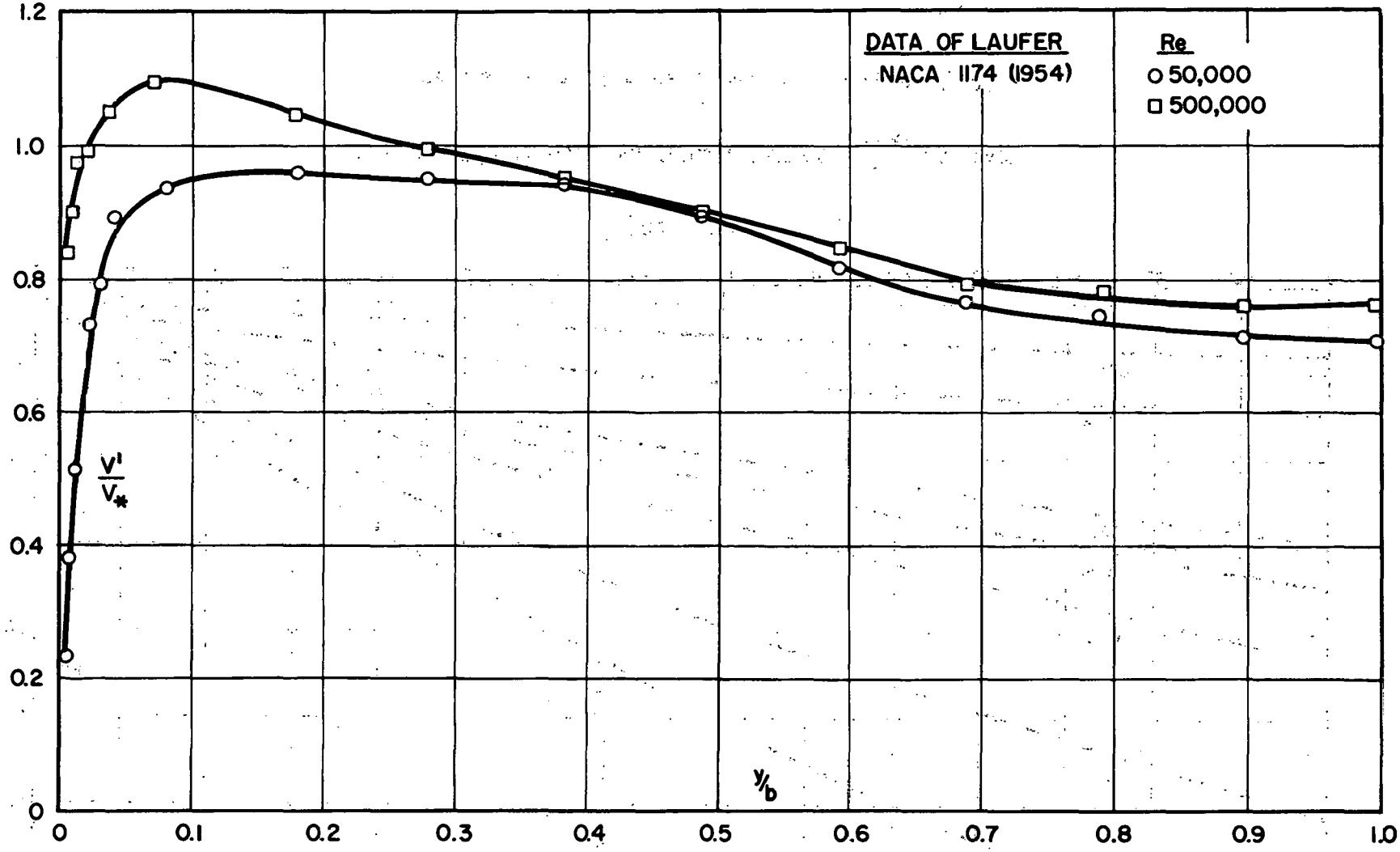


FIGURE VII-7

VARIATION OF THE TURBULENT FLUCTUATING VELOCITY COMPONENT WITH REYNOLDS NUMBER AND DISTANCE FROM THE WALL

Data of Laufer for Air Flow in a 10-inch Diameter Round Pipe (ref. (26))

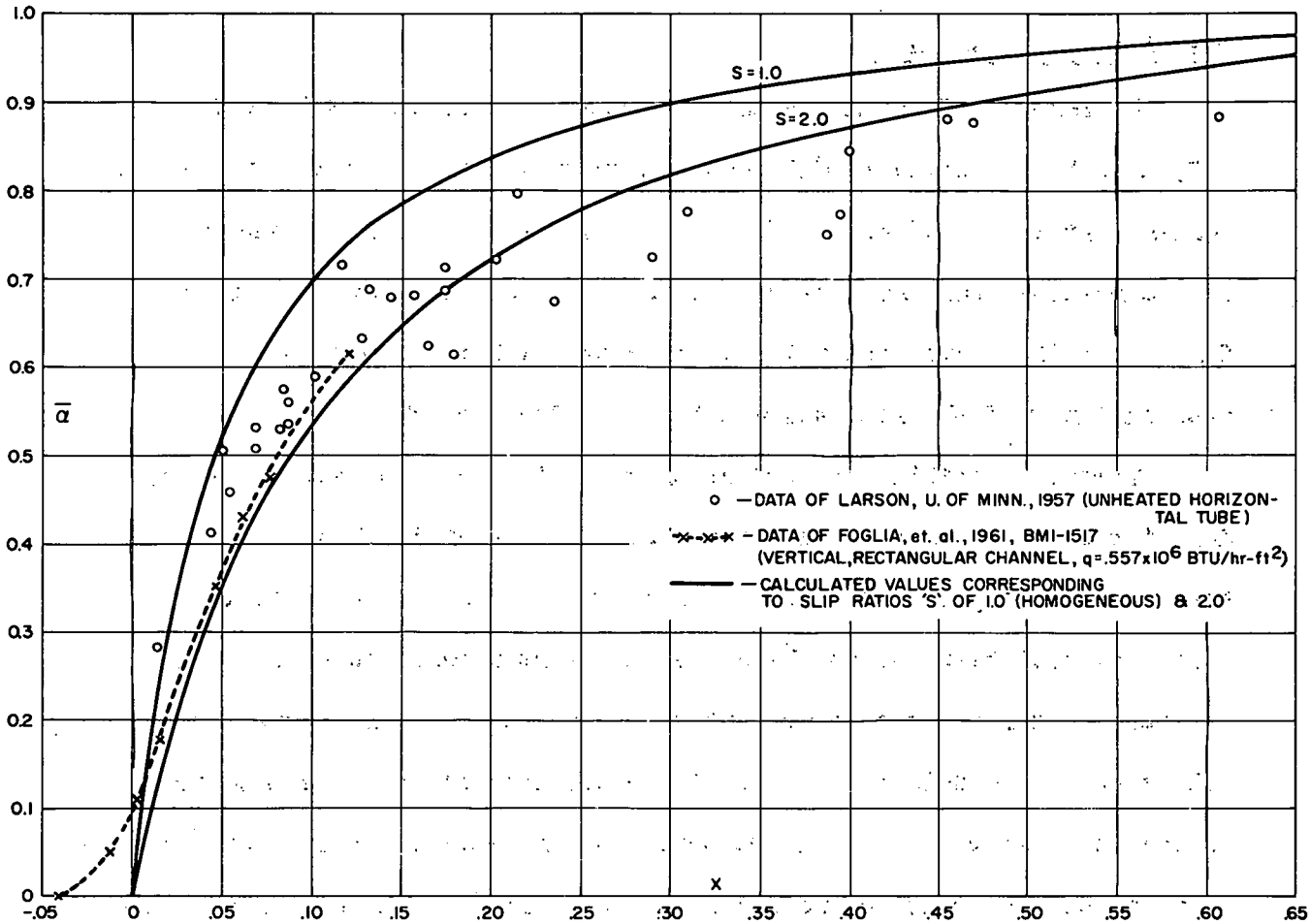


FIGURE VII-8

GRAPH OF THE CHANNEL AVERAGE STEAM VOLUME FRACTION, SHOWING:

1. Data of Larson for water flow in a .484 in. diameter unheated horizontal tube at 1015 psia (ref. (49)).

2. Data of Foglia, et.al., for water flow upward in a vertical heated rectangular channel .100 in. thick, at 1030 psia and 557,000 Btu/hr-ft$^2$ (ref. (52)).

3. Calculated values using equation (48) for S = 1.0 and 2.0 at 1000 psia.

## VIII. COMPARISON OF THEORETICAL RESULTS WITH CRITICAL HEAT FLUX DATA

### Description of the Data

The results of the analysis, expressed by equation (52) in Section VII, have been applied to 822 measured critical heat flux data points for boiling water, including the 80 valid points tabulated in Appendix C and selections from the data of others. The selection of data was confined to bulk boiling conditions, in accord with the limits of applicability of the analysis mentioned in Section VII ($X \geqslant 0$).

Wherever possible, the criterion for selection was that there was definite evidence that the critical heat flux condition had actually been experienced, as indicated by an abrupt increase or oscillation of heater element temperature while the flow system remained steady. The Critical Heat Flux Detector output signal was used as the basis for selection of the data in Appendix C. Recordings of both the Detector signal and heater element thermocouple outputs were the basis for selection from the data of Janssen and Kervinen (ref. (15)). This criterion could not be rigorously applied in selecting from the data of Westinghouse (ref. (1)), Harwell (ref. (8)), CISE (refs. (12),(13), Italy), and Aladyev, et.al. (ref. (11), Russia), as there are no records in these references which substantiate in detail the character of each critical heat flux determination.

There is an indication that some of the CISE data may have been taken when the system was in an unstable condition, as characterized by the critical heat flux levels being less than for data taken with the

same geometry, mass velocity and pressure but at higher steam quality.[1] Part of the Russian data (ref. (11)) was taken with a flow system designed to have a tendency for flow oscillations to develop. This data also displays maxima in $q_c(X)$, similar to some of the CISE data. Only those portions of the CISE data and the data of Aladyev for which stable loop operation was indicated were selected for comparison here.

The Westinghouse data, the data of Janssen and Kervinen, and the data in Appendix C were all obtained with sub-cooled liquid water flow into the inlet of the test sections. In contrast, the data of Harwell, CISE, and Aladyev, et.al., were obtained in systems using a two-phase mixture at the test section inlet.

The data of Janssen and Kervinen (ref. (15)) was obtained using thermocouples attached to the heater element wall together with either the Detector used in the present work (Section V) or another detector similar in function. The Westinghouse data (ref. (1)) was obtained using thermocouples attached to the heater element in conjunction with a power trip device set to shut off the test section power at a prescribed thermocouple output level. The Harwell data (ref. (8)) and the CISE data (refs. (12), (13)) were obtained using heater element voltage differential measurements with a detector and power trip circuit apparently similar in general function to the Detector described in

---

[1] Silvestri discusses the significance of the "maxima" in $q_c(X)$ for the CISE data and suggests they are the boundaries between stable and unstable operation (ref. (12).

Appendix B.[2] For the Russian data critical heat flux detection was apparently based on observation of abrupt increase of measured heater element wall temperature (ref. (11)).

The experimental data selected for comparison with the theoretical results are summarized in Appendix E. The particular values of the constants C', C" and m used in each case for the corresponding calculations of $q_c$ by equation (52) and the deviations of the calculated values from experimental values are included in the tabulation.

A large range of variables for boiling water flow is covered by the 822 selected data points, as shown in Table VIII-1.

TABLE VIII-1

| | |
|---|---|
| Geometry | Rectangular; Circular; Annular |
| Mass Velocity, G | 27 to 1096 lbs/sec-ft$^2$ |
| Steam Quality, $X_c$ | 0.00 to 0.75 |
| Pressure | 585 to 2500 psia |
| Hydraulic Diameter, De | 0.095 to 0.875 in. |
| Heated Length, L | 6.0 to 108 in. |
| $L/D_e$ | 20:1 to 390:1 |

[2] For the CISE data simultaneous measurements of heater element temperature at exit were also made. According to Silvestri (ref. (12)), several of the critical heat flux determinations were based on recorded start of oscillation of the heater element temperature alone, there having been an insufficient rise in temperature to cause the detector circuit to trip the power. Apparently the detector output signal was not recorded, but was used solely to trip power in the Harwell and CISE experiments.

Characteristic fluctuations of the detector signal as displayed by an oscilloscope were noted for some of the Harwell data in the steam quality range above about 20 per cent (ref. (8)).

Application of Equation (52)

Initial determination of the constants C', C" and m in equation (52) was made using the 80 valid critical heat flux points tabulated in Appendix C. The procedure followed was to first take the constant C' in equation (52b) as 1.00, corresponding to nearly homogeneous flow as expected for high heat flux conditions in ducts with a heated to total surface ratio of nearly unity. Equation (52) was then graphed in Figure VIII-1 in the non-dimensional form,

$$\xi q_c = f(\psi)$$

using the critical heat flux data given in Appendix C. An approximate best fit was obtained with the constants m and C" in equation (52) evaluated as m = 0.75, C" = 0.53. The resulting correlation was tested by using these values of the constants in equation (52) and then calculating the corresponding critical heat flux for each of the 80 valid data points presented in Appendix C and Figure VI-1. A comparison of the calculated values with the measured data is shown in Figure VIII-2. Agreement is seen to be reasonably good (approximately 85 per cent of the calculated points lie within $\pm$ 30 per cent of the measured values).

Finally, critical heat fluxes were calculated with equation (52) using the constants m = 0.75, C" = 0.53 and C' adjusted as required to provide an approximate "best fit" of the data, for each of the 742 additional data points selected from the other sources (Appendix E). It was found that for the thinner ducts there is apparently a dependence of the critical heat flux on duct spacing or hydraulic diameter which is not correctly represented by equation (52). As a consequence, the data is fitted better for the thin ducts ($b < b_o$ = .084 in.) by varying C" in proportion to $(b/b_o)^{0.9}$. For the thicker ducts ($b >$ .084 in.), C" is

held constant[3] at 0.53. With these values of C", and taking the exponent m constant throughout at 0.75, it was found that the data was fitted reasonably well by equation (52) using C' = 1.0 for the rectangular channel and circular tube data and C' = 6.5 for the annular test section data. Since the ratio of heated surface to total surface in the circular tubes and rectangular channels is from .80 to 1.0 while for the annular channels the ratio is from .23 to .40, it is suggested that the variation in C' required in order to have equation (52) fit the data is due primarily to retention of a relatively larger amount of the available liquid in the film on the unheated surfaces at the expense of the effective liquid concentration in the channel core at the critical heat flux condition.[4]

Figure VIII-3 compares calculated values using equation (52) with measured critical heat fluxes for each of the selected 235 data points of Janssen and Kervinen. Except for a few points agreement of measured and calculated values is seen to be quite good (approximately 92 per cent of the calculated points lie within $\pm$ 30 per cent of the measured values).

---

[3] An exception to this was found in the Russian data for a short circular tube (ref. (11)), for which $b/b_o = 1.88$. For this data, adjustment of C" to C" = 1.4 x .53 = .74 resulted in 92 per cent of the data points being predicted to within less than $\pm$ 30 per cent deviation from measured critical heat fluxes, reflecting either a continuation of the trend of variation with duct size displayed by the thinner ducts; or perhaps a dependence on length to diameter ratio, not included in equation (52), which appears to become evident at small length to diameter ratios (refs. (92),(96)). (See footnote 7, Sec. III.) For this data $L/D_e = 20$, the least ratio of all the data treated.

[4] Refer to the discussion in Section VII relevant to equation (49). As noted later, this hypothesis is further substantiated by the fact that Group I of Janssen and Kervinen's annular test section data (Appendix E), taken with a ribbed outer wall designed to minimize attachment of liquid on the unheated surface are in good agreement with calculations using C'= 1.00, in analogy to the effect of an adjacent "heated" wall. Additional evidence of the unheated wall effect is indicated in motion picture sequence 12-2 (Reel V,Appendix D; also Fig. VI-23c) showing a relatively thicker, more placid layer of liquid flowing up the unheated wall, compared to the thinner, more agitated liquid film on the heated wall.

The Westinghouse 2000 psia data (ref. (1)) was calculated with equation (52) using initially C" = .53. These results compared poorly with the data. In order to investigate the trend of the deviation with duct size, the graph in Figure VIII-4 was prepared, which includes for reference mean deviations for the other data groups also. Based on the results in Figure VIII-4, a correction factor of $(b/b_o)^{0.9}$ was applied to C" for the range of duct sizes $b < b_o$, which resulted with substantial improvement in agreement of calculated and measured values for the Westinghouse data (approximately 68 per cent of the calculated points are within $\pm$ 30 per cent of measured values). Calculations of the Group F data of Janssen and Kervinen ($b/b_o = 0.536$) and the Harwell data ($b/b_o = 0.510$) were also brought into better agreement with the measurements. The requirement for the correction is probably due to the fact that the analysis from which equation (52) resulted was constructed for relatively "thin" liquid films. That is, $\delta$ should be small in comparison with the duct dimension b. In consequence, as shown by these comparisons with the data, the analysis is apparently invalid for very thin ducts ($b < 0.084$ in.) and for these cases a correction has to be applied.

The trends of the experimental data with the main system parameters and the corresponding values calculated with equation (52) are displayed in Figures VIII-5 through VIII-13. Agreement between calculated and measured values is seen to be reasonably good for both the data from Appendix C (Figure VIII-5) and the data of Janssen and Kervinen (Figures VIII-6 to VIII-9).

Somewhat greater deviation of calculated from measured values is seen for a representative selection of the Westinghouse data (Figure VIII-10), although the main trend of the data with mass velocity is

predicted correctly by the calculations.[5]

Some of the calculated points for the Harwell data (Figure VIII-11) and the CISE data (Figure VIII-12) deviate substantially from the measured values, although again the main trend of the data with mass velocity appears to be correctly predicted by the calculations. At the higher mass velocities the experimental critical fluxes apparently reduce much more sharply with increased steam quality than is predicted by equation (52) with the constants used, for both the Harwell and the CISE data. The calculations agree reasonably well with the measurements at the lowest mass velocity for both sets of data. The trend in the Harwell and CISE data of a rapid drop in critical heat flux with increasing steam quality at the higher mass velocities is not evidenced in the other data treated. The possibility is suggested that this may be due to an inlet condition resulting from the method used in the Harwell and CISE experiments of entering the test section with a two-phase mixture.[6]

The trends of the Russian data with mass velocity and pressure appear to be predicted reasonably well by equation (52) (Figure VIII-13).

---

[5] Part of the deviation between calculated and measured values in Figure VIII-10 is due to the fact that each grouping by mass velocity actually covered a substantial range of experimental mass velocities whereas the calculations were based on the mean mass velocity for each group.

---

[6] For example, it seems possible that in some conditions of two-phase flow at inlet with high mass velocity, the liquid might not be able to attach to the wall even though the heat flux may be substantially less than the critical heat flux level which would be experienced if the fluid entered the duct as a liquid. Corresponding oscillations of wall temperature, characteristic of the behavior observed by Silvestri during "slow burnout" (ref. (12)), caused by liquid momentarily contacting the wall but immediately disengaging, would not be unexpected in such a situation.

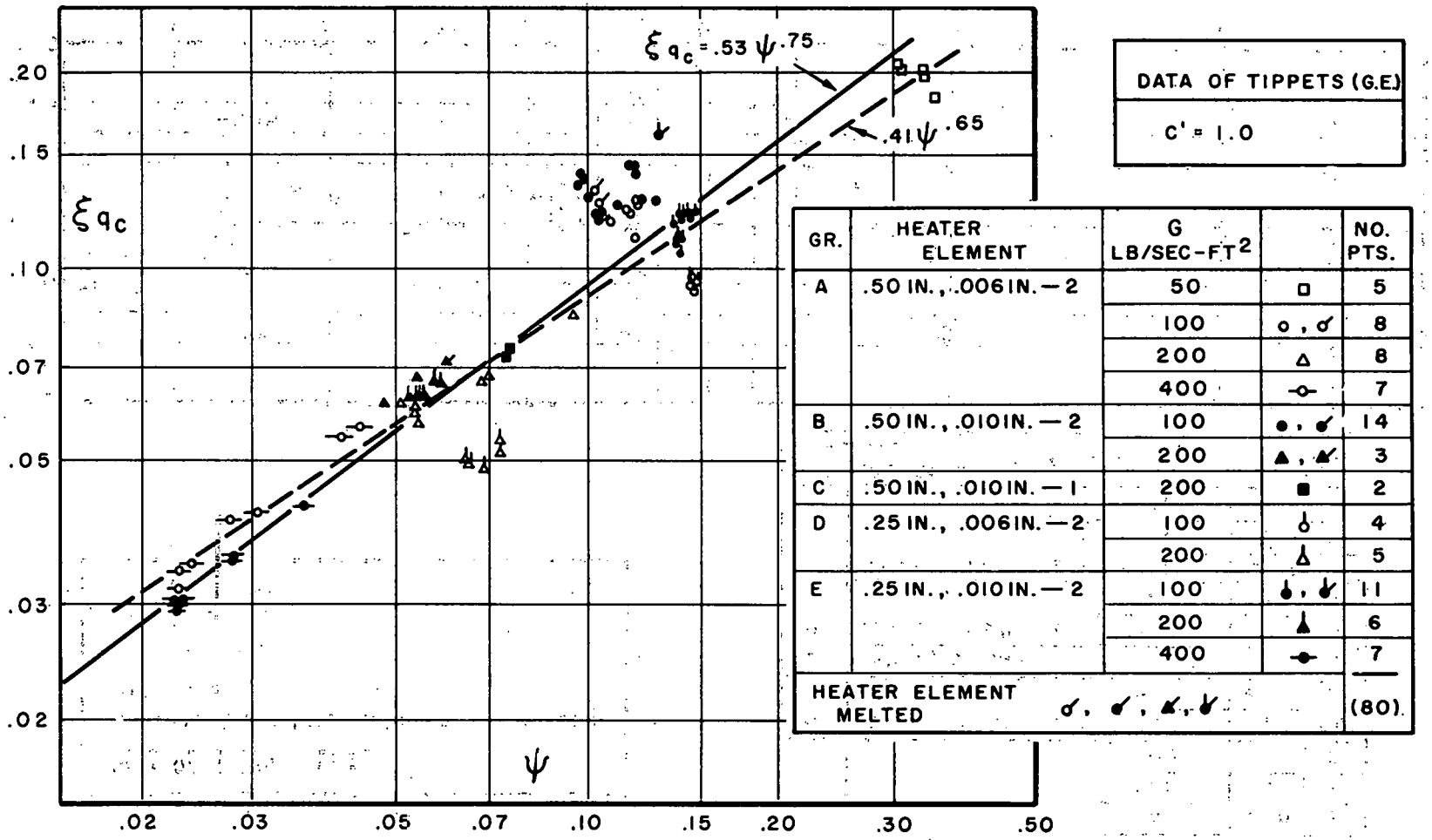


| DATA OF TIPPETS (G.E.) |
|---|
| C' = 1.0 |

| GR. | HEATER ELEMENT | G LB/SEC-FT$^2$ | | NO. PTS. |
|---|---|---|---|---|
| A | .50 IN., .006 IN. — 2 | 50 | □ | 5 |
| | | 100 | ○, ◁ | 8 |
| | | 200 | △ | 8 |
| | | 400 | ⊸ | 7 |
| B | .50 IN., .010 IN. — 2 | 100 | ●, ◢ | 14 |
| | | 200 | ▲, ◤ | 3 |
| C | .50 IN., .010 IN. — 1 | 200 | ■ | 2 |
| D | .25 IN., .006 IN. — 2 | 100 | ◊ | 4 |
| | | 200 | ◬ | 5 |
| E | .25 IN., .010 IN. — 2 | 100 | ◆, ◥ | 11 |
| | | 200 | ▲ | 6 |
| | | 400 | ⊸ | 7 |
| HEATER ELEMENT MELTED | | | ◁, ◢, ◤, ◥ | (80) |

FIGURE VIII-1

NON-DIMENSIONAL GRAPH OF DATA OF APPENDIX C AND EQUATION (52)
USED TO SELECT THE CONSTANTS: C" = .53, m = .75

FIGURE VIII-2

ERROR PLOT COMPARING DATA FROM APPENDIX C WITH CORRESPONDING HEAT FLUXES CALCULATED BY EQUATION (52)

DATA OF TIPPETS (G.E.)

RECTANGULAR DUCT, 2.1 IN. WIDE, 37 IN. LONG

1000 PSIA

C' = 1.0

C'' = .53

m = .75

| GR. | HEATER ELEMENT | G LB/SEC-FT$^2$ | | NO. PTS. |
|---|---|---|---|---|
| A | .50 IN., .006 IN. — 2 | 50 | □ | 5 |
| | | 100 | ○, ♂ | 8 |
| | | 200 | △ | 8 |
| | | 400 | -○- | 7 |
| B | .50 IN., .010 IN. — 2 | 100 | ●, ♂ | 14 |
| | | 200 | ▲, ◢ | 3 |
| C | .50 IN., .010 IN. — 1 | 200 | ■ | 2 |
| D | .25 IN., .006 IN. — 2 | 100 | ♁ | 4 |
| | | 200 | ♁ | 5 |
| E | .25 IN., .010 IN. — 2 | 100 | ♁, ♂ | 11 |
| | | 200 | ♁ | 6 |
| | | 400 | -●- | 7 |
| HEATER ELEMENT MELTED | | | ♂, ♂, ◢, ◢ | (80) |

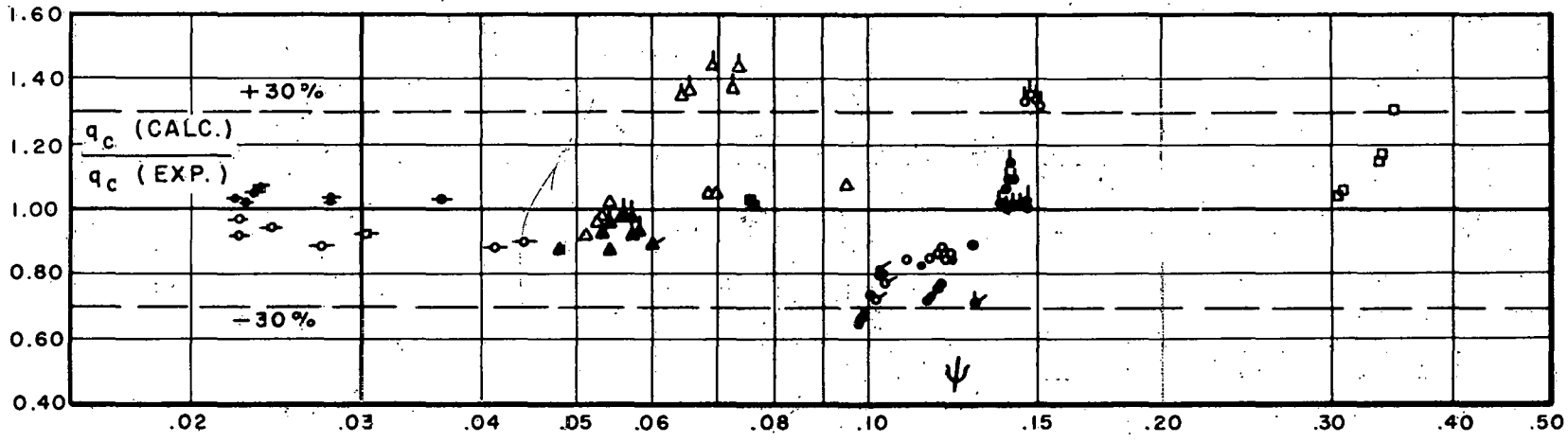

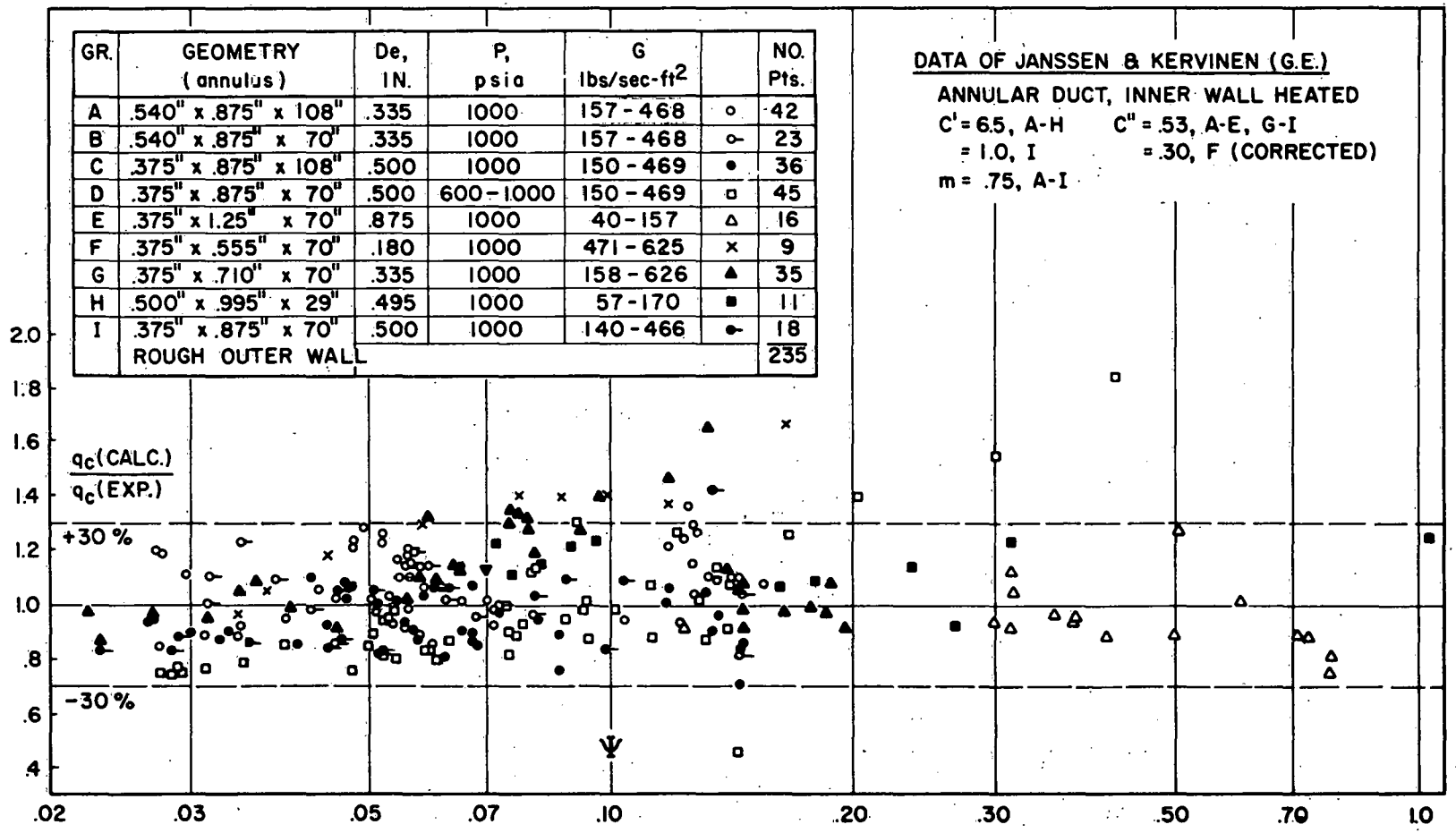


FIGURE VIII-3

ERROR PLOT COMPARING DATA OF REF. (15) WITH
CORRESPONDING HEAT FLUXES CALCULATED BY EQUATION (52)

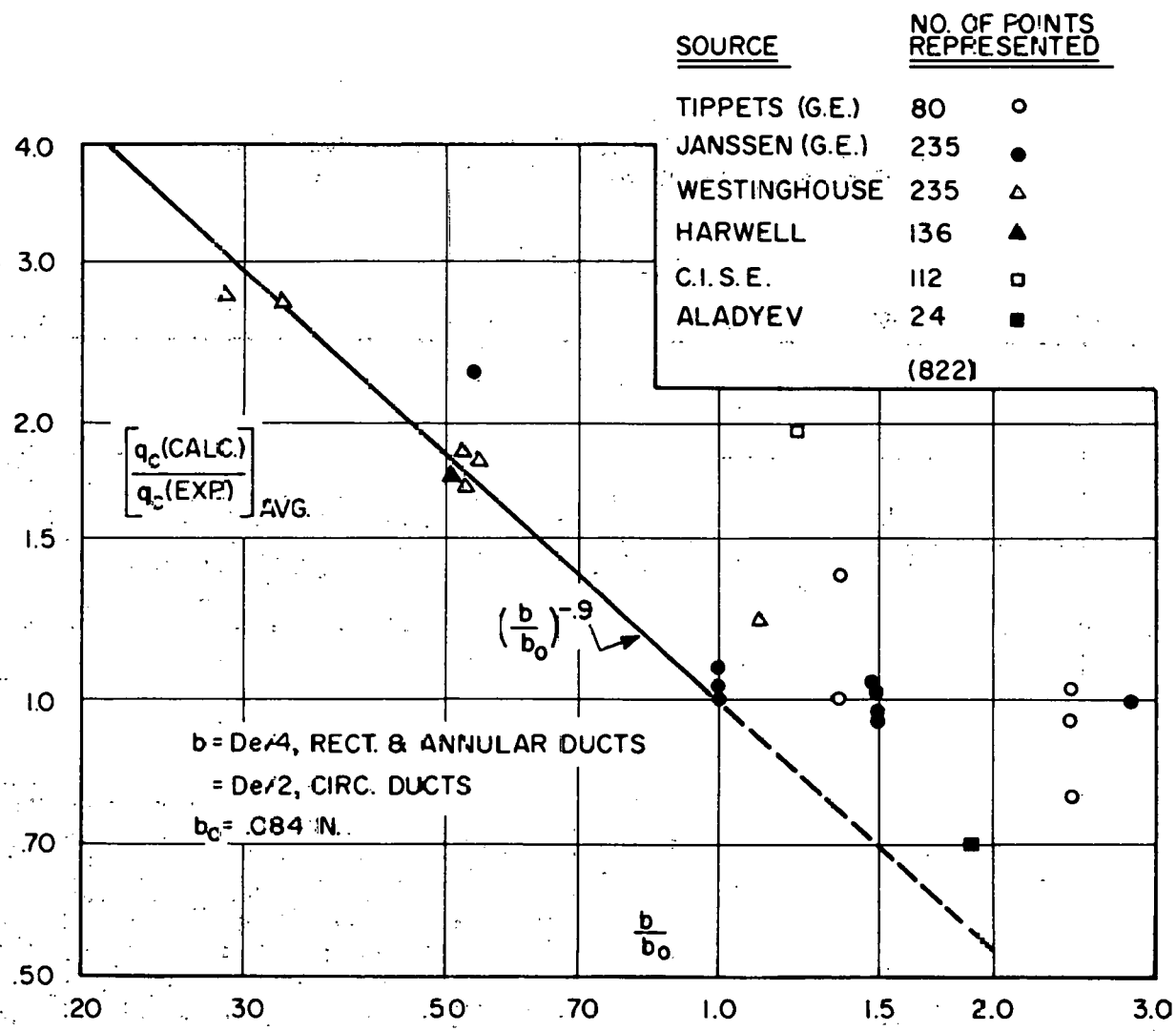


FIGURE VIII-4

ERROR PLOT SHOWING EFFECT OF DUCT SIZE ON DEVIATION BETWEEN HEAT FLUXES CALCULATED BY EQ. (52) AND MEASURED DATA

Plotted points are arithmetic averages of all data points for each duct size indicated for each source group.

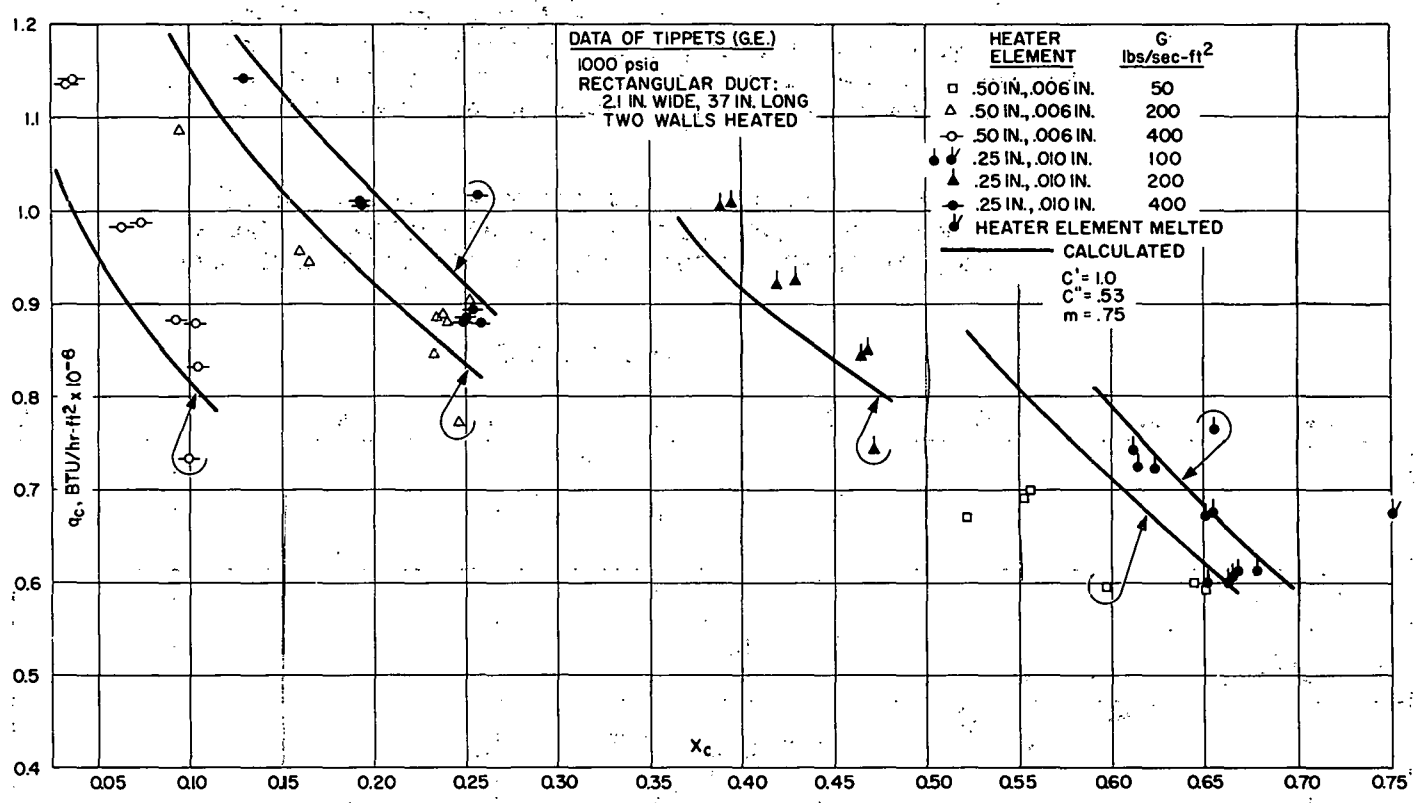


FIGURE VIII-5

GRAPH OF DATA OF APPENDIX C AND CALCULATIONS BY EQUATION (52) SHOWING VARIATION OF CRITICAL HEAT FLUX WITH STEAM QUALITY, MASS VELOCITY AND CHANNEL SPACING (HYDRAULIC DIAMETER)

1. Critical heat flux decreases with increased steam quality.
2. Critical heat flux increases with decreased mass velocity.
3. Critical heat flux increases with decreased channel spacing (hydraulic diameter).

Note: The point located at $q = .673 \times 10^6$ Btu/hr-ft$^2$, $X = .751$ is from run No. 18RR-1, operated to deliberate destruction of the heater element at a heat flux 11 per cent above normal critical heat flux "trip" point. The corresponding normal trip point was at $q_c = .606 \times 10^6$ Btu/hr-ft$^2$, $X_c = .667$, in agreement with the calculations and other data.

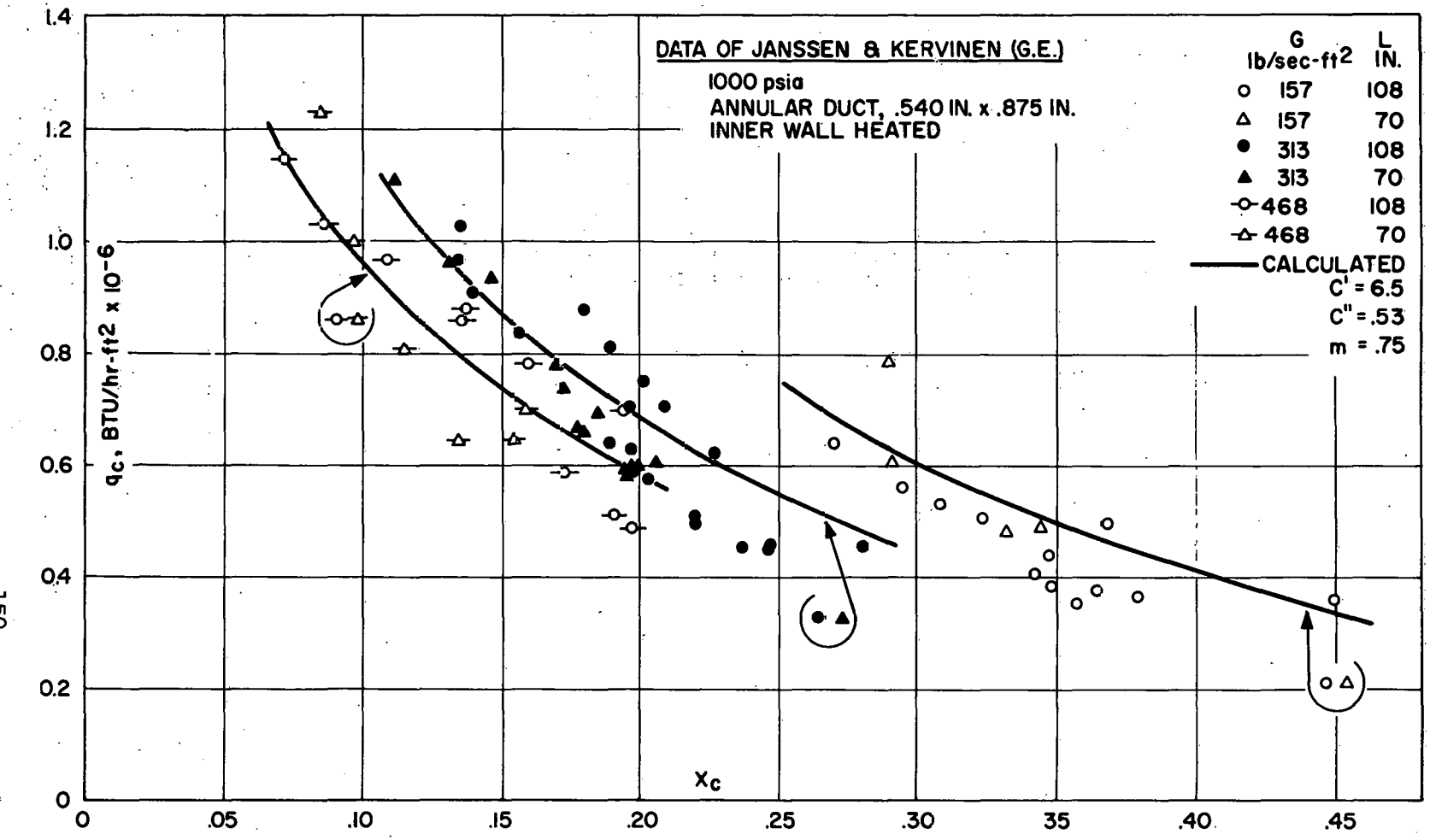


FIGURE VIII-6

GRAPH OF DATA OF REF. (15) AND CALCULATIONS BY EQ. (52) SHOWING VARIATION OF CRITICAL HEAT FLUX WITH STEAM QUALITY AND MASS VELOCITY FOR TWO HEATED LENGTHS

1. Critical heat flux decreases with increased steam quality.
2. Critical heat flux increases with decreased mass velocity.
3. Critical heat flux not affected by change of heated length, for $210 \ll L/D_e \ll 322$.

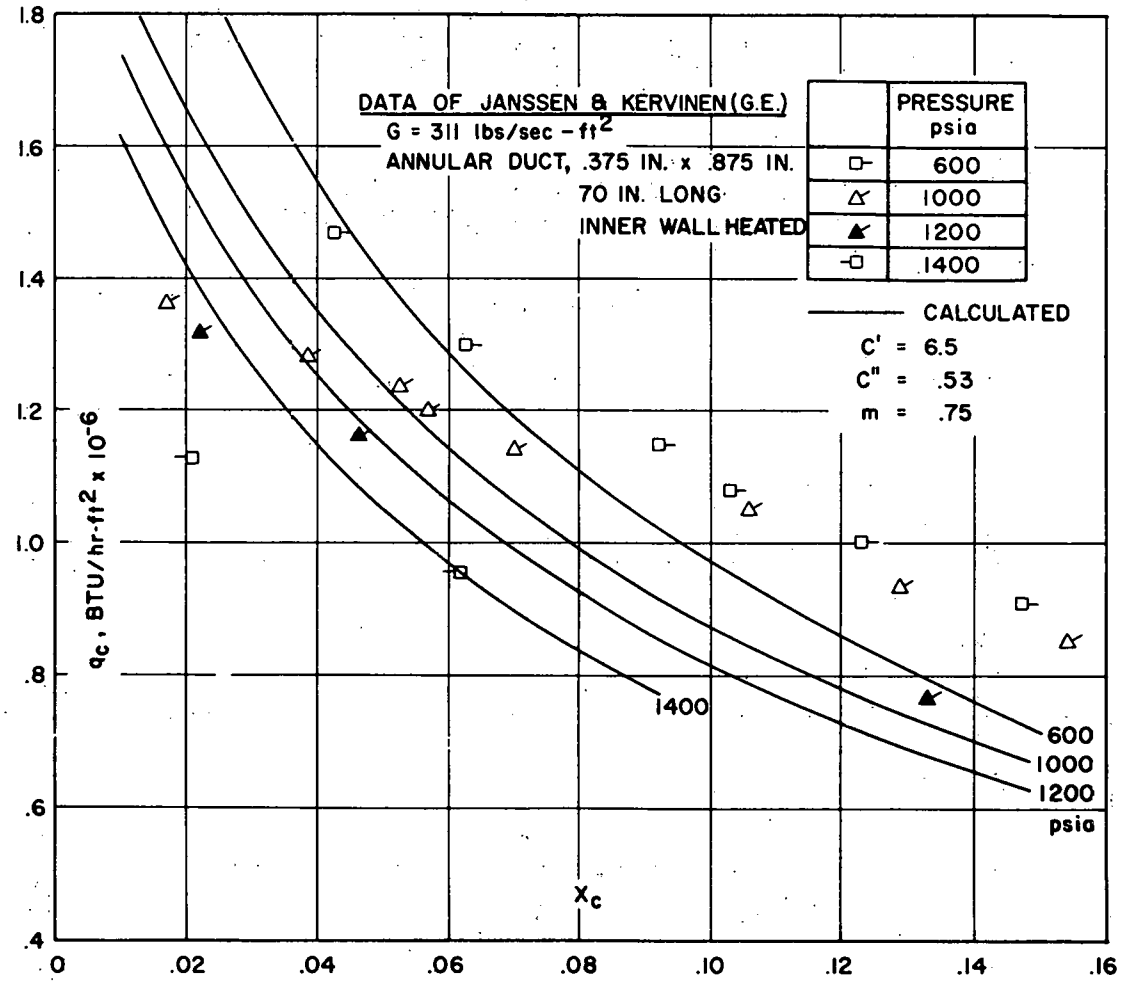


FIGURE VIII-7

GRAPH OF DATA OF REF. (15) AND CALCULATIONS BY EQUATION (52) SHOWING VARIATION OF CRITICAL HEAT FLUX WITH STEAM QUALITY AND PRESSURE

1. Critical heat flux decreases with increased steam quality.
2. Critical heat flux decreases with increased pressure over the range 600 to 1400 psia.

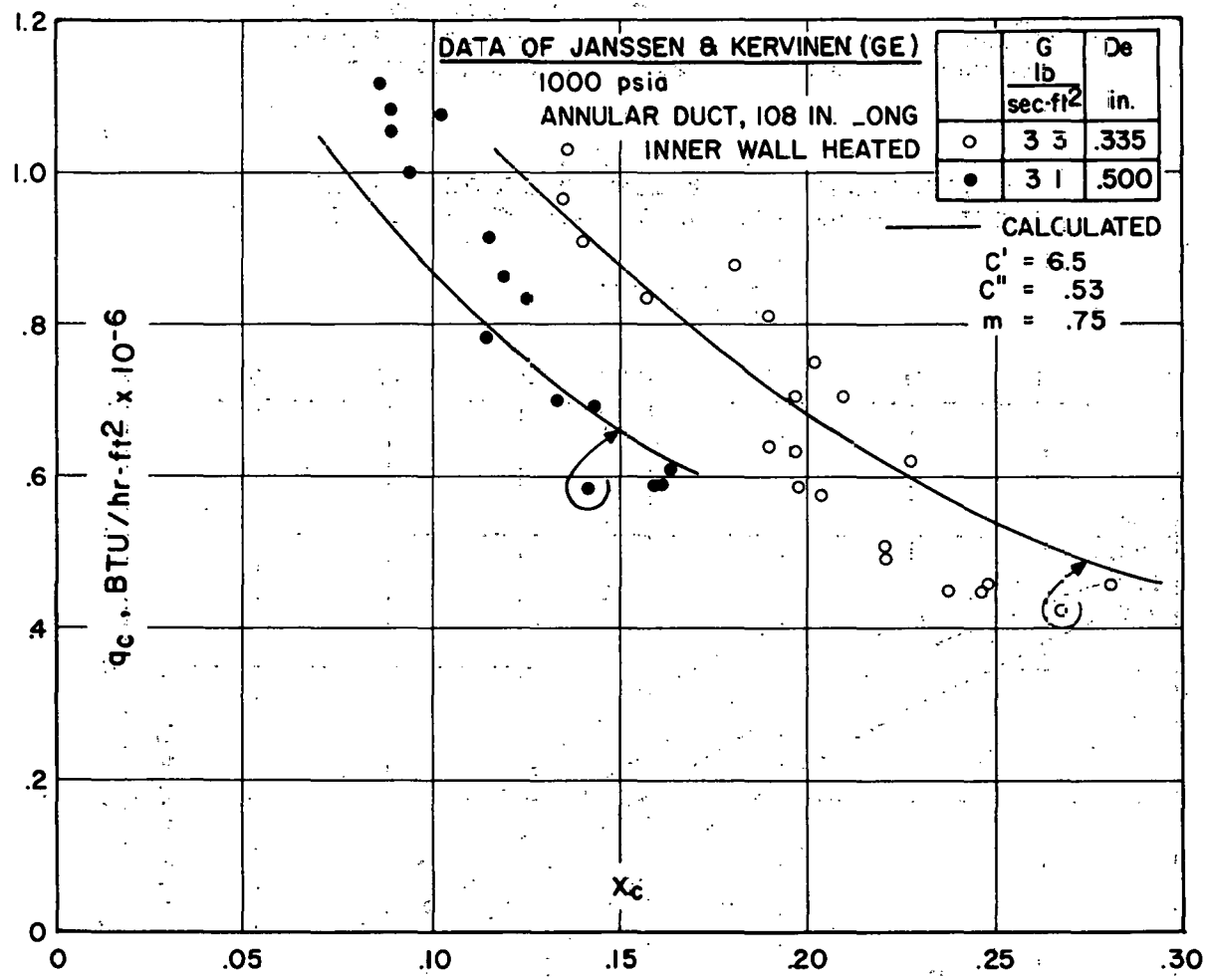


FIGURE VIII-8

GRAPH OF DATA OF REF. (15) AND CALCULATIONS BY EQUATION (52) SHOWING VARIATION OF CRITICAL HEAT FLUX WITH STEAM QUALITY AND HYDRAULIC DIAMETER

1. Critical heat flux decreases with increased steam quality.
2. Critical heat flux increases with decreased hydraulic diameter.

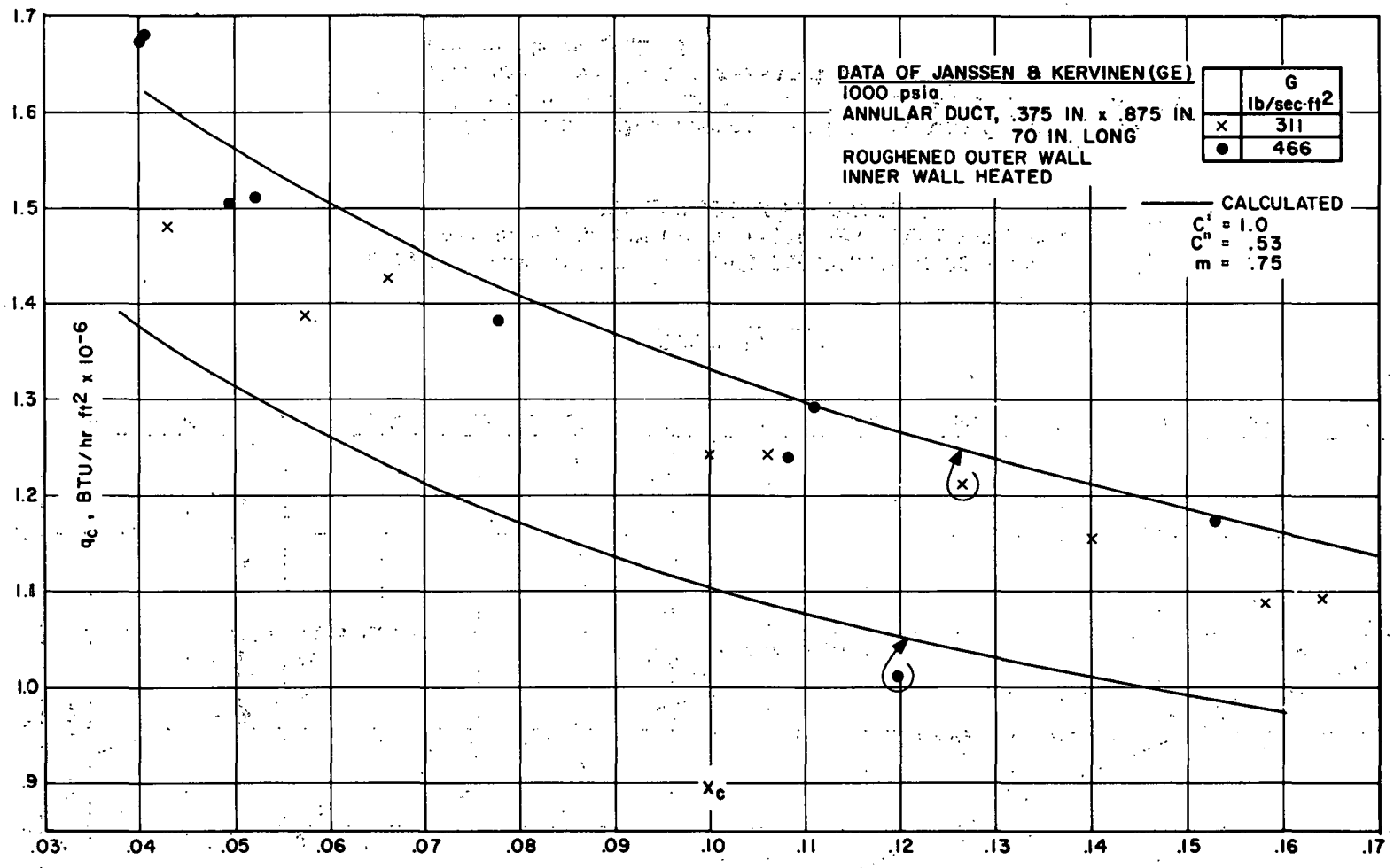


FIGURE VIII-9

GRAPH OF DATA OF REF. (15) AND CALCULATIONS BY EQUATION (52) SHOWING VARIATION OF CRITICAL HEAT FLUX WITH STEAM QUALITY AND MASS VELOCITY FOR ANNULUS WITH ROUGHENED OUTER UNHEATED WALL

1. Critical heat flux decreases with increased steam quality.
2. Experimental data shows slight increase of critical heat flux with increased mass velocity, contrary to prediction of Equation (52).

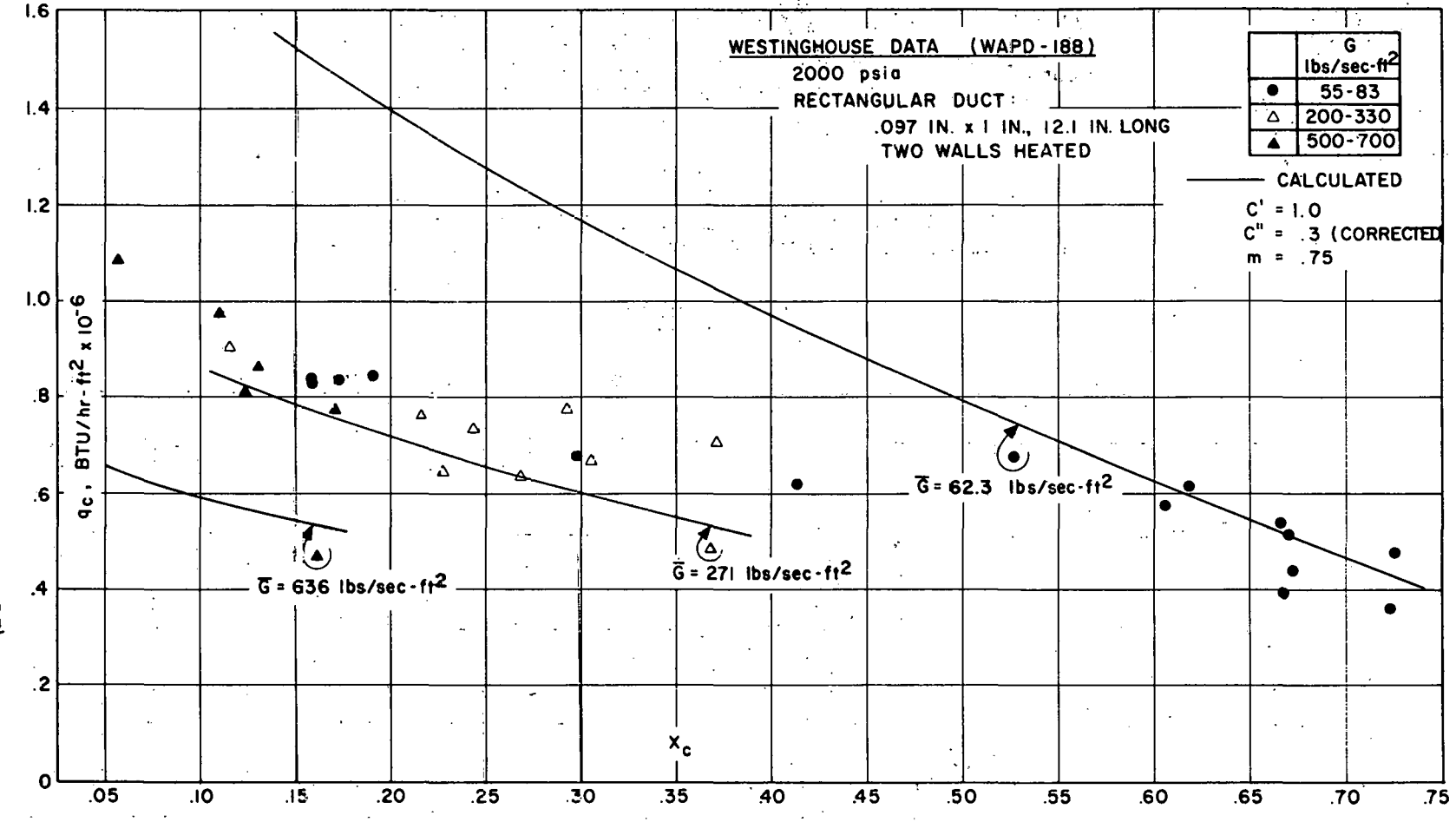


FIGURE VIII-10

GRAPH OF DATA OF REF. (1) AND CALCULATIONS BY EQUATION (52) SHOWING VARIATION OF CRITICAL HEAT FLUX WITH STEAM QUALITY AND MASS VELOCITY

1. Critical heat flux decreases with increased steam quality.
2. Critical heat flux increases with decreased mass velocity with the trend in the measured data tending to reverse at lesser steam qualities.

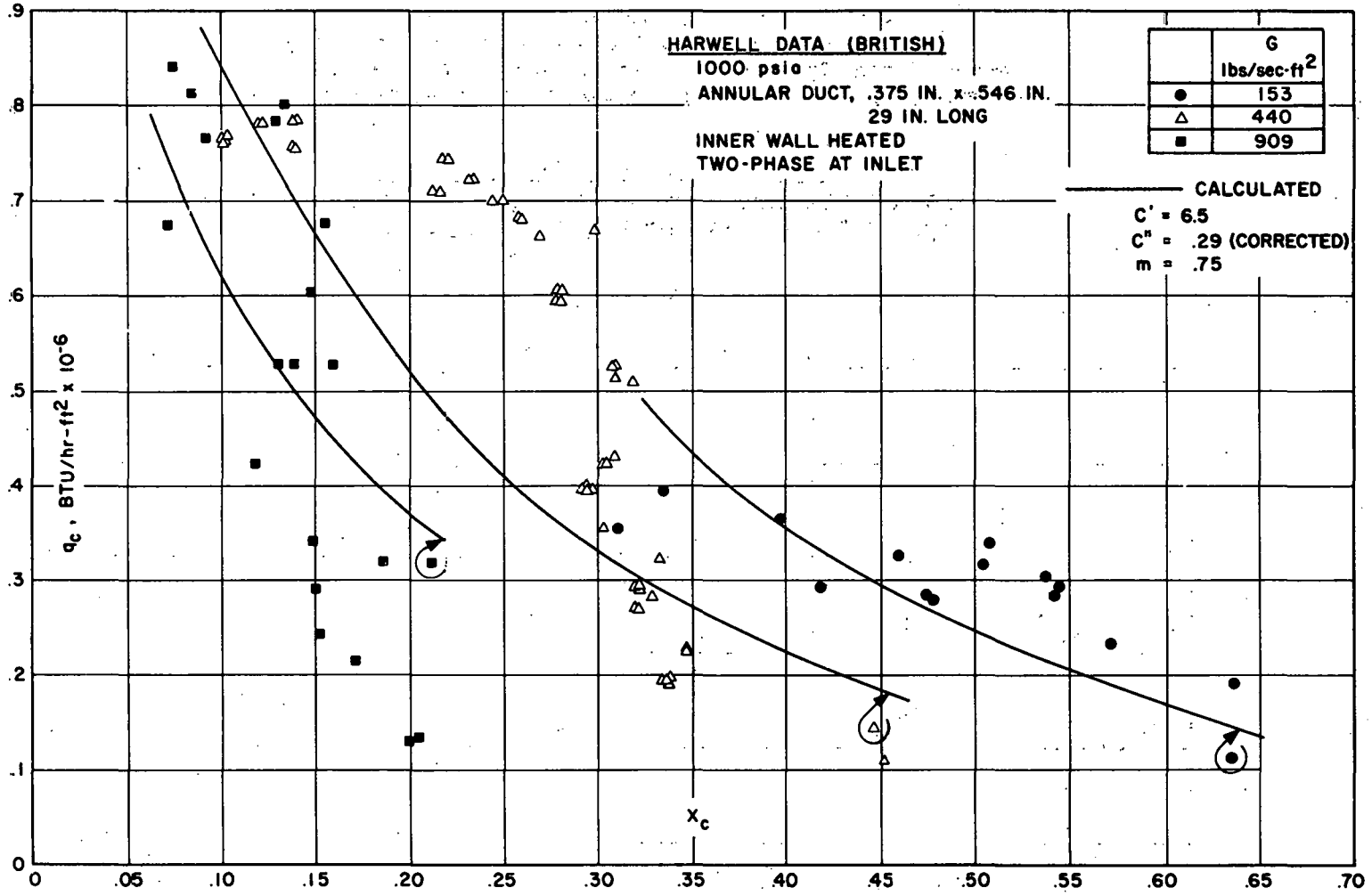


FIGURE VIII-11

GRAPH OF DATA OF REF. (8) AND CALCULATIONS BY EQUATION (52) SHOWING VARIATION OF CRITICAL HEAT FLUX WITH STEAM QUALITY AND MASS VELOCITY

1. Critical heat flux decreases with increased steam quality, with measured values reducing more sharply than predicted by Equation (52) at the higher mass velocities.
2. Critical heat flux increases with decreased mass velocity.

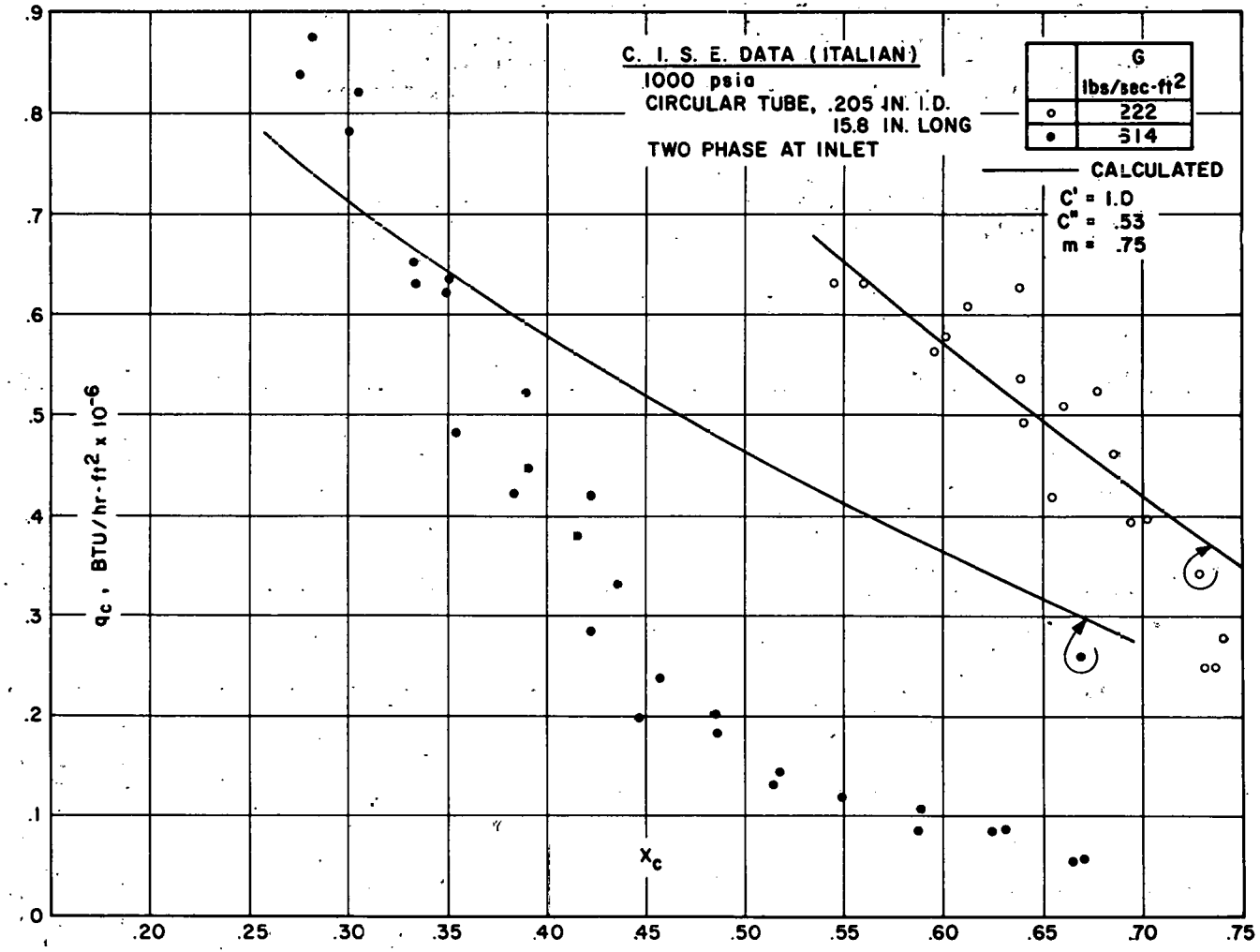


FIGURE VIII-12

GRAPH OF DATA OF REFS. (12) AND (13) AND CALCULATIONS BY EQUATION (52) SHOWING VARIATION OF CRITICAL HEAT FLUX WITH STEAM QUALITY AND MASS VELOCITY

1. Critical heat flux decreases with increased steam quality, with measured values reducing more sharply than predicted by Equation (52) at the highest mass velocity.
2. Critical heat flux increases with decreased mass velocity.

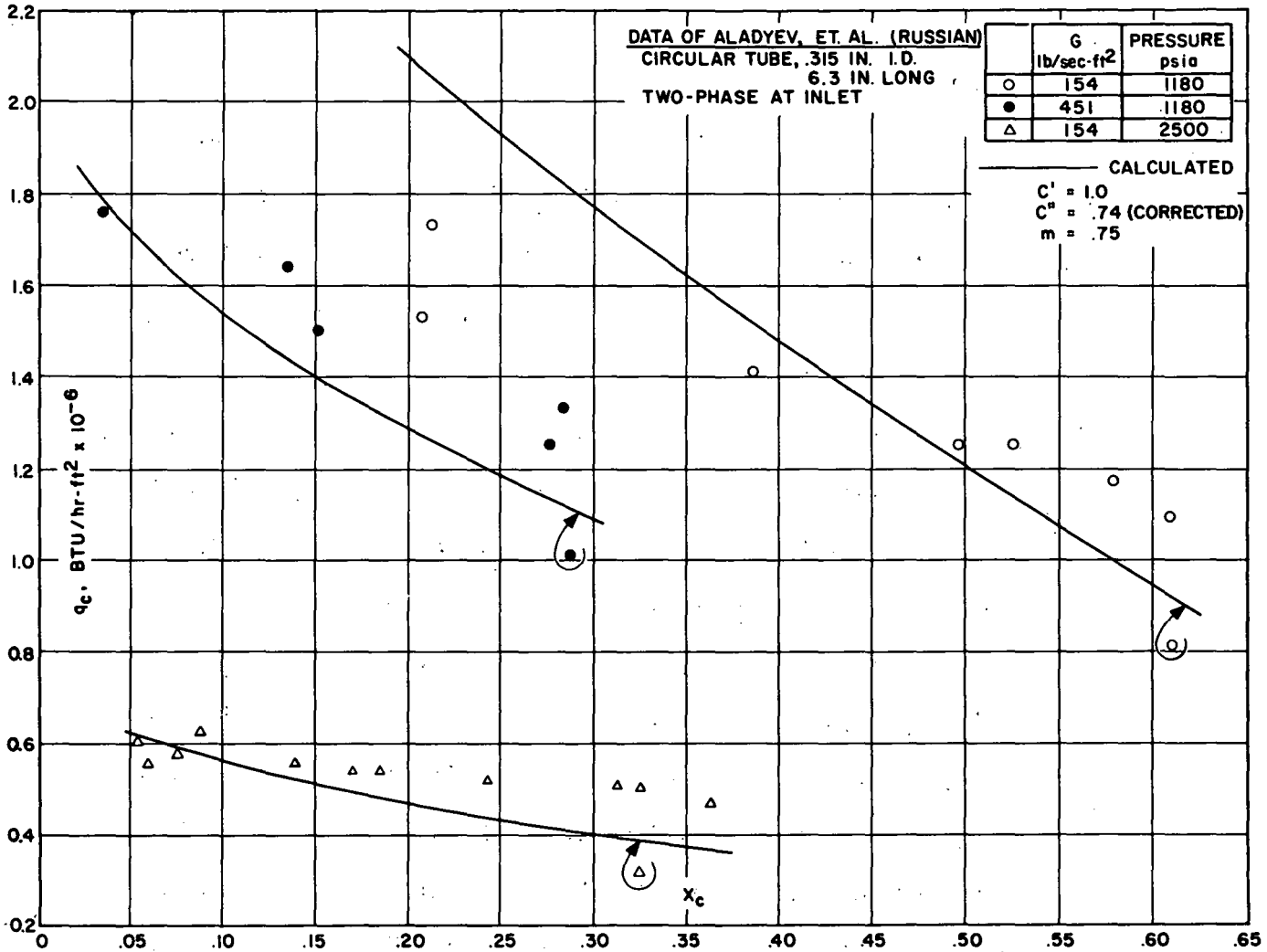


FIGURE VIII-13

GRAPH OF DATA OF REF. (11) AND CALCULATIONS BY EQUATION (52) SHOWING VARIATION OF CRITICAL HEAT FLUX WITH STEAM QUALITY, MASS VELOCITY AND PRESSURE

1. Critical heat flux decreases with increased steam quality, with measured values reducing slightly less rapidly than predicted by Equation (52).
2. Critical heat flux increases with decreased mass velocity.
3. Critical heat flux decreases with increased pressure over the range 1180 to 2500 psia.
4. Uncorrected calculations (C" = 0.53) predict critical heat flux levels about 70 per cent of these data (see footnote 3, Section VIII).

# IX. DISCUSSION OF RESULTS

## Summary

The results of the work can be summarized briefly as follows:

(1) Development of a new set of apparatus for direct observation and photography of boiling water flow patterns at pressures, mass velocities and steam qualities representative of modern nuclear reactor design, with heat fluxes up to and including the critical heat flux (Section IV, Appendices A and B).

(2) Eighty valid critical heat flux determinations covering the range of variables: p, 1000 psia; G, 50 to 400 lbs/sec-ft$^2$; $X_c$, .033 to .751; $D_e$, .46 in. and .81 in., in a rectangular channel (Section VI, Appendix C).

(3) Thirty-three high speed motion picture sequences of boiling water flow patterns, made up in convenient form for additional study, taken at flow and heat transfer conditions covering the range of variables: p, 1000 psia; G, 50 to 400 lbs/sec-ft$^2$; fluid state, sub-cooled at $\Delta h_s$ = 170 Btu/lb to bulk boiling at X = .656; q, up to and including the critical heat flux; $D_e$, .81 in. mainly, in a rectangular channel heated on both sides and on one side (Section VI, Appendix D).

(4) Theoretical analysis of the critical heat flux condition in forced flow with bulk boiling ($X \geqslant 0$) leading to derivation of a convenient working equation (equation (52)), which was used to correlate and study the critical heat flux data obtained in the present work together with a selection, intended to be representative, of 742 additional data points from all major

sources (Sections VII, VIII, Appendix E).

Detailed discussions of the results are given in the respective Sections. The purpose of this Section is to synthesize the findings from a more general point of view and to briefly relate them to the results of other works.

Flow Pattern Observations

The main characteristics of the boiling water flow patterns observed in the course of detailed examination of the motion picture sequences are tabulated in Appendix D. Figures VI-19 through VI-23 present enlarged frames selected from the motion pictures together with brief descriptions of the corresponding flow patterns.

The following general characteristics of the boiling water flow patterns at 1000 psia are evident in the motion picture sequences, corresponding to increasing fluid enthalpy from sub-cooled nucleate surface boiling conditions up to bulk boiling at high steam qualities, with heat fluxes up to and including the critical heat flux level.

(1) $\Delta h_s \gtrsim 20$ Btu/lb for G = 100 to 400 lbs/sec-ft$^2$ ($q \ll q_c$):

Growing (and shrinking) bubbles slide along the heated surface, at a velocity slightly less than the mean channel velocity, in an irregular frothy layer of liquid and bubbles mixed. The bubbles are not attached to the heated surface during their stage of principal growth. There is almost pure liquid in the regions of the channel away from the heated wall, indicating little tendency for general mixing (Figs. VI-20a, -22a, -23a, b).

(2a) $0 \lesssim \Delta h_s \lesssim 20$ Btu/lb for G = 200 to 400 lbs/sec-ft$^2$ ($q < q_c$):
$0 \lesssim X \lesssim .10$ for G = 100 lbs/sec-ft$^2$ ($q < q_c$):

The arrangement is a frothy mixture of large and small

bubbles interlaced with pure liquid as continuous phase, with highly agitated, frothy layer of tiny bubbles and liquid adjacent to heated surfaces. There are slight fluctuations of the pattern, indicative of a tendency for "slug" flow to develop, apparent at the low mass velocity (Figs. VI-20b, -21a, -22b).

(2b) $.10 \lessapprox X \lessapprox .30$ for $G \lessapprox 100$ lbs/sec-ft$^2$ ($q < q_c$):

A definite "slug" pattern develops as the steam quality is raised, which becomes less distinct and disappears at the high range of steam qualities.[1] The slugging pattern appears to be composed of a finely divided almost homogeneous froth of vapor and liquid alternating periodically (.05 to .10 sec. period) with an arrangement which appears to be a thick, relatively placid layer of liquid against the wall surfaces with probably high vapor concentration in the middle of the channel. This pattern is not observed at the higher mass velocities ($G = 200, 400$ lbs/sec-ft$^2$) (Figs. VI-20c, d).

(3) $X \gtrsim 0$ for $G = 400$ lbs/sec-ft$^2$ ($q \lessapprox q_c$):
$X \gtrsim .10$ for $G = 200$ to 400 lbs/sec-ft$^2$ ($q \lessapprox q_c$):
$X \gtrsim .30$ for $G = 50$ to 400 lbs/sec-ft$^2$ ($q \lessapprox q_c$):

An irregular wavy continuous film of liquid, flowing with the stream, is attached to the unheated surfaces and at least a portion of the heated surfaces. The remainder of the

---

[1] It is of interest to note that of the nine critical heat flux determinations rejected because of evidence of the critical heat flux condition having occurred substantially upstream from the exit (Appendix C), eight were in the range of mean exit steam qualities 0.12 to 0.39 at $G = 100$ lbs/sec-ft$^2$, corresponding to the "slug" flow regime described in 2b. Film sequence 4-5-a in Reel II (rejected run 4-4) shows evidence of substantial "slugging (Appendix D).

liquid is apparently carried along in the core as either: dispersed droplets in continuous vapor (at the lesser mass velocities and higher steam qualities (Figs. VI-19, -20e)); or a finely divided emulsion of liquid and vapor (Figs. VI-21b, c, -22c, e). Interfacial wave-lengths range from about one to five times the film thickness. The liquid film is apparently thicker and much less agitated at the unheated surfaces than at the heated surfaces (e.g., Fig. VI-23c). Irregular, agitated streamers of vapor (or irregular bubbles) can be seen forming at the edges of the heated surfaces and issuing into the liquid film (especially evident in Figs. VI-21c, -22e).

There is no apparent abrupt change of the flow pattern (in the field of view) as the critical heat flux condition develops other than an increase of the intensity of agitation of the film at the heated surface (e.g., Figs. VI-19c, d, -20e, -21c, -22c, e). There is no evidence of "slugging" or other general irregularities in the flow at any of the valid critical heat flux conditions.[1]

Except for the considerable differences due to local heating at moderate and high heat flux levels and the different range of flow variables and fluid properties used, the observed flow patterns have a general similarity to those observed by others for low pressure systems (Sec. III).

Evidence of a thermal boundary layer can be seen clearly against the unheated wall in some of the sequences in Reel V (also Figs. VI-23a, b). This optical effect results from local density differences caused by the temperature gradient associated with the heat transfer rate to

the wall (heat loss). This indicates the possibility of a technique for studying boundary layer phenomena in single-phase flow using shadow-graph or Schlieren equipment in conjunction with high speed motion pictures.[2]

As noted above under (3), there is evidence in the motion picture sequences of vapor formation in the liquid film against the heated wall. An approximate estimate of the wall to saturated liquid temperature difference $\Delta T_{SH}$ (liquid superheat) which would prevail if there were no local boiling in the liquid adjacent to the wall can be made by using the Reynolds Analogy (ref. (41), p. 209) in the following form, for saturated bulk fluid,

$$\Delta T_{SH} = \frac{qG}{c_p \rho_L^2 \nu_{*L}^2} ,$$

together with equation (41) of Section VII for the liquid-phase friction velocity

$$\nu_{*L}^2 = \frac{1}{2} \Phi_{TPF} f_F \frac{G^2}{\rho_L^2}$$

Combining these gives for the liquid superheat corresponding to no boiling at the wall

$$\Delta T_{SH} = \frac{2q}{c_p \Phi_{TPF} f_F G}$$

Calculated values for several critical heat flux runs selected from Appendix C to represent the least liquid superheats at the wall over the range of the experiment are tabulated in Table IX-1.[3]

---

[2] Suggestion of Dr. S. Levy, General Electric Company.

---

[3] Based on $c_p$ = 1.3 Btu/lb-F° (ref. (55)), $\Phi_{TPF}$ determined from Fig. VII-6 and $f_F$ calculated as in Appendix E.

TABLE IX-1

| Run No. | G, lbs/sec-ft$^2$ | $q_c$, $10^6$ Btu/hr-ft$^2$ | $X_c$ | $\Delta T_{SH}$, $^oF$ |
|---|---|---|---|---|
| 1-3 | 50.1 | .591 | .650 | 48.5 |
| 18-5 | 99.2 | .570 | .607 | 25.4 |
| 3R-4 | 99.4 | .857 | .465 | 50.5 |
| 6-3 | 199 | .847 | .233 | 49.4 |
| 15-2 | 394 | .880 | .258 | 24.3 |
| 9-1 | 397 | .832 | .104 | 40.5 |

According to the data of Mead, Romie and Guibert (ref. (54)), the maximum liquid superheat that can be sustained at a heated stainless steel-distilled water interface at 1000 psia, for both static and flowing systems, without bubble nucleation and growth is about 15°F to 20°F. For all of the cases in Table IX-1, the estimated liquid superheats which would have existed if there had been no bubble formation at the heater element surface are substantially larger than the maximum threshold level required for nucleation (ref. (54)). Since the runs selected are representative of the least liquid superheats which would have existed, it is therefore not surprising that evidence of vapor formation in the liquid film adjacent to the heater element surfaces can be seen in the motion pictures.[4]

[4] Larson (ref. (104)) presents additional theoretical discussion related to the maximum liquid superheat that can be sustained without nucleation. It is worth noting that the data of ref. (54) was taken with clean surfaces in distilled water. Surface deposits on the heater elements and impurities in the water used in the present experiment would be expected to lower the maximum liquid superheat above which bubble nucleation would start.

Critical Heat Flux Determinations

The experimental data is tabulated in Appendix C and presented graphically in Figure VI-1. Figures VI-2 through VI-14 show several representative Sanborn recorder traces of the system flow rate, heat flux changes, Critical Heat Flux Detector signal and sequencing of the camera, at conditions up to and including the critical heat flux level. Figures VI-14 a, b, c show recorder traces of these data during deliberate operation to destruction of one element at heat fluxes above the normal critical heat flux "trip" level (run 18RR-1). Figures VI-15 through VI-18 are photographs of heater elements showing various representative types of damages sometimes caused at the critical heat flux condition.

The main trends of variation of the critical heat flux can be summarized as follows (Figure VI-1):

(1) For all of the valid data the critical heat flux decreases monotonically with increasing steam quality. The nine data points which were rejected because of evidence of overheating in the upstream sections of the channel substantially away from the exit show a general trend that appears to have a maximum for $q_c$ with respect to steam quality at the exit, and they occurred at notably lesser heat flux levels than did the valid data points.[5]

(2) The critical heat flux decreases with increased mass velocity.

(3) The critical heat flux decreases with increased duct spacing (hydraulic diameter).

(4) The critical heat fluxes for the thin heater ribbons (.006 in.) are of the order of 10 per cent lower than for the

thicker ribbons (.010 in.). In some cases the difference is substantially more.[6]

(5) Although the data taken with the single-ribbon heaters are too few upon which to base a firm conclusion, indication is that the reduced ratio of heated surface to total surface resulted with lesser critical heat fluxes than for the double-ribbon heater elements.

Not allowing for the possible variations in $q_c$ due to the causes mentioned in footnote 6, the maximum deviations in measurement of the

---

[5] This trend is similar to those noted in refs. (11) and (12) for points taken during apparently oscillating or unstable flow conditions. There is some evidence that the flow may have been "slugging" during the rejected runs (see footnote 1). It is suggested that if there was "slug" flow during these runs, the cause of the critical heat flux condition occurring upstream from the exit may have been due to the fact that the higher steam quality "slugs" would have a local quality at any point during their path along the channel which would be higher than would exist at the same points if the flow were not "slugging." Therefore, depending on the heat flux level, it is not unreasonable to expect that in such a condition a "slug" might in the course of its travel up the channel have its steam quality reach the critical value corresponding to the particular channel heat flux, before the "slug" reached the exit. The critical heat flux condition would in this instance still be due to a local situation, but would not be capable of prediction or correlation using the usual energy balance based on mean flow parameters. It was due largely to this uncertainty of correlation that the nine points mentioned were rejected.

---

[6] Part of the reason for this difference may be due to the lesser thermal capacity in the thin elements coupled with the 60 cps alternating current used for resistance heating. An estimate using the results of Houston's analysis (ref. (105)) for a mean heat flux of 900,000 Btu/hr-ft$^2$ and a mean convection coefficient of 16,000 Btu/hr-ft$^2$-F$^o$ (allows for surface depositions) indicates the peak heat flux for the thin ribbon to be about 7 per cent higher than for the thicker ribbon. It is possible that larger differences may have occurred due to local thin spots caused by overheating of the ribbons at the exit end during fabrication of the silver-soldered joint there (see Appendix A). The thinner ribbons would be expected to be more susceptible to such damages during fabrication.

data are estimated to be less than 5 per cent for the critical heat fluxes and less than 2 per cent for the exit enthalpy at the critical heat flux condition.[7] Repeatability of the data is good, indicating that the phenomenon is a definite one not subject to significant statistical variation and that the main variables have been accounted for in the experiment[8] (Section VI).

Calculated data in Figure B-3 relating the Critical Heat Flux Detector output signal to heater element temperature rise indicates by comparison with the recorder traces in Figures VI-2 through VI-14 that onset of the critical heat flux condition initially causes only modest local temperature rises (probably of the order of a few tens of degrees Fahrenheit). The photographs in Figures VI-15, -16 indicate that the length of the zone of local temperature rise at onset of the critical heat flux condition is probably quite small (less than one inch).

Theoretical Analysis and Application

The analysis in Section VII is constructed to represent the critical heat flux condition corresponding to flow pattern type number 3, mentioned under "Flow Pattern Observations," in bulk boiling ($X \geq 0$). Figure VII-1A shows an artist's representation of the system assumed.

---

[7] Corresponding variations of the exit steam quality are somewhat larger (see Table VI-1, pg. 51).

---

[8] Since surface conditions and water purity (demineralized tap water) were not controlled except by flushing and venting gases during the four-hour warm-up period, the good repeatability of the data indicates that these are probably not significant variables in the range of conditions investigated. Surface deposits on the heater elements were noticeable after use.

Elements of the derivation are:

(1) Expression of the maximum liquid film thickness for incipient instability, caused by dynamic forces on the interface becoming larger than the stabilizing forces due to surface tension.

(2) Expression of the net liquid flow to the film at a point as the algebraic sum of the vaporization rate at the film, liquid re-entrainment rate, and liquid transfer rate from the core to the interface by turbulent diffusion.[9]

(3) Association of onset of the critical heat flux condition with momentary thinning of the film (but not necessarily immediate disruption of it), due to excess of liquid consumption rate over liquid supply rate, resulting with momentary stabilization of the film and consequent reduction to zero of the re-entrainment rate.

(4) Calculation of the critical heat flux condition at the limit as the re-entrainment rate becomes zero and the local rate of turbulent diffusion of liquid from the core to the interface approaches a maximum, corresponding to all liquid that comes in contact with the interface being pulled into the film due to surface tension effects and none being removed.

The rate of turbulent diffusion of liquid to the interface is

---

[9] This part of the analysis has a general similarity to the analyses by Isbin, et.al., (ref. (2)) and Goldmann, et.al., (ref. (3)) to the extent that a liquid flow balance to the vicinity of the wall is considered and a principal component is turbulent diffusion of liquid. Treatment of the diffusion process here, however, is more detailed and includes as an essential part variation of the local diffusion rate as a function of the distance from the wall (i.e., according to the thickness of the film at onset of the critical heat flux condition).

expressed in terms of the local fluctuating turbulent velocity component and, hence, based on the data of Laufer (refs. (26), (27)), is taken as a function of distance from the wall. The consequence of this assumption is far-reaching, inasmuch as it results with the liquid diffusion rate and, consequently, the critical heat flux condition being functions of the initial liquid film thickness at onset of instability.

All heat transferred is assumed to result in vaporization of liquid in the film and at the interface. The heat transferred by turbulent convection from the interface to the core is ignored.

The derivation suffers from the fact that the present experimental data and methods of analysis relevant to ascertaining the structure of the wall turbulence in two-phase flow, the relationships between interfacial wave motion and the properties of the mean flow, and the liquid concentration distribution in the core[10] are far from adequate for application in the type of analysis attempted in Section VII. Consequently, rather gross assumptions had to be made regarding some of the processes involved, which resulted in introduction of three empirical constants.

The result of the derivation is equation (52) in Section VII, which expresses the critical heat flux in terms of the relevant fluid properties (liquid and vapor densities, liquid-vapor surface tension and latent heat of vaporization), steam quality, mass velocity, and duct size (hydraulic diameter), with three empirical constants to be

---

[10] Levy's analysis of the mean local density distribution in two-phase flow (refs. (46) and (47)) holds promise of being capable of combination with the liquid film model treated here to more accurately represent the liquid concentration distribution in the core.

determined by fitting to the critical heat flux data.

Equation (52) has been applied to a representative selection of 822 data points from the major available sources (Section VIII, Appendix E). The following values of the constants in equation (52) were found to give reasonably good agreement with the data:

$m = 0.75$

$C' = 1.00$ (fraction of channel surface heated, .80 to 1.0)

$= 6.5$ (fraction of channel surface heated, .23 to .40)

$C'' = .53$ $(b > b_o = .084$ in.)

$= .53\ (b/b_o)^{.9}$ $(b < b_o = .084$ in.)

Detailed discussion of the basis for determination of these constants and comparison of results calculated by equation (52) with the data are given in Section VIII.

The fact that the exponent m could be held constant for the entire span of data treated indicates a certain universality in its character. Examination of equation (52) shows (for $f_F \sim G^{-0.2}$) that calculated $q_c$ decreases with increasing mass velocity G for $m > 0.5$. Hence, for $m = 0.75$ equation (52) predicts decreasing critical heat flux with increasing mass velocity in proportion to $G^{-0.45}$, in good agreement with the data.[11] Equation (52) predicts decreasing critical heat flux with increasing pressure over the range examined, 585 to 2500 psia, in good agreement with the data (Figs. VIII-7, -13).

For the range of duct sizes $b > b_o = .084$ in., equation (52) predicts decreasing critical heat flux with increasing duct size b

---

[11] Examination of the graphs in Section VIII (e.g., Fig. VIII-3) indicates better agreement might have been obtained if m had been taken slightly smaller, say m = 0.65, and C" correspondingly smaller (see Fig. VIII-1).

(hydraulic diameter) in proportion to $b^{-0.7} \sim D_e^{-0.7}$ for a particular geometry, in reasonably good agreement with the data (Figs. VIII-5,-8)). Except for the Russian data (Fig. VIII-13), for which a correction of 1.4 had to be applied, C" was held constant for the entire range of data for ducts larger than $b = b_o = .084$ in. This indicates a tendency for C" to be universal, provided the duct thickness (or radius) is large compared to the liquid film thickness.[12]

The fact that the particular Russian data treated is uniformly about 40 per cent higher than calculations by equation (52) predict may be due to the trend of increased critical heat flux with decreased length to diameter ratios over the range less than about 100, found in some of the Russian data (refs. (92), (96)). The length to diameter ratio for the Russian data in Fig. VIII-13 was 20:1. This trend is not evident in the other data treated, for which $L/D_e \geq 33$ (see Appendix E).

The two values for C' used, 1.00 and 6.5, are empirical. The difference between these values of C' reflects the effect of adjacent unheated surfaces on the local liquid concentration in the core. Larger values of C' result in decreased predicted critical heat flux, corresponding to reduced liquid concentration in the core due to

---

[12] For duct sizes less than $b = b_o = .084$ in. predictions by equation (52) deviate markedly from the data, indicative of the fact that the analysis in Section VII is not valid for thin ducts in which the liquid film thickness is not small compared to the duct half-width (or radius). Since the corresponding correction factor $(b/b_o)^{.9}$ applied to C" brings the predictions back into fair agreement with the data (Fig. VIII-4), the measured critical heat fluxes therefore tend to increase with increasing duct size in proportion to $b^{0.2}$, for thin ducts ($b < b_o = .084$ in.)

increased liquid attachment to the unheated surfaces.[13]

Uses of the Results

It is hoped that the results will be found useful in the following applications:

(1) Application of the experience obtained and recorded here to further improve and extend the technique and apparatus initiated in this work to more precise and comprehensive research and measurement of the structure of high pressure boiling water flows with heat fluxes up to and beyond the critical heat flux condition into the transition and film boiling (liquid deficit) regimes.

(2) Incorporation of the critical heat flux data tabulated in Appendix C into the body of nuclear reactor design data for direct application.

(3) Use by other researchers of the high speed motion pictures tabulated in Appendix D as a source of basic data and means for further study of the nature of high pressure boiling water flows and the critical heat flux phenomenon.

(4) Application of the theoretical analysis in Section VII as a starting point for continued theoretical investigation of

---

[13] Figure VIII-9 shows general agreement between calculated values using C' = 1.00 and measured values in an annulus (heated/total surface ratio = .30) for which the unheated surface was roughened to minimize attachment of liquid, in some support of this idea. Recent data from CISE (ref. (98)) shows an increase of the critical heat flux at one surface of an annular channel as the sub-critical heat flux at the other surface is raised, in further support of the argument.

the critical heat flux phenomenon.

(5) Direct application of the present theoretical result, equation (52) in Section VII, as a means for correlating and interpreting experimental data and as a tool for nuclear reactor design analysis.

# X. CONCLUSIONS

1. The critical heat flux to water in conditions of bulk boiling (X>0) with steady forced flow has the following trends, over the range of conditions investigated experimentally and analytically:

   (a) $q_c$ decreases with increasing mass velocity over the range from 50 lbs/sec-ft$^2$ to 900 lbs/sec-ft$^2$.

   (b) $q_c$ decreases with increasing pressure over the range from 600 psia to 2500 psia.

   (c) $q_c$ decreases with increasing hydraulic diameter over the range of duct dimensions[1] "b" from .084 in. to .24 in. and increases slightly with hydraulic diameter for the range of duct dimensions "b" less than .084 in. down to .024 in.

   (d) $q_c$ decreases monotonically with increasing steam quality over the range from 0.00 to 0.75.

   (e) $q_c$ increases with increasing ratio of heated surface to total surface.

   (f) $q_c$ is approximately independent of heated length over the range from 12 inches to 108 inches and range of length to diameter ratios from about 100 to 400. The Russian data indicates $q_c$ increases with decreasing $L/D_e$ ratios for $L/D_e < 100$.

   (g) $q_c$ appears to be calculable using local fluid properties and local flow conditions such as mass velocity, steam quality and pressure.

---

[1] b is the radius for circular tubes and one-fourth the hydraulic diameter for annular and rectangular ducts.

(h) The critical heat flux condition appears to be a distinct repeatable phenomenon rather than subject to significant statistical variation.

2. There is substantial evidence in the high speed motion pictures that the general arrangement of the flow, over the range of variables investigated, at heat fluxes near and including the critical heat flux level, is characteristically a wavy turbulent liquid film in which there is vapor formation, flowing along the channel walls with the balance of the liquid being carried as either dispersed droplets or as an emulsion with the vapor in an adjacent more rapidly and steadily moving core. This conclusion is not indisputable, due to lack of corresponding precise physical measurements of the arrangement of the flow pattern.

3. Theoretical analysis based on a representation of the flow pattern which is generally consistent with conclusion 2 resulted with a useful working equation which relates the critical heat flux to the significant local fluid properties and flow parameters (equation (52), Section VII). Critical heat fluxes calculated by this expression are in good general agreement with measured values over the range of variables considered. The expression includes three empirical constants which were determined by application to a limited portion of the data treated.

## XI. RECOMMENDATIONS

1. Although the evidence in the present work indicates strongly that the heated surface is covered by a liquid film through the inception of the critical heat flux condition, incontrovertible proof is lacking. It is therefore recommended that the next step in the research be development and use of an apparatus, similar in function to the observational test section but more specifically adapted to investigation of the process at the heated surface, to explore this aspect further.

   In particular, the apparatus should include provisions for close-up photography both normal and parallel to the surface and should include appropriate instrumentation for simultaneous measurement of the local heated surface temperature. It is recommended that the apparatus use high pressure boiling water as the working fluid in order that there be adequate assurance, at the present state of development of the technology, that the results will be applicable to nuclear power reactor design, for which the need for early application is probably greatest.[1]

2. It is suggested that equation (52) be used as a tool in nuclear reactor design analysis. In preparation for this, the three empirical constants should be refined by fitting them to a limited selection of data which is most representative of reactor design conditions.

---

[1] Professor J. W. Westwater has suggested use of: (a) smaller systems, each designed for investigation of a specific aspect of the problem; (b) liquids other than water to vary fluid properties over a wider range at modest pressures; (c) heater elements made of pure metals and used as resistance thermometers. (Professor Westwater was consultant to the project during the early experimental stage. Ref. (70) includes his report.)

3. Theoretical effort should be continued, to refine the analysis of the critical heat flux condition in forced flow with bulk boiling. In particular, the representations of the liquid concentration distribution in the core, turbulent diffusion of liquid to the interface, and the inter-relationship between the local turbulence, the film thickness and the dominant length of the interfacial waves should be improved.

4. Consideration should be given to the practicality of conducting a set of small scale experiments to make measurements of the local structure of two-phase flow, both with and without heating, in conjunction with the theoretical effort. Particular attention should be given to measuring liquid concentration distributions, local turbulence structure and the motion of the liquid film interface.

## APPENDIX A

## DESCRIPTION OF THE OBSERVATIONAL TEST SECTION

### Introduction

The observational test section was developed as part of this work to provide a means for direct visual observation and high speed photography of the two-phase flow, critical heat flux conditions and heat transfer processes with boiling water at elevated pressures. The test section was designed and built at General Electric Company Atomic Power Equipment Department, San Jose, California, and was put into initial operation in the Building G Heat Transfer Test Facility in July 1960.[1] Further development work on the photographic window assembly, the heater elements and the associated instrumentation and general experimental setup was then done to improve performance of the equipment. The final experimental phase of the program, during which most of the critical heat flux data and all of the selected motion pictures of boiling water flow patterns were obtained, was executed during the first four months of 1961.

The test section is shown installed in its safety enclosure in Figure IV-2 and in disassembly in Figures IV-3 and IV-4. Figures A-1 and A-2 are reductions of the main assembly and heater element assembly design drawings.

### Test Section Body

The test section body, shown partially in Figure A-1 and in full in Figure IV-3, was formed by welding together, with reinforcing ribs, two

---

[1] Detail design-drafting of the test section was done by Mr. C.E. Nessle, Draftsman-Designer. The test section was built by Mr. R. C. Dixon, Machinist.

bars of stainless steel five feet long and 3-1/2 inches square in cross-section, which were grooved on their mating faces to form a heavy-walled rectangular channel five feet long and about 7/8 inches by 2-1/8 inches in cross-section. To each end of this 5-inch schedule-80 stainless steel pipe fittings were welded to form the terminal heads for the flow connections and the heater element electrical power connections. The resulting integral assembly was then broached to achieve the required tolerances on channel dimensions and machined to final size and shape to accommodate the window assemblies and instrumentation taps. The resulting piece has provisions for seven pressure taps spaced along its length, twelve voltage taps for critical heat flux detection, twenty blind holes for possible later use to measure steam volume fractions by the gamma attenuation technique, and observation windows at any of the four window sections along its length.

The structural members of the test section are all made of stainless steel type-304, and all welds were made in accordance with the ASME Boiler and Pressure Vessel Code. The pressure-bearing pyrex glass windows, window covers, cover bolts, gasket seats and gaskets are either standard parts used on the Penberthy Liquid Level Gage, model WT-16 or were fabricated to conform to critical design specifications provided as a courtesy by Penberthy Manufacturing Company, Detroit, Michigan.

Analysis of the stresses in the test section together with a formal hydrostatic test at 2100 psig and room temperature conditions established the maximum service rating in accordance with the ASME Boiler and Pressure Vessel Code to be 1100 psig maximum operating pressure at 600°F maximum operating temperature (refs. (60), (61), (62)).

Photographic Window

Assembly of the photographic window is shown in Figure IV-4. The photographic window was located adjacent to the exit end of the heater element at the second window section from the outlet. The other three window sections were fitted with stainless steel "blanks" to form a smooth flow channel (See Figure IV-3).

The window assembly shown in Figure IV-4 was installed on the front side of the test section together with a coated front-surface mirror (shown in Figure IV-3) which directed the optical image into the camera lens. The front edge of the flow channel was formed by a rectangular mono-crystalline sapphire filler block (inside face 4.320 in. long, .585 in. wide, .390 in. thick) together with a stainless steel filler block holder into which it is fitted and clamped. The filler block holder contains several small drilled holes which serve to equalize pressures and permit a small bleed of flow channel liquid through a thin (approximately .03 in. thick) liquid filled space between the filler block and the outer pressure-bearing pyrex window glass. The size and number of the bleed holes were selected by trial-and-error so as to provide enough bleed flow to wipe deposits from the pyrex window and still prevent excessive passage of steam bubbles into the space between the pyrex window and the filler block. Compressed asbestos gaskets were used as a pressure seal between the pyrex pressure-bearing window glass and machined gasket surface on the test section body and as a cushion to absorb differential thermal expansion between the window glass and the retaining cover. The carbon steel retaining cover or frame clamps the window glass tightly in place by means of stud bolts which extend through the test section body to the matching

cover on the back side. The window gaskets, pyrex window glass and retaining cover are standard stock items used on the Penberthy Liquid Level Gage, Model No. WT-16. The window glass is Macbeth brand, Type A, made by Corning Glass Company. The manufacturer's service rating for these is 1660 psig at 600°F. The sapphire filler block is a fully annealed synthetic crystal made to order by Linde Company, Division of Union Carbide and Chemicals Corporation.

The arrangement at the back side of the test section was identical with the front side, except that in place of the sapphire filler block and holder a full-length pyrex filler block was used (inside face 9.355 in. long, .610 in. wide, .385 in. thick). The pyrex filler block was made by Braun-Knecht-Heimann Company, Belmont, California, using Corning Glass Company pyrex, code No. 7740.

The original test section design used a one-piece pyrex window glass which, in effect, incorporated the filler block with the pressure-bearing window as an integral piece. This design was replaced by the two-piece window arrangement early in the trial operation period due to the high breakage rate of the integral windows, caused by their relative stiffness and high surface stress concentrations.

The two-piece window design which was next used incorporated full-length pyrex filler blocks at both the front and back sides of the test section. After some operation it was found that the rate of damage of the pyrex surfaces due to erosion and dissolution caused by the adjacent rapidly flowing two-phase stream was too large at 1000 psia saturated conditions to be practical from the standpoint of maintaining satisfactory optical characteristics for the photographic window. As a result, the filler block at the front side of the test section was

replaced with the special sapphire crystal filler block and holder. Since the only requirement of the filler block at the back side was that it be translucent and reasonably smooth, the full-length pyrex filler block design was retained there. Frequent replacement of the outer pressure-bearing pyrex window glasses and the pyrex filler block at the back side was required due to surface damage and dimensional changes caused by erosion and dissolution.[2] The sapphire filler block was used throughout the remainder of the experiment, for over 200 hours of operation at 1000 psia saturated test conditions, with negligible deterioration of its optical qualities.

Mirror

The optical mirror and holder are attached to the front retaining cover of the photographic window assembly as shown in Figure IV-3. The mirror is 10 inches long by 2 inches wide with an aluminum reflector coating on the front surface to avoid parallax and a silicon oxide overcoating to protect the reflector and to increase reflectivity. The mirror was made by Spectracoat, Inc., Belmont, California.

Heater Element

Details of the heater element construction are specified in Figure A-2 and can be discerned in Figures IV-3 and IV-4 and Figures VI-15 through VI-18.

The heated portion of the heater elements was fabricated from

---

[2] Material removal rates due to erosion and dissolution of the pyrex in contact with the flowing two-phase stream at 1000 psia saturated conditions were measured to be about .001 in. per hour. Damage rates to the outer pressure-bearing pyrex window were less due to the protection afforded by the inner filler block. A small amount of damage to the pyrex surface could be tolerated without excessive deterioration of optical characteristics due to the relatively small refraction at the liquid water-pyrex interface.

stainless steel, type 302 precision shim stock,[3] made by Precision Steel Warehouse, Inc., Downers Grove, Illinois. The shim steel heater ribbons are connected at the bottom to the lower electrode assembly by means of a silver-soldered, clamped terminal located below the inlet to the rectangular flow channel in the inlet terminal head, leaving about 2-1/2 inches of unobstructed heater ribbon in the terminal head. The heater ribbons extend upward through the flow channel to a point at about the middle of the second window section from the top where they are joined by silver-soldered step-joints to nickel-plated copper connector-strips which continue, with no change in flow geometry, to a silver-soldered joint with the upper terminal located about 2-1/2 inches above the outlet of the rectangular flow channel in the outlet terminal head. The overall heated length inside the rectangular flow channel is 37.0 inches. The unheated section of the rectangular flow channel to the outlet is 21.8 inches, giving an overall length of unobstructed rectangular flow channel of 58.8 inches.

The electrical terminals at each end of the heater element are connected by means of a U-shaped clamp to one-inch diameter connector rods which serve to make electrical connection through a flexible cable assembly to copper electrodes which penetrate the head closure covers of the two terminal heads through insulated pressure seals. The connector rods are positioned by respective sets of two stainless steel spiders which are bolted through insulated holes to mating flanges welded on the inside of each terminal head. The transverse positions of the spiders are adjustable in order to provide means for adjusting the transverse

---

[3] Measured thickness variation of this stock is less than .00005 in. (Measurements made on a Pratt and Whitney 48-inch Standard External Length Measuring Machine.)

and azimuthal position of the heater element in the flow channel. Tension on the heater element and means for adjustment of its axial position are provided by a large nut on the threaded portion of each connector rod. The force causing tension on the heater element is transmitted through a bushing to the outermost spider at the outlet end and through a double spring assembly to both spiders at the inlet end. The double spring assembly serves to compensate for differential thermal expansion between the heater ribbons and the test section body. All copper parts of the heater element are nickel plated.

The heater element was insulated electrically and thermally from the test section body by accurately cut laminations of rubberized compressed asbestos (Durabla), which also served to accurately fix the spacing between heater ribbons and, consequently, the channel thickness. This material had the characteristic of becoming adhered quite tightly to the backs of the heater ribbons as the section was brought to hot operating conditions, as shown by the stained appearance of the heater ribbon back of the used heater element in Figure VI-15. This was a useful aid to maintain the heater element properly positioned and to prevent flow between the heater ribbons and the insulation. All other insulations in the heater element assembly were made from Rulon-A, a high temperature resistant fluorocarbon compound similar to Teflon, manufactured by the Dixon Corporation, Providence, Rhode Island.

A combination of stainless steel leaf springs and U-shaped wire springs, spot-welded periodically along the heater element between the ribbons, as shown in sections B-B and D-D of Figure A-2, was used to press the heater ribbons tightly against the insulation strips in back in opposition to the electrical forces tending to draw the ribbons together.

Three sets of these springs at the upper end of the heated section served also to equalize voltages between ribbons in connection with the Critical Heat Flux Detector circuit (Appendix B). One heater ribbon of each heater element assembly had spot-welded to it a .020-inch diameter stainless steel wire focusing target, as shown in enlarged view E of Figure A-2, used for focusing the high speed motion picture camera.

After assembly in the test section, each heater ribbon was connected to voltage taps for the Critical Heat Flux Detector circuit. The voltage taps were made of short lengths of annealed stainless steel wire, spot-welded to the backs of the heater ribbons and threaded through holes in the test section body, insulated by tubes of Rulon-A, and threaded through insulated packing glands (made by Conax Corporation) screwed into the test section body.

The heater elements used were of five basic types, corresponding to the heater ribbon thickness, spacing between ribbons (flow channel thickness), and number of sides of the channel heated (single-ribbon or double-ribbon). The heater element types are defined in Appendix C.

For heater element types 1A and 1B (.50 in. spacing), all of the space between the backs of the heater ribbons and the inside walls of the test section channel was filled with the Durabla insulation. For types 2A and 2B (.25 in. spacing), additional space was filled by .125 inch thick full-length stainless steel shims on each side, laminated between the Durabla insulation and the test section walls. Type 3 (single-ribbon) was formed by installing only one heater ribbon in the heater element assembly.

For type 3 (single-ribbon, .50 in. spacing) the unheated wall of

the flow channel was formed by one of the .125 inch thick full-length shims installed with a layer of Durabla behind to properly locate it in the flow channel. Special insulated leaf springs, not shown in any of the Figures, were spot-welded at points along the shim to press the opposite heater ribbon back against its insulation.

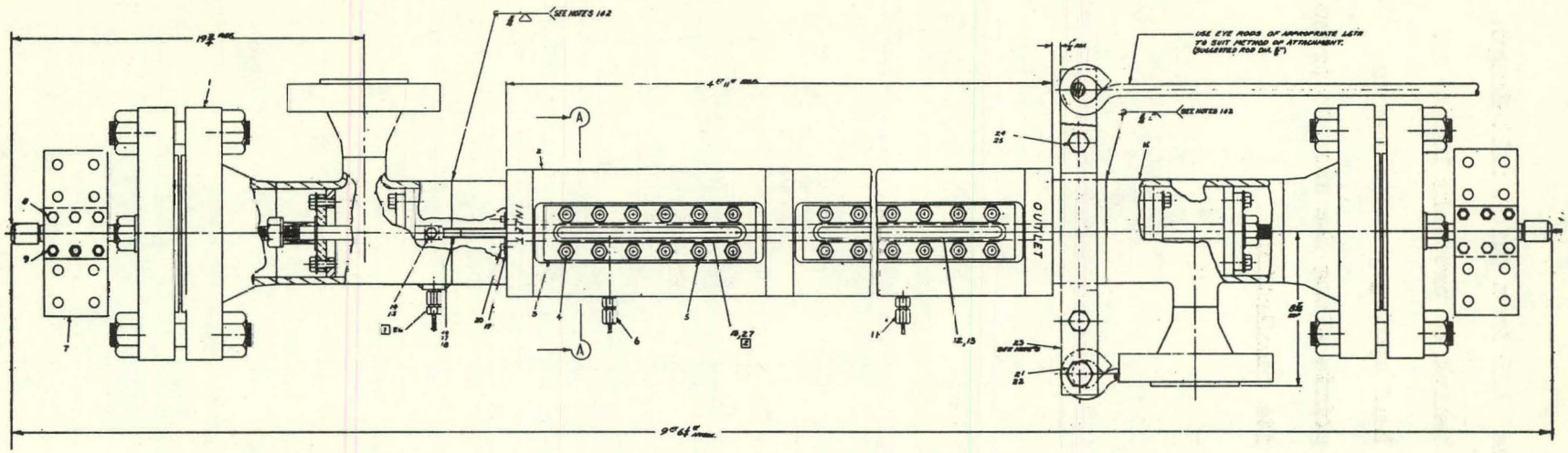


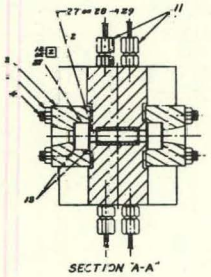


(6-1) ASSEMBLY WITH PT-14 HEATER ELEMENT 980 WATTS

(6-2) ASSEMBLY WITH PT-17 HEATER ELEMENT OTHERWISE SAME AS 6-1

(6-3) ASSEMBLY WITH PT-18 HEATER ELEMENT OTHERWISE SAME AS 6-1

NOTES:

1. ALL WELDS SHALL BE PERFORMED AND INSPECTED IN ACCORDANCE WITH ASME BOILER AND PRESSURE VESSEL CODE SECTION I, LATEST EDITION AND ADDENDA IN EFFECT.
2. ALL CHANNEL WELDS AND ENTIRE ASSEMBLY TO BE POSTWELD HEAT TREATED AS A UNIT.
3. PT-16 SHALL BE MARKED "NOT FOR TRUE PRESSURE".
4. MAXIMUM OPERATING PRESSURE 1100 PSIG
MAXIMUM OPERATING TEMPERATURE 600°F.
ASME BOILER AND PRESSURE VESSEL CODE STAMP, PER THIS RATING PLACED THEREON, BASED ON HYDROSTATIC TEST DEFINED IN P-144, 6-4-6.
(FILED, GENERAL ELECTRIC CO. ARCO EQUIP DWG.)

# OBSERVATIONAL TEST SECTION ASSEMBLY
## (G.E. DWG. NO. 197E635)

FIGURE A-1

OBSERVATIONAL TEST SECTION ASSEMBLY

(Drawing Number 197 E 635)

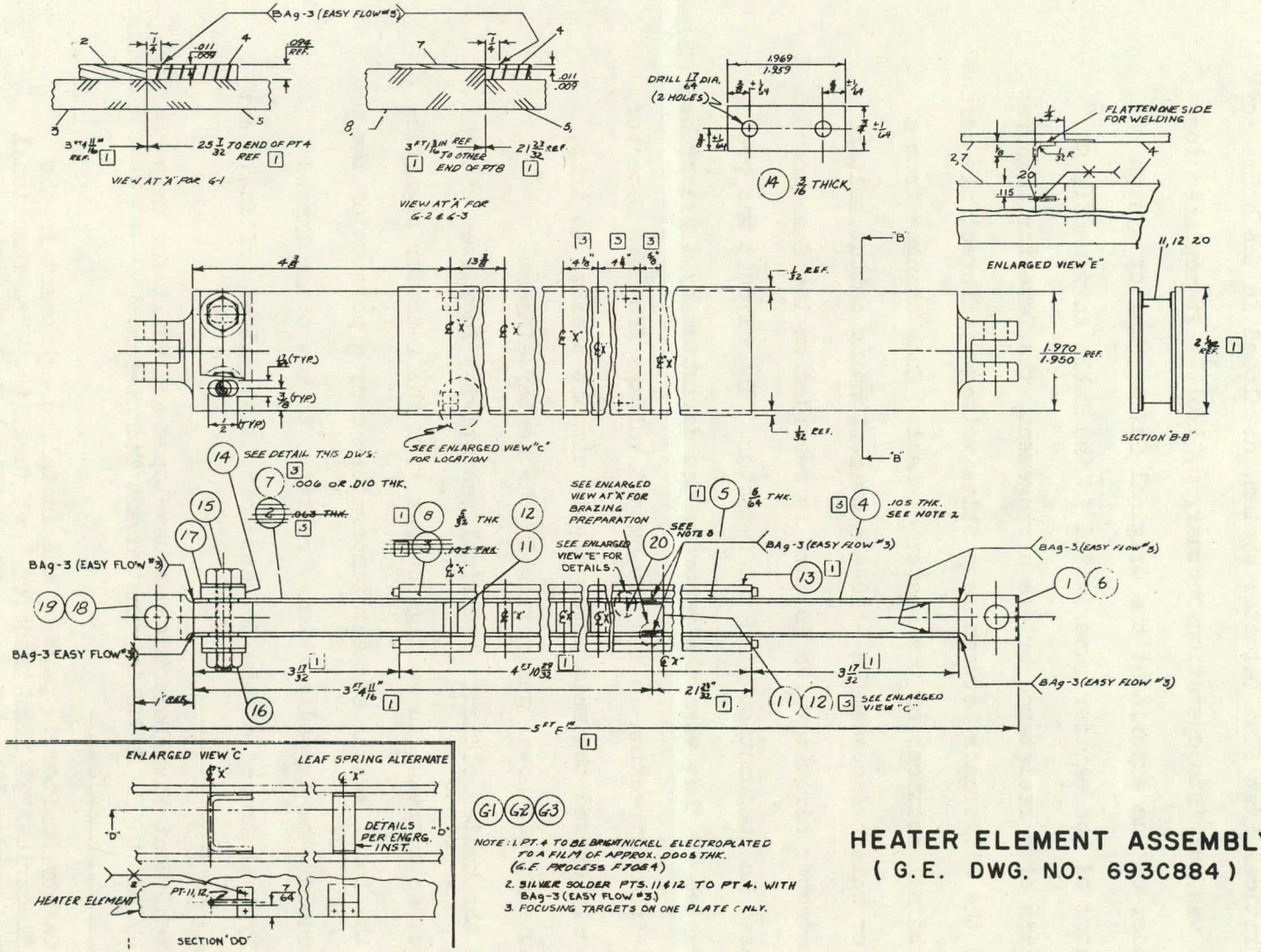


**HEATER ELEMENT ASSEMBLY**
**( G.E. DWG. NO. 693C884 )**

FIGURE A-2

HEATER ELEMENT ASSEMBLY

(Drawing Number 693 C 884)

## APPENDIX B

## DESCRIPTION OF THE CRITICAL HEAT FLUX DETECTOR

### General

The Critical Heat Flux Detector system, developed in the course of this work, was put into operation February 6, 1961.[1] It replaced for the remainder of the experiment the original Safety Monitor system used for some of the earlier runs (noted in the Table in Appendix C).[2]

By means of a resistance bridge arrangement, the Detector measures changes in the difference between respective voltage differentials across two longitudinal sections of the heater element. Such changes from a reference or balanced condition cause a corresponding output voltage from the Detector circuit which in turn is recorded on the Sanborn recorder used in conjunction with the Detector. The circuit was precisely adjusted so that when the recorder pen deflected by a prescribed amount in either direction (6 mm) the output voltage from the Detector simultaneously caused the main power supply circuit breaker to trip, thereby shutting off power generation in the heater element.

Since the heater element electrical resistivity increases with temperature, an increase in voltage output from the Detector signifies a rise of the local heater element temperature over a portion of the length of one of the tapped sections, relative to the other tapped section. Typical traces of the Detector output signal at critical heat

---

[1] The Critical Heat Flux Detector was developed and built for this project by Mr. C. H. McCubbin, Instrument Technician.

[2] The GEL Safety Monitor is part of the installed equipment in the General Electric-APED heat transfer test facility. Its functional operation is generally similar to the Critical Heat Flux Detector, except that it has no recording provisions.

flux conditions are shown in Figures VI-2 through VI-14. The distinctive character of the Detector output voltage variation with time at establishment of the critical heat flux conditions, as recorded by the Sanborn recorder, formed the main basis for judging when to start the motion picture camera in order to synchronize with onset of the critical heat flux condition. Deflection of the recorder pen to the right (towards the time marker) corresponds to increase in heater element temperature at the outlet end.

The particular Detector voltage output level selected as the threshold to cause the main power circuit breakers to trip was high enough to avoid spurious power trips due to occasional small electrical transients not related to the critical heat flux condition and to permit normal operational adjustments of the test section power, flow, pressure and inlet sub-cooling without causing spurious trips due to the disturbances caused by these adjustments. The selected threshold level was low enough to give adequate assurance of shutting off the test section power in time to avoid damage to the heater element during the critical heat flux condition. The time delay in the external circuit for the main power circuit breaker to trip after the Detector output voltage reached the trip threshold level is estimated from the Sanborn recorder traces to be about 0.1 second.

During each approach to a critical heat flux condition, the Detector circuit was maintained in approximate null balance by manual adjustment using the continuous recorder trace of the voltage output as a guide, up to power levels within a few per cent of the critical heat flux. This procedure assured adequate compensation for any initial unbalances in the circuit, which tend to be amplified as the test

section power and voltage differences are increased, thereby maintaining the change in voltage output from the Detector required to trip the main power circuit at approximately the prescribed value.

Detector Circuit

The Critical Heat Flux Detector circuit is diagrammed in Figure B-1, showing the connection to the heater element at voltage taps VT-1, VT-2, and VT-3, the connection through relay $K_5$ to the main power circuit breaker, and the connection to the Sanborn recorder. The heater element voltage taps were made by three insulated stainless steel wire probes spot-welded to each heater ribbon to make one pair of taps connected in parallel at each of the three voltage tap locations. The top pair was located at the outlet end of the heated section (VT-1), the next lower pair was located 4-1/4 inches upstream from the outlet end (VT-2) and the lowest pair was located 4-1/8 inches further upstream (VT-3). The heater element construction included internal electrical connections between the two heater ribbons at each of these locations in order to equalize heater ribbon voltages at these points. The resistances of the two tapped sections of the heater element are designated by $R_1$ and $R_2$ in Figure B-1.

Heater element resistances $R_1$ and $R_2$ form two legs of a resistance bridge circuit. The other two legs are $R_3$ and $R_4$ together with a variable resistance $R_5$ used as a potentiometer for balancing of the bridge. The primary side of transformer $T_1$ is connected between VT-2 and the potentiometer tap. Transformer $T_1$ provides a gain in output voltage from the bridge of about 36:1.

An unbalance in the bridge caused by a change in the relative resistance of either $R_1$ or $R_2$ from an initial balanced condition causes

current flow in the primary side of $T_1$, thereby inducing an output voltage from the secondary side of $T_1$. This output voltage feeds as an alternating-current error signal through taps A and E to a Sanborn servo-monitor type preamplifier (Model 150-1200).

The preamplifier is both amplitude and phase sensitive. It includes two stages of amplification, a mixer stage, demodulation and an output amplifier.

Output from transformer $T_2$ provides a 12-volt alternating-current reference voltage to the preamplifier through taps E and C. Output voltages from $T_1$ and $T_2$ are either in phase or 180° out of phase, depending on which of the resistances $R_1$ and $R_2$ changes to unbalance the bridge. This determines the direction of deflection of the recorder pen.

The preamplifier delivers a demodulated signal, corresponding to the direction and amount of bridge unbalance, to a Sanborn driver type amplifier (Model 150-200 B/400). Output from this amplifier causes deflection of the pen of a direct-writing center-tapped galvanometer in a Sanborn recording oscillograph (Model 150-100 BW). An internal direct-current power supply (not shown) provides the plate, bias and heater voltages required in both the preamplifier and the driver amplifier. The galvanometer circuit is parallel tapped at 1 and 2 to impress the direct current galvanometer voltage difference across relay $K_3$.

$K_3$ is an Advance relay (Model SV/1C/20,000 D), single-pole, double throw type of high sensitivity. $K_3$ is in the normally open position and is tripped closed by the galvanometer voltage difference. Variable resistors $R_6$ and $R_7$ connected in series with $K_3$ and the galvanometer circuit taps 1 and 2 provide the means for fine adjustment of the trip

point for $K_3$ in terms of the galvanometer voltage difference and, hence, the degree of unbalance of the Detector bridge circuit and the magnitude of the change of the relative heater element voltage difference across either of the two resistances $R_1$ or $R_2$.

When the bridge is balanced by adjustment of $R_5$ so that its output voltage from $T_1$ is zero, the galvanometer pen is centered and no current flows through the relay $K_3$. $K_3$ and the variable resistors $R_6$ and $R_7$ were set so that an increase of the bridge output voltage from null balance by an amount sufficient to cause deflection of the galvanometer pen 6 mm in either direction would cause relay $K_3$ to trip.

Tripping of relay $K_3$ energizes an auxiliary direct current circuit, which causes the main power breaker switch relay $K_5$ to trip open, thereby shutting off the power supply to the heater element.

Calibration

Electrical measurements made during the course of the experiment established the linearity of the galvanometer pen deflection with bridge output voltage. The measured bridge output voltage to the primary side of transformer $T_1$ was .078 millivolts output per millimeter deflection of the recorder pen (recorder set on a scale factor of unity). The following analysis employs this information to interpret recorder pen deflections in terms of estimated heater element temperature increments.

Analysis of Heater Element Temperature Changes

For the purpose of this analysis, the bridge circuit connecting the heater element taps VT-1, VT-2 and VT-3 with the amplifier, recorder and power trip devices at taps A and E in Figure B-1 is represented by diagram A in Figure B-2. The effects of transients

are neglected.

Resistances $R_1$ and $R_2$ in diagram A are the respective resistances of the tapped sections of the heater element at the outlet end, as shown in diagram B of Figure B-2. When the bridge is balanced, the bridge output voltage e' and the output voltage e from the secondary side of transformer $T_1$ to the preamplifier are zero, the corresponding resistance of the outlet section of the heater element is $R_1 = R_1'$, and the potentiometer resistance $R_5$ is split into $R_{5a}$ and $R_{5b}$. At balance the bridge resistances are therefore related according to

$$\frac{R_1'}{R_1' + R_2} = \frac{R_3 + R_{5a}}{R_3 + R_4 + R_5} \qquad (1)$$

Onset of the critical heat flux condition is considered to be characterized by an abrupt rise (or fluctuation) of the local heater element temperature in a patch in the outlet section between taps VT-1 and VT-2, with a corresponding increase in the resistance $R_1$ to $R_1 = R_1' + r$. At this condition the bridge circuit is unbalanced causing the voltage output from the secondary side of transformer $T_1$ to become

$$e = \frac{r R_2 E N_1}{(R_1' + R_2)(R_1' + R_2 + r)} \qquad (2)$$

where $N_1$ is the voltage ratio for $T_1$, E is the heater element voltage difference between VT-1 and VT-3 and the resistance increment r is recognized to be sufficiently small that the corresponding changes in E and in the heater element current I are negligible (less than 0.1 per cent). Since r is small compared to $(R_1' + R_2)$, equation (2) reduces to

$$e = \frac{r R_2 E N_1}{(R_1' + R_2)^2}$$

Hence, for the test section current $I = E/(R_1' + R_2)$ taken as constant the transformer output voltage to the amplifier circuit is

$$e = r I N_1/(1 + R_1'/R_2) \qquad (3)$$

As an idealization consider the zone of inception of the critical heat flux condition to be represented by a rectangular patch on one of the heater ribbons of length "a", width "b" and average temperature $\Delta T$ above the average temperature T of the rest of the heater element, as depicted in diagram B of Figure B-2. The heater ribbons are considered to have an average electrical resistivity $\rho_1$ corresponding to T, except for the hot patch "ab" which has a higher average resistivity $\rho_2$ corresponding to $T + \Delta T$. Considering the patch "ab" to behave as a separate resistor in simple series-parallel electrical connection with the rest of the heater element gives for the resistance increment $r = R_1 - R_1'$,

$$r = R_1' \frac{a}{L_1} \left[ \frac{d/b}{d/b - 1 + \rho_1/\rho_2} - 1 \right] \qquad (4)$$

where $L_1$ is the length of the heater element section corresponding to $R_1$ between taps VT-1 and VT-2 and d is twice the width of each heater element ribbon.

For the stainless steel heater element material,

$$\frac{\rho_1}{\rho_2} = \frac{1}{1 + \alpha_T \Delta T/\rho_1} ,$$

where $\alpha_T$ is the mean temperature coefficient of resistivity over the temperature interval T to $T + \Delta T$. Using this relation in equation (4), substituting for r in equation (3) and noting that $I R_1' = E_1$ gives

$$e = E_1 N_1 \frac{a}{L_1} \left[ \frac{d/b}{\frac{d}{b} - 1 + \frac{1}{1 + \alpha_T \Delta T/\rho_1}} - 1 \right] \qquad (5)$$

Calibration of the Detector circuit in conjunction with the Sanborn recorder established the recorder pen deflection $\delta_R$ as a function of the bridge output voltage to be

$$\delta_R = K_c N_T e' = K_c e$$

where $K_c$ = 350 mm/volt.

Thus, substituting this into equation (5) for e and solving for the temperature rise of the patch $\Delta T$ gives as a general working equation in terms of the patch dimensions "a", "b"

$$\Delta T = \frac{\rho_1/\alpha_T}{\frac{b}{d}\left[1 + N_1 K_c E_1 a/L_1 \delta_R\right] - 1} \qquad (6)$$

Critical heat fluxes found in the experiment range from about 550,000 Btu/hr-ft$^2$ to 1,115,000 Btu/hr-ft$^2$. Taking 800,000 Btu/hr-ft$^2$ as representative with the coolant in bulk boiling at 1000 psia, the voltage difference $E_1$ and mean internal heater ribbon temperatures $\overline{T}_i$ for the two double ribbon heater element types, .006 in. and .010 in. ribbon thickness, are calculated to be as follows:

| Heater Ribbon Thickness, in. | $E_1$, volts | $\overline{T}_i$, °F |
|---|---|---|
| .006 | 14.0 | 569.4 |
| .010 | 10.8 | 573.4 |

The Jens-Lottes equation, $\Delta T_{sat} = 1.9\, q^{\frac{1}{4}}/e^{p/900}$, was used to estimate the wall surface to coolant temperature differences (ref. (41)), and the mean internal temperature differences were estimated from the derived

relation, corresponding to negligible end and edge effects, for ribbon thickness t' and thermal conductivity k,

$$\Delta \bar{T}_i = qt'/6k$$

k was taken as 11 Btu/hr-ft-°F, for stainless steel at about 600°F and $E_1$ was calculated using measured cold heater element resistances adjusted to operating temperature according to data given in ref. (59) for stainless steel. Taking 600°F as representative of the mean temperature for both elements, data in ref. (59) for type 304 stainless steel was used to calculate $\rho_1/\alpha_T = 3100°F$.

Using these values together with d = 3.92 in., $N_1 = 36$ and $L_1 = 4.25$ in. calculations of the temperature rise $\Delta T$ corresponding to various deflections of the recorder pen $\delta_R$ were made for each of the two heater element types for two representative hot patch geometries. The results are plotted in Figure B-3.

Cases 1 and 3 in Figure B-3 for the 1/4 in. square patch are intended to be representative of the type of critical heat flux zone geometry indicated by the elongated circular area of overheated metal seen about one-fourth inch from the end of the heater ribbon in Figure VI-16. (approximately 0.3 in. diameter). Cases 2 and 4 for a 1/2 in. long by 1 inch wide rectangular patch show in comparison the effect of patch geometry on the relationship between recorder pen deflection and corresponding hot patch temperature rise. The patches of overheated metal seen in the burned heater elements of Figures VI-15 and VI-18 are roughly represented by the larger hot patch geometry assumed for Cases 2 and 4.

The calculated results indicate that at the initial inception of the critical heat flux condition, as manifested by a slight deflection

of the recorder pen (less than 6 mm), the order of magnitude of the local heater element temperature rise is probably less than 100°F, even for relatively small patches in the critical heat flux condition. It is likely, however, that as the critical heat flux condition becomes more completely established, especially at the higher critical heat flux levels for which full establishment of the condition appears to be abrupt, the heater element temperature may actually rise substantially above the values indicated in Figure B-3, due to the heretofore neglected transient response characteristics of the Detector circuit.

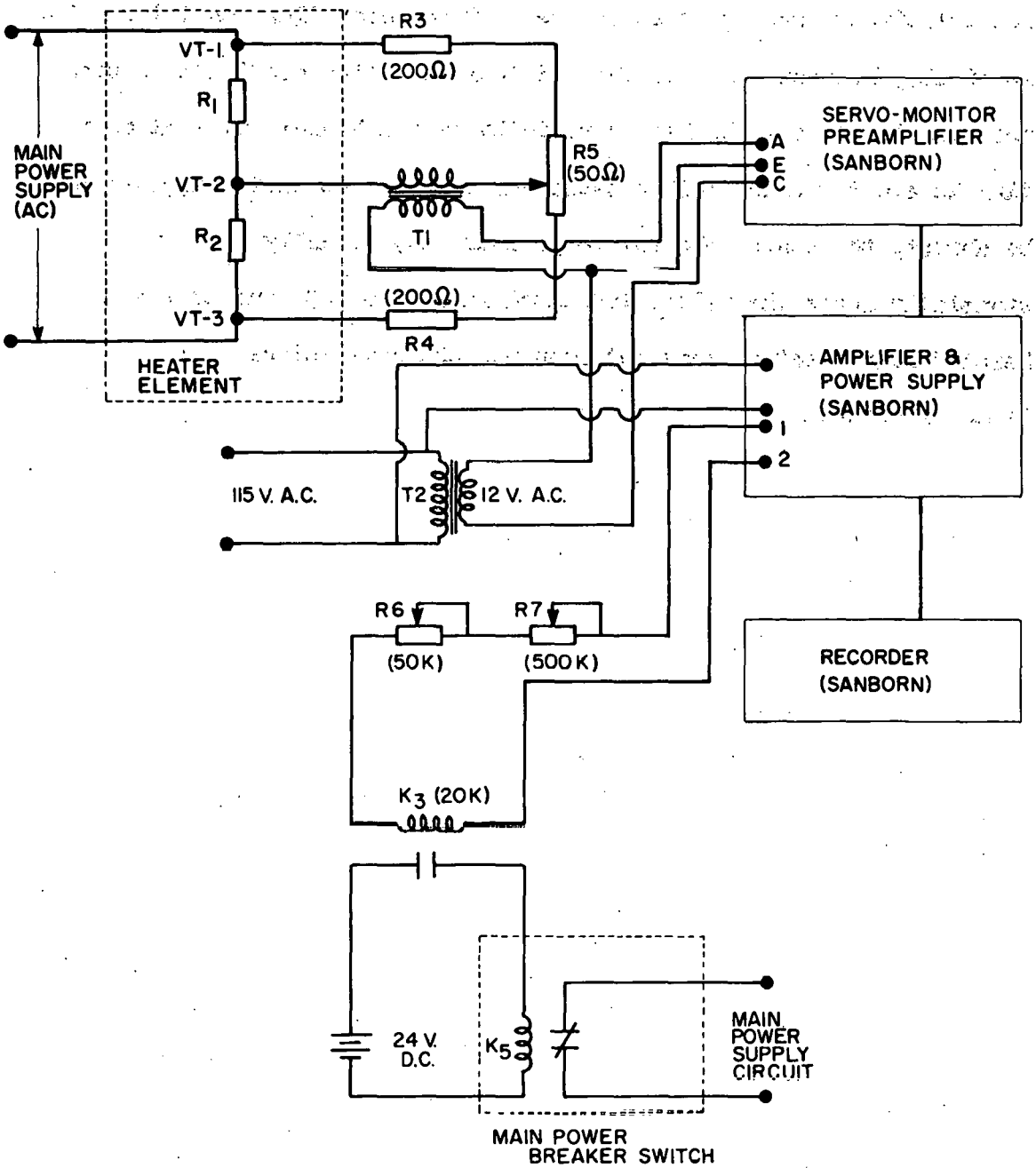


FIGURE B-1

CRITICAL HEAT FLUX DETECTOR CIRCUIT

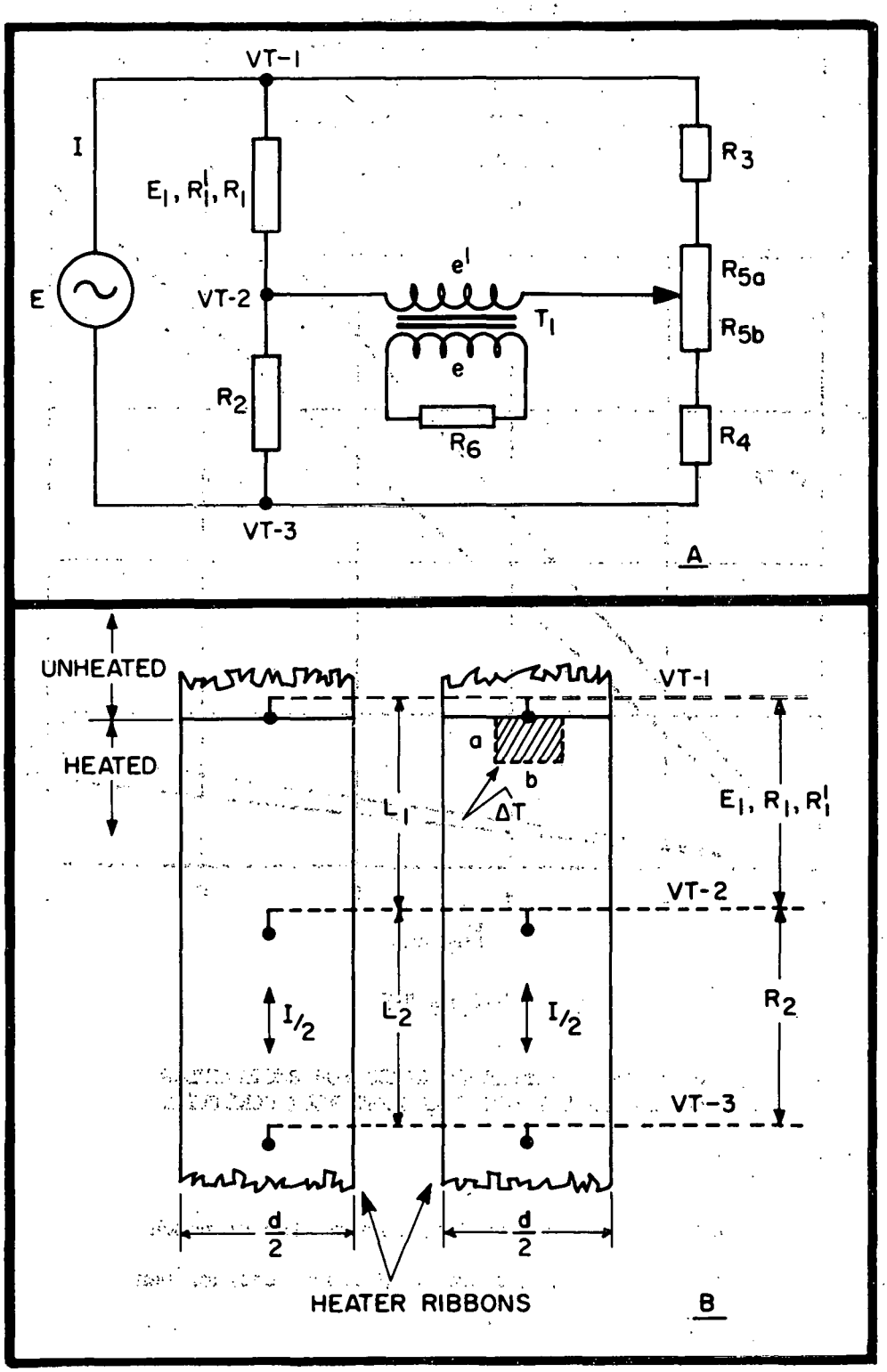


FIGURE B-2

REPRESENTATION OF CRITICAL HEAT FLUX DETECTOR BRIDGE CIRCUIT FOR ANALYSIS

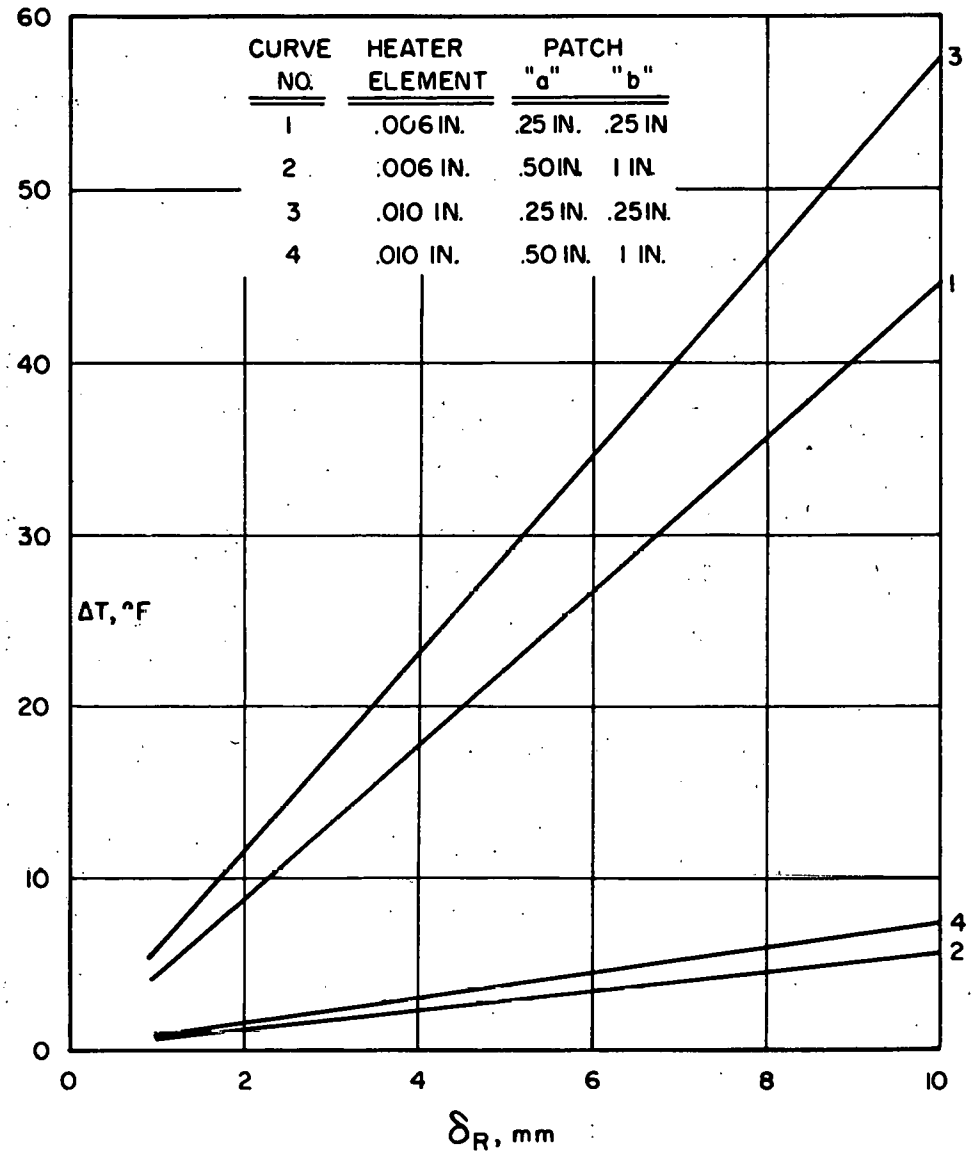


FIGURE B-3

CALCULATED TEMPERATURE RISES FOR RECTANGULAR PATCHES IN THE CRITICAL HEAT FLUX CONDITION

| | |
|---|---|
| $\Delta T$ | Average temperature rise of patch |
| $\delta R$ | Deflection of Sanborn recorder pen |
| "a" | Patch length |
| "b" | Patch width |

Double-ribbon heater elements, 1.96 in. wide, .006 in. and .010 in. thick ribbons.
800,000 Btu/hr-ft$^2$ heat flux.

## APPENDIX C

## EXPERIMENTAL CRITICAL HEAT FLUX DATA

All of the critical heat flux data obtained in the experiment are tabulated in reduced form in the following table[1] and are graphed in Figure VI-1. Properties of water used for reduction of the data are those given in reference (55) for the respective state conditions.

The heater element types are defined according to the following coding:

| Type | Spacing, in. | Ribbon Thickness, in. | No. of Sides Heated | Hydraulic Diameter, in. |
|---|---|---|---|---|
| 1A | .50 | .006 | 2 | .81 |
| 1B | .50 | .010 | 2 | .81 |
| 2A | .25 | .006 | 2 | .46 |
| 2B | .25 | .010 | 2 | .46 |
| 3 | .50 | .010 | 1 | .81 |

The types of runs are defined according to the following coding, which includes coding pertaining to steady-state camera runs described in Appendix D.

Critical Heat Flux Runs

BO: Critical heat flux run, without camera operation.

BOC: Critical heat flux run, with camera operation.

-T: Automatic power trip at critical heat flux condition.

-S: Manual reduction of power from critical heat flux condition.

-A: Physical damage to heater element interrupted electrical circuit.

-R: Critical heat flux data judged invalid.

Camera Runs Only

SC: Steady-state operation at subcooled conditions, with camera.

---

[1] Calculations involved in reduction of the data were done by Mr. M. G. McBride, Engineering Assistant.

SSC: Steady-state operation at bulk boiling conditions, with camera.

SSC-O: Steady-state operation in bulk boiling near critical heat flux conditions, with camera.

The respective critical heat flux determinations and associated instrumentation features are described by the following notes, referred to in the tabulation of data.

Notes

(1) Recorder trace of voltage unbalance indicates oscillations or sharp rise of heater element temperature within 4-1/4 inches of outlet end.

(2) Recorder trace of voltage unbalance indicates oscillations or rise of heater element temperature upstream, more than 4-1/4 inches from outlet end.

(3) Recorder trace of voltage unbalance does not indicate oscillations or sharp rise of heater element temperature within 8-3/8 inches of outlet end.

(4) Physical damage to heater element, due to overheating, within 4-1/4 inches of outlet end.

(5) Physical damage to heater element, due to overheating, in upstream regions, more than 4-1/4 inches from outlet end.

(6) GEL Safety Monitor used, together with either heater element thermocouples or voltage unbalance recordings.[2]

(7) Recorder traces of thermocouple outputs indicate oscillations or sharp rise of heater element temperature at outlet end (with GEL Safety Monitor only).

---

[2] The critical heat flux detector system described in Section IV and Appendix B was used for all runs except those indicated by note (6).

(8) Heater element thermocouples defective; no recording made of heater element voltage unbalance; judgment of validity of critical heat flux detection based on visual appearance of GEL safety monitor oscilloscope pattern (with GEL Safety Monitor only) and comparison of data with valid repeat runs.

# EXPERIMENTAL CRITICAL HEAT FLUX DATA

| Run No. | Type Run | Date | Type Heater Element | $\Delta h_s$, inlet Btu/lb. | P, psia | G $\frac{lb.}{sec\text{-}ft^2}$ | $X_c$ | $q_c$, $\frac{10^6 \text{ Btu}}{hr - ft^2}$ | Notes |
|---|---|---|---|---|---|---|---|---|---|
| 1-3 | BOC-T | 2/7/61 | 1A | 67.0 | 1000 | 50.1 | .650 | .591 | (1) |
| 1-4 | BOC-T | 2/7/61 | 1A | 71.0 | 1000 | 50.6 | .644 | .597 | (1) |
| 2-2 | BO-T | 2/7/61 | 1A | 211.0 | 1010 | 50.1 | .553 | .689 | (1) |
| 2-3 | BO-T | 2/7/61 | 1A | 214.0 | 1000 | 50.1 | .522 | .668 | (1) |
| 2-5 | BOC-T | 2/7/61 | 1A | 216.0 | 1000 | 50.1 | .556 | .698 | (1) |
| 3T-3 | BOC-T | 9/28/60 | 1B | 24.0 | 1003 | 101 | .496 | .845 | (6), (7) |
| 3T-4 | BOC-T | 9/29/60 | 1B | 21.0 | 997 | 101 | .501 | .845 | (6), (7) |
| 3T-6 | BO-A | 9/29/60 | 1B | 22.0 | 1002 | 101 | .500 | .832 | (6), (7) |
| 3TR-3 | BOC-T | 10/18/60 | 1B | 26.0 | 995 | 101 | .534 | .906 | (6), (8) |
| 3TR-4 | BOC-T | 10/18/60 | 1B | 26.0 | 995 | 101 | .536 | .909 | (6), (8) |
| 3TR-5 | BOC-T | 10/18/60 | 1B | 26.0 | 995 | 101 | .542 | .918 | (6), (8) |
| 3RR-1 | BO-T | 4/13/61 | 1B | 38.0 | 1000 | 97.6 | .515 | .878 | (1) |
| 3TRR-5 | BO-A | 12/27/60 | 1A | 52.0 | 1000 | 98 | .493 | .881 | (6), (1), (4) |
| 3-5 | BO-A | 1/6/61 | 1A | 45.5 | 1005 | 98.6 | .511 | .898 | (6), (1), (4) |
| 3R-4 | BOC-T | 2/15/61 | 1A | 55.0 | 1000 | 99.4 | .465 | .857 | (1) |
| 3A-1 | BO-T-R | 3/4/61 | 1A | 109 | 1000 | 99.4 | .368 | .835 | (2) |
| 3A-2 | BO-A-R | 3/4/61 | 1A | 107.5 | 995 | 99.4 | .389 | .864 | (5), (3) |
| 3AR-1 | BO-T | 3/25/61 | 1A | 107.5 | 995 | 99.4 | .425 | .920 | (1) |
| 3AR-2 | BO-T | 3/25/61 | 1A | 111.0 | 1000 | 99.4 | .415 | .913 | (1) |
| 3AR-3 | BO-T | 3/25/61 | 1A | 107.5 | 1000 | 99.4 | .427 | .923 | (1) |
| 3ARR-1 | BO-T | 4/13/61 | 1B | 104.0 | 995 | 98.1 | .441 | .925 | (1) |
| 3B-1 | BO-T | 3/25/61 | 1A | 131.5 | 1000 | 99.4 | .412 | .957 | (1) |
| 3B-2 | BO-T | 3/25/61 | 1A | 131.5 | 1000 | 99.4 | .410 | .955 | (1) |
| 3BR-1 | BO-T | 4/13/61 | 1B | 131.5 | 1005 | 99.4 | .410 | .955 | (1) |
| 4T-2 | BO-T | 10/27/60 | 1B | 153.5 | 1000 | 103 | .415 | 1.053 | (6), (7) |
| 4T-3 | BO-T | 10/27/60 | 1B | 153.5 | 1000 | 103 | .420 | 1.062 | (6), (7) |
| 4T-4 | BO-T | 10/27/60 | 1B | 153.5 | 1000 | 103 | .430 | 1.077 | (6), (7) |
| 4T-5 | BO-T | 10/27/60 | 1B | 153.5 | 1000 | 103 | .430 | 1.077 | (6), (7) |
| 4R-1 | BO-T | 4/13/61 | 1B | 161.0 | 1000 | 99.4 | .381 | .979 | (1) |
| 4-4 | BOC-S-R | 1/24/61 | 1A | 163.5 | 1005 | 101 | .303 | .876 | (6), (2) |
| 4-5 | BOC-T-R | 1/24/61 | 1A | 164.0 | 1005 | 99.4 | .321 | .894 | (6), (2) |
| 5A-1 | BO-T-R | 4/13/61 | 1B | 212.0 | 1005 | 99.4 | .315 | .999 | (2) |
| 5-1 | BO-T-R | 1/26/61 | 1A | 253.5 | 999 | 99.4 | .138 | .823 | (6), (2) |
| 5-2 | BOC-S-R | 1/26/61 | 1A | 259.0 | 1005 | 99.4 | .156 | .864 | (6), (2) |
| 6-3 | BOC-T | 2/2/61 | 1A | 25.0 | 1000 | 199 | .233 | .847 | (6), (1) |
| 6R-3 | BO-T | 3/24/61 | 1A | 32.0 | 1000 | 199 | .234 | .884 | (1) |
| 6R-4 | BOC-T | 3/24/61 | 1A | 28.5 | 1000 | 199 | .239 | .881 | (1) |
| 6R-5 | BOC-T | 3/24/61 | 1A | 31.0 | 1000 | 199 | .237 | .889 | (1) |
| 6R-6 | BOC-T | 3/24/61 | 1A | 27.0 | 1000 | 196 | .252 | .903 | (1) |
| 6RR-1 | BO-T | 4/14/61 | 1B | 16.0 | 1000 | 199 | .269 | .916 | (1) |
| 6A-1 | BO-T | 4/14/61 | 1B | 56.0 | 1000 | 199 | .232 | .991 | (1) |
| 7-3 | BOC-T | 2/6/61 | 1A | 90.0 | 1000 | 199 | .165 | .945 | (1) |
| 7-5 | BOC-S | 2/6/61 | 1A | 94.0 | 1000 | 199 | .160 | .957 | (1) |
| 7R-1 | BO-A | 4/4/61 | 1B | 88.3 | 1015 | 199 | .200 | 1.043 | (4), (1) |
| 8-2 | BOC-T | 2/6/61 | 1A | 166.4 | 1055 | 199 | .095 | 1.089 | (1) |
| 9-1 | BOC-T | 2/6/61 | 1A | 19.0 | 1000 | 397 | .104 | .832 | (1) |
| 9R-2 | BOC-S | 3/24/61 | 1A | 32.0 | 1000 | 395 | .093 | .884 | (1) |
| 9R-3 | BOC-T | 3/24/61 | 1A | 25.0 | 1000 | 397 | .103 | .879 | (1) |
| 9A-1 | BO-T | 3/25/61 | 1A | 61.5 | 1000 | 397 | .063 | .984 | (1) |
| 9A-2 | BOC-T | 3/25/61 | 1A | 55.0 | 1000 | 398 | .074 | .987 | (1) |
| 9B-1 | BOC-T | 3/25/61 | 1A | 97.3 | 1015 | 397 | .033 | 1.136 | (1) |
| 9B-2 | BOC-T | 3/25/61 | 1A | 95.0 | 1005 | 398 | .037 | 1.141 | (1) |

## EXPERIMENTAL CRITICAL HEAT FLUX DATA - CONT'D.

| Run No. | Type Run | Date | Type Heater Element | $\Delta h_s$ inlet Btu/lb. | P, psia | G lb./sec-ft$^2$ | $X_c$ | $q_c$ $10^6$ Btu/hr-ft$^2$ | Notes |
|---|---|---|---|---|---|---|---|---|---|
| 12-3 | BO-T | 4/6/61 | 3 | 15.0 | 1007 | 199 | .140 | 1.018 | (1) |
| 12-4 | BOC-T | 4/6/61 | 3 | 16.0 | 1005 | 199 | .140 | 1.027 | (1) |
| 12-5 | BO-A-R | 4/6/61 | 3 | 20.0 | 1000 | 201 | .126 | 1.027 | (5),(3) |
| 13-3 | BOC-T | 2/27/61 | 2A | 49.0 | 1000 | 195 | .388 | .715 | (1) |
| 13-4 | BOC-T | 2/27/61 | 2A | 49.0 | 1000 | 197 | .382 | .712 | (1) |
| 13-5 | BOC-T | 2/27/61 | 2A | 49.0 | 1000 | 205 | .362 | .710 | (1) |
| 13R-1 | BO-T | 3/18/61 | 2B | 50.0 | 1000 | 197 | .464 | .843 | (1) |
| 13R-2 | BO-T | 3/18/61 | 2B | 49.0 | 1000 | 197 | .468 | .846 | (1) |
| 14-1 | BO-T | 2/27/61 | 2A | 104.0 | 995 | 196 | .334 | .764 | (1) |
| 14-2 | BO-T | 2/27/61 | 2A | 109.0 | 1005 | 197 | .337 | .786 | (1) |
| 14R-1 | BO-T | 3/19/61 | 2B | 104.0 | 1000 | 201 | .419 | .920 | (1) |
| 14R-2 | BO-T | 3/19/61 | 2B | 107.5 | 1000 | 197 | .429 | .925 | (1) |
| 14A-1 | BO-T | 3/18/61 | 2B | 161.0 | 1005 | 199 | .389 | 1.004 | (1) |
| 14A-2 | BO-T | 3/18/61 | 2B | 163.5 | 1000 | 197 | .394 | 1.006 | (1) |
| 15-1 | BO-T | 3/18/61 | 2B | 22.0 | 1000 | 394 | .249 | .882 | (1) |
| 15-2 | BO-T | 3/18/61 | 2B | 16.0 | 1001 | 394 | .258 | .880 | (1) |
| 15R-1 | BO-T | 3/19/61 | 2B | 22.0 | 1000 | 394 | .250 | .884 | (1) |
| 15R-2 | BO-T | 3/19/61 | 2B | 21.0 | 1000 | 394 | .254 | .894 | (1) |
| 16-1 | BO-T | 3/18/61 | 2B | 86.0 | 1000 | 394 | .192 | 1.011 | (1) |
| 16-2 | BO-T | 3/18/61 | 2B | 85.0 | 1000 | 394 | .193 | 1.009 | (1) |
| 17-1 | BO-T | 3/18/61 | 2B | 154.8 | 1015 | 394 | .129 | 1.143 | (1) |
| 18-4 | BOC-S | 3/9/61 | 2A | 78.0 | 1000 | 99.2 | .613 | .575 | (1) |
| 18-5 | BO-S | 3/9/61 | 2A | 78.0 | 1000 | 99.2 | .607 | .570 | (1) |
| 18R-1 | BO-T | 3/20/61 | 2B | 71.0 | 1005 | 99.0 | .651 | .595 | (1) |
| 18R-2 | BO-T | 3/20/61 | 2B | 69.0 | 1005 | 98.7 | .662 | .600 | (1) |
| 18R-3 | BO-T | 3/21/61 | 2B | 72.0 | 1000 | 99.2 | .667 | .611 | (1) |
| 18R-4 | BO-T | 3/21/61 | 2B | 66.0 | 1000 | 99.2 | .678 | .612 | (1) |
| 18R-5 | BO-T | 3/21/61 | 2B | 69.0 | 1000 | 99.2 | .664 | .605 | (1) |
| 18RR-1 | BO-A | 3/21/61 | 2B | 69.0 | 1000 | 99.2 | .751 | .673 | (4),(1) |
| 19-1 | BO-T | 3/10/61 | 2A | 132.0 | 1000 | 97.8 | .587 | .612 | (1) |
| 19-2 | BO-T | 3/10/61 | 2A | 128.5 | 1000 | 98.4 | .588 | .612 | (1) |
| 19R-1 | BO-T | 3/20/61 | 2B | 132.0 | 1002 | 99.2 | .654 | .673 | (1) |
| 19R-2 | BO-T | 3/20/61 | 2B | 132.0 | 1005 | 99.2 | .650 | .670 | (1) |
| 20-1 | BO-A-R | 3/10/61 | 2A | 221.0 | 1005 | 99.7 | .356 | .550 | (5),(3) |
| 20R-1 | BO-T | 3/20/61 | 2B | 200.0 | 1002 | 99.2 | .614 | .723 | (1) |
| 20R-2 | BO-T | 3/20/61 | 2B | 198.0 | 1000 | 99.2 | .623 | .722 | (1) |
| 20R-3 | BO-T | 3/20/61 | 2B | 215.0 | 1000 | 99.2 | .612 | .740 | (1) |

## APPENDIX D

## MOTION PICTURES OF BOILING WATER FLOW PATTERNS

Thirty three edited sequences of high speed motion pictures, selected as part of the data of the experiment, are listed in the following table in the order of their appearance in five data reels and a summary reel.[1,2] The coding designating the types of runs is the same as defined in Appendix C. Operating conditions for each sequence are tabulated and a set of notes describing the salient features of the flow patterns observed in each case are included. Specific measurements mentioned in the notes were made directly on the projected image using the Projector-Analyzer described in Section IV. The measurements are approximate.

Each sequence is continuous and is approximately the last half of the corresponding 100-foot negative exposed (approximately 1850 frames). The camera speed is nearly uniform over this portion of the films, varying from about 3900 pps at beginning of each sequence to about 4500 pps at the end, with a mean speed of about 4300 pps. The actual operating time of each edited sequence is about .43 second and the projection time at a projection speed of 16 pps is about 115 seconds, giving a mean speed reduction ratio of about 270:1. Precise camera speed at any portion of the sequences can be calculated from measurement of the camera timer marks in the sprocket track of each film (120 marks

---

[1] Complete records of the individual photographic settings found after some trial to give the best positive prints of the original negatives are filed at Cinechrome Laboratories, Inc., Palo Alto, California (General Electric Company Order No. 205-75445-G).

[2] Sequence and reel titles were made by Mr. C. L. Swan, Engineering Assistant.

per second).

The camera was in each case sharply focused on the wire focusing target attached perpendicular to one heater ribbon about .15 in. inside the channel and .25 in. upstream from the end of the heated zone. The target is .020 in. diameter and .125 in. long. The view seen is the last .56 in. of the end of the heated section (Figure IV-6).

Properties of water used for calculation of the operating conditions are those given in reference (55) for the state conditions corresponding to each sequence. The nominal operating pressure for each sequence was 1000 psia.

Relevant fluid property data for water at 1000 psia saturated pressure are[3]:

| | | | |
|---|---|---|---|
| $T_{sat}$: | 544.6 F. | $\sigma/\sigma_{212\ F}$: | 0.3 |
| $\rho_L$: | 46.3 lbs/ft$^3$ | $\mu_L/\mu_g$ : | 5.1 |
| $\rho_L/\rho_g$: | 20.6 | $k_L/k_g$ : | 11.1 |
| $c_L/c_g$: | 1.0 | | |

Heater elements used for all reels except Reel V were: .50 in. spacing, .006 in. ribbon thickness, heated on both sides. Heater elements used for all sequences in Reel V except 18S-1 were: .50 in. spacing, .010 in. ribbon thickness, heated on one side. The heater element used for 18S-1 was: .25 in. spacing, .006 in. ribbon thickness, heated on both sides.

Millimeter lengths noted under "Heater Element Temperature" are the deflections of the recorder pen corresponding to the heater element voltage unbalance (Appendix B, Figure B-3).

---

[3] $\rho$, density; c, specific heat; $\sigma$, vapor-liquid surface tension; $\mu$, dynamic viscosity; k, thermal conductivity.

# MOTION PICTURES OF BOILING WATER FLOW PATTERNS

SUMMARY REEL

| Seq. No. (Reel) | Type | Run No. | Date | G, $\frac{lb.}{sec\text{-}ft^2}$ | X | $\Delta h_s$, $\frac{Btu}{lb.}$ | q, $\frac{10^6\ Btu}{hr\text{-}ft^2}$ | $\frac{q}{q_c}$ | Heater Element Temp. | P, psia | $\Delta h_s$, inlet Btu/lb. |
|---|---|---|---|---|---|---|---|---|---|---|---|
| 3S-1 (II) | SC | 3S-1 | 3/3/61 | 102 | | 91.4 | .245 | $<<1.0$ | Steady | 940 | 182 |

(1) Sub-cooled nucleate boiling at heater surfaces. (2) Growing bubbles are not attached to surface but are sliding along near the surface with the stream at about 1.5 ft/sec. (75% of mean velocity). (3) Bubbles tend to grow in irregular clumps spaced about .10 in. apart and extending from the heater surface about .04 to .06 in. (4) Bubble diameters .01 to .05 in. (5) Bubbles in center are slowly collapsing. (6) General flow pulsation at 120 cps. (7) Bubble population appears to be reduced for about .10 sec. during the middle of the sequence, due probably to a momentary slight increase of $\Delta h_s$, inlet.

| | | | | | | | | | | | |
|---|---|---|---|---|---|---|---|---|---|---|---|
| 3S-2 (II) | SSC | 3S-2 | 3/3/61 | 99.4 | .056 | | .492 | $<<1.0$ | Steady | 1015 | 171 |

(1) General froth-like appearance with large bubbles interlaced with continuous liquid containing a range of smaller bubbles (.01 to .15 in. diameter). (2) Larger bubbles tend to be more centrally located, but with nearly continuous liquid predominant at middle of channel. (3) Highly agitated frothy structure of fine bubbles in liquid layer adjacent to heater surfaces (layer thickness $\approx$ .08 in.). (4) No evidence of flow pulsations. (5) Bubbles deeper in channel behind the target can be seen clearly.

| | | | | | | | | | | | |
|---|---|---|---|---|---|---|---|---|---|---|---|
| 3S-4 (II) | SSC | 3S-4 | 3/3/61 | 99.4 | .166 | | .491 | $<<1.0$ | Steady | 1005 | 97.0 |

(1) Agitated frothy structure of fine bubbles in liquid against heater surface. (2) "Slugging" is quite distinct, as evidenced by varying illumination from rear (.05 sec. period). (3) "Dark" slugs indicative of finely divided "froth" of vapor and liquid in core; "light" slugs indicative of thick, relatively placid, liquid layer on window (shadows of wave structure evident), containing some small bubbles moving at about 4 ft/sec., with probably high vapor content in core. (4) Irregular motion (downward) of bubbles outside channel indicates some pressure pulsing (120 cps), apparently affected by "slugs". (5) Motion of fluid adjacent to heater surfaces changes according to type of "slug" passing.

| | | | | | | | | | | | |
|---|---|---|---|---|---|---|---|---|---|---|---|
| 3R-3 (II) | SSC-O | 3R-3 | 2/15/61 | 99.4 | .465 | | .857 | .96 | Oscill. - 2 mm | 1000 | 55.0 |

(1) No evidence of "slugging". (2) Shadow of profile of highly turbulent wavy liquid film evident on both heater surfaces ( $\delta \approx$ .02 in.). Spectrum of small waves superimposed on longest wave lengths ($1 < \lambda/\delta < 5$). (3) Fine, rapid moving structure of waves on liquid film against window. (4) No evidence of definite bubbles visible in channel. (5) Appearance similar to Seq. No. 1-2, but with more liquid evident in corners and finer wave structure on window. (6) Evidence of irregular, wavy streamers of vapor moving from edges of heater ribbons into liquid film at edges of window. (7) Motion of liquid film at heater element surfaces very irregular, tending sometimes to almost stop.

SUMMARY REEL (Continued)

| Seq. No. (Reel) | Type | Run No. | Date | G, $\frac{lb.}{sec\text{-}ft^2}$ | X | $\Delta h_s$, $\frac{Btu}{lb.}$ | q, $\frac{10^6\ Btu}{hr\text{-}ft^2}$ | $\frac{q}{q_c}$ | Heater Element Temp. | P, psia | $\Delta h_s$, inlet Btu/lb. |
|---|---|---|---|---|---|---|---|---|---|---|---|
| 1-2 (I) | SSC-0 | 1-2 | 2/7/61 | 50.1 | .656 | | .588 | ≈1.0 | Oscill. - 4 mm | 1035 | 70.0 |

(1) Wave structure of liquid film on window is sharply defined. (2) Small bubbles in liquid film traveling upward at about 5 ft/sec. (3) Profile of wavy liquid film on right-hand side is distinct ( $\delta \approx .025$ in.). The wave structure on the film includes a spectrum of short wave-lengths superimposed on the longest waves ($1 \lesssim \lambda/\delta \lesssim 5$). (4) "Pulsing" of fluid normal to left-hand heater ribbon ( 120 cps), possibly associated with slight warp in ribbon (cavity back of ribbon). Evidence of irregular streamers of vapor pulsing from edge of heater ribbon into liquid film at edge of window. (5) Motion of the liquid film at heater element surfaces is very irregular, tending to almost stop occasionally. (6) No "slugging". (7) Intense back-light indicates high vapor content in core.

| | | | | | | | | | | | |
|---|---|---|---|---|---|---|---|---|---|---|---|
| 7-5 (III) | BOC-S | 7-5 | 2/6/61 | 199 | .160 | | .957 | 1.0 | Oscill. - 4 mm | 1000 | 94.0 |

(1) Highly agitated pulsing streamers of vapor appear to be moving from edge of heater ribbons into liquid film. High frequency pulsing of fluid normal to surface at top of left-hand ribbon. (2) Shadow of profile of highly agitated wavy liquid film against right-hand heater ribbon ( $\delta \approx .03$ in.). Motion of liquid film is very irregular, occasionally appearing to almost stop. Spectrum of superimposed wave lengths ($1 \lesssim \lambda/\delta \lesssim 3$). (3) No "slugging." (4) Smooth motion of bubbles outside channel (upward) indicates no pressure pulsing. (5) Finely divided, rapid moving liquid film structure on window.

| | | | | | | | | | | | |
|---|---|---|---|---|---|---|---|---|---|---|---|
| 9A-1 (IV) | BOC-T | 9A-2 | 3/25/61 | 398 | .074 | | .987 | 1.0 | Oscill. + Pulse-trip | 1000 | 55.0 |

(1) Highly agitated, wavy streamers of vapor flowing in liquid film at edges of both heater ribbons. (2) Shadow of profile of turbulent, wavy liquid film vaguely evident against both heater surfaces, in contrast with more rapidly moving, finely divided flow structure across majority of window face ( $\delta \approx .04$ in., $\lambda \lesssim 2\delta$). (3) Intensity of agitation of flow structure at heater ribbon appears to increase during about .10 sec. period before power trip. Flow structure along ribbon surface very irregular, sometimes almost stopping, just before power trip. (4) No "slugging". (5) Small pressure pulsing at 120 cps indicated by irregular motion of bubbles outside channel. (6) Power trip with brief flow reversal .22 sec. before end of sequence. (7) Flow pattern after power trip markedly different than before: pure liquid covering heater; vapor re-arranges into large irregular bubbles as mixture enthalpy decreases toward end of sequence.

REEL I: G = 50 lbs/sec-ft$^2$

| Seq. No. | Type | Run No. | Date | G, $\frac{lb.}{sec\text{-}ft^2}$ | X | $\Delta h_s$, $\frac{Btu}{lb.}$ | q, $\frac{10^6\ Btu}{hr\text{-}ft^2}$ | $\frac{q}{q_c}$ | Heater Element Temp. | P, psia | $\Delta h_s$, inlet Btu/lb. |
|---|---|---|---|---|---|---|---|---|---|---|---|
| 2-1 | SSC | 2-1 | 2/7/61 | 50.1 | .258 | | .465 | $\ll 1.0$ | Steady | 1000 | 217 |

(1) Turbulent wavy liquid film evident on window surface. (2) Occasional small bubble in film on window. (3) Shadow of liquid film profile on right-hand heater ribbon, of thickness $\delta \approx .05$ in. (4) Wave structure on film on window ($\lambda \approx .05$ in.). (5) Some "slugging" indicated at period of .10 to .15 sec. (6) Intensity of back-lighting in center indicates high vapor content in core.

| | | | | | | | | | | | |
|---|---|---|---|---|---|---|---|---|---|---|---|
| 1-1 | SSC | 1-1 | 2/7/61 | 50.1 | .318 | | .343 | $\ll 1.0$ | Steady | 1000 | 69.0 |

(1) General appearance similar to that for No. 2-1. (2) Occasional small bubbles in liquid film on window. (3) Edge of heater element more clearly visible at upper left corner. (4) "Slugging" less distinct (.10 to .15 sec. period). (5) Increased intensity of back-lighting in center indicates more nearly single-phase vapor in core than in No. 2-1.

| | | | | | | | | | | | |
|---|---|---|---|---|---|---|---|---|---|---|---|
| 2-2 | SSC-0 | 2-4 | 2/7/61 | 50.1 | .450 | | .616 | $\ll 1.0$ | Steady | 1000 | 216 |

(1) Increased intensity of back-lighting indicating higher vapor content in core than in No. 1-1. (2) Occasional small bubbles in liquid film on window. (3) "Pulsing" of fluid normal to surface at top of left-hand heater ribbon (120 cps). (4) Very slight "slugging". (5) Shadows of focusing target and profile of liquid film visible on right-hand side.

| | | | | | | | | | | | |
|---|---|---|---|---|---|---|---|---|---|---|---|
| 2-3 | BOC-T | 2-5 | 2/7/61 | 50.1 | .556 | | .698 | 1.0 | Pulse-Trip | 1000 | 216 |

(1) Liquid film on window and its wave structure more sharply defined. (2) No "slugging" evident. (3) Shadow of profile of liquid film on right-hand side, with wavy, undulating surface more definite. (4) Occasional small bubble in film on window. (5) Intensity of back-lighting in center increased further, indicating higher vapor content than in previous sequences. (6) "Pulsing" of fluid normal to left-hand heater ribbon (120 cps), possibly associated with slight warp in left heater ribbon (cavity back of ribbon). Some evidence of irregular streamers of vapor pulsing from edge of heater ribbon into liquid film at edge of window.

| | | | | | | | | | | | |
|---|---|---|---|---|---|---|---|---|---|---|---|
| 1-2 | SSC-0 | 1-2 | 2/1/61 | 50.1 | .656 | | .588 | $\approx 1.0$ | Oscill. $\pm$ 4 mm | 1035 | 70.0 |

(1) Wave structure of liquid film on window is sharply defined. (2) Small bubbles in liquid film traveling upward at about 5 ft/sec. (3) Profile of wavy liquid film on right-hand side is distinct ($\delta \approx .025$ in.). The wave structure on the film includes a spectrum of short wave-lengths superimposed on the longest waves ($1 \lesssim \lambda/\delta \lesssim 5$). (4) "Pulsing" of fluid normal to left-hand heater ribbon (100 cps), possibly associated with slight warp in ribbon (cavity back of ribbon). Evidence of irregular streamers of vapor pulsing from edge of heater ribbon into liquid film at edge of window. (5) Motion of the liquid film at heater element surfaces is very irregular, tending to almost stop occasionally. (6) No "slugging." (7) Intense back-light indicates high vapor content in core.

# MOTION PICTURES OF BOILING WATER FLOW PATTERNS - CONT'D.

REEL II: $G = 100$ lbs/sec-ft$^2$

| Seq. No. | Type | Run No. | Date | G, lb./sec-ft$^2$ | X | $\Delta h_s$, Btu/lb. | q, $10^6$ Btu/hr-ft$^2$ | q/qc | Heater Element Temp. | P, psia | $\Delta h_s$, inlet Btu/lb. |
|---|---|---|---|---|---|---|---|---|---|---|---|
| 3S-1 | SC | 3S-1 | 3/3/61 | 102 | | 91.4 | .245 | $\ll 1.0$ | Steady | 940 | 182 |

(1) Sub-cooled nucleate boiling at heater surfaces. (2) Growing bubbles are not attached to surface but are sliding along near the surface with the stream at about 1.5 ft/sec. (75% of mean velocity). (3) Bubbles tend to grow in irregular clumps spaced about .10 in. apart and extending from the heater surface about .04 to .06 in. (4) Bubble diameters .01 to .05 in. (5) Bubbles in center are slowly collapsing. (6) General flow pulsation at 120 cps. (7) Bubble population appears to be reduced for about .10 sec. during the middle of the sequence, due probably to a momentary slight increase of $\Delta h_s$, inlet.

| | | | | | | | | | | | |
|---|---|---|---|---|---|---|---|---|---|---|---|
| 3S-2 | SSC | 3S-2 | 3/3/61 | 99.4 | .056 | | .492 | $\ll 1.0$ | Steady | 1015 | 171 |

(1) General froth-like appearance with large bubbles interlaced with continuous liquid containing a range of smaller bubbles (.01 to .15 in. diameter). (2) Larger bubbles tend to be more centrally located, but with nearly continuous liquid predominant at middle of channel. (3) Highly agitated frothy structure of fine bubbles in liquid layer adjacent to heater surfaces (layer thickness $\approx$ .08 in.). (4) No evidence of flow pulsations. (5) Bubbles deeper in channel behind the target can be seen clearly.

| | | | | | | | | | | | |
|---|---|---|---|---|---|---|---|---|---|---|---|
| 3S-3 | SSC | 3S-3 | 3/3/61 | 99.4 | .097 | | .491 | $\ll 1.0$ | Steady | 1020 | 145 |

(1) Agitated frothy structure of bubbles in liquid adjacent to heater surfaces is more finely divided than in No. 3S-2. (2) Varying back-light intensity indicates some "slugging" (.04 sec. period). (3) Irregular motion (downward) of small bubbles outside channel indicates some pressure pulsing.

| | | | | | | | | | | | |
|---|---|---|---|---|---|---|---|---|---|---|---|
| 3S-4 | SSC | 3S-4 | 3/3/61 | 99.4 | .166 | | .491 | $\ll 1.0$ | Steady | 1005 | 97.0 |

(1) Agitated frothy structure of fine bubbles in liquid against heater surface. (2) "Slugging" is quite distinct, as evidenced by varying illumination from rear (.05 sec. period). (3) "Dark" slugs indicative of finely divided "froth" of vapor and liquid in core; "light" slugs indicative of thick, relatively placid, liquid layer on window (shadows of wave structure evident), containing some small bubbles moving at about 4 ft/sec., with probably high vapor content in core. (4) Irregular motion (downward) of bubbles outside channel indicates some pressure pulsing (120 cps), apparently affected by "slugs". (5) Motion of fluid adjacent to heater surfaces changes according to type of "slug" passing.

| | | | | | | | | | | | |
|---|---|---|---|---|---|---|---|---|---|---|---|
| 3R-1 | SSC | 3R-1 | 2/15/61 | 99.4 | .223 | | .465 | $\ll 1.0$ | Steady | 1000 | 49.0 |

(1) "Slugging" less distinct. (2) Left-hand heater ribbon appears to have agitated "froth" against its surface; pulsing of fluid suggestive of vapor formation in liquid against right-hand heater ribbon. (3) Liquid film on window surface with wave structure. (4) Bubbles in liquid film on window moving at about 5 ft/sec. (5) Shadow of liquid film profile with agitated wavy surface evident on right-hand heater ribbon (most evident during "light" slugs).

REEL II (Continued)

| Seq. No. | Type | Run No. | Date | G, lb./sec-ft² | X | $\Delta h_s$, Btu/lb. | q, $10^6$ Btu/hr-ft² | $\frac{q}{q_c}$ | Heater Element Temp. | P, psia | $\Delta h_s$, inlet Btu/lb. |
|---|---|---|---|---|---|---|---|---|---|---|---|
| 4-5-a | BOC-S-R | 4-4 | 1/24/61 | 101 | .303 | | .876 | ≈.80 | Oscill. (upstream) | 1005 | 164 |

(1) Camera apparently out of focus. (2) Fluctuating back-light intensity indicates distinct "slugging" (.07 sec. period). (3) Definite appearance of wave structure on liquid film on window during "light" slugs (similar to Seq. Nos. 2-3 and 1-2). (4) Shadow of liquid film profile with very agitated wavy surface against heater ribbons evident during "light" slugs. (5) Motion of liquid film at heater surfaces is very irregular, occasionally appearing to almost stop.

| | | | | | | | | | | | |
|---|---|---|---|---|---|---|---|---|---|---|---|
| 3R-2 | SSC-O | 3R-2 | 2/15/61 | 99.4 | .454 | | .857 | .92 | Pulsing - 1 mm | 1000 | 54.0 |

(1) Little evidence of distinct "slugging". (2) Shadow of profile of liquid film with agitated wavy surface against right-hand ribbon. (3) Structure of waves on liquid film against window, with finer, more rapidly moving structure towards middle of window. (4) Evidence of irregular, wavy streamers of vapor moving from edges of heater ribbons into liquid film at edge of window.

| | | | | | | | | | | | |
|---|---|---|---|---|---|---|---|---|---|---|---|
| 3R-3 | SSC-O | 3R-3 | 2/15/61 | 99.4 | .465 | | .857 | .96 | Oscill. - 2 mm | 1000 | 55.0 |

(1) No evidence of "slugging". (2) Shadow of profile of highly turbulent wavy liquid film evident on both heater surfaces ( $\delta \approx .02$ in.). Spectrum of small waves superimposed on longest wave lengths ($1 \lesssim \lambda/\delta \lesssim 5$). (3) Fine, rapid moving structure of waves on liquid film against window. (4) No evidence of definite bubbles visible in channel. (5) Appearance similar to Seq. No. 1-2, but with more liquid evident in corners and finer wave structure on window. (6) Evidence of irregular, wavy streamers of vapor moving from edges of heater ribbons into liquid film at edges of window. (7) Motion of liquid film at heater element surfaces very irregular, tending sometimes to almost stop.

---

REEL III: G = 200 lbs/sec-ft²

| | | | | | | | | | | | |
|---|---|---|---|---|---|---|---|---|---|---|---|
| 6S-1 | SC | 6S-1 | 3/23/61 | 199 | | 2.8 | .298 | << 1.0 | Steady | 1000 | 65.0 |

(1) General froth-like appearance, similar to No. 3S-2, with large bubbles interlaced with continuous liquid containing a range of smaller bubbles (.01 to .25 in. diameter). (2) Larger bubbles tend to be centrally located. (3) Agitated structure of fine bubbles in liquid layer adjacent to heater surface (layer thickness .06 in.). (4) No "slugging" or "pulsing". (5) Large filament-like bubble attached to target.

| | | | | | | | | | | | |
|---|---|---|---|---|---|---|---|---|---|---|---|
| 6R-1 | SSC | 6R-1 | 3/23/61 | 199 | .167 | | .612 | << 1.0 | Steady | 1000 | 19.0 |

(1) Flow structure appears to be finely divided, indistinct and rapid moving near middle of window, suggestive of short, high frequency waves on liquid film against window. (2) Slower moving, turbulent, wavy streamers of vapor in liquid film at edges of heater ribbons. (3) Very slight evidence of "slugging". (4) Smooth motion of bubbles outside channel (upward) indicates no pressure pulsing.

| | | | | | | | | | | | |
|---|---|---|---|---|---|---|---|---|---|---|---|
| 6R-5 | BOC-T | 6R-6 | 3/24/61 | 196 | .252 | | .903 | 1.0 | Oscill. + Pulse-trip | 1000 | 27.0 |

(1) Appearance similar to No. 6R-1 except streamers of vapor flowing in liquid film at edge of left-hand heater ribbon more agitated. (2) No "slugging". (3) Smooth motion of bubbles outside channel.

# MOTION PICTURES OF BOILING WATER FLOW PATTERNS - CONT'D.

REEL III (Continued)

| Seq. No. | Type | Run No. | Date | G, lb./sec-ft² | X | $\Delta h_s$, Btu/lb. | q, $10^6$ Btu/hr-ft² | q/$q_c$ | Heater Element Temp. | P, psia | $\Delta h_s$, inlet Btu/lb. |
|---|---|---|---|---|---|---|---|---|---|---|---|
| 7-1-b | SSC | 7-1 | 2/6/61 | 202 | .104 | | .796 | <<1.0 | Steady | 995 | 96.0 |

(1) Agitated, wavy streamers of vapor flowing in liquid film at edge of left-hand heater ribbon. (2) Shadow of profile of turbulent wavy liquid film against right-hand heater ribbon evident. (3) Wave structure on liquid film on glass more distinct. (4) High frequency pulsing of fluid against upper edge of left-hand heater ribbon. (5) No "slugging". (6) Smooth motion of bubbles outside channel.

| | | | | | | | | | | | |
|---|---|---|---|---|---|---|---|---|---|---|---|
| 7-2 | SSC-O | 7-2 | 2/6/61 | 199 | .151 | | .911 | .91 | Pulsing - 1 mm | 1000 | 92.0 |

(1) Appearance similar to No. 7-1-b, except both the liquid film and vapor streamers at edge of left-hand heater ribbon and the wavy profile of the liquid film against the right-hand heater ribbon appear more agitated. (2) No "slugging." (3) Smooth motion of bubbles outside channel.

| | | | | | | | | | | | |
|---|---|---|---|---|---|---|---|---|---|---|---|
| 7-5 | BOC-S | 7-5 | 2/6/61 | 199 | .160 | | .957 | 1.0 | Oscill. - 4 mm | 1000 | 94.0 |

(1) Highly agitated pulsing streamers of vapor appear to be moving from edge of heater ribbons into liquid film. High frequency pulsing of fluid normal to surface at top of left-hand ribbon. (2) Shadow of profile of highly agitated wavy liquid film against right-hand heater ribbon ( $\delta \approx .03$ in.). Motion of liquid film is very irregular, occasionally appearing to almost stop. Spectrum of superimposed wave lengths ($1 \ll \lambda/g \ll 3$). (3) No "slugging". (4) Smooth motion of bubbles outside channel (upward) indicates no pressure pulsing. (5) Finely divided, rapid moving liquid film structure on window.

| | | | | | | | | | | | |
|---|---|---|---|---|---|---|---|---|---|---|---|
| 8-1 | SSC | 8-1 | 2/6/61 | 199 | .084 | | .989 | <<1.0 | Steady | 1035 | 158.0 |

(1) Appearance similar to No. 7-5. (2) Structure of liquid film on window rather indistinct. (3) Shadow of profile of agitated wavy liquid film against right-hand heater ribbon evident. (4) Agitated liquid film and vapor streamers flowing at edge of left-hand heater ribbon. (5) No "slugging". (6) Occasional glimpses of focusing target on right-hand side.

| | | | | | | | | | | | |
|---|---|---|---|---|---|---|---|---|---|---|---|
| 8-3 | SSC-O | 8-3 | 2/6/61 | 199 | .105 | | 1.080 | ≈1.0 | Pulsing - 1 mm | 1060 | 166.0 |

(1) Appearance similar to No. 8-1, except shadow of profile of liquid film against right-hand heater ribbon and vapor streamers in liquid film at edges of ribbons appear to be more highly agitated and more irregular in motion. (2) Rather indistinct, rapid moving liquid film structure on window. (3) No "slugging".

# MOTION PICTURES OF BOILING WATER FLOW PATTERNS — CONT'D.

REEL IV: G = 400 lbs/sec-ft$^2$

| Seq. No. | Type | Run No. | Date | G, $\frac{lb.}{sec\text{-}ft^2}$ | X | $\Delta h_s$, $\frac{Btu}{lb.}$ | q, $\frac{10^6\ Btu}{hr\text{-}ft^2}$ | $\frac{q}{q_c}$ | Heater Element Temp. | P, psia | $\Delta h_s$, inlet Btu/lb. |
|---|---|---|---|---|---|---|---|---|---|---|---|
| 9S-1 | SC | 9S-1 | 3/24/61 | 398 | | 61.3 | .245 | $<<1.0$ | Steady | 995 | 87.0 |

(1) Start of sub-cooled nucleate boiling. (2) Evidence of "hot patches" or preferred nucleation sites slightly below target on left-hand heater ribbon. (3) Bubbles grow from "hot patches" as flat, irregular domes about .05 in. wide, changing as they grow to irregular streamers of vapor up to .15 in. long before disattaching or breaking into smaller bubbles. (4) Large irregular bubbles up to .15 in.x .30 in. slide along right-hand heater ribbon at about 4 ft/sec. (50% of mean channel velocity). (5) No evidence of flow pulsing. (6) Collapse rate of bubbles in stream is slow. (7) Considerable asymmetry of bubble shape and size in stream.

| | | | | | | | | | | | |
|---|---|---|---|---|---|---|---|---|---|---|---|
| 9S-2 | SC | 9S-2 | 3/24/61 | 398 | | 17.6 | .493 | $<<1.0$ | Steady | 995 | 69.0 |

(1) Very smooth flow of discrete bubbles, ranging from .01 to .10 in. diameter, interlaced by almost pure liquid near middle of channel. (2) Agitated, frothy structure of tiny bubbles and liquid in a layer about .13 in. thick against both heater surfaces. (3) No flow pulsing of "slugging". (4) Velocity of fluid in channel center is markedly faster than velocity in frothy layer against wall. (5) Bubble collapse rate in free stream from wall to near channel center is too slow to detect, indicating incomplete mixing of colder and hotter parts of fluid.

| | | | | | | | | | | | |
|---|---|---|---|---|---|---|---|---|---|---|---|
| 9R-1 | SSC | 9R-1 | 3/24/61 | 398 | .096 | | .857 | .98 | Pulsing - 1 mm | 1005 | 27.0 |

(1) Evidence of turbulent, wavy streamers of vapor with highly agitated wave structure flowing in liquid film at edges of both heater ribbons. (2) Structure of liquid film on window is more finely divided, becoming rather indistinct with increasingly high flow velocity toward middle of window. (3) No "slugging". (4) Smooth flow of bubbles outside channel indicates negligible pressure pulsing.

| | | | | | | | | | | | |
|---|---|---|---|---|---|---|---|---|---|---|---|
| 9R-2 | BOC-S | 9R-2 | 3/24/61 | 395 | .093 | | .884 | 1.0 | Oscill. - 4 mm | 1000 | 32.0 |

(1) Appearance similar to No. 9R-1, but with vapor streamers in liquid film at edges of heater ribbons being more agitated. (2) No "slugging." (3) Slight irregularity of motion of bubbles outside channel indicates small pressure pulsing at about 120 cps.

| | | | | | | | | | | | |
|---|---|---|---|---|---|---|---|---|---|---|---|
| 9A-1 | BOC-T | 9A-2 | 3/25/61 | 398 | .074 | | .987 | 1.0 | Oscill. + Pulse-trip | 1000 | 55.0 |

(1) Highly agitated, wavy streamers of vapor flowing in liquid film at edges of both heater ribbons. (2) Shadow of profile of turbulent, wavy liquid film vaguely evident against both heater surfaces, in contrast with more rapidly moving, finely divided flow structure across majority of window face ($\delta \approx .04$ in., $\lambda \approx 2\delta$). (3) Intensity of agitation of flow structure at heater ribbon appears to increase during about .10 sec. period before power trip. Flow structure along ribbon surface very irregular, sometimes almost stopping, just before power trip. (4) No "slugging." (5) Small pressure pulsing at 120 cps indicated by irregular motion of bubbles outside channel. (6) Power trip with brief flow reversal .22 sec. before end of sequence. (7) Flow pattern after power trip markedly different than before; pure liquid covering heater; vapor re-arranges into large irregular bubbles as mixture enthalpy decreases toward end of sequence.

REEL IV (Continued).

| Seq. No. | Type | Run No. | Date | G, $\frac{lb.}{sec\text{-}ft^2}$ | X | $\Delta h_s$, $\frac{Btu}{lb.}$ | q, $\frac{10^6\ Btu}{hr\text{-}ft^2}$ | $\frac{q}{q_c}$ | Heater Element Temp. | P, psia | $\Delta h_s$, inlet Btu/lb |
|---|---|---|---|---|---|---|---|---|---|---|---|
| 9B-2 | BOC-T | 9B-2 | 3/25/61 | 398 | .037 | | 1.141 | 1.0 | Oscill. + Pulse-trip | 1005 | 95.0 |

(1) Appearance very similar to No. 9A-1, with highly agitated liquid film and vapor streamers moving irregularly at edges of both heater ribbons, and finely divided, rapidly moving liquid film structure on window. (2) No "slugging". (3) More pronounced pressure pulsing (120 cps) indicated by irregular motion of bubbles outside channel. (4) Power trip with brief flow reversal .02 sec. before end of sequence. (5) Re-arrangement of flow pattern after power trip similar to No. 9A-1.

---

REEL V: G = 100 and 200 lbs/sec-ft$^2$

| | | | | | | | | | | | |
|---|---|---|---|---|---|---|---|---|---|---|---|
| 11S-1 | SC | 11S-1 | 3/30/61 | 99.4 | | 112.3 | .489 | <<1.0 | Steady | 985 | 212 |

(1) Sub-cooled nucleate boiling. (2) Bubbles appear to grow in large clumps sliding along the heater surface at about 1.7 ft/sec. (85% of channel velocity), spaced about .10 to .15 in. apart and extending about .15 in. from the wall, with a frothy structure of tiny bubbles between clumps. (3) Almost all bubbles are in heated half of channel with sizes from .01 to .07 in. diameter. (4) Flow is pulsing slightly (120 cps). (5) Shadow of profile of wavy thermal boundary layer evident along unheated right-hand wall. (about .04 to .05 in. thick).

| | | | | | | | | | | | |
|---|---|---|---|---|---|---|---|---|---|---|---|
| 11S-2 | SC | 11S-2 | 3/30/61 | 99.4 | | 72.4 | .612 | << 1.0 | Steady | 1000 | 200 |

(1) Appearance is similar to No. 11S-1, except: bubbles tend to be more uniform, more numerous and smaller; more bubbles in free stream; bubbles at heater surface less distinct. (2) Arrangement at heater surface appears to be an irregular layer (about .05 to .10 in. thick) of frothy mixture of tiny bubbles and liquid sliding along the surface at about 2 ft/sec. with occasional distinct larger bubbles forming from the layer (.03 to .07 in. diameter). (3) Flow is pulsing markedly, occasionally stopping and momentarily reversing (120 cps). (4) Thermal boundary layer evident along unheated wall, similar to No. 11S-1 but more irregular and not as well defined (varies up to about .04 in. thick).

| | | | | | | | | | | | |
|---|---|---|---|---|---|---|---|---|---|---|---|
| 12S-1 | SC | 12S-1 | 3/30/61 | 199 | | 170.0 | .489 | << 1.0 | Steady | 1000 | 221 |

(1) Beginning of sub-cooled nucleate boiling. (2) Bubbles tend to grow at heater element surface in small irregular clumps, spaced about .05 in. apart and extending about .03 in. from the wall (seen mainly as shadows in profile). (3) These clumps together with occasional small discrete bubbles slide along the surface at about 2 ft/sec. (50% of channel velocity). (4) Bubbles shrink rapidly as they approach top of heater element. (5) No evidence of flow pulsations. (6) Shadow of profile of irregular wavy thermal boundary layer moving along unheated right-hand wall (about .03 in. thick).

REEL V (Continued)

| Seq. No. | Type | Run No. | Date | G, $\frac{lb.}{sec\text{-}ft^2}$ | X | $\Delta h_s$, $\frac{Btu}{lb.}$ | q, $\frac{10^6\ Btu}{hr\text{-}ft^2}$ | $\frac{q}{q_c}$ | Heater Element Temp. | P, psia | $\Delta h_s$, inlet Btu/lb. |
|---|---|---|---|---|---|---|---|---|---|---|---|
| 12S-2 | SC | 12S-2 | 3/30/61 | 199 | | 151.2 | .612 | $<<1.0$ | Steady | 1000 | 215 |

(1) Sub-cooled nucleate boiling. (2) Irregular clumps of bubbles growing at heater element surface, similar to, but longer and more distinct than in No. 12S-1. (3) Clumps are spaced about .10 in. apart and extend about .10 in. from wall. (4) In between the clumps is a frothy mixture of tiny bubbles and liquid in an irregular layer about .05 in. thick. (5) The whole mass of bubbles and clumps slides along the heater surface at about 3 ft/sec. (75% of channel velocity). (6) Almost all bubbles are in heated half of channel. (7) Slight flow pulsation (120 cps). (8) Thermal boundary layer evident along unheated wall, similar to No. 12S-1 (about .03 to .04 in. thick).

| | | | | | | | | | | | |
|---|---|---|---|---|---|---|---|---|---|---|---|
| 12-2 | SSC-0 | 12-2 | 4/6/61 | 199 | .113 | | .844 | $\approx .80$ | Pulsing - 1 mm | 1013 | 17.0 |

(1) Image hazy due to fouled window surface. (2) Evidence of greater proportion of liquid in unheated side of channel. (3) Hazy profile of shadow of agitated wavy liquid film on heater element at left ($\delta \approx .03$ in.); streamers of vapor moving in liquid film at edge of heater ribbon; relatively thick, more placid layer of high liquid concentration against unheated wall at right (.10 to .15 in. thick). (4) Occasional flashes of light from back-lights at right-hand side indicates pure liquid in contact with unheated surface. (5) No evidence of flow pulsations or "slugging". (6) Dark curved line at right is edge of window gasket, out of position.

| | | | | | | | | | | | |
|---|---|---|---|---|---|---|---|---|---|---|---|
| 18S-1 | SSC | 18S-1 | 3/9/61 | 99.2 | .234 | | .367 | $<<1.0$ | Steady | 1005 | 152 |

(1) Only sequence with .25 in. spacing heater element. (2) Appearance is very similar to No. 3S-4 with distinct rather irregular "slugging" indicated by varying illumination intensity (.05 to .10 sec. period). (3) "Dark" slugs indicative of finely divided "froth" of vapor and liquid in core; "light" slugs indicative of thick, placid layer of liquid on window (wave structure evident), with high vapor content in core. (4) Finely divided, agitated froth of tiny bubbles and vapor at heater element surfaces. (5) Occasional small bubbles (.03 in. diameter) carried along in "light" liquid slugs at about 5 ft/sec. (6) Edge of left-hand heater ribbon clearly visible. Thick edges of heater element insulation visible back of heater ribbons.

## APPENDIX E

## EXPERIMENTAL CRITICAL HEAT FLUX DATA USED FOR COMPARISON WITH THEORETICAL ANALYSIS

The following table summarizes the 822 measured critical heat flux data points used for comparison with the results calculated by equation (52).[1,2] This experimental data and the corresponding analytical predictions are discussed in Section VIII and are plotted in Figures VIII-2 through VIII-13. Included in the table are the values used for the constants C', C" and m in equation (52) and the deviations of the calculated critical heat fluxes from the corresponding measured values.

Values of the fluid properties used for the calculations are listed below. Wherever a set of data was taken at saturation pressures slightly different than those listed, the corresponding fluid properties were obtained directly from the original source references. Symbols and dimensional units are defined in the Nomenclature.

| $P_{sat}$, psia | $T_{sat}$, °F | $\sigma$, lb/sec$^2$ x $10^2$ | $\rho_L$, lb/ft$^3$ | $\rho_L/\rho_g$ | $h_{fg}$, Btu/lb. | $\mu_L$, lb/sec-ft x $10^5$ |
|---|---|---|---|---|---|---|
| 600 | 486.2 | 5.855 | 49.75 | 38.30 | 731.6 | 7.013 |
| 800 | 518.2 | 4.906 | 47.84 | 27.21 | 688.9 | 6.498 |
| 1000 | 544.6 | 4.118 | 46.29 | 20.63 | 649.4 | 6.112 |
| 1200 | 567.2 | 3.539 | 44.84 | 16.23 | 611.7 | 5.919 |
| 1400 | 587.1 | 2.976 | 43.29 | 13.04 | 574.7 | 5.823 |
| 2000 | 635.8 | 1.609 | 38.91 | 7.307 | 463.4 | 5.726 |
| 2500 | 668.1 | .7077 | 34.84 | 4.554 | 360.5 | 5.694 |

Values of $\rho_L$, $\rho_g$, $h_{fg}$, $T_{sat}$, and $\mu_L$ were taken from Keenan and Keyes (ref. (55)). Values of $\sigma$, the surface tension of liquid water

[1] Most of the calculations for this part of the work were done by Mr. C. W. Hewitt, Engineering Assistant.

[2] The data of Janssen and Kervinen (ref. (15)) were obtained under the U.S. Atomic Energy Commission Fuel Cycle Development Program at General Electric Company, Atomic Power Equipment Department (Contract No. AT(04-3)-189,P.A. 11). The data is used here, previous to issue of reference (15), through the courtesy of Dr. E. Janssen.

against its vapor, were taken from a graph in reference (56) of: the surface tension equation of Penn and Chang (ref. (57)); and the data of Volyak (ref. (58)) (measurements from 248°F to 662°F).

The two-phase friction multiplier $\Phi_{TPF}$ was determined from the correlation of Martinelli and Nelson (ref. (38)), plotted in Figure VII-6. Values of the Fanning friction factor $f_F$ for the saturated liquid were calculated from the modified Blasius equation given by McAdams (ref. (41)):

$$f_F = .046/R_e^{0.2}$$

# SUMMARY OF EXPERIMENTAL CRITICAL HEAT FLUX DATA USED FOR COMPARISON WITH THEORETICAL ANALYSIS

| Source | Group | Geometry[1] | $D_e$, in. | P, psia | $X_c$ | G, $\frac{lbs.}{sec\text{-}ft^2}$ | $b/b_o$[5] | No. | $\left[\frac{q_c(calc.)}{q_c(exp.)}\right]_{ave.}$ | $\frac{L}{De}$ |
|---|---|---|---|---|---|---|---|---|---|---|
| Tippets | A | Rect.[2], 37" long .50"x 2.1"-2 | .814 | 1000 | .033-.65 | 50-400 | 2.43 | 28 | .959 | 45 |
| C' = 1.0 | | | | | | | | | | |
| | B | Rect.[3], 37" long .50"x 2.1"-2 | .814 | 1000 | .20-.59 | 100-200 | 2.43 | 17 | .787 | 45 |
| C" = .53 | | | | | | | | | | |
| m = .75 | C | Rect.[3], 37" long .50"x 2.1"-1 | .814 | 1000 | .14 | 200 | 2.43 | 2 | 1.028 | 45 |
| | D | Rect.[2], 37" long .25"x 2.1"-2 | .455 | 1000 | .33-.61 | 100-200 | 1.36 | 9 | 1.368 | 81 |
| | E | Rect.[3], 37" long .25"x 2.1"-2 | .455 | 1000 | .13-.75 | 100-400 | 1.36 | 24 | 1.006 | 81 |
| | | (sub-cooled at inlet) | | (.85 within ± 30%)[6] | | | | (80) | | |
| Janssen and Kervinen (Ref. 15) | A | Ann., 108" long .540"x .875" | .335 | 1000 | .072-.449 | 157-468 | 1.00 | 42 | 1.041 | 322 |
| | B | Ann., 70" long .540"x .875" | .335 | 1000 | .085-.344 | 157-468 | 1.00 | 23 | 1.019 | 209 |
| C' = 6.5, A-H = 1.0, I | | | | | | | | | | |
| | C | Ann., 108" long .375" x .875" | .500 | 1000 | .037-.29 | 150-311 | 1.49 | 36 | .968 | 216 |
| C" = .53, A-E, G-I = .30, F | | | | | | | | | | |
| | D | Ann., 70" long .375"x .875" | .500 | 600-1400 | .00-.25 | 150-469 | 1.49 | 45 | 1.023 | 140 |
| m = .75 | | | | | | | | | | |
| | E | Ann., 70" long .375"x 1.25" | .875 | 1000 | .007-.35 | 40-157 | 2.83 | 16 | 1.004 | 80 |
| | F | Ann., 70" long .375"x .555" | .180 | 1000 | .005-.13 | 471-625 | .536 | 9 | 1.306 | 389 |
| | G | Ann., 70" long .375"x .710" | .335 | 1000 | .00-.31 | 158-626 | 1.00 | 35 | 1.088 | 209 |
| | H | Ann., 29" long .500"x .995" | .495 | 1000 | .042-.26 | 57-170 | 1.48 | 11 | 1.050 | 59 |
| | I | Ann., 70" long .375"x .875", rough[4] | .500 | 1000 | .040-.16 | 140-466 | 1.49 | 18 | .956 | 140 |
| | | (sub-cooled at inlet) | | (.92 within ± 30%)[6] | | | | (235) | | |
| Westinghouse (Ref. 1) | A | Circ., .186"x 12" long | .186 | 2000 | .044-.67 | 58-978 | 1.11 | 21 | 1.213 | 65 |
| | B | Rect., 6" long .101"x 1"-2 | .183 | 2000 | .028-.74 | 27-213 | .547 | 28 | 1.066 | 33 |
| C' = 1.0 | | | | | | | | | | |
| C" = .53, A = $.53(b/b_o)^{.9}$, B-F | C | Rect., 12.1" long .097"x 1"-2 | .177 | 2000 | .009-.75 | 35-811 | .524 | 70 | 1.046 | 68 |
| | D | Rect., 12.1" long .050"x 1"-2 | .095 | 2000 | .017-.73 | 60-580 | .286 | 47 | .834 | 127 |
| m = .75 | | | | | | | | | | |
| | E | Rect., 27" long .097"x 1"-2 | .177 | 2000 | .015-.73 | 83-1098 | .524 | 42 | .958 | 153 |
| | F | Rect., 27" long .059"x 1"-2 | .111 | 2000 | .27-.74 | 89-294 | .333 | 27 | 1.077 | 243 |
| | | (sub-cooled at inlet) | | (.68 within ± 30%)[6] | | | | (235) | | |

## SUMMARY OF EXPERIMENTAL CRITICAL HEAT FLUX DATA USED FOR COMPARISON WITH THEORETICAL ANALYSIS – CONT'D.

| Source | Geometry[1] | $D_e$, in. | P, psia | $X_c$ | G, $\frac{lbs.}{sec\text{-}ft^2}$ | $b/b_o$[5] | No. | $\left[\frac{q_c(calc.)}{q_c(exp.)}\right]_{ave}$ | $\frac{L}{D_e}$ |
|---|---|---|---|---|---|---|---|---|---|
| Harwell (Ref. 8) | Ann., 29" long .375"x .546". | .171 | 1000 | .073-.64 | 153-909 | .510 | (136) | .964 | 170 |
| C' = 6.5, C" = .29, m = .75 | (Two-phase at inlet) | | (.55 within ± 30%)[6] | | | | | | |
| C.I.S.E. (Refs.12, 13) | Circular, .205"x 15.8"long | .205 | 585-1195 | .28-.74 | 222-459 | 1.22 | (112) | 1.975 | 77 |
| C' = 1.0, C" = .53, m = .75 | (Two-phase at inlet) | | (.44 within ± 30%)[6] | | | | | | |
| Alndyev,et.al.(Ref. 11) | Circular, .315" x 6.3"long | .315 | 1180-2500 | .00-.61 | 154-451 | 1.88 | (24) | .978 | 20 |
| C' = 1.0, C" = .74, m = .75 | (Two-phase at inlet) | | (.92 within ± 30%)[6] | | | | | | |
| | | | | | | | (822 Total) | | |

[1] The numbers -1 and -2 for rectangular geometries designate the number of heated sides. For all of the annular geometries listed, the inner wall only was heated.

[2] Heater ribbon .006 in. thick.

[3] Heater ribbon .010 in. thick.

[4] Outer wall roughened with transverse circular ridges, .080 in. square cross-section, spaced on 1.00 in. centers.

[5] $b_o$ = .084 in.

[6] Fraction of data points for which theoretical prediction of $q_c$ does not differ from measured values by more than 30%.

## APPENDIX F

### ANALYSIS OF THE LIQUID FILM INTERFACE VELOCITY

The purpose of this analysis is to derive from the results obtained in Section VII an expression for the velocity of the liquid at the interface. This expression (equation (F-3)) is intended for application in future work to correlate measurements from the high speed motion pictures of the liquid film interface velocities.

A prediction of the mean velocity distribution for turbulent single-phase flow can be derived from Prandtl's mixing length theory by integrating equation (29) in Section VII, with the idealizations: $\tau = \tau_0$, constant and $\ell = Ky$. The result, with constants evaluated from Nikuradse's velocity data, is[1]

$$\frac{U(y)}{v_*} = 2.5 \ln (y v_*/\nu) + 5.5 \qquad \text{(F-1)}$$

For vertical upward two-phase flow with a liquid film at the wall of thickness $\delta$, a simple analysis of the forces on fluid elements gives for the shear stress distribution in the liquid film, for thin rectangular and annular ducts of half-width $b$ and circular tubes of radius $b$,

$$\frac{\tau_L(y)}{\tau_0} = 1 - \frac{y/\delta}{1 + \dfrac{g\rho_g + dp/dz}{g\rho_L + dp/dz}\left(\dfrac{b}{\delta} - 1\right)}$$

---

[1] See Schlicting (ref. (25), chs. 19 and 20; also ref. (33)).

Equation (F-1) gives excellent agreement with measured data for the region $y v_*/\nu > 30$ where turbulent effects are dominant. Close to the wall where viscous effects predominate, $y v_*/\nu < 5$, excellent agreement with data is obtained with the linear relation $U(y)/v_* = y v_*/\nu$. Equal values are given by both relations, in fair agreement with the data, at $y v_*/\nu \cong 11.6$. However, in the so-called "buffer zone," $5 < y v_*/\nu < 30$ where both viscous and turbulent effects are prominent better prediction is obtained with different values for the constants (ref. (25)).

In order to simplify the analysis, the conditions of the two-phase flow are assumed to be such that the forces of gravity are negligible compared to the pressure gradient $dp/dz$ . With this assumption the shear stress distribution reduces to

$$\frac{\tau_L(y)}{\tau_0} = 1 - \frac{y}{b}$$

which is seen to be identical with the shear stress distribution for single-phase flow. No measurements of velocity distributions for two-phase liquid-vapor flows have been reported. In the absence of these and because of the similarity of the shear stress distribution in the liquid film (for two-phase flows with negligible effects of gravity forces compared to the pressure gradient) to that for single-phase flow, it is assumed that equation (F-1) correctly gives the velocity distribution in the liquid film.[2]

Thus, evaluating (F-1) at the interface $y = \delta$ for $U_L(\delta)$ gives

$$\frac{U_L(\delta)}{v_{*_L}} = 2.5 \ln \left( \delta v_{*_L} / \nu_L \right) + 5.5 \qquad \text{(F-2)}$$

where $v_{*_L} = \sqrt{\tau_0 / \rho_L}$

Finally, substitution into equation (F-2) from equation (42) in Section VII for the film thickness $\delta$ and from equation (41) for the liquid friction velocity $v_{*_L}$ gives, in terms of non-dimensional

---

[2] Several investigators have employed variations of this approach to derive formulations for predicting the relationships between the shear stress (pressure gradient), liquid film thickness and film flow rate, using generalized velocity distributions similar to, or the same as equations (F-1) and (F-2) to calculate the liquid film flow rate. The measured data (usually with air-water systems) are in reasonably good agreement with the theoretical predictions, especially if allowance is made for the uncertainty of the measurements due to liquid entrainment in the flowing gas stream and the difficulties of measuring the liquid film thicknesses (refs. (28), (29), (30), (31), (32)).

ratios, for the liquid film interface velocity $U_L(\delta)$:

$$\frac{U_L(\delta)}{\sqrt{\frac{1}{2}\Phi_{TPF} f_F \, G/\rho_L}} = 2.5 \ln\left[\frac{K_3 K_4 \sigma (1+\rho_L/\rho_g)}{\sqrt{\frac{1}{2}\Phi_{TPF} f_F}\, G \nu_L (1+\sqrt{\rho_L/\rho_g})^2}\right] + 5.5 \qquad \text{(F-3)}$$

where the constants $K_3$ and $K_4$ are given by equations (36a) and (40a) in Section VII as

$$2\pi < K_3 < 3\pi$$

and

$$K_4 = (K/K_2)^2/K_1$$

## REFERENCES


1. DeBartoli, R.A., Green, S.J., LeTourneau, B.W., Troy, M., Weiss, A., "Forced-Convection Heat Transfer Burnout Studies for Water in Rectangular Channels and Round Tubes at Pressures Above 500 psia," WAPD-188, October 1958.

2. Isbin, H.S., Vanderwater, R., Fauske, H., Singh, S., "A Model for Correlating Two-Phase, Steam-Water, Burnout Heat-Transfer Fluxes," Trans. ASME, C, 83, (2), May 1961, pp. 149-157.

3. Goldmann, K., Firstenberg, H., Lombardi, C., "Burnout in Turbulent Flow - A Droplet Diffusion Model," Trans. ASME C, 83, (2), May 1961, pp. 158-162.

4. Bell, D.W., "Correlation of Burnout Heat Flux Data at 2000 psia," Nuc. Sci. and Eng. 7, pp. 245-251 (1960) (presented ANS meeting, June 1959).

5. Chang, Y., "Heat Transfer and Critical Conditions in Nucleate Boiling of Subcooled and Flowing Liquids," TID-6045, August 1960, (US-OTS).

6. Cicchetti, A., Silvestri, M., Soldaini, G., Zavattarelli, R., "A Critical Survey of the Literature on Burnout Studies with Wet Steam," Energia Nucleare, 6, (10), October 1959, pp. 637-660 (edited by CISE, Milano, Italy).

7. Collier, J.G., "Burnout in Liquid Cooled Reactors," Part 1 in Nuclear Power, June 1961, pp. 61-66; Part 2 in Nuclear Power, July 1961, pp. 64-67.

8. Bennett, A.W., Collier, J.G., Lacey, P.M.C., "Heat Transfer to Mixtures of High Pressure Steam and Water in an Annulus," Part II, AERE - R 3804, Harwell, England, August 1961 (to be published).

9. Zuber, N., "Hydrodynamic Aspects of Boiling Heat Transfer," AECU-4439 (USAEC - TIS), June 1959, (Ph.D. Thesis, Univ. of Calif. at Los Angeles, 1959).

10. Zuber, N., Tribus, M., Westwater, J.W., "The Hydrodynamic Crisis in Pool Boiling of Saturated and Subcooled Liquids," 1961 International Heat Transfer Conference, Boulder, Colo., Part II-A (27), pp. 230-236 (ASME).

11. Aladyev, I.T., Miropolsky, Z.L., Doroshchuk, V.E., Styrikovich, M.A., "Boiling Crisis in Tubes," 1961 International Heat Transfer Conference, Boulder, Colo., Part II-A, (28), pp. 237-243 (ASME).

12. Silvestri, M., "Two-Phase (Steam and Water) Flow and Heat Transfer," 1961 International Heat Transfer Conference, Boulder, Colo., Part II-A (39), pp. 341-353 (ASME).

13. Berkowitz, L., Bertoletti, S., Lesage, J., Peterlongo, G., Soldaini, G., Zaratterelli, R., "Results of Wet Steam Cooling Experiments: Pressure Drop, Heat Transfer and Burnout Measurements With Round Tubes (1960)," CISE Report No. R-27, pp. 148-160, October 1960.

14. Polomik, E. E., Levy, S., Sawochka, S. G., "Heat Transfer Coefficients With Annular Flow During 'Once-Through' Boiling of Water to 100 Per Cent Quality at 800, 1100, and 1400 psi," GEAP 3703 (report to USAEC), May 1961. (to be published).

15. Janssen, E. and Kervinen, J. A., "Burnout Limits for Single Rod in Annular Geometry, 600 to 1400 psia," GEAP-3899 (1962), (report to USAEC, in preparation).

16. Lamb, H., "Hydrodynamics," Dover, 6th ed.

17. York, J. L., Stubbs, H. E., Tek, M.R., "The Mechanism of Disintegration of Liquid Sheets," Trans. ASME, 75, (7), pp. 1279-1286 (1953).

18. Hagerty, W. W. and Shea, J. F., "A Study of the Stability of Plane Fluid Sheets," Jour. Appl. Mech., 22 (4), pp. 509-514 (1955).

19. Lilleleht, L. U. and Hanratty, T. J., "Measurement of Interfacial Structure for Co-Current Air-Water Flow," Jour. Fl. Mech., 11, (1), pp. 65-81, August 1961.

20. Miles, J. W., "On the Generation of Surface Waves by Shear Flows": Part 1 in Jour. Fl. Mech., 3, pp. 185-204 (1957); Part 2 in Jour. Fl. Mech., 6, pp. 568-582 (1959).

21. Miles, J. W., "On the Generation of Surface Waves by Turbulent Shear Flows," Jour. Fl. Mech., 7, pp. 469-478 (1960).

22. Stewart, R. W., "The Wave Drag of Wind Over Water," Jour. Fl. Mech., 10, pp. 189-194 (1961).

23. Gazley, C., Jr., "Co-Current Gas-Liquid Flow-III: Interfacial Shear and Stability," 1949 - Heat Trans. and Fl. Mech. Inst., pp. 29-40, (Berkeley Meeting).

24. Goldstein, S., "Modern Developments in Fluid Dynamics," Vol. I, Ch. 5, Oxford, (1958).

25. Schlicting, H., "Boundary Layer Theory," Pergammon (1955).

26. Laufer, J., "Some Recent Measurements in a Two-Dimensional Turbulent Channel," Jour. Aero. Sc., pp. 277-287, May 1950.

27. Laufer, J., "The Structure of Turbulence in Fully Developed Pipe Flow," NACA Report No. 1174, (1954).

28. Calvert, S. and Williams, B., "Upward Co-Current Annular Flow of Air and Water in Smooth Tubes," Jour. AIChE, March 1958, pp. 78-86.

29. Kinney, G. R., Abramson, A. E., Sloop, J. L., "Internal-Liquid-Film Cooling Experiments with Air-Stream Temperatures to 2000°F in 2-inch and 4-inch Diameter Horizontal Tubes," NACA Report No. 1087, (1952).

30. Charvonia, D. A., "A Study of the Mean Thickness of the Liquid Film and the Characteristics of the Interfacial Surface in Annular, Two-Phase Flow in a Vertical Pipe," Purdue Res. Found. Report No. I-50-1, May 1959 (ASME Paper 61-WA-243).

31. Collier, J. G. and Hewitt, G. F., "Data on the Vertical Flow of Air-Water Mixtures in the Annular and Dispersed Flow Regions, Part-B," AERE-R3455, Harwell, England, August 1960 (to be published).

32. Hewitt, G. F., King, I., Lovegrove, P. C., "Holdup and Pressure Drop Measurements in the Two-Phase Annular Flow of Air-Water Mixtures," AERE-R3764, Harwell, England, June 1961 (to be published).

33. Sleicher, C. A., Jr., "Experimental Velocity and Temperature Profiles for Air in Turbulent Pipe Flow," Trans. ASME, 80, pp. 693-702, (1958).

34. Knuth, E. L., "The Mechanics of Film Cooling": Part 1 in Jet Propulsion, Nov-Dec 1954, pp. 359-365; Part 2 in Jet Propulsion, Jan. 1955, pp. 16-25.

35. Laird, A.D.K., "Stability Considerations in Vertical Annular Two-Phase Fluid Flow," Ph.D. Thesis, Univ. of Calif. at Berkeley (1951).

36. Dryden, H. L., "Turbulence and Diffusion," Ind. and Eng. Chem., April 1939, pp. 416-425.

37. Hanratty, T. J., "Turbulent Exchange of Mass and Momentum with a Boundary," Jour. AIChE, 2, (3), pp. 359-366 (1956).

38. Martinelli, R. C. and Nelson, D. B., "Prediction of Pressure Drops During Forced Circulation Boiling of Water," Trans. ASME, 70, 695, (1948).

39. Isbin, H.S., Moen, R.H., Wickey, R.O., Mosher, D.R., Larson, H.C., "Two-Phase Steam-Water Pressure Drops," 1958 Nuc.Eng.Conf., 147(AIChE).

40. Chisholm, D. and Laird, A.D.K., "Two-Phase Flow in Rough Tubes," Trans. ASME, pp. 276-286 (1958).

41. McAdams, W. H., "Heat Transmission," 3rd ed., ch. 6, McGraw-Hill (1954).

42. Moody, L. F., "Friction Factors for Pipe Flow," Trans. ASME, 66, pp. 671-684 (1944).

43. Frenkel, J., "Kinetic Theory of Liquids," Dover (1946).

44. Norman, W. S. and McIntyre, V., "Heat Transfer to a Liquid Film on a Vertical Surface," Trans. Inst. Chem. Eng., 38, pp. 301-307 (England).

45. Longwell, J. P. and Weiss, M. A., "Mixing and Distribution of Liquids in High Velocity Air Streams," Ind. and Eng. Chem., 45, pp. 667-677 (1953).

46. Levy, S., "Prediction of Two-Phase Flow From Mixing Length Theory," GEAP-3628 (Dec. 1960), (report to USAEC).

47. Levy, S., "Prediction of Two-Phase Pressure Drop and Density Distribution From Mixing Length Theory," May 1961, (report to USAEC issued as an extension to GEAP 3628, ref. (46)), (to be published).

48. Petrick, M. P., "Investigation of Two-Phase Air-Water Flow Phenomena," ANL 5787, (1958), (US-OTS).

49. Larson, H. C., "Void Fractions in Two-Phase Steam-Water Systems," M. S. Thesis, Dept. of Chem. Eng., Univ. of Minn. (1957).

50. Maurer, G. W., "A Method of Predicting Steady-State Boiling Vapor Fraction in Reactor Coolant Channels," Bettis Technical Review, WAPD-BT-19, pp. 59-70, (1960), (US-OTS).

51. Marchaterre, J. F., et.al., "Natural and Forced Circulation Boiling Studies," ANL-5735, (1960), (US-OTS).

52. Foglia, J.J., Peter, F.G., Epstein, H.M., Wooton, R.O., Dingee, D.A., Chastain, J.W., "Boiling-Water Void Distribution and Slip Ratio in Heated Channels," BMI-1517, (1961),(US-OTS).

53. Krasiakova, L.I., "Some Characteristics of the Flow of a Two-Phase Mixture in a Horizontal Pipe," Zhur. Tekh. Fiz., 22, (4), pp. 654-669 (AERE Lib/Trans. 695, Harwell, 1957).

54. Mead, B. R., Romie, F. E. and Guibert, A. G., "Liquid Superheat and Boiling Heat Transfer," Proc. 1951 - Heat Trans. and Fl. Mech. Inst., pp. 209-216, (Stanford, 1951).

55. Keenan, J. H. and Keyes, F. G., "Thermodynamic Properties of Steam," 1st ed., Wiley (1936).

56. Hoyt, J. G., "Surface Tension of Water at Elevated Temperatures," (internal General Electric Co. memorandum, August 1956).

57. Penn, A.B.K. and Chang, E., "Changes of Viscosity and Surface Tension of Water with Temperature," Bull. Chunking Inst. of Industrial Research, No. 17, pp. 1-5 (1948).

58. Volyak, L. D., "Temperature Dependence of the Surface Tension of Water," Dokladie Akad. Nauk., 74, pp. 307-310 (1950).

59. Everhart, J.L., Lindlief, W.E., Kanegis, J., Weissler, P.G., Siegel, F., "Mechanical Properties of Metals and Alloys," Nat'l. Bur. Stds., Bull. C-447, (1943).

60. Perl, M. G., "Hydrostatic Test Report No. 18," (General Electric Co. internal report, June 1960).

61. "ASME Code Form U-2, Certificate of Shop Inspection for Part 7-1," (filed at General Electric Co., APED, July 1961).

62. Tippets, F. E., "Preliminary Stress Analysis - Observational Test Section," (General Electric Co. internal memorandum, Dec. 1959).

63. Fage, A. and Townend, H.C.H., "An Examination of Turbulent Flow With an Ultramicroscope," Proc. Roy. Soc., 135A, 656 (1932), London.

64. Isbin, H. S., Moen, R. H. and Mosher, D. R., "Two-Phase Pressure Drops," AECU-2994, Nov. 1954.

65. Bennett, J.A.R., "Two-Phase Flow in Gas-Liquid Systems," AERE CE/R 2497, (Harwell, England) (1958).

66. Collier, J. G., "A Review of Two-Phase Heat Transfer (1935-1957)," AERE CE/R 2496, (Harwell, England) (1958).

67. Emmerson, G. S., "Heat Transmission with Boiling," Nuc. Eng., pp. 493-500, Nov. 1960.

68. Leiby, D. W., "Boiling Heat Transfer Literature Survey, II: Selected Papers," General Electric Laboratory Report DF55GL 307, Nov. 1955.

69. Charvonia, D. A., "A Review of the Published Literature Pertaining to the Annular, Two-Phase Flow of Liquid and Gaseous Media in a Pipe," PUR-32-R, Dec. 1958.

70. Westwater, J. W., "Comments on Visual Flow Studies with Boiling in a Flow Channel," letter of May 16, 1961, to F. E. Tippets, GEAP-3709, 3rd Quart. Rep., AEC Fuel Cycle Prog., pp. 32-37.

71. Gresham, W. A., Foster, P. A. and Kyle, R. J., "Review of the Literature on Two-Phase (Gas-Liquid) Fluid Flow in Pipes," WADC-TR-55-422 (Pt. 1), June 1955.

72. Roberts, H. A., "A Review of Net Boiling Heat Transfer and Pressure Drop From the Literature," AERE-ED/M-22, (British), Aug. 1955.

73. Forster, K. Engelberg- and Grief, R., "Heat Transfer to a Boiling Liquid - Mechanism and Correlations," Trans. ASME, 81, C, pp. 43-53, Feb. 1959.

74. Kutateladze, S. S., "Heat Transfer in Condensation and Boiling," AEC-tr-3770, 2nd ed. (Moscow, 1952).

75. Janssen, E., "Multi-Rod Burnout at Low Pressure," GEAP-3467, June 1960 (to be published).

76. Vohr, J., "Forced Convection Boiling," Quarterly Progress Report No. IX-QPR-3-61, NYO-9648, Columbia Univ., Eng. Res. Lab., October 1961 (also earlier Quarterly Reports, from October 1960).

77. Westwater, J. W. and Santangelo, J. G., "Photographic Study of Boiling," Ind. and Eng. Chem., 47, (8), pp. 1605-1610 (1955).

78. Rohsenow, W. M. and Clark, J. A., "A Study of the Mechanism of Boiling Heat Transfer," Trans. ASME, 609 (July 1951).

79. Ellion, M. E., "A Study of the Mechanism of Boiling Heat Transfer," Cal. Inst. Tech. Jet Propulsion Lab. Memo No. 20-88, March 1954.

80. Dengler, C. E., "Heat Transfer and Pressure Drop for Evaporation of Water in a Vertical Tube," Ph.D. Thesis, MIT (1952).

81. Kozlov, B. K., "Forms of Flow of Gas-Liquid Mixtures and Their Stability Limits in Vertical Tubes," Zhur. Tekh. Fiz., 24 (12), 2285 (1954).

82. Govier, G. W., Radford, B. A. and Dunn, J.S.C., "The Upward Vertical Flow of Air-Water Mixtures; I - Effect of Air and Water Rates on Flow Pattern, Holdup and Pressure Drop," Canadian Jour. of Chem. Engr., 35, 58 (1957).

83. Govier, G. W., Radford, B.A. and Dunn, J.S.C., "The Upward Vertical Flow of Air-Water Mixtures; II - Effect of Tubing Diameter on Flow Pattern, Holdup and Pressure Drop," Canadian Journal of Chem. Engr., 36, 195 (1958).

84. Kosterin, S. I., "Investigation of the Effect of the Diameter and the Position of the Pipe Upon the Hydraulic Resistance and the Structure of the Flow of a Gas-Liquid Mixture," Izvestia Akad. Nauk., 12 (1949).

85. Baker, O., "Simultaneous Flow of Oil and Gas," Oil and Gas Journal 53, 185 (1954).

86. Richardson, B. L., "Some Problems in Horizontal Two-Phase Two-Component Flow," ANL-5949 (1959).

87. Mologin, M. A., "Types of Flow of Gas-Liquid Mixtures in Horizontal Pipes," Dokl. Akad. Nauk., 94, (5), 807 (1954).

88. Brooks, C. H. and Badger, W. L., "Heat Transfer Coefficients in the Boiling Section of a Long-Tube, Natural Circulation Evaporator," Trans AIChE, 33, pp. 392-416 (1937).

89. Dukler, A.E., "Fluid Mechanics and Heat Transfer in Vertical Falling Film Systems," Preprint-101 (AIChE), 3rd Nat'l. ASME-AIChE Heat Transfer Conference, Storrs, August 1959.

90. Bergelin, O.P., Kegel, P.K., Carpenter, F.G., Gazley, C., Jr., "Co-Current Gas-Liquid Flow - I. Flow in Horizontal Tubes; II. Flow in Vertical Tubes," 1949- Ht. Trans. Fl. Mech. Inst., pp. 5-28 (Berkeley meeting).

91. Adorni, N., Casagrande, I., Cravarolo, L., Hassid, A., Silvestri, M., "Experimental Data on Two-Phase Adiabatic Flow: Liquid Film Thickness, Phase and Velocity Distribution, Pressure Drops in Vertical Gas-Liquid Flow," CISE Report R-35, March 1961.

92. Ivashkevich, A.A., "Critical Heat Flux for Forced Flow of Liquids in Channels," Atomnaya Energia, Jan. 1960, pp. 51-54.

93. Green, S.J., LeTourneau, B.W., and Troy, M., "Forced Circulation Uniform Flux Burnout Studies for High-Pressure Water," ASME Paper No. 59-HT-25, August 1959.

94. Averin, E.K., and Kruzhilin, G.N., "Heat Transfer in the Boiling of Water in Conditions of Forced Circulation," (from "Heat Transfer and Thermal Simulation," ed. by M.A. Mikheev, pp. 239-271 (Moscow, 1959), AERE-Trans 847.

95. Miropolsky, Z.L., Shitsman, M.E., Mostinsky, I.L., Stavrovsky, A.A., "The Effect of Inlet Conditions on the Critical Heat Flux for the Case of Boiling Water in Tubes," Teploenergetika, 1 (1959), pp. 80-83, (RTS-1525).

96. Styrikovich, M.A. and Faktorovich, L.E., "Effect of Tube Length on the Magnitude of Critical Heat Flow with Forced Convection of Steam-Water Mixture," Sov. Fiz. Dokladie, 3, 518 (1959).

97. Aladyev, I.T., Dadonov, L.D., Udalov, V.S., "Burnout Heat Flux for Flow of Water in Pipes," Sov. Jour. Atomic Energy, 6, (1), Jan. 1959, pp. 42-45.

98. Bertoletti, S., Lesage, J., Lombardi, C., Peterlongo, G., Silvestri, M., Soldaini, G., Weckermann, F., "Heat Transfer and Pressure Drop with Steam-Water Spray," CISE Report No. R-36, April 1961.

99. AMU-ANL Heat Transfer Conference, Argonne National Laboratory, Sept. 5-6, 1961 (General Discussion, Session III).

100. Reynolds, J.M., "Burnout in Forced Convection Nucleate Boiling of Water," MIT Tech. Report No. 10, July 1957.

101. Galson, A.E. and Polomik, E.E., "Burnout Data Applicable to Boiling Water Reactors," (paper presented at Amer. Nuc. Soc. meeting, June 1957).

102. Lacey, P.M.C., Hewitt, G.F. and Collier, J.G., "Climbing Film Flow," AERE-R 3962, Harwell, England, January 1962.

103. Schmidt, K. R., "Thermodynamic Investigations of Highly-Loaded Boiler Heating Surfaces," translation from Mitteilunger der Vereinigung der Grosskesselbesitzer, 63, 391 (1959) by L. Venters, AEC-tr-4033.

104. Larson, R. F., "Factors that Influence Heat Transfer in Boiling," Proc. 1953 - Heat Trans. and Fl. Mech. Inst., pp. 163-172, (UCLA, 1953).

105. Houston, R. W., "Temperature Fluctuations in Resistance Heating With Alternating Current," CU-3-53-AT-dp-Ch.E., June 1953.

106. Ebasco Services Inc. and General Electric Co., "Steam Quality Optimization," Separate Study No. 3R, Boiling Water Reactor Study, IDO-24030 (1959).

107. Kline, S. J. and McClintock, F. A., "Describing Uncertainties in Single-Sample Experiments," Mechanical Engineering, Jan. 1953, pp. 3-8.

108. Leppert, G., Jakob, M. and Reynolds, J. B., "Pressure Drop During Forced Circulation Boiling," Heat Transfer Symposium, Louisville, Preprint 5, (AIChE), March 1955.

109. Styrikovich, M. A. (editor), "Hydrodynamics and Heat Transfer During Boiling in High Pressure Boilers," Acad. Sci., USSR, Moscow, 1955, (AEC-tr-4490, June 1961), (US-OTS).